FUNCTIONALIZATION OF WHITE PHOSPHORUS MEDIATED BY LOW VALENT COBALT COMPLEXES

Dissertation zur Erlangung des

Doktorgrades der Naturwissenschaften

DR. RER. NAT.

am Institut für Anorganische Chemie

der Fakultät für Chemie und Pharmazie

der Universität Regensburg

vorgelegt von

CHRISTIAN M. HOIDN

aus Zwiesel

Regensburg 2019

Der experimentelle Teil der vorliegenden Arbeit wurde von November 2015 bis Oktober 2019 unter Anleitung von Prof. Dr. Robert Wolf am Institut für Anorganische Chemie der Universität Regensburg angefertigt.

Diese Arbeit wurde angeleitet von: Prof. Dr. Robert Wolf

Promotionsgesuch eingereicht am: 23.10.2019

Tag der mündlichen Prüfung: 04.12.2019

Promotionsausschuss: Vorsitz: Apl. Prof. Dr. Rainer Müller

                                    Erstgutachter: Prof. Dr. Robert Wolf

                                    Zweitgutachter: Prof. Dr. Manfred Scheer

                                    Dritter Prüfer: Prof. Dr. Frank-Michael Matysik

PROLOGUE

This thesis reports on the synthesis and characterization of cobalt complexes and their application in the functionalization of white phosphorus. Chapter 1 reviews the versatile chemistry of transition metal-mediated P_4 functionalization and categorizes this research field into systematic subunits. Chapter 2 addresses the synthesis of a novel heterobimetallic Co_2Sn_2 cluster and its reactivity toward white phosphorus. Chapter 3 reports on the cyanide-induced [3+2] fragmentation of pentaphosphido ligands, which were obtained by stepwise P_4 activation and functionalization. In Chapter 4, the construction of polyphosphido complexes from a tetraphosphido cobaltate precursor is discussed. The final chapter 5 summarizes the results of this thesis and gives a brief outlook.

PROLOG

Diese Dissertation behandelt die Synthese und Charakterisierung von niedervalenten Cobaltkomplexen und deren Anwendung in der Funktionalisierung von weißem Phosphor. Kapitel 1 setzt sich mit dem aktuellen Forschungsstand zur übergangsmetallvermittelten P_4 Funktionalisierung auseinander und gruppiert die bisherige Literatur in systematische Untereinheiten. Kapitel 2 beschreibt die Synthese eines neuen heterobimetallischen Co_2Sn_2-Clusters und seine Reaktivität gegenüber weißem Phosphor. In Kapitel 3 wird die durch Cyanidanionen ausgelöste [3+2] Fragmentierung von Pentaphosphidoliganden thematisiert. Kapitel 4 befasst sich mit dem Aufbau von Polyphosphidokomplexen durch Reaktion von einem Tetraphosphido-Komplex mit einer P_2 Spezies. Das letzte Kapitel 5 fasst die Ergebnisse dieser Arbeit zusammen und gibt einen kurzen Ausblick.

TABLE OF CONTENTS

1   TRANSITION METAL-MEDIATED TRANSFORMATIONS OF WHITE PHOSPHORUS

1.1   Introduction

The element phosphorus is essential for life. In every organism, phosphorus serves as a building block of DNA and of the cellular energy carrier ATP.[1] But the biological relevance is far from the only reason why phosphorus containing molecules have a huge impact on daily life.[1] Phosphorus compounds are also found in detergents, fertilizers, insecticides, food products, flame retardants, and organophosphorus derivatives in particular play a crucial role in the chemical and pharmaceutical industries (Figure 1).
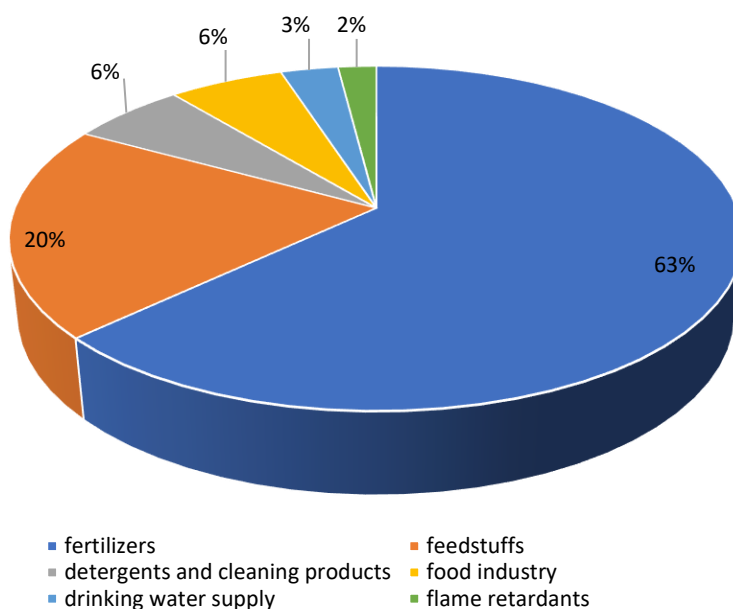
Figure 1. Percentage distribution of phosphorus usage in Germany in 2011 estimated by the Federal Environment Agency.[2]

The industrial precursor for the vast majority of these synthetic compounds is white phosphorus (P_4), the most reactive allotrope of the element, which is produced from phosphate rock on a megaton scale annually.[3,4] Tremendous amounts of energy are required to generate P_4 from the mineral apatite, $Ca_5(PO_4)_3(OH,F,Cl)$, quartz sand (SiO_2) and coke (C) at around 1500 °C in an electric arc furnace (Scheme 1a).[1] A significant amount of P_4 produced worldwide is converted into valuable organophosphorus compounds which are used for example as specialty chemicals, pharmaceuticals and catalyst components. The synthesis of these target organophosphorus derivatives is a

1

multistep process involving the initial chlorination of P_4 to PCl_3, followed by subsequent functionalization with Grignard or organolithium reagents (Scheme 1b).[3,4]
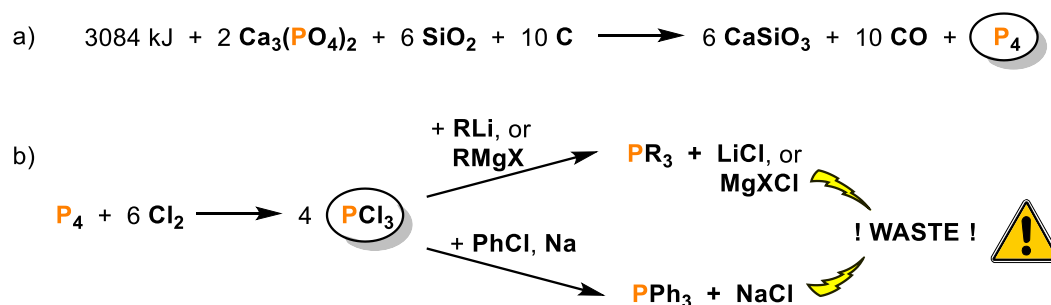
Scheme 1. Production of white phosphorus (P_4) from the calcium phosphate part of apatite minerals (a) and the synthesis of organophosphorus compounds via PCl_3 (b) (R = organic residue; X = Cl, Br, I).

Triphenylphosphane (PPh_3), for example, being one of the synthetically most important organophosphorus compounds, is industrially prepared by high-temperature reaction of chlorobenzene with PCl_3 in the presence of molten sodium.[5] Furthermore, huge amounts of inorganic salt waste are accumulated as by-products. Thus, both sustainability and safety issues render an overall improvement of those processes urgently needed. The development of alternative routes that avoid the use of chlorine gas and circumvent the highly toxic intermediate PCl_3 is currently of great interest. A promising approach to gain fundamental understanding of phosphorus transformations is the mild activation of P_4 and its successive functionalization with organic substrates. It is hoped that studying these reactions may ultimately pave the way to effective catalytic methods for converting P_4 directly to organophosphorus derivatives.

1.2   Activation of White Phosphorus

The controlled and consecutive cleavage of P−P bonds within the P_4 tetrahedron (often referred to as P_4 activation) plays a crucial role in the formation of reactive P_n (n = 1 − 4) units, potentially suitable for further functionalizations. As outlined in several reviews, a large number of reactive main group element or transition metal compounds has been applied to the activation and degradation of the P_4 molecule.[4,6,7] Scheme 2 illustrates conceivable degradation pathways starting with the initial formation of [1.1.0]bicyclo-P_4 ("butterfly") species. The stepwise cleavage of further P−P single bonds results in cyclic, branched and linear P_n fragments stabilized by transition metals or main group compounds.
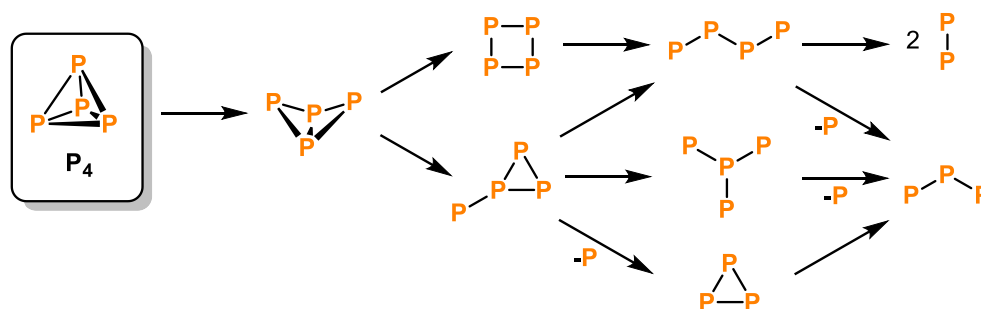
Scheme 2. A selection of possible reaction pathways for the activation of white phosphorus (P_4). Only the P_n backbones of the fragments are shown; charges and substituents are omitted for clarity.

Especially the transition metal-mediated activation of P_4 has attracted considerable attention over the last several decades has given rise to a plethora of fascinating complexes bearing highly versatile P_n units.[4,6] A complete description of all literature known P_n ligands would exceed the scope of this introduction. Nevertheless, only a compendious overview of common structural P_n motifs is illustrated in Figure 2. Monophosphido ligands, P_2 dumbbells or *cyclo*-P_3 rings derive from fragmented P_4 molecules (n ≤ 3). Tetraphosphido ligands (n = 4) are typically observed either as metal-bound retained P_4 tetrahedra, or as partially degraded "butterfly" species, P_4 rings and chains. Sometimes, the aggregation of multiple phosphorus atoms n ≥ 5 is also observed, which may result in aromatic *cyclo*-P_5 and *cyclo*-P_6 ligands, or even extended polyphosphorus cages (bridging motifs, metal−phosphorus multiple bonding, and varying hapticity can also be observed, but are not discussed here).
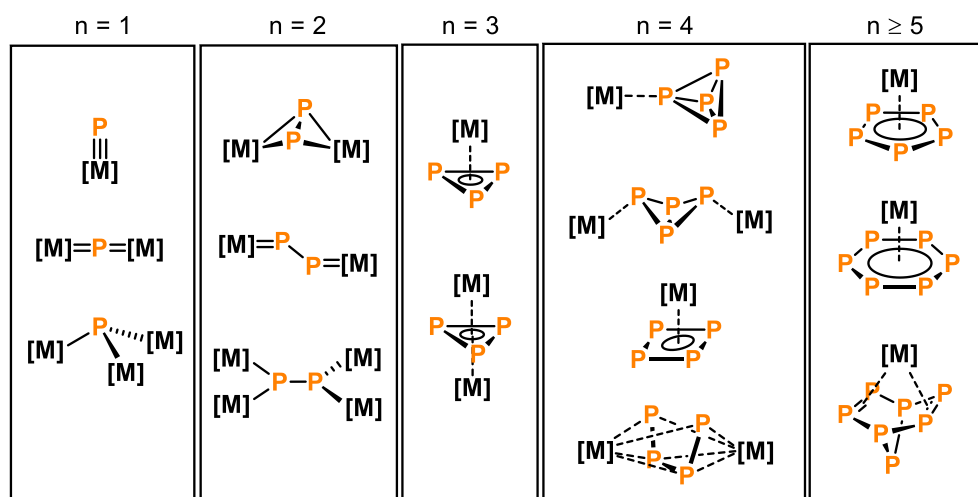
Figure 2. Structural motifs of selected transition metal complexes bearing P_n ligands; [M] = transition metal complex fragment.

3

1.3 Transition Metal-Mediated Functionalization of White Phosphorus

Whereas the activation of P_4 has been extensively investigated, subsequent functionalization is far less explored. In the last few years, the interest in transfer and incorporation of P_4-derived phosphorus atoms into organic or main group substrates has grown substantially, yet the controlled and selective functionalization of activated phosphorus units is still challenging. In the following section, a detailed review is presented which addresses the functionalization of white phosphorus promoted by transition metals.

1.3.1 One Step Activation and Functionalization

The first transition metal-mediated P_4 functionalization reaction was reported in 1974 by *Green* and co-workers.[8] They described the reaction of [Cp$_2$MoH$_2$] (**1**) with an excess of P_4 in hot toluene, affording the deep red diphosphene complex [Cp$_2$Mo(η^2-P$_2$H$_2$)] (**2**), which was crystallographically characterized by *Canillo* et al. three years later (Scheme 3a).[9] This discovery represents a landmark in phosphorus chemistry, since not only P_4 activation, but also functionalization was observed. Specifically, five P−P bonds of the P_4 tetrahedron were cleaved and, simultaneously, new P−H bonds were formed by transfer of the hydride ligands from the metal center to phosphorus.
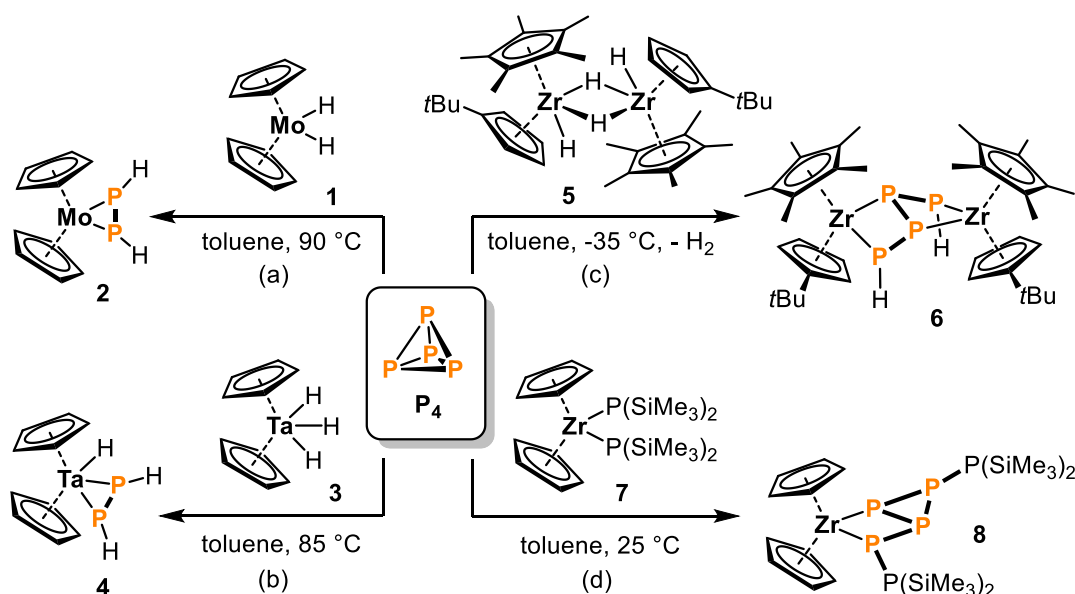
Scheme 3. Early transition metallocene-mediated activation of P$_4$ with concomitant functionalization.

More than 20 years later, *Stephan* and co-workers provided a further example of such a fragmentation/hydrogenation process (Scheme 3b). Reaction of the tantalocene trihydride

complex [Cp$_2$TaH$_3$] (**3**) with P$_4$ results in the hydridodiphosphene complex [Cp$_2$Ta(H)(η^2-P$_2$H$_2$)] (**4**).[10] Interestingly, *Chirik* et al. found that an analogous reaction of the related zirconium dihydride complex [Cp*$_2$ZrH$_2$] with P$_4$ proceeds differently, and does not give a diphosphene complex. Instead, only P$_4$ activation to the [1.1.0]-tetraphosphabicyclobutane (butterfly) complex [Cp*$_2$Zr(η^2-P$_4$)] occurs, along with reductive elimination of H$_2$.[11] They further described the treatment of the sterically more encumbered dinuclear complex [Cp*Cp′ZrH$_2$]$_2$ (**5**, Cp′ = η^5-C$_5$H$_4$tBu) with P$_4$ (Scheme 3c). The product molecule [{Cp*Cp′Zr}$_2$(μ_2,η^2,η^2-P$_4$H$_2$)] (**6**) features a bridging P$_4$ chain best described as a P$_4$H$_2^{4-}$ tetraanion. *Lappert* and co-workers used the zirconium diphosphido complex [Cp$_2$Zr(P(SiMe] (**7**) for a related insertion of a rearranged P$_4$ scaffold into both Zr−P bonds to yield the hexaphosphane-3,5-diide complex **8** (Scheme 3d).[12]

A late transition metal based approach for the one-step activation and functionalization of P$_4$ was initially reported by *Peruzzini* et al. in 1998 (Scheme 4).[13] Rhodium(III) and iridium(III) hydride complexes [(triphos)MH$_3$] (**9a**: M = Rh, **9b**: M = Ir; triphos = 1,1,1-tris(diphenylphosphanylmethyl)ethane) enable the direct hydrogenation of P$_4$ to PH$_3$, if conducted in a closed system. The stoichiometric by-products are the highly stable *cyclo*-P$_3$ compounds **10**. Upon carrying out the reaction of **9a** with P$_4$ at lower temperature, or
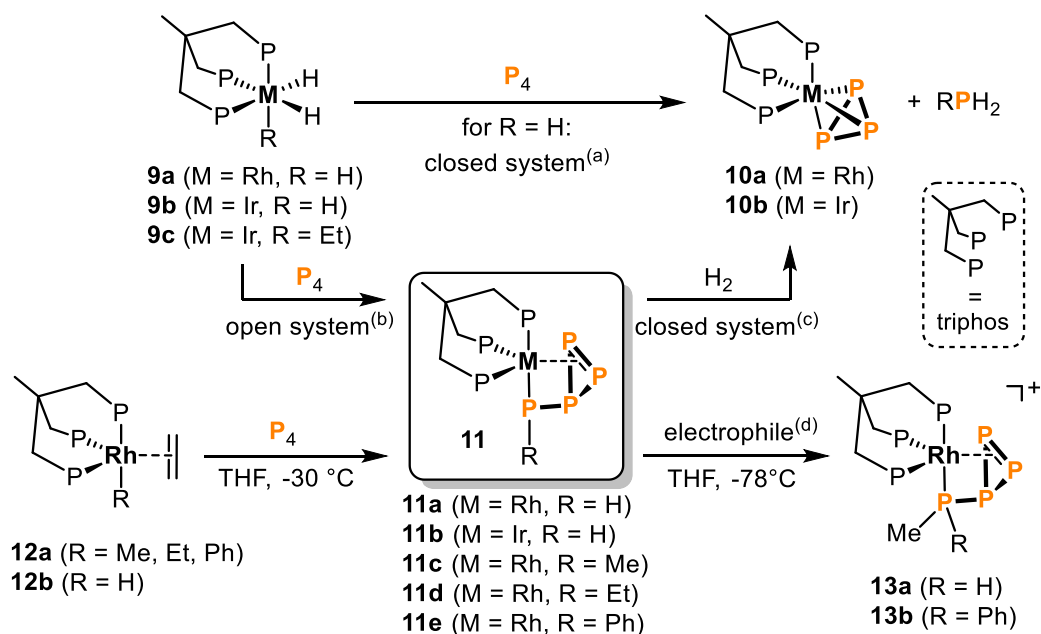
Scheme 4. Functionalization of P$_4$ mediated by rhodium and iridium triphos complexes. Reaction conditions: (a) for **9a**: THF, 70 °C; for **9b** THF, 120 °C. (b) for **9a**: open system, THF, 70 °C, −H$_2$ or closed system, THF, 40 °C, −H$_2$; for **9c**: open system, THF, reflux, −C$_2$H$_6$. (c) for **11a**, **11b**: THF, 70 °C; for **11c**, **11d**, **11e**: THF, 60 °C, 20 atm H$_2$. (d) for **11a**, **11e**: +MeOTf; for **11c**: +HBF$_4$·OMe$_2$.

in an open system, the evolution of dihydrogen gas and an isolable intermediate species [(triphos)Rh(η^1:η^2-HP$_4$)] (**11a**) was observed. Further mechanistic studies performed with the kinetically more stable dihydridoethyl iridium complex [(triphos)IrH$_2$(Et)] (**9c**) revealed the initial formation of a butterfly compound [(triphos)M(H)(η^2-P$_4$)], which slowly isomerizes to [(triphos)Ir(η^1:η^2-HP$_4$)] (**11b**). Finally, when solutions of either **11a** or **11b** were saturated with H$_2$, the reactions proceeded to completion, forming PH$_3$ and **10**.

Only a year later, *Peruzzini* et al. successfully extended this concept to P−C bond formation by reporting on analogous hydrocarbon-substituted tetraphosphido rhodium complexes [(triphos)Rh(η^1:η^2-RP$_4$)] (**11c**: R = Me; **11d**: R = Et, **11e**: = Ph) derived from the corresponding ethylene complexes [(triphos)Rh(R)(η^2-C$_2$H$_4$)] (**12a**) and P$_4$ (Scheme 4).[14] During the reaction the labile ethylene ligand is released while the alkyl and aryl moieties previously bound to the metal center in **12a** selectively migrate to the activated P$_4$ scaffold. Notably, the reaction of P$_4$ with the corresponding hydrido-ethylene derivative [(triphos)Rh(H)(η^2-C$_2$H$_4$)] (**12b**) does not afford the expected product **11a**. Instead, the ethylene ligand inserts into the Rh−H bond and successively gives the ethyltetraphosphido species **11d**. Moreover, the pressurization of **11c**, **11d** and **11e** with H$_2$ at 60 °C induced the formation of **10a** along with the phosphanes RPH$_2$ in moderate yields. The reactivity of complexes **11** was further explored through reactions with electrophiles.[15] The reaction of **11a** and **11e** with MeOTf or MeI gave the doubly functionalized and highly temperature sensitive cations [(triphos)Rh(η^1:η^2-MeRP$_4$)]$^+$ (**13a**: R = H, **13b**: R = Ph). The fact that **13a** is also obtained by treating **11c** with HBF$_4$·OMe$_2$ supports the idea that in this system electrophilic attack generally takes place at the already-functionalized phosphorus atom.

A very recent collaboration by the groups of *Caporali* and *Grützmacher* dealt with the chlorination of P$_4$ by the 16 valence electron species [Cp*RuCl(PCy$_3$)] (**14**, Scheme 5).[16] Promoted by two equivalents of **14**, the migration of two chloride ligands from ruthenium to an activated P$_4$ unit yields the dinuclear complex [Cp*Ru(PCy$_3$)(μ_2,η^2:η^4-P$_4$Cl$_2$)RuCp*] (**15**), containing a planar and unsymmetrically bridging 1,4-dichloro-tetraphosphabutadiene ligand. A selective exchange of the chloro substituents with alkyl groups was achieved by salt metathesis with *n*BuLi. The product was the tetranuclear compound [(Cp*Ru)$_4$(μ_3,η^2:η^2:η^4-P$_4$*n*Bu$_2$)$_2$] (**16**), which features two coplanar [P$_4$*n*Bu$_2$] moieties.
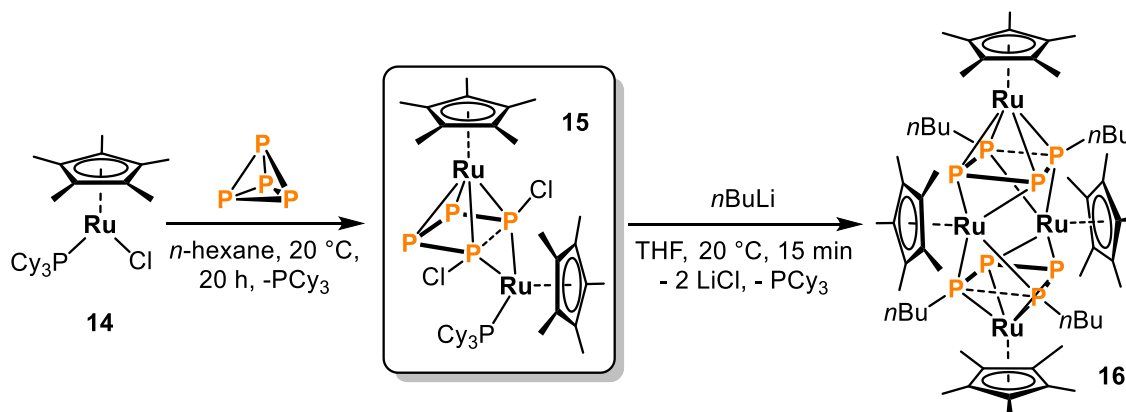
Scheme 5. Ruthenium-mediated halogenation and subsequent alkylation of P_4.

1.3.2 Functionalization of P_1 and P_2 Ligands

In comparison to the one-step reactions mentioned above, more versatile transformations can be made feasible by separating P_4 activation from the subsequent functionalization step. The following section deals with functionalizations of P_1 and P_2 ligands derived from P_4, which date back to the pioneering work of *Scherer* et al. in 1991. Oxidation of the Ni_2WP_2 complex **17** with $(Me_3SiO)_2$ afforded **18a**, the first complex of PO, the heavier congener of the ubiquitous nitric oxide (NO, Scheme 6a).[17] Oxidation of **17** with S_8
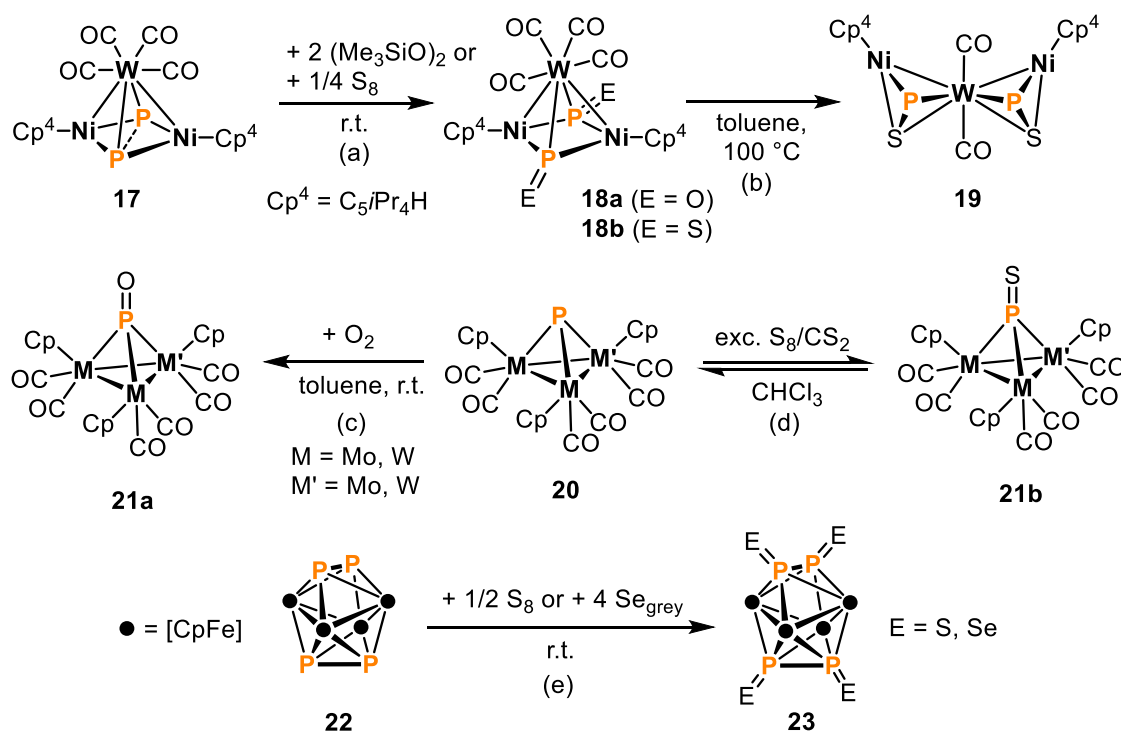
Scheme 6. Oxidation of P_4-derived P_1 and P_2 ligands in the coordination sphere of transition metals.

similarly affords the isoelectronic PS species **18b**, which undergoes partial loss of CO and rearrangement from $\mu_3{:}\eta^1$ to $\mu_2{:}\eta^2$ coordination of the PS ligands when heated to 100 °C (**19**, Scheme 6b).[18] *Mays* and co-workers found that a similar μ_3-PO compound (**21a**) is formed if the trinuclear species **20** is exposed to atmospheric oxygen (Scheme 6c).[19] The corresponding oxidation with elemental sulfur is fully reversible and leads to **21b** in the presence of an excess of S_8 in CS_2 (Scheme 6d).[20] The reverse reaction to **20** takes place in common organic solvents in the absence of an excess S_8. *Scherer* et al. reported on the synthesis of E=P−P=E ligands in **23** by oxidation of the P_2 dumbbells in the Fe_4P_4 clusters **22** with elemental sulfur or grey selenium (Scheme 6e).[21]

A series of remarkable functionalizations was performed by *Cummins* and co-workers using early transition metals triply bound to a terminal phosphido (P^{3-}) ligand. The molybdenum phosphide **24** was reacted with monomeric acetone peroxide, elemental sulfur and mesityl azide ($MesN_3$), giving complexes with terminally-bound phosphorus monoxide (**25a**), phosphorus monosulfide and iminophosphenium (**25b**) ligands (Scheme 7a).[22,23] In addition, the phosphaalkyne $AdC{\equiv}P$ (Ad = 1-adamantyl) adds to the $Mo{\equiv}P$ triple bond in **24** to yield the *cyclo*-CP_2 complex **26** (Scheme 7b).[24]
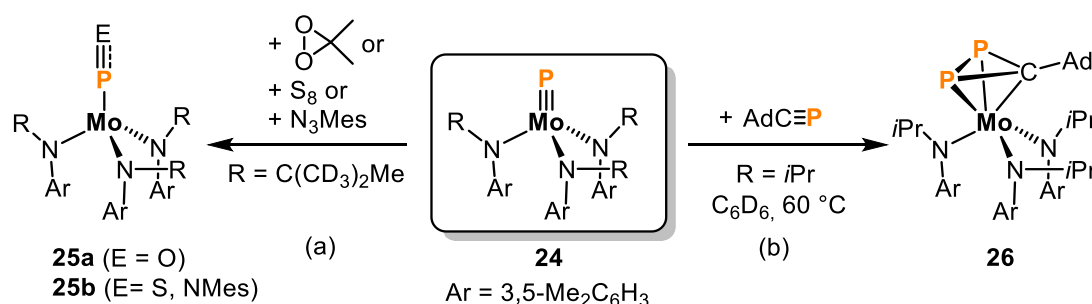
Scheme 7. P_1 functionalizations mediated by the molybdenum phosphido complex **24**.

Cummins and co-workers also subsequently demonstrated the impressive synthetic potential of the anionic niobium complex **27**, which is isoelectronic with **24** (Scheme 8). The $Nb{\equiv}P$ triple bond in **27** participates in further solvent-dependent P_4 activation. Trapping of 0.5 equivalents of P_4 in weakly coordinating solvents affords [(*cyclo*-P_3)Nb(N[Np]Ar)$_3$]$^-$ (Np = CH_2tBu, Ar = 3,5-$Me_2C_6H_3$), which is structurally related and isolobal to **26**.[25] In THF, however, addition of the entire P_4 tetrahedron occurs and concomitant migration of one amide ligand onto phosphorus gives the amino functionalized *cyclo*-P_5 anion **28** (Scheme 8a). Moreover, the anionic nature of **27** opened up avenues to salt metathesis reactions with electrophiles. Treatment of **27** with divalent group 14 element salts at low temperatures provided the dinuclear compounds **29** contai-
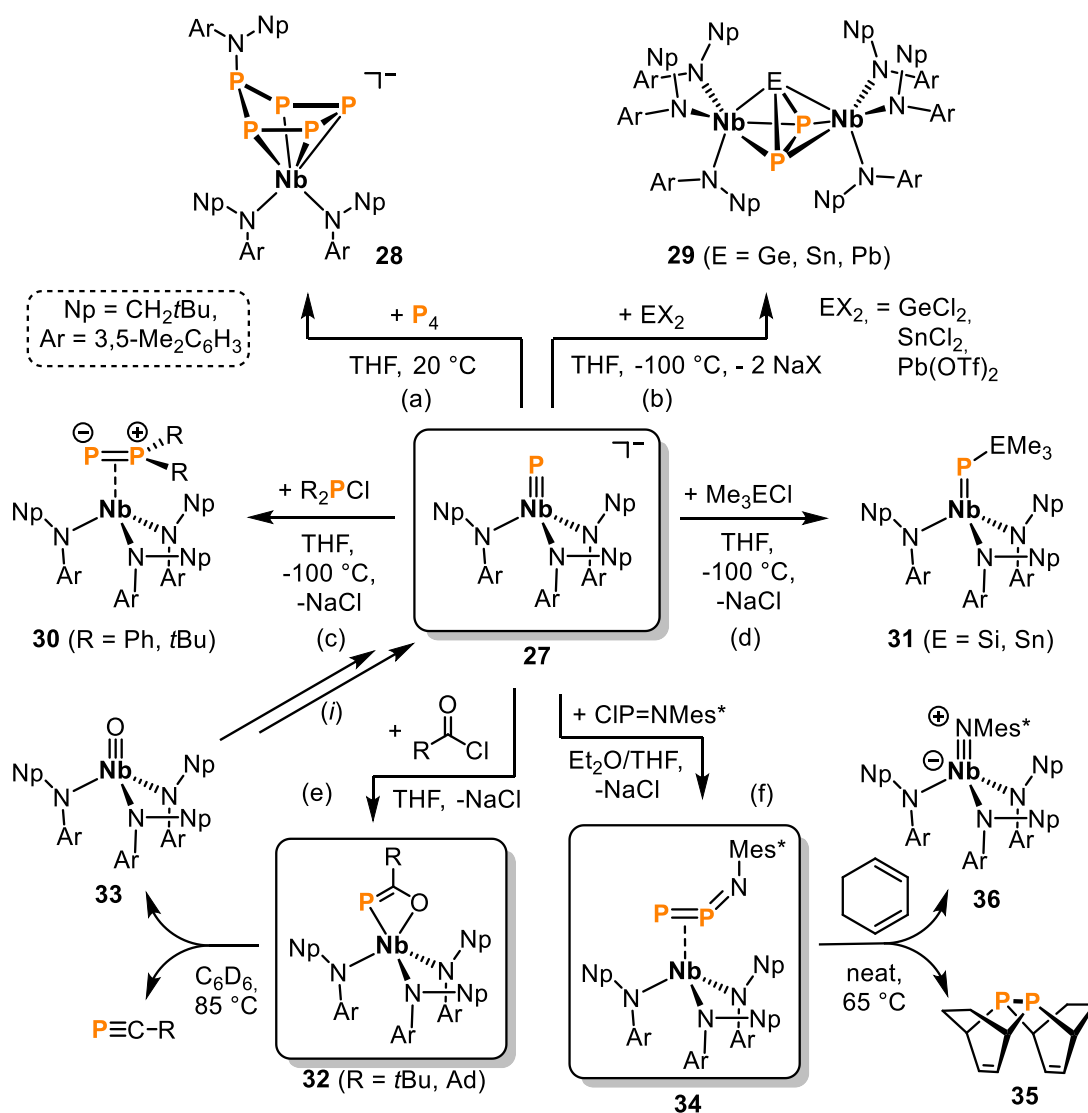
Scheme 8. Phosphorus functionalization mediated by the niobium phosphide anion **27**. (*i*) Recovery of starting material **27** from **33** proceeds by: 1. +Tf$_2$O in Et$_2$O at −35 °C; 2. +[Mg(thf)$_3$(C$_{14}$H$_{10}$)]/−Mg(OTf)$_2$, −C$_{14}$H$_{10}$ in THF at −100 °C; 3. +0.25 equiv. P$_4$ in THF at r.t.; 4. +Na-amalgam/−Hg in THF at r.t.

ning bridging μ$_2$:η^3-η^3-*cyclo*-EP$_2$ (E = Ge, Sn, Pb) triangles (Scheme 8b).[26] The η^2-phosphanyl phosphinidene complexes **30** were accessible by reacting **27** under similar conditions with chlorophosphanes (Scheme 8c).[27] Silylation and stannylation (compounds **31**) at the nucleophilic phosphorus atom were achieved by treating **27** with Me$_3$ECl (E = Si, Sn, Scheme 8d). *Cummins* and co-workers further reported that **27** enables the remarkable transformation of acyl chlorides into the corresponding phosphaalkynes (Scheme 8e).[28] In fact, the authors described a complete synthetic cycle involving an initially formed niobacyclic intermediate **32**, [2+2] fragmentation to give the phosphaalkynes P≡C−R (R = *t*Bu, Ad) and the niobium(V) oxo product **33**, and finally the recycling of **33** by step-wise deoxygenation, P$_4$ activation and reduction.[29] The reaction of **27** with the chloroiminophosphane ClP=NMes* (Mes* = 2,4,6-*t*Bu$_3$C$_6$H$_2$)

9

gives **34**, which bears the diphosphorus analogue of an organic azide ligand (P=P=N-Mes*) coordinating through the P=P unit in an η^2-fashion (Scheme 8f).[30] Remarkably, compound **34** serves as a precursor for the thermal release of formal [P≡P] units, which can be quantitatively trapped by using 1,3-cyclohexadiene to form the Diels-Alder adduct **35** via a double diene addition. The by-product of this process is the niobium imide complex [(Mes*N)Nb([Np]NAr)$_3$] (**36**).

Moreover, *Cummins* and co-workers presented additional functionalizations of the terminal PO ligand in the above-mentioned molybdenum complex **25a**, mediated by added more oxophilic metal species. The nucleophilic attack of one methyl group in [Cp$_2$ZrMe$_2$] at phosphorus gives the Mo(IV) complex **37** in up to 75% yield (Scheme 9a).[23] An uncommon phospha-Wittig reaction takes place upon treatment of **25a** with the silyl phosphinidene complex **31a** (Scheme 9b).[31] This O=P/Nb=PSi*i*Pr$_3$ metathesis generates the oxo niobium compound **33** along with the silyl substituted diphosphenido molybdenum complex **38**. In solution, **38** decomposes within days to the phosphido molybdenum complex **24** and the unstable diphosphene **39**. Elevated temperatures accelerate this decomposition reaction. The reactive intermediate **39** readily oligomerizes to a mixture of the phosphinidene trimer **40** and tetramer **41**, or can be trapped with dienes to form the [2+4] cycloaddition products **42**.
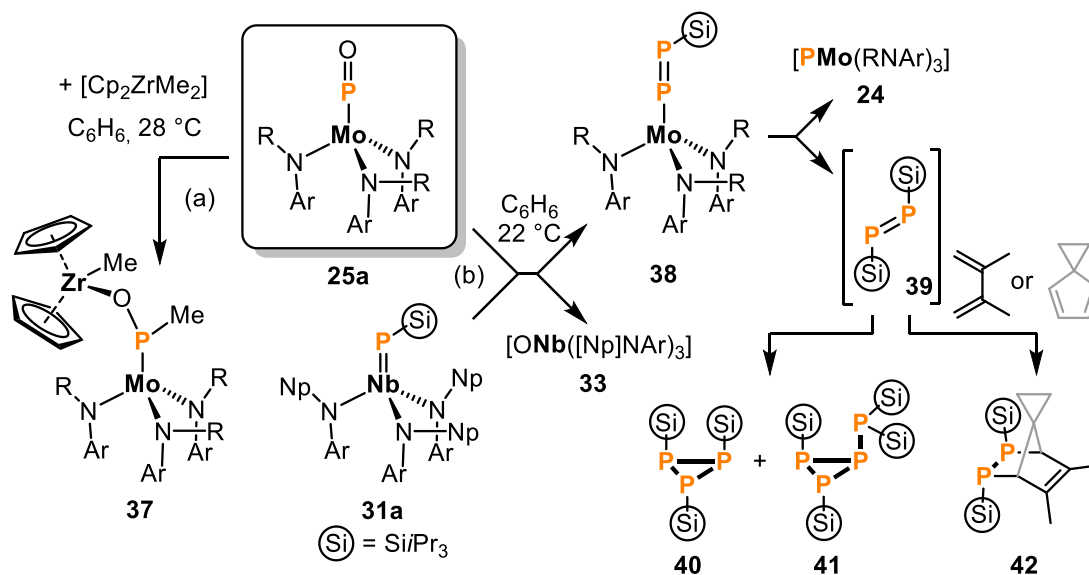
Scheme 9. Transformations of the phosphorus monoxide ligand P=O promoted by combinations of two metal complexes (Ar = 3,5-Me$_2$C$_6$H$_3$; R = C(CD$_3$)$_2$Me; Np = CH$_2$*t*Bu).

In 2000, *Scheer* and co-workers described the functionalization of the chromium complex **43** with group 15 halides (Scheme 10a).[32] While reactions with PCl$_5$ and PCl$_3$, led to the *cyclo*-P$_3$ complex **44** and the dinuclear chromium chloride **45**, respectively, the reactions

with ECl$_3$ (E = As, Sb) were very unselective. A complex mixture of products was obtained, including **44**, **45**, the *cyclo*-EP$_2$ complex **46** and various triple-decker compounds **47**. Interestingly, *Ruiz* and co-workers found that the closely related heavier group 6 complex anions **48** can readily be functionalized with electrophiles affording the methyl- or stannyldiphosphenyl bridged species **49** (Scheme 10b).[33]
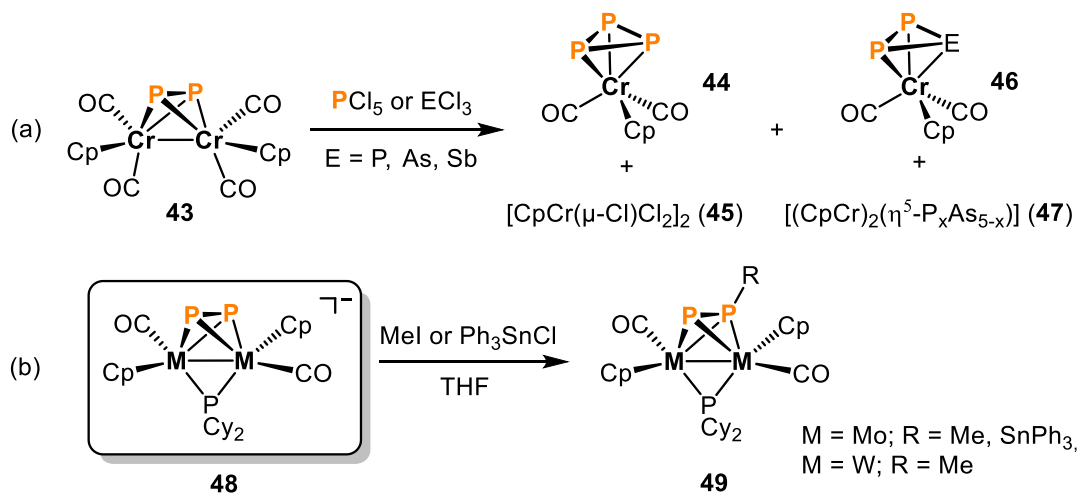
Scheme 10. Functionalization of P$_2$ units mediated by dinuclear group 6 complexes.

1.3.3   Functionalization of P$_3$ Ligands

The first functionalization of a P$_3$ ligand was reported by *Peruzzini* and *Stoppioni* in 1986. Highly electrophilic alkylating agents MeOTf and [Me$_3$O]BF$_4$ were used for the methylation of the *cyclo*-P$_3$ moiety in the group 9 triphos complexes **50** (Scheme 11a).[34] The products **51** contain methyltriphosphirene ligands coordinating in an η^3-mode. It is noteworthy that these alkylations represent the first examples of successful transition metal-mediated functionalization of any polyphosphorus ligand with carbon-based electrophiles. Under the same conditions, the protonation of **50** with HOTf gave a different outcome (Scheme 11b).[35] Spectroscopic and crystallographic investigations indicated that H$^+$ interacts weakly with the heteroatomic CoP$_3$ cluster core in **52** and is most likely located between both phosphorus and cobalt.

The reactivity of the *cyclo*-P$_3$ ligand toward main group *nucleophiles* was explored by *Scheer* and co-workers 30 years later using a related nickel complex.[36] According to variable temperature ^{31}P NMR studies, the reaction of the nickel *cyclo*-P$_3$ sandwich compound **53** with LiPPh$_2$ initially forms the intermediate triphosphirene species **54a**, which then rapidly incorporates a second equivalent of **53** and concomitantly rearranges

11

to the heptaphosphane compound **55a**. Since crystallization and purification of **55a** was unsuccessful due to its high sensitivity, protonation with HBF$_4$ was investigated to afford the more stable neutral species **56**. The two nickel centers in **56** are bridged by a remarkable bicyclic P$_6$ ligand with an exocyclic PPh$_2$ substituent. By contrast, the reaction of **53** with LiNMe$_2$ gives the η^2-triphosphirene complex **54b** as isolable main product, and **55b** was detected only in minor quantities by ^{31}P NMR spectroscopy.
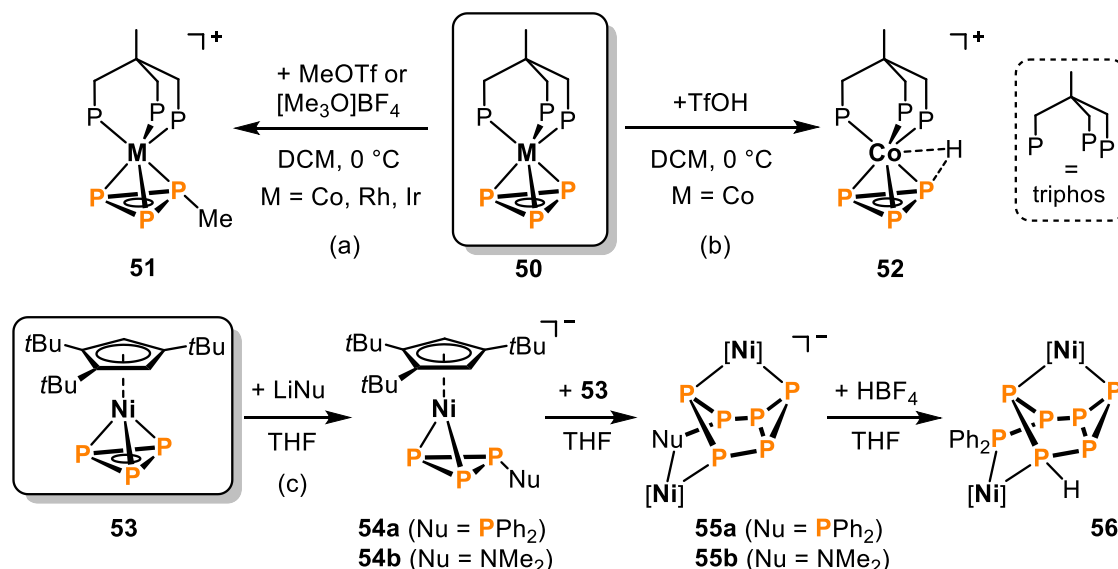
Scheme 11. Reactivity of neutral *cyclo*-P$_3$ complexes with electrophiles (top) and nucleophiles (bottom); [Ni] = [Ni(C$_6$H$_2$tBu$_3$)] (triphos = 1,1,1-tris(diphenylphosphanylmethyl)ethane).

Further η^2-triphosphirene complexes were obtained by *Piro* and *Cummins* by reacting the di- and trinuclear *cyclo*-P$_3$ complex anions **57a** and **57b**, respectively, with electrophiles (Scheme 12).[24] Treatment of the dinuclear **57a** with Ph$_3$SnCl affords the P-stannylated compound **58a**, and the reaction of trinuclear **57b** with 1-adamantylcarbonyl chloride gave the analogous, yet thermally unstable, P-acylated species **58b**. When **57b** is reacted with ClP=NMes*, one [W(CO)$_5$] fragment is lost and a shift of the second [W(CO)$_5$] moi-
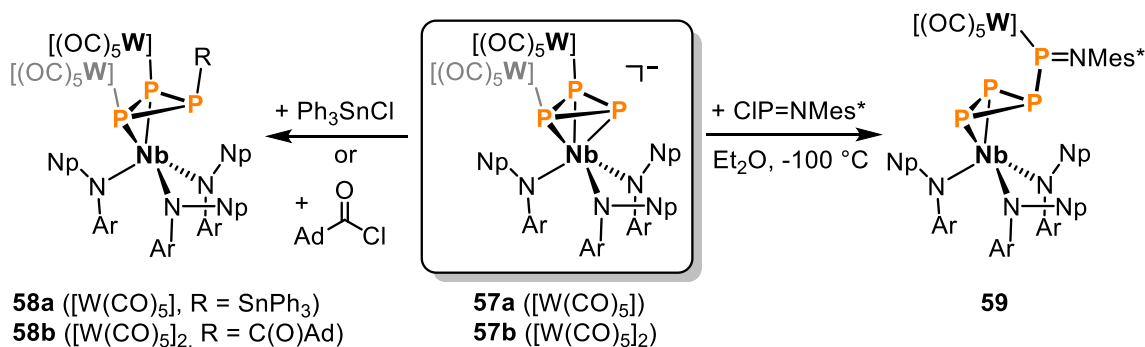
Scheme 12. Functionalization of cyclo-P$_3$ units with electrophiles mediated by oligonuclear complex anions (Ar = 3,5-Me$_2$C$_6$H$_3$; Np = CH$_2$tBu; Mes* = 2,4,6-tBu$_3$C$_6$H$_2$).

ety to the iminophosphane P is observed. The product **59** features a Mes*NP[W(CO)$_5$]$^+$ unit that circumambulates around the unsaturated triphosphorus cycle in solution at ambient temperature.

Cummins and co-workers further demonstrated the exceptional utility of anionic niobium complexes for phosphorus transfer by using the niobate **60** (Scheme 13), which bears phenolato instead of the more established anilido ligands (cf. **27**, **57**). The reaction of **60** with Ph$_3$SnCl yields the stannyldiphosphirene complex **61**, where the Ph$_3$Sn$^+$ moiety rapidly migrates around the *cyclo*-P$_3$ ring in solution even at −90 °C (Scheme 13a).[37] Subsequent liberation of the diphosphirene molecule from the metal center was achieved by converting **61** with the oxidant pyridine-*N*-oxide in the presence of the trapping agent 1,3-cyclohexadiene. This procedure gave the uncommon Diels-Alder adduct **62** along with the niobium oxo dimer [ONb(ODipp)$_3$]$_2$. Remarkably, **62** serves as a P$_3$$^{3-}$ synthon and readily transfers its *cyclo*-P$_3$ unit onto [ClRh(PPh$_3$)$_3$]. This reaction involves chloride abstraction from rhodium to eliminate Ph$_3$SnCl, and the release of 1,3-cyclohexadiene from the diphosphene by [4+2] retrocycloaddition which ultimately affords the *cyclo*-P$_3$ rhodium complex **63**.
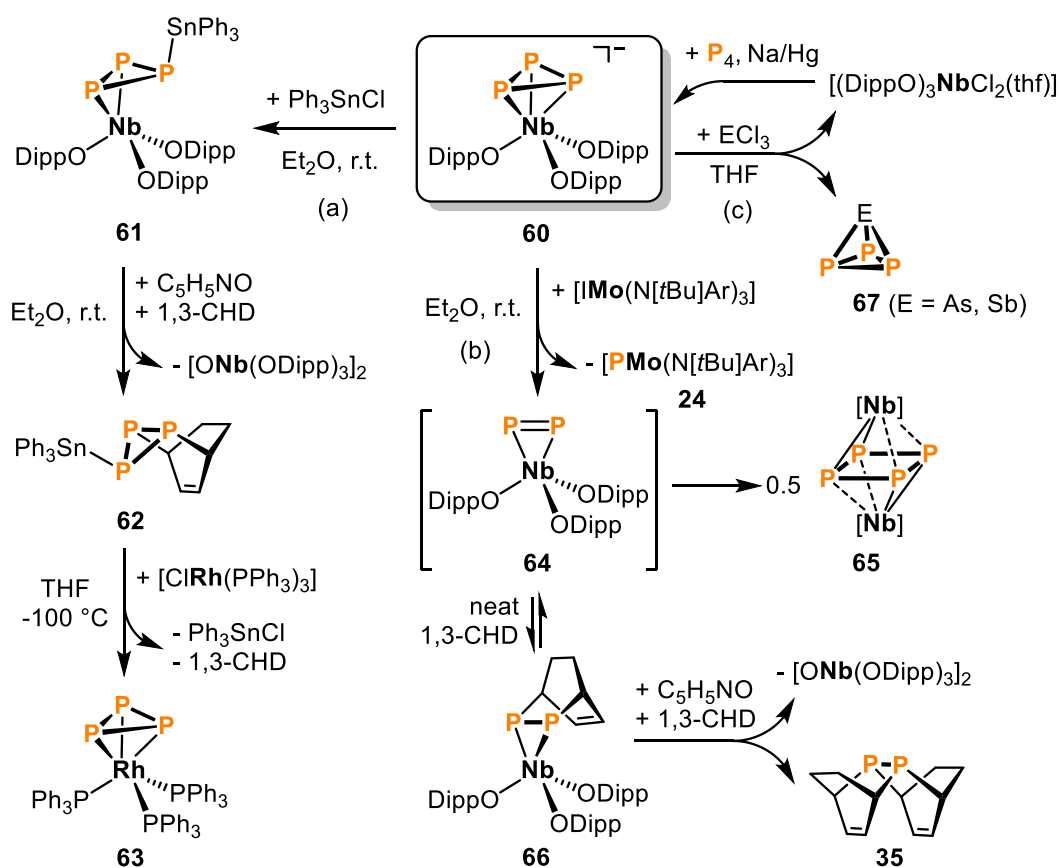
Scheme 13. Phosphorus transfer reactions promoted by the anionic niobium *cyclo*-P$_3$ complex **60**; [Nb] = [Nb(ODipp)$_3$] (1,3-CHD = 1,3-cyclohexadiene).

In a different approach, **60** was reacted with the iodo molybdenum(IV) species [IMo(N[tBu]Ar)$_3$] (Ar = 3,5-Me$_2$C$_6$H$_3$, Scheme 13b), which acts as a P$^-$ abstractor to form [PMo(N[tBu]Ar)$_3$] (c.f. **24**, Scheme 7).[38] In this manner, the dinuclear *cyclo*-P$_4$ cluster **65** was quantitatively obtained, presumably via an irreversible dimerization of an intermediate P$_2$ species **64**. In the presence of the trapping agent 1,3-cyclohexadiene, an equilibrium with the Diels-Alder product **66** was detected by ^{31}P NMR spectroscopy. Complex **66** could not be isolated as a pure compound due to this equilibrium with **64**, which irreversibly dimerizes to **65**. However, upon addition of the oxidizing agent pyridine-*N*-oxide, liberation of the diphosphene ligand occurs, affording the above-mentioned double cycloaddition product **35** (Scheme 8). *Cummins* and co-workers also reported on the facile synthesis of the fascinating binary interpnictogen molecules EP$_3$ (**67**, E = As, Sb) via salt metathesis reactions of **60** with ECl$_3$ (Scheme 13c).[39] The niobium dichloride by-product [(DippO)$_3$NbCl$_2$(thf)] can easily be recycled to the *cyclo*-P$_3$ precursor **60** by reduction in the presence of P$_4$.

1.3.4 Functionalization of P$_4$ Ligands

As the formation of P$_4$ ligands is the most common result of transition metal-mediated P$_4$ activation,[4,6] it is not surprising that phosphorus functionalization has mostly been explored for these complexes. These reactions are particularly versatile depending on the precise nature of the P$_4$ ligand. Thus, the following section is divided into four parts correlating with the successive degradation of the P$_4$ tetrahedron: tetrahedral P$_4$ ligands, [1.1.0]bicyclo-P$_4$ compounds ("butterfly-P$_4$" ligands), *cyclo*-P$_4$ units, and *catena*-P$_4$ species.

1.3.4.1 Tetrahedral P$_4$ Ligands

Stoppioni, *Peruzzini* and co-workers reported on the hydrolytic disproportionation of intact P$_4$ tetrahedra in the coordination sphere of ruthenium. Such reactivity is remarkable given that free P$_4$ is well known to be indefinitely stable in water at room temperature.[6] The authors found that [CpRu(PPh$_3$)$_2$(η^1-P$_4$)]$^+$ (**68a**) almost quantitatively forms the phosphane complex **69a** upon reaction with 100 equiv. H$_2$O (Scheme 14a).[40] By-products are oxophosphorus species such as phosphorus acid (H$_3$PO$_3$) and phosphoric acid (H$_3$PO$_4$). Substitution of the triphenyl phosphane ligands for the bidentate 1,2-(bisdiphenylphosphino)ethane (dppe), or the sodium salt of *meta*-sulfonated triphenylphosphane (TPPMS = Ph$_2$P(*m*-C$_6$H$_4$SO$_3$Na) (compounds **68b** and **68c**,

respectively), resulted in formation of minor quantities of hydroxyphosphane complexes such as **70b,c** and **71b,c** as side-products.[41] The composition of the final mixtures strongly depends on the solvent, the temperature and the excess amount of H_2O. When **71b** is dissolved in DCM, it reacts with the PF_6^- counter anion and gives the fluorodihydroxyphosphane complex $[CpRu(dppe)\{PF(OH)_2\}]PF_2O_2$ (**72**) by F/OH substitution.
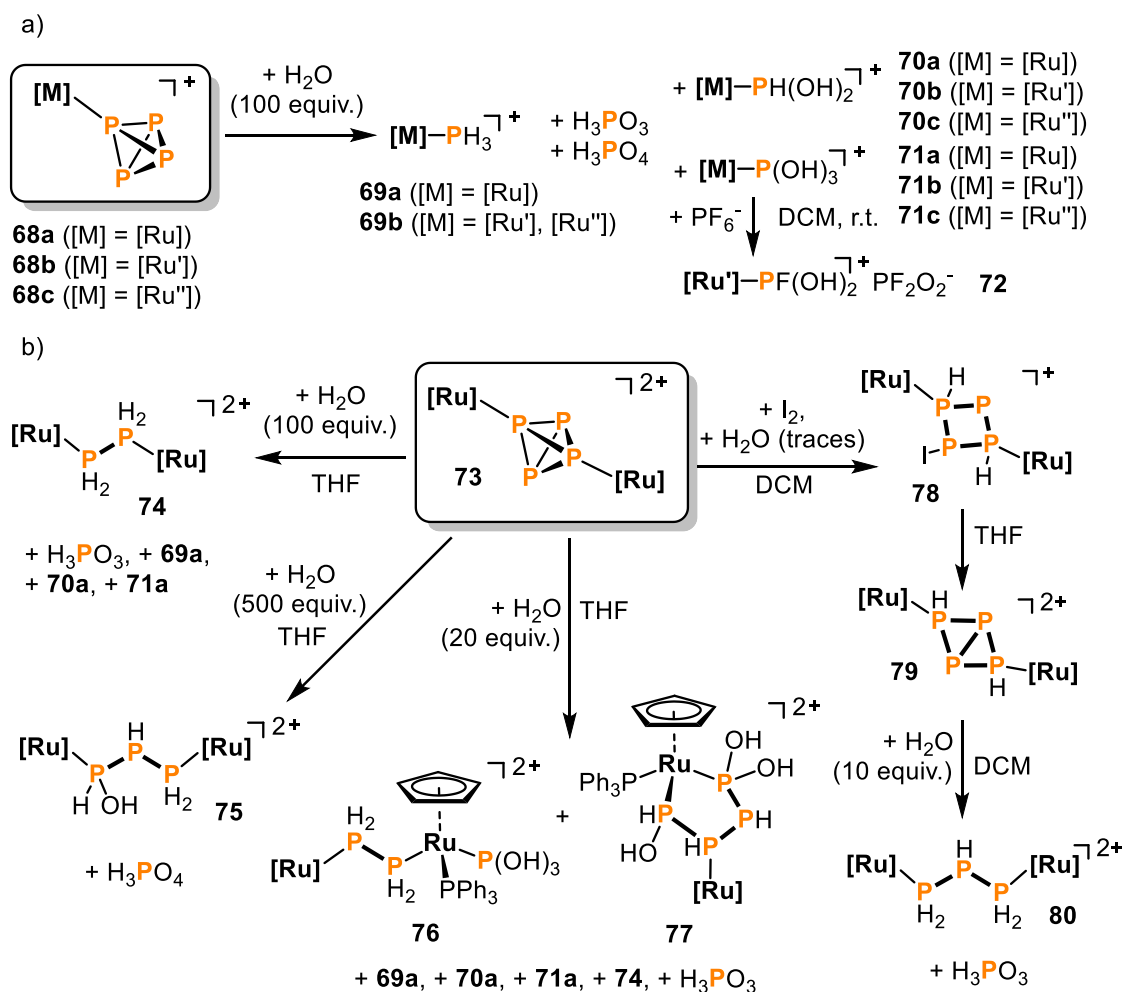
Scheme 14. Hydrolysis of P_4 in the coordination sphere of mononuclear (a) and dinuclear (b) ruthenium complexes; [Ru] = [CpRu(PPh$_3$)$_2$]; [Ru'] = [CpRu(dppe)] (dppe = 1,2-bis(diphenylphosphino)ethane); [Ru''] = [CpRu(TPPMS)$_2$] (TPPMS = Ph$_2$P(m-C$_6$H$_4$SO$_3$Na)).

The dicationic diruthenium complex **73** displays a very complex hydrolysis behavior. When treated with 100 equiv. H_2O, in a similar manner to **68a**, a diphosphane complex **74** is obtained along with **69a**, **70a**, **71a** and H_3PO_3 as by-products (Scheme 14b).[42] With a much higher excess of water (500 equiv.), the reaction becomes selective and gives rise to H_3PO_3 and the remarkable 1-hydroxytriphosphane complex **75** in 93% isolated yield.[43] Reducing the amount of water to only 20 equiv. slows down the reaction rate significantly and affords two different compounds as major products:[44] the 1,1,4-

tris(hydroxy)tetraphosphane complex **77** and a dinuclear species **76**, which comprises a bridging diphosphane and a $P(OH)_3$ ligand. The reaction mixture further contains small amounts of several other species, namely **69a**, **70a**, **71a**, **74** and H_3PO_3. A different reactivity is observed when **73** is first oxidized with iodine in the presence of traces of water.[45] The initial product is the monocationic diruthenium complex **78**, stabilizing the cyclic $(P_4H_2I)^-$ anion. In THF, the iodide anion dissociates from the tetraphosphorus ligand, resulting in the [1.1.0]bicyclotetraphosphane complex **79** that further hydrolyzes to the triphosphane complex **80** and phosphorous acid.

In a different approach recently reported by *Lammertsma* and co-workers, the *N*-heterocyclic carbene (NHC) gold complex **81**, which binds an intact P_4 tetrahedron in an η^2-fashion, readily reacts with aryl lithium compounds at low temperatures (Scheme 15).[46] The controlled P−C bond formation and concomitant cleavage of one P−P bond gives rise to the proposed intermediate butterfly species **82**. Immediate addition of a second [(NHC)Au] fragment, derived through formal loss of P_4 from a second equivalent of **81**, affords the cationic complex **83** in high yield.
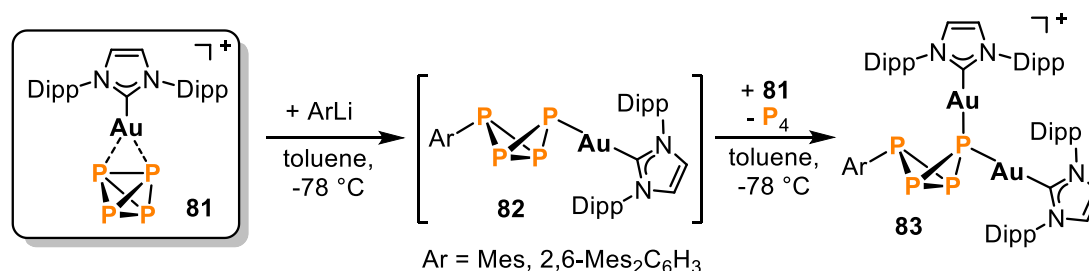
Scheme 15. Functionalization of P_4 with organolithium compounds in the coordination sphere of *N*-heterocyclic carbene (NHC) gold cations.

1.3.4.2 [1.1.0]bicyclo-P₄ Ligands

The first functionalizations of [1.1.0]bicyclo-P_4 ("butterfly-P_4") ligands were reported by *Scherer* et al. Thermolysis of the diiron complexes **84** in the presence of diphenylacetylene affords the triphospholyl species **85a** in moderate yields (Scheme 16a).[47] In the case of the related compound containing a sterically more demanding pentaisopropylcyclopentadienyl ligand (**84b**), the remarkable P_{11} cage compound **86** is also formed in low quantities. *Scheer* and co-workers later extended this concept to other alkynes. Phenylacetylene gives a mixture of the monophospholyl (**87**) and 1,2,3-triphospholyl species (**85b**).[48] The reaction of **84a** with the phosphaalkyne *t*BuC≡P produces several compounds (Scheme 16b).[49] While the tetraphospholyl (**88**)

and the 1,2,4-triphospholyl (**89**) complexes are the main products, minor amounts of pentaphosphaferrocene **90** and the dinuclear triphosphaallyl complex **91** can also be isolated. It is proposed that key steps in these reactions are the [3+1] fragmentation of the butterfly framework and the subsequent addition of one or two equivalents of alkyne.
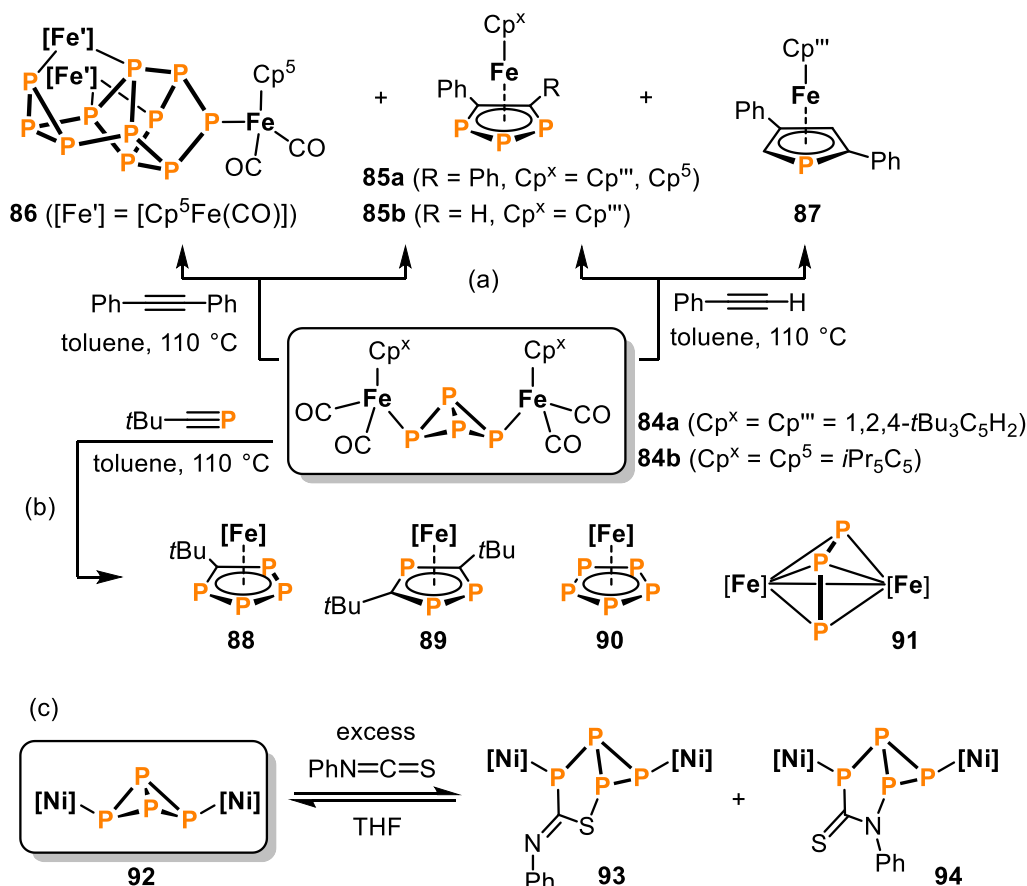
Scheme 16. Addition reactions of unsaturated organic molecules to P_4 butterfly complexes; [Ni] = [CpNi(IMes)] (IMes = 1,3-bis(2,4,6-trimethylphenyl)imidazolin-2-ylidene); [Fe] = [Cp'''Fe].

Wolf and co-workers found that the N=C and C=S bonds of the heterocumulene phenyl isothiocyanate (PhNCS) reversibly insert into a P−P bond of the P_4 butterfly scaffold of the dinuclear nickel complex **92** (Scheme 16c).[50] The products are the two isomeric bicyclo[3.1.0]heterohexane species **93** and **94**, which can be isolated as pure compounds, although they slowly equilibriate with the starting materials **92** and PhNCS in solution.

Protonation of the iron butterfly compound **84a** was also investigated by *Scheer* and co-workers. According to ^{31}P NMR and computational studies, the acidic proton selectively attacks the more nucleophilic, metal-bound ("wing tip") P atom to give the cation **95** (Scheme 17a).[51] A similar observation was made by *Lammertsma* and co-workers.[52] The reaction of the anionic Lewis acid stabilized P_4-butterfly compound **96** with [Me$_3$NH][BPh$_4$] initially forms the intermediate "wing tip" protonated species **97**

17

(Scheme 17b). Immediate loss of the amine-borane adduct Me$_3$N·BAr$_3$ (Ar = Ph, C$_6$F$_5$) leads to the formation of the neutral bicyclo[1.1.0]tetraphosphabutane isomers *exo,endo*-**98** and *exo,exo*-**98**. The two isomers were calculated to lie close in energy and readily undergo Lewis acid-catalyzed isomerization. Moreover, they decompose within one day due to a lack of kinetic stabilization.
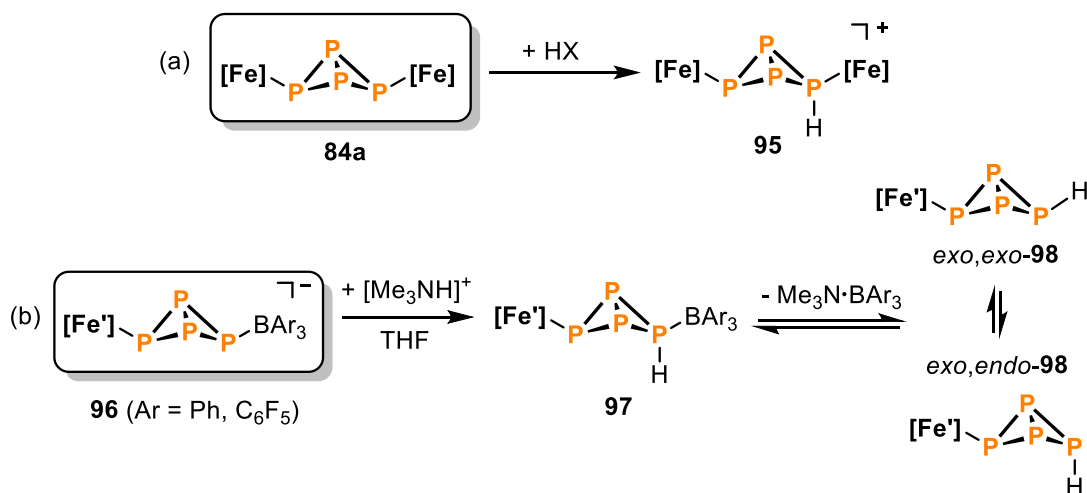
Scheme 17. Iron-mediated protonation of P$_4$-butterfly ligands; HX = [(Et$_2$O)H][BF$_4$], [(Et$_2$O)$_2$H][Al(OC(CF$_3$)$_3$)]; [Fe] = [Cp'''Fe(CO)$_2$]; [Fe'] = [Cp*Fe(CO)$_2$].

As also reported by *Scheer* and co-workers, the reaction of [Cp''$_2$Zr(η^1:η^1-P$_4$)] (**99**, Cp'' = 1,3-*t*Bu$_2$C$_5$H$_3$) with the monochlorosilylene **100** in toluene at room temperature gives compounds **101** and **102**, which are remarkable phosphorus/silicon analogues of benzene and cyclobutadiene, respectively (Scheme 18).[53] Computational studies indicated that **101** possesses considerable aromatic character, whereas **102** is weakly antiaromatic. The aromaticity in both compounds is substantially influenced by the additional donating nitrogen lone pairs of the bidentate PhC(N*t*Bu)$_2$ substituents.
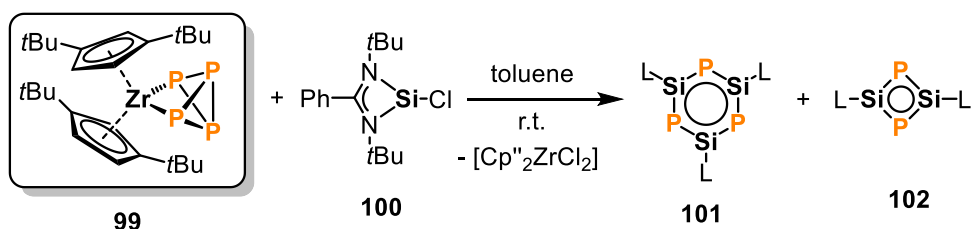
Scheme 18. Synthesis of phosphorus/silicon analogues of benzene by P$_4$ functionalization (L = [PhC(N*t*Bu)$_2$]).

1.3.4.3 *cyclo*-P$_4$ ligands

Functionalization at *cyclo*-P$_4$ ligands is far less common than at tetrahedral and butterfly-P$_4$ ligands, and was first demonstrated by *Scheer* and co-workers (Scheme 19).[54] When a tenfold excess of PCl$_5$ is reacted with the pentanuclear *cyclo*-P$_4$ complex **103**, the main products in the reaction mixture are [WCl$_4$(MeCN)$_2$], PCl$_3$, [W(CO)$_5$(PCl$_3$)], and the dinuclear tetrachlorodiphosphane complex **104**. However, these species are only found in minor quantities when the reaction is performed with a smaller amount of PCl$_5$ (4 equiv.). The main product in this case is **105**, in which a [WCl(CO)$_2$(MeCN)$_2$] fragment is coordinated by a chlorinated *cyclo*-P$_4$ ligand through its triphosphaallyl subunit. The isolation of **105** as a pure compound was not successful, because it readily reacts with traces of moisture to give the corresponding hydrolysis product **106**.
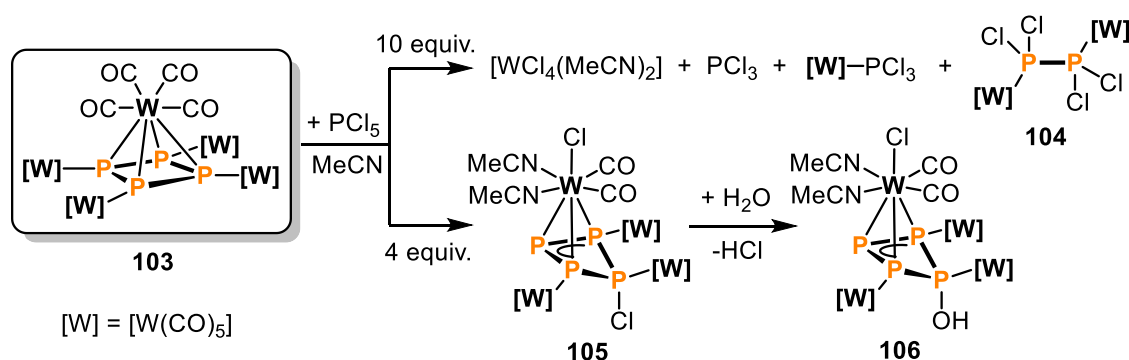
Scheme 19. Chlorination of a *cyclo*-P$_4$ ligand in the pentanuclear tungsten complex **103**; [W] = [W(CO)$_5$].

Recently, *Mézailles* and co-workers investigated the reactivity of the end-deck *cyclo*-P$_4$ iron complex **107** toward electrophiles (Scheme 20a).[55] The P-borylated Lewis adduct **108** is formed in an equilibrium reaction upon treatment of **107** with B(C$_6$F$_5$)$_3$ in DCM. *Scheer* and co-workers reported on ring expansions of the related end-deck *cyclo*-P$_4$ cobalt sandwich complex **109** upon reaction with the pnictinidene complexes [Cp*E{W(CO)$_5$}$_2$] (E = P, As, Scheme 20b).[56] The insertion of the phosphinidene into the P$_4$ ring is followed by a shift of one [W(CO)$_5$] unit and affords the two isomeric η^4-*cyclo*-P$_5$ species **110a** and **110b**, which differ only in the orientation of the tungsten pentacarbonyl and the Cp* substituents. Interestingly, when **109** is reacted with the arsinidene, all substituents previously bound to arsenic migrate to phosphorus resulting in numerous η^4-*cyclo*-P$_4$As isomers (**111a-c**), which differ by the location of the arsenic atom within the five-membered ring.

19
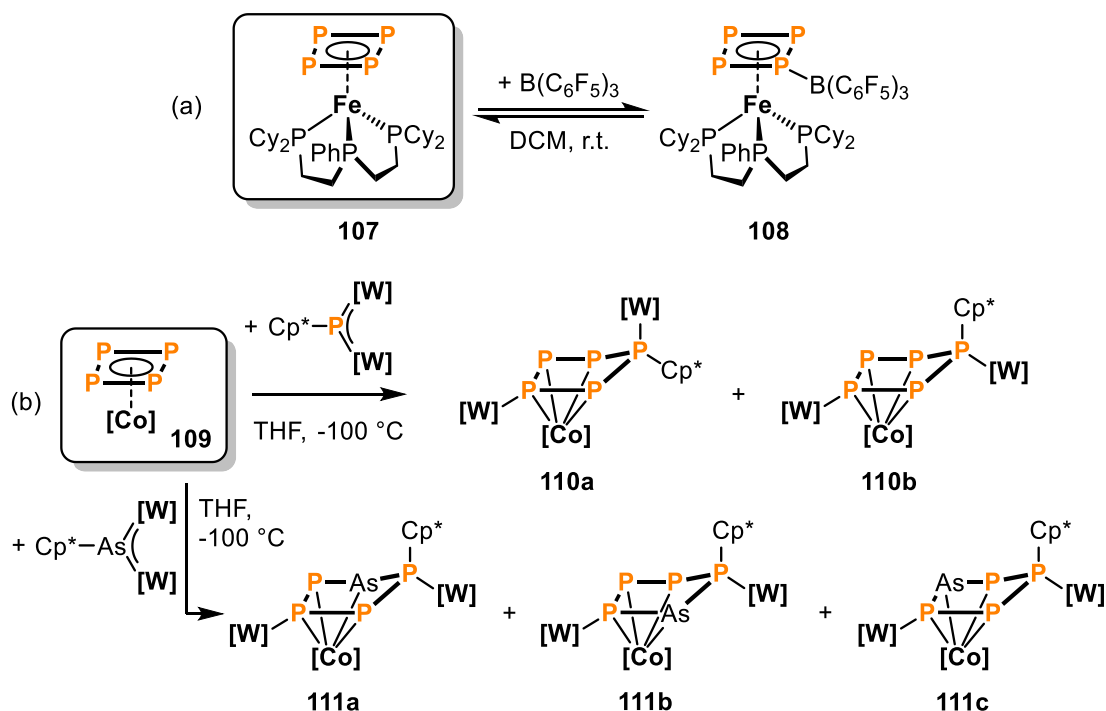
Scheme 20. Late transition metal complex-promoted functionalization of *cyclo*-P$_4$ ligands; [Co] = [(1,2,4-*t*Bu$_3$C$_5$H$_2$)Co].

1.3.4.4 P$_4$ Chains

Wolf and co-workers first demonstrated the functionalization of P$_4$ chains in the coordination sphere of 3d metalate anions. Reaction of the diiron compound **112** with one equivalent of Et$_3$N·HCl or [H(Et$_2$O)$_2$][BAr$^F_4$] (Ar^F = 3,5-(CF$_3$)$_2$C$_6$H$_3$) affords the protonated ferrate **113** in moderate yields (Scheme 21).[57] Crystallographic, spectroscopic and computational investigations indicate that the proton is highly mobile, and simultaneously bound to both iron and phosphorus. Treatment of **112** with an excess of Me$_3$SiCl results in liberation of the phosphorus scaffold from the iron center to give a
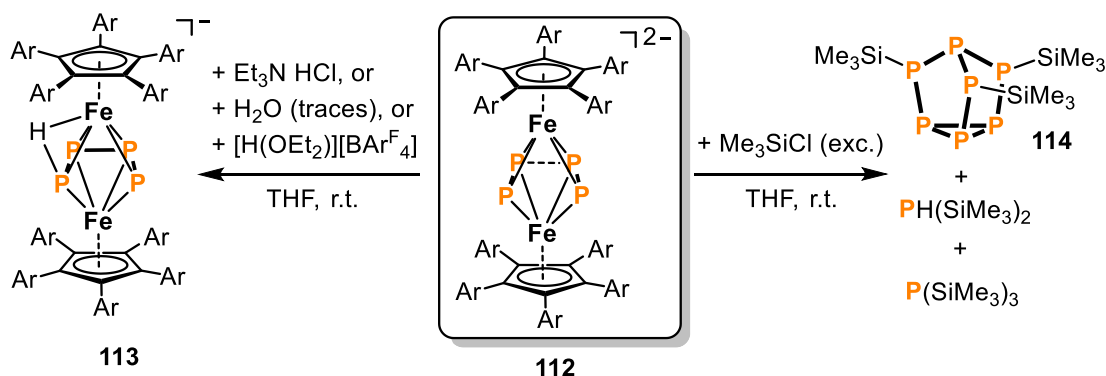
Scheme 21. Functionalization of the bridging P$_4$ chain in the ferrate **112** with electrophiles (Ar = 4-ethylphenyl; Ar^F = 3,5-(CF$_3$)$_2$C$_6$H$_3$).

mixture of $PH(SiMe_3)_2$, $P(SiMe_3)_3$ and the nortricyclane compound $P_7(SiMe_3)_3$ (**114**) in a ratio of 1:1:10.

The heterodinuclear complex **115**, which features a *catena*-P_4 unit, readily undergoes P−P condensation reactions with chlorophosphanes (Scheme 22).[58] The reaction with *t*BuPCl$_2$ affords a *cyclo*-P_5 cobalt complex **116** with a concomitant chloride shift from P to Ga. By contrast, a different outcome is observed upon reaction of **115** with the dialkylmonochlorophosphanes R_2PCl (R = *i*Pr, Cy, *t*Bu). In this case, the *N*-heterocyclic gallylene [Ga(nacnac)] (nacnac = CH[CMeN(2,6-*i*Pr$_2$C$_6$H$_3$)]$_2$) is released, affording the mononuclear *cyclo*-P_5R_2 cobalt complexes **117**. Variable temperature NMR studies on the reaction with *i*Pr$_2$PCl revealed the formation of two intermediate species, likely being constitutional isomers, of which the more abundant one could be crystallographically identified as the neutral *catena*-P_5iPr$_2$ complex **118**.
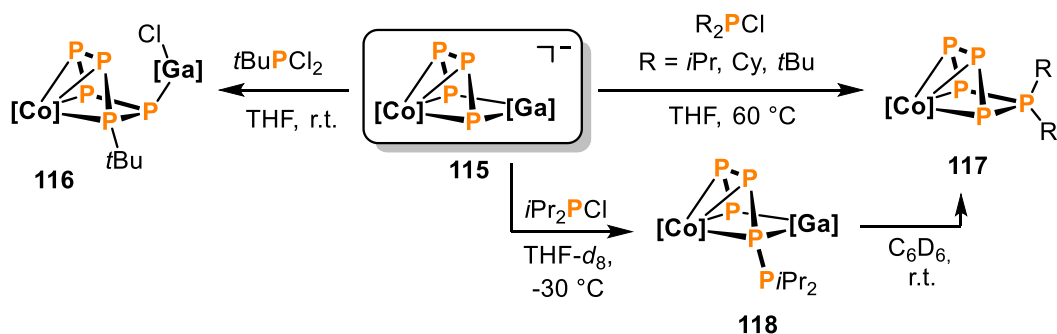
Scheme 22. Functionalization of the *catena*-P_4 unit in the cobaltate complex **115** with chlorophosphanes; [Co] = [CoBIAN] (BIAN = bis(mesityl)iminoacenaphthene); [Ga] = [Ga(nacnac)] (nacnac = CH[CMeN(2,6-*i*Pr$_2$C$_6$H$_3$)]$_2$).

1.3.5   Functionalization of P$_n$ Ligands (n ≥ 5)

The functionalization of white phosphorus-derived P$_n$ ligands with n ≥ 5 has hitherto been only scarcely explored. *Scheer* and co-workers treated the pentaphosphaferrocene [Cp*Fe(η^5-P$_5$)] (**119**) with a set of main group nucleophiles and thus obtained P-functionalized η^4-P$_5$ ferrate complexes (Scheme 23a).[59] Distinct reactivity was observed depending on the nucleophile. While LiCH$_2$SiMe$_3$, LiNMe$_2$, and LiPH$_2$, give rise to mononuclear complexes of the type of **120** (minor product for LiPH$_2$), the formation of dinuclear complexes of the type of **121** occurs upon reaction with NaNH$_2$ and LiPH$_2$ (major product), respectively.
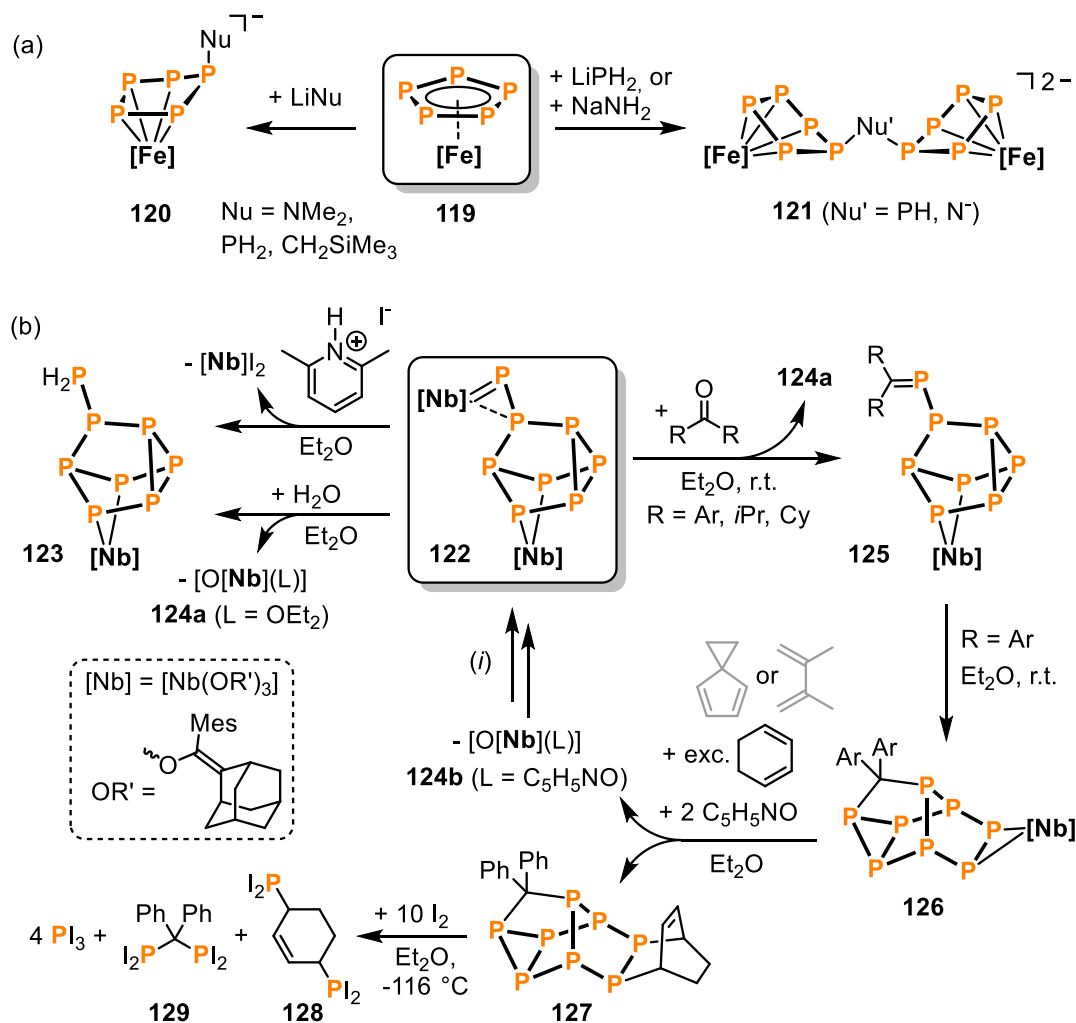
Scheme 23. Transition metal-mediated functionalization of a *cyclo*-P_5 ligand (a) and a P_8 framework (b); [Fe] = [Cp*Fe]; [Nb] = [Nb(OR')$_3$] (OR' = (adamantane-2-ylidene)(mesityl)methanolate); Ar = Ph, 4-Cl-C$_6$H$_4$, 4-Me-C$_6$H$_4$, 4-OMe-C$_6$H$_4$, 4-NMe$_2$-C$_6$H$_4$, 4-CF$_3$-C$_6$H$_4$). (*i*) Recovery of starting material **122** (0.5 equiv.) proceeds by: 1. + O(OCCF$_3$)$_2$, +2 equiv. Me$_3$SiI/−Me$_3$SiO(OCCF$_3$) in Et$_2$O; 2. + SmI$_2$/−SmI$_3$ in THF; 3. +P$_4$ in toluene.

Cummins and co-workers found that the diniobium octaphosphide complex **122** possesses a reactive phosphinidene moiety, which readily hydrolyzes to give the oxo niobium species **124a** and the mononuclear phosphanyl-substituted heptaphosphide complex **123** (Scheme 23b).[60] The latter compound could also be synthesized in a more selective manner by protonation of **122** with two equivalents of 2,6-dimethylpyridinium iodide. The corresponding niobium diiodide complex is the stoichiometric by-product. Remarkably, **122** also undergoes Nb=P/O=C metathesis with ketones.[61] While the resulting alkyl substituted phosphaalkene complexes **125** are stable for up to several days at ambient temperature, the corresponding aryl derivatives immediately undergo an electrocyclic rearrangement ultimately affording the saturated organophosphorus cluster compounds **126**. The carbophosphorus cluster can be liberated from niobium by treatment

with two equivalents of pyridine-*N*-oxide in the presence of an excess of 1,3-cyclohexadiene, leading to the Diels-Alder product **127**.[62] Moreover, [4+2] cycloaddition with the niobium bound diphosphene moiety in **126** also takes place when 2,3-dimethylbutadiene or spiro[2.4]hepta-1,6-diene are used as dienes, and the niobium oxo compounds **124a** and **124b** can be recycled by step-wise deoxygenation, reduction and P$_4$ activation. Furthermore, *Cummins* and co-workers described the remarkable reactivity of **127** towards ten equivalents of iodine, which cleanly affords four molecules of PI$_3$ along with the bis(diiodophosphanyl)-substituted hydrocarbons **128** and **129**.

1.3.6 Radical Functionalization

A further approach to P$_4$ functionalization not necessarily involving the formation of intermediate phosphido complexes is the functionalization of P$_4$ with main group radicals mediated by transition metal complexes. The key step is the controlled generation of carbon (or other main group element) centered radicals, which induce successive, homolytic P−P bond cleavage reactions, resulting in stepwise degradation of the P$_4$ molecule. This concept was originally demonstrated by *Barton* and co-workers in a metal free system using alkyl radicals generated by the decomposition of pyridine thione oxycarbonyl esters (Barton's PTOC esters).[63] *Cummins* and co-workers used the three-coordinate Ti(III) complex [Ti(N[tBu]Ar)$_3$] (**130**, Ar = 3,5-C$_6$H$_3$Me$_2$) for the stoichiometric halogen radical abstraction from main group element halides RX (RX = PhBr, CyBr, Me$_3$SiI, Ph$_3$SnCl) to give the Ti(IV) species **131** (Scheme 24a).[64] The concomitantly formed R$^•$ radicals successively break down the P$_4$ tetrahedron, ultimately affording the respective phosphane species PR$_3$ in certain cases. While a similar, quantitative conversion is also observed for the heavier group 14 element halides Me$_3$SiI and Ph$_3$SnCl, considerable amounts of the diphosphane species P$_2$R$_4$ are found as by-products in the analogous reactions with CyBr and PhBr. However, with an excess (5 equiv.) of **130** and RX, these reactions also become quantitative. When sterically more demanding aryl groups such as Mes and Ar* (= 2,6-Mes$_2$C$_6$H$_3$) are used, the stepwise P$_4$ degradation does not proceed to completion, but results in the triphosphirane P$_3$Mes$_3$ and the bicyclo[1.1.0]tetraphosphabutane ("butterfly") species *exo,endo*-Ar*$_2$P$_4$, respectively.
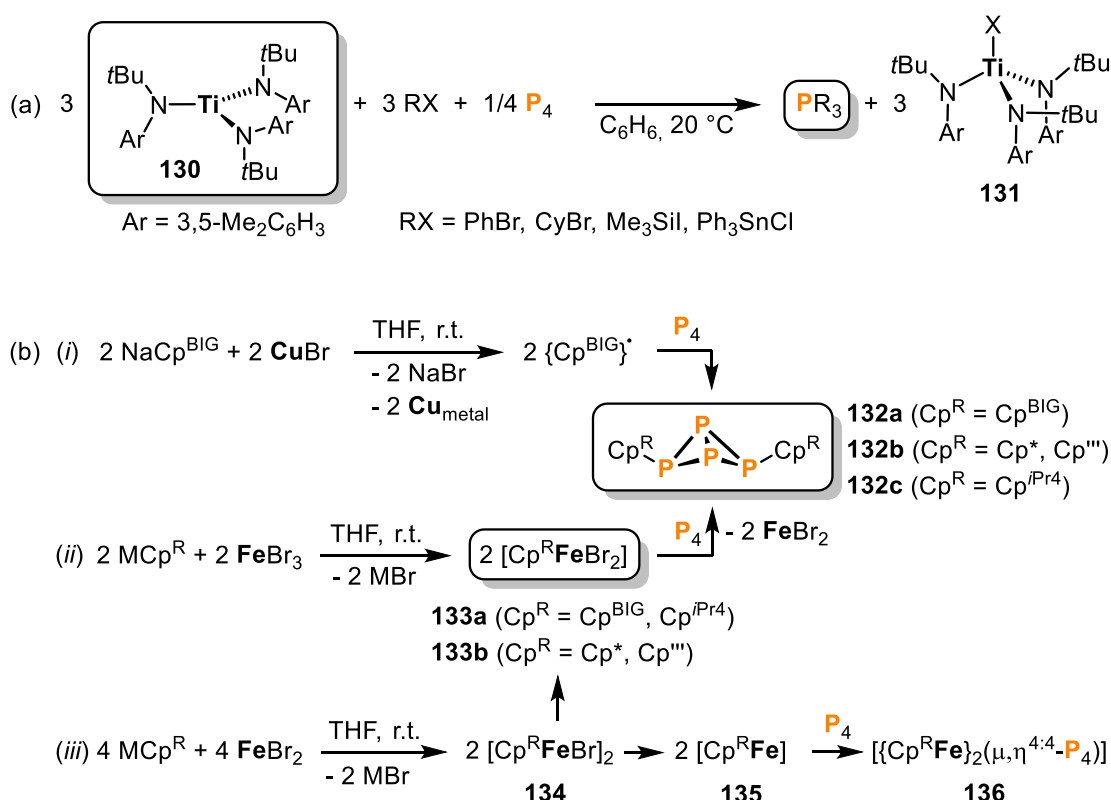
Scheme 24. Radical functionalization of P_4 mediated by early (a) and late (b) transition metals. (*i*) only for Cp^{BIG}; (*ii*) MCp^R = $NaCp^{BIG}$, $NaCp'''$, $LiCp^*$, $NaCp^{iPr4}$; (*iii*) only for MCp^R = $NaCp'''$, $LiCp^*$ (Cp^{BIG} = $C_5(4\text{-}n\text{Bu-}C_6H_4)_5$; Cp''' = $C_5H_2tBu_3$; Cp^* = C_5Me_5; Cp^{iPr4} = C_5HiPr_4).

Scheer reported on the synthesis of the organic *exo,exo*-substituted P_4 butterfly compounds **132** by the one-pot reactions of P_4 with metal-generated cyclopentadienyl radicals (Scheme 24b).[65] The required radicals were formed via three different pathways: (*i*) The treatment of $NaCp^{BIG}$ (Cp^{BIG} = $C_5(4\text{-}n\text{Bu-}C_6H_4)_5$) with CuBr led to precipitation of metallic copper along with dark blue $\{Cp^{BIG}\}^•$ radicals, which were detected by EPR spectroscopy and selectively gave **132a** upon addition of P_4. (*ii*) The reaction of the alkali cyclopentadienide salts MCp^R (= $NaCp^{BIG}$, $NaCp'''$, $LiCp^*$, $NaCp^{iPr4}$) with $FeBr_3$ afforded the intermediate Fe^{III} complexes **133**, which readily transfer $Cp^{R•}$ radicals onto the P_4 tetrahedron, giving **132** upon loss of $FeBr_2$. (*iii*) The corresponding Fe^{II} complexes **134** synthesized from MCp^R (= $NaCp'''$, $LiCp^*$) and $FeBr_2$ resulted in the P_4 butterfly species **132b** when reacted with P_4. The reaction mechanism in this case is suggested to involve disproportionation of **134** into the Fe^{III} complexes **133b**, which undergo the abovementioned reaction with P_4, and Fe^I intermediates **135** that form the dinuclear species **136** bearing a bridging *catena*-P_4 ligand.

Furthermore, *Yakhvarov* and *Budnikova* have reported on electrochemical methods for radical functionalization of P_4.[66,67] Their work has recently been reviewed in detail.[68,69]

The reaction principle is based on the electrocatalytic C−P bond formation mediated by bipyridine (bpy) nickel complexes. Figure 3 exemplifies a suggested schematic catalytic cycle for the nickel-promoted transformation of P_4 into organophosphorus compounds. The proposed mechanism involves the cathodic electrogeneration of active Ni^0 complexes from the corresponding Ni^{II} species, followed by the oxidative addition of aryl halides ArX.[67] The resulting organonickel aryl complex [NiX(Ar)(bpy)] is inert towards P_4. However, after electrochemical one-electron reduction, the radical species [Ni(Ar)(bpy)]$^{-}$ immediately incorporates the P_4 molecule.[69] Subsequent aqueous work-up ultimately affords tertiary phosphanes and phosphane oxides. Note that the metal ions generated from the electrochemically soluble (sacrificial) anode are required to stabilize anionic phosphido intermediates and thus prevent undesired phosphorus polymerization processes. Depending on the anode material, different organophosphorus products are formed.[70] While a zinc anode mainly leads to the formation of tertiary phosphanes, an aluminium anode rather results in phosphane oxide formation. By contrast, use of a magnesium anode gives cyclic polyphosphorus compounds, such as $(PhP)_5$.
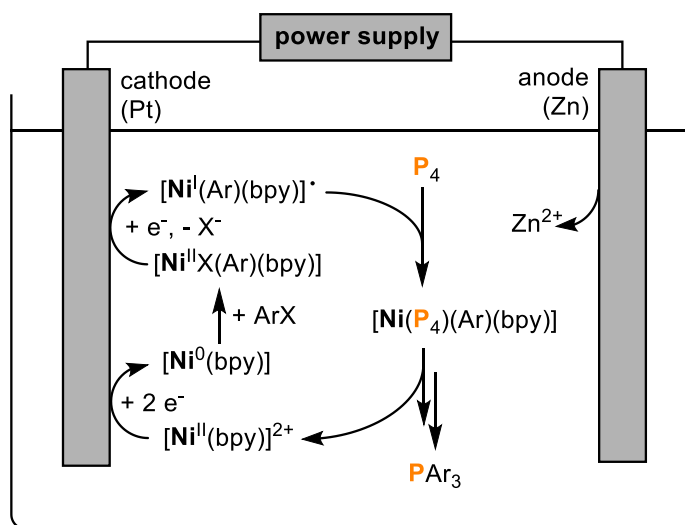
Figure 3. Proposed mechanism for nickel-electrocatalyzed arylation of white phosphorus in DMF or MeCN carried out in an undivided cell (bpy = 2,2′-bipyridine).

1.4   Conclusion

Starting with the pioneering work of *Green*, *Stoppioni* and *Peruzzini* in the 1970s and 1980s, the transition metal-mediated functionalization of white phosphorus has developed greatly over the last two decades. Scientists around the globe have contributed to this part of phosphorus chemistry and demonstrated the synthetic potential of P_4 functionalization in the formation of versatile and unprecedented phosphorus compounds. A considerable number of transition metal complexes bearing P_n ligands derived from P_4 activation have been used for subsequent P_4 functionalization (sections 1.3.2-1.3.5). By contrast, only a few hydrido or alkyl complexes have shown the potential to activate and functionalize P_4 in a single step (section 1.3.1), and even fewer complexes have been capable of promoting radical functionalization (section 1.3.6). Generally, neutral complexes have been employed more often for P_4 functionalization than ionic ones. Yet, anionic complexes have generally proven to serve as better platforms than cations. This may be attributed to the fact that by far the most common reactants for P_4 functionalizations are electrophiles. The attack at the nucleophilic phosphorus sites is often accompanied with metathetical halide abstraction, which provides the driving force for the reaction. Hydrolyses, oxidations, cycloadditions, and reactions with nucleophiles have been reported much less frequently. Most of these functionalizations have given rise to remarkable new mono- or oligophosphorus complexes. However, the liberation of these P-rich species from the complexing metal centers is challenging and has thus far seldom been achieved. Nevertheless, some fascinating compounds, such as EP_3 (E = As, Sb) prepared by *Cummins* and the P-Si analogue of benzene reported by *Scheer* have been synthesized via this approach. It is noteworthy that, while P_4 functionalization at both early and late transition metals has been established to similar extents, release from the metal has mostly been observed at early transition metal systems. This is probably due to the higher oxophilicity of these metals, which can be exploited in ligand liberation reactions with oxidizing agents (e.g. pyridine-*N*-oxide).

In summary, despite the growing number of successful phosphorus functionalization reactions, the ultimate goal, namely the circumvention of chlorine gas and PCl_3 in the industrial formation of useful organophosphorus species, is still far from being reached. However, careful evaluation of the above-mentioned literature may begin to allow chemists to predict the outcome of their prospective functionalization reactions, and hence accelerate the progress in this fundamental area of modern phosphorus chemistry.

1.5 References

[1] A. F. Holleman, E. Wiberg, N. Wiberg, *Anorganische Chemie*, *Band 1 Grundlagen und Hauptgruppenelemente*, de Gruyter, Berlin, **2017**, pp. 846.

[2] LAGA - Bund/Länder-Arbeitsgemeinschaft Abfall, **2012**, *Evaluation of Options for the Sustainable Use of Secondary Phosphorus Reserves*. [online] 30.01.2012. [cited: 17.06.2019]. URL: https://www.laga-online.de/Publikationen-50-Informationen.html?command=downloadConte.

[3] M. Peruzzini, L. Gonsalvi, A. Romerosa, *Chem. Soc. Rev.* **2005**, *34*, 1038–1047.

[4] B. M. Cossairt, N. A. Piro, C. C. Cummins, *Chem. Rev.* **2010**, *110*, 4164–4177.

[5] D. Corbridge, *Phosphorus: An Outline of its Chemistry, Biochemistry, and Technology*, Elsevier, New York, **1994**.

[6] M. Caporali, L. Gonsalvi, A. Rossin, M. Peruzzini, *Chem. Rev.* **2010**, *110*, 4178–4235.

[7] M. Scheer, G. Balázs, A. Seitz, *Chem. Rev.* **2010**, *110*, 4236–4256.

[8] J. C. Green, M. L. H. Green, G. E. Morris, *J. Chem. Soc., Chem. Commun.* **1974**, 212–213.

[9] E. Cannillo, A. Coda, K. Prout, J.-C. Daran, *Acta Cryst. B* **1977**, *33*, 2608–2611.

[10] N. Etkin, M. T. Benson, S. Courtenay, M. J. McGlinchey, A. d. Bain, D. W. Stephan, *Organometallics* **1997**, *16*, 3504–3510.

[11] P. J. Chirik, J. A. Pool, E. Lobkovsky, *Angew. Chem. Int. Ed.* **2002**, *41*, 3463–3465, *Angew. Chem.* **2002**, *114*, 3613–3615.

[12] E. Hey, M. F. Lappert, J. L. Atwood, S. G. Bott, *J. Chem. Soc., Chem. Commun.* **1987**, 597–598.

[13] M. Peruzzini, J. A. Ramirez, F. Vizza, *Angew. Chem. Int. Ed.* **1998**, *37*, 2255–2257, *Angew. Chem.* **1998**, *110*, 2376–2378.

[14] P. Barbaro, M. Peruzzini, J. A. Ramirez, F. Vizza, *Organometallics* **1999**, *18*, 4237–4240.

[15] P. Barbaro, A. Ienco, C. Mealli, M. Peruzzini, O. J. Scherer, G. Schmitt, F. Vizza, G. Wolmershäuser, *Chem. Eur. J.* **2003**, *9*, 5196–5210.

[16] M. Bispinghoff, Z. Benkő, H. Grützmacher, F. D. Calvo, M. Caporali, M. Peruzzini, *Dalton Trans.* **2019**, *48*, 3593–3600.

[17] O. J. Scherer, J. Braun, P. Walther, G. Heckmann, G. Wolmershäuser, *Angew. Chem. Int. Ed.* **1991**, *30*, 852–854, *Angew. Chem.* **1991**, *103*, 861–863.

[18] O. J. Scherer, C. Vondung, G. Wolmershäuser, *Angew. Chem. Int. Ed.* **1997**, *36*, 1303–1305, *Angew. Chem.* **1997**, *109*, 1360–1362.

[19] J. E. Davies, M. C. Klunduk, M. J. Mays, P. R. Raithby, G. P. Shields, P. K. Tompkin, *Dalton Trans.* **1997**, 715–720.

[20] J. E. Davies, M. J. Mays, E. J. Pook, *Chem. Commun.* **1997**, *60*, 1997.

[21] O. J. Scherer, G. Kemény, G. Wolmershäuser, *Chem. Ber.* **1995**, *128*, 1145–1148.

[22] C. E. Laplaza, W. M. Davis, C. C. Cummins, *Angew. Chem. Int. Ed.* **1995**, *34*, 2042–2044, *Angew. Chem.* **1995**, *107*, 2181–2183.

[23] M. J. A. Johnson, A. L. Odom, C. C. Cummins, *Chem. Commun.* **1997**, 1523–1524.

[24] N. A. Piro, C. C. Cummins, *J. Am. Chem. Soc.* **2008**, *130*, 9524–9535.

[25] D. Tofan, B. M. Cossairt, C. C. Cummins, *Inorg. Chem.* **2011**, *50*, 12349–12358.

[26] J. S. Figueroa, C. C. Cummins, *Angew. Chem. Int. Ed.* **2005**, *44*, 4592–4596, *Angew. Chem.* **2005**, *117*, 4668–4672.

[27] J. S. Figueroa, C. C. Cummins, *Angew. Chem. Int. Ed.* **2004**, *43*, 984–988, *Angew. Chem.* **2004**, *116*, 1002–1006.

[28] J. S. Figueroa, C. C. Cummins, *J. Am. Chem. Soc.* **2004**, *126*, 13916–13917.

[29] J. S. Figueroa, C. C. Cummins, *J. Am. Chem. Soc.* **2003**, *125*, 4020–4021.

[30] N. A. Piro, J. S. Figueroa, J. T. McKellar, C. C. Cummins, *Science* **2006**, *313*, 1276–1279.

[31] N. A. Piro, C. C. Cummins, *J. Am. Chem. Soc.* **2009**, *131*, 8764–8765.

[32] S. Umbarkar, P. Sekar, M. Scheer, *Dalton Trans.* **2000**, 1135–1137.

[33] a) M. A. Alvarez, M. E. García, D. García-Vivó, A. Ramos, M. A. Ruiz, *Inorg. Chem.* **2011**, *50*, 2064–2066; b) M. A. Alvarez, M. E. García, D. García-Vivó, M. A. Ruiz, M. F. Vega, *Organometallics* **2015**, *34*, 870–878.

[34] G. Capozzi, L. Chiti, M. Di Vaira, M. Peruzzini, P. Stoppioni, *J. Chem. Soc., Chem. Commun.* **1986**, 1799–1800.

[35] M. Di Vaira, P. Stoppioni, S. Midollini, F. Laschi, P. Zanello, *Polyhedron* **1991**, *10*, 2123–2129.

[36] E. Mädl, G. Balázs, E. V. Peresypkina, M. Scheer, *Angew. Chem. Int. Ed.* **2016**, *55*, 7702–7707, *Angew. Chem.* **2016**, *128*, 7833–7838.

[37] B. M. Cossairt, C. C. Cummins, *Angew. Chem. Int. Ed.* **2010**, *49*, 1595–1598, *Angew. Chem.* **2010**, *122*, 1639–1642.

[38] A. Velian, C. C. Cummins, *Chem. Sci.* **2012**, *3*, 1003.

[39] B. M. Cossairt, M.-C. Diawara, C. C. Cummins, *Science* **2009**, *323*, 602.

[40] M. Di Vaira, P. Frediani, S. S. Costantini, M. Peruzzini, P. Stoppioni, *Dalton Trans.* **2005**, 2234–2236.

[41] a) M. Di Vaira, M. Peruzzini, S. Seniori Costantini, P. Stoppioni, *J. Organomet. Chem.* **2006**, *691*, 3931–3937; b) M. Caporali, L. Gonsalvi, R. Kagirov, V. Mirabello, M. Peruzzini, O. Sinyashin, P. Stoppioni, D. Yakhvarov, *J. Organomet. Chem.* **2012**, *714*, 67–73.

[42] P. Barbaro, M. Di Vaira, M. Peruzzini, S. Seniori Costantini, P. Stoppioni, *Chem. Eur. J.* **2007**, *13*, 6682–6690.

[43] P. Barbaro, M. Di Vaira, M. Peruzzini, S. Seniori Costantini, P. Stoppioni, *Angew. Chem. Int. Ed.* **2008**, *47*, 4425–4427, *Angew. Chem.* **2008**, *120*, 4497–4499.

[44] P. Barbaro, M. Di Vaira, M. Peruzzini, S. Seniori Costantini, P. Stoppioni, *Inorg. Chem.* **2009**, *48*, 1091–1096.

[45] P. Barbaro, C. Bazzicalupi, M. Peruzzini, S. Seniori Costantini, P. Stoppioni, *Angew. Chem. Int. Ed.* **2012**, *51*, 8628–8631, *Angew. Chem.* **2012**, *124*, 8756–8759.

[46] J. E. Borger, M. S. Bakker, A. W. Ehlers, M. Lutz, J. C. Slootweg, K. Lammertsma, *Chem. Comm.* **2016**, *52*, 3284–3287.

[47] O. J. Scherer, T. Hilt, G. Wolmershäuser, *Angew. Chem. Int. Ed.* **2000**, *39*, 1425–1427, *Angew. Chem.* **2000**, *112*, 1483–1485.

[48] S. Deng, C. Schwarzmaier, C. Eichhorn, O. Scherer, G. Wolmershäuser, M. Zabel, M. Scheer, *Chem. Comm.* **2008**, 4064–4066.

[49] M. Scheer, S. Deng, O. J. Scherer, M. Sierka, *Angew. Chem. Int. Ed.* **2005**, *44*, 3755–3758, *Angew. Chem.* **2005**, *117*, 3821–3825.

[50] S. Pelties, A. W. Ehlers, R. Wolf, *Chem. Comm.* **2016**, *52*, 6601–6604.

[51] C. Schwarzmaier, S. Heinl, G. Balázs, M. Scheer, *Angew. Chem. Int. Ed.* **2015**, *54*, 13116–13121, *Angew. Chem.* **2015**, *127*, 13309–13314.

[52] J. E. Borger, M. K. Jongkind, A. W. Ehlers, M. Lutz, J. C. Slootweg, K. Lammertsma, *ChemistryOpen* **2017**, *6*, 350–353.

[53] A. E. Seitz, M. Eckhardt, A. Erlebach, E. V. Peresypkina, M. Sierka, M. Scheer, *J. Am. Chem. Soc.* **2016**, *138*, 10433–10436.

[54] M. Scheer, M. Dargatz, P. G. Jones, *J. Organomet. Chem.* **1993**, *447*, 259–264.

[55] A. Cavaillé, N. Saffon-Merceron, N. Nebra, M. Fustier-Boutignon, N. Mézailles, *Angew. Chem. Int. Ed.* **2018**, *57*, 1874–1878, *Angew. Chem.* **2018**, *130*, 1892–1896.

[56] M. Piesch, M. Seidl, M. Stubenhofer, M. Scheer, *Chem. Eur. J.* **2019**, *25*, 6311–6316.

[57] U. Chakraborty, J. Leitl, B. Mühldorf, M. Bodensteiner, S. Pelties, R. Wolf, *Dalton Trans.* **2018**, *47*, 3693–3697.

[58] C. G. P. Ziegler, T. M. Maier, S. Pelties, C. Taube, F. Hennersdorf, A. W. Ehlers, J. J. Weigand, R. Wolf, *Chem. Sci.* **2019**, *10*, 1302–1308.

[59] E. Mädl, M. V. Butovskii, G. Balázs, E. V. Peresypkina, A. V. Virovets, M. Seidl, M. Scheer, *Angew. Chem. Int. Ed.* **2014**, *53*, 7643–7646, *Angew. Chem.* **2014**, *126*, 7774–7777.

[60] B. M. Cossairt, C. C. Cummins, *Angew. Chem. Int. Ed.* **2008**, *47*, 169–172, *Angew. Chem.* **2008**, *120*, 175–178.

[61] B. M. Cossairt, C. C. Cummins, *Inorg. Chem.* **2008**, *47*, 9363–9371.

[62] B. M. Cossairt, C. C. Cummins, *Angew. Chem. Int. Ed.* **2008**, *47*, 8863–8866, *Angew. Chem.* **2008**, *120*, 8995–8998.

[63] a) D. H. R. Barton, J. Zhu, *J. Am. Chem. Soc.* **1993**, *115*, 2071–2072; b) D. H.R. Barton, R. A. Vonder Embse, *Tetrahedron* **1998**, *54*, 12475–12496.

[64] B. M. Cossairt, C. C. Cummins, *New J. Chem.* **2010**, *34*, 1533.

[65] S. Heinl, S. Reisinger, C. Schwarzmaier, M. Bodensteiner, M. Scheer, *Angew. Chem. Int. Ed.* **2014**, *53*, 7639–7642, *Angew. Chem.* **2014**, *126*, 7769–7773.

[66] a) Y. G. Budnikova, D. I. Tazeev, A. G. Kafiyatullina, D. G. Yakhvarov, V. I. Morozov, N. K. Gusarova, B. A. Trofimov, O. G. Sinyashin, *Russ. Chem. Bull.* **2005**, *54*, 942–947; b) Y. G. Budnikova, D. G. Yakhvarov, Y. M. Kargin, *Mendeleev Commun.* **1997**, *7*, 67–68.

[67] D. G. Yakhvarov, Y. G. Budnikova, O. G. Sinyashin, *Russ. J. Electrochem.* **2003**, *39*, 1261–1270.

[68] a) Y. H. Budnikova, D. G. Yakhvarov, O. G. Sinyashin, *J. Organomet. Chem.* **2005**, *690*, 2416–2425; b) Y. H. Budnikova, T. V. Gryaznova, V. V. Grinenko, Y. B. Dudkina, M. N. Khrizanforov, *Pure App. Chem.* **2017**, *89*, 311–330; c) D. G. Yakhvarov, E. V. Gorbachuk, R. M. Kagirov, O. G. Sinyashin, *Russ. Chem. Bull., Int. Ed.* **2012**, *61*, 1300–1312.

[69] D. G. Yakhvarov, E. V. Gorbachuk, O. G. Sinyashin, *Eur. J. Inorg. Chem.* **2013**, *2013*, 4709–4726.

[70] D. G. Yakhvarov, Y. H. Budnikova, D. I. Tazeev, O. G. Sinyashin, *Russ. Chem. Bull., Int. Ed.* **2002**, *51*, 2059–2064.

2 Synthesis of Cyclic M_2E_2 Clusters (M = Fe, Co; E = Ge, Sn) Using M⁻ Synthons[a,b]

Christian M. Hoidn, Christian Rödl, Peter Coburger, Madison L. McCrea-Hendrick, Theresa Block, Rainer Pöttgen, Andreas W. Ehlers, Bas De Bruin, Philip P. Power and Robert Wolf

2.1 Introduction

Tin compounds have played a pivotal role in the chemistry of multiple bonded heavier main group species.[1] The ability of heavy p-block elements to form isolable homodinuclear multiple bonds was first demonstrated by the structural characterization of the distannene $R_2Sn=SnR_2$ (R = CH{SiMe₃}₂) by *Lappert* and co-workers in 1976.[2] Distannyne Ar′SnSnAr′ (Ar′ = C_6H_3-2,6(C_6H_3-2,6-*i*Pr₂)₂), one of the first heavier group 14 element alkyne analogues, was described in 2002.[3,4] Moreover, homo- and heterometallic Zintl ions,[5] metalloid cages $[SnR]_n$,[6] and metalloid clusters $[Sn_nR_m]$ (n > m)[7] have attracted significant attention. Various transition metal stannyl and stannylidene complexes were reported, while stannylidyne complexes and metallostannylenes are still scarce.[1,8,9] Known examples such as **A−C** (Figure 1a) are stabilized by phosphane, cyclopentadienyl or carbonyl coligands.
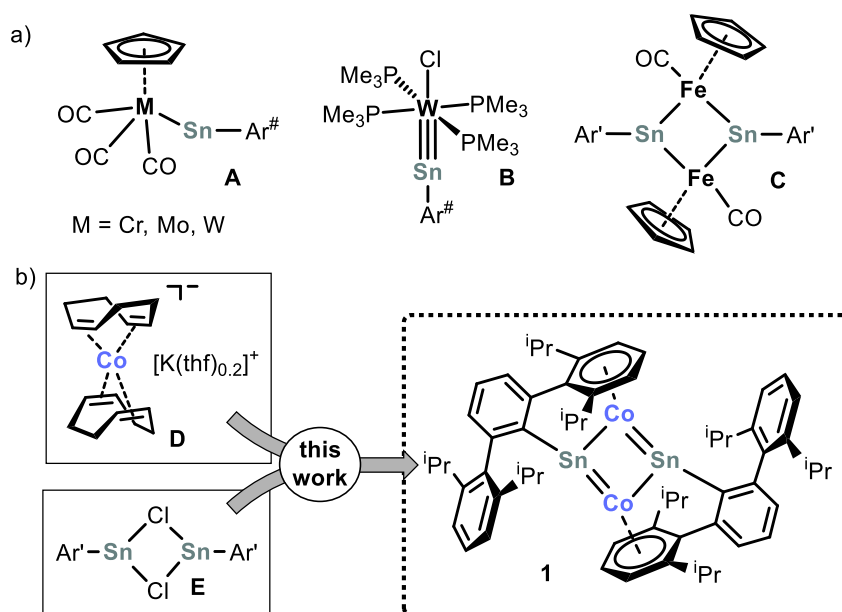
Figure 1. (a) Selected metallostannylene and stannylidyne complexes (Ar# = C_6H_3-2,6(C_6H_2-2,4,6-Me₃)₂); (b) synthesis of Co₂Sn₂ compound **1**, reagents and byproducts: [Ar′Sn(μ-Cl)]₂ + 3[K(thf)₀.₂][Co(η⁴-1,5-cod)₂]/−2KCl, −4 1,5-cod; conditions: toluene, −30 °C → r.t., 20 h

Herein, we describe a new strategy for the synthesis of unusual p-block/d-block element clusters. Pioneering work by *Jonas* and *Ellis* established the synthesis and reactivity of [K(thf)₀.₂][Co(η⁴-1,5-cod)₂] (**D**, cod = cyclooctadiene)[10] and many related alkene and polyarene metalates.[11,12] However, such anions were employed mainly in redox-neutral ligand exchange reactions.[12,13] We now show that anion **D** can be used to obtain the unusual [Ar′SnCo]₂ cluster (**1**), which features a cyclic Co₂Sn₂ core with two three coordinate tin atoms. The preparative oxidation of **1** with [Cp₂Fe][BArᶠ₄] (Arᶠ = 3,5-

$(CF_3)_2C_6H_3)$ led to the cationic cluster $[Ar'SnCo]_2^+$ (**2**). In addition, reactivity studies of **1** with white phosphorus afforded $[Ar'_2Sn_2Co_2P_4]$ (**3**), which is the first molecular cluster composed of tin, cobalt and phosphorus atoms. Furthermore, the synthesis of the analogous heterobimetallic clusters $[Ar'GeCo]_2$ (**4**) and a related iron tin compound **5** is discussed.

2.2   Results and Discussion

2.2.1   Synthesis, Characterization and Reactivity of [Ar'SnCo]₂ (1)

$[Ar'SnCo]_2$ (**1**) was obtained by reacting $[K(thf)_{0.2}][Co(\eta^4\text{-}1,5\text{-cod})_2]$ (**D**) with $[Ar'Sn(\mu\text{-}Cl)]_2$ (**E**) in toluene (Figure 1b). An excess of cobaltate **D** (three equiv. per $[Ar'Sn(\mu\text{-}Cl)]_2$ dimer) was required to produce **1** in up to 42% isolated yield. Deep-green single crystals suitable for single crystal XRD were obtained from a concentrated *n*-hexane solution. The structure of **1** (Figure 2) shows a centrosymmetric, rhomboidal Co_2Sn_2 core with two distinct Co−Sn bond lengths.
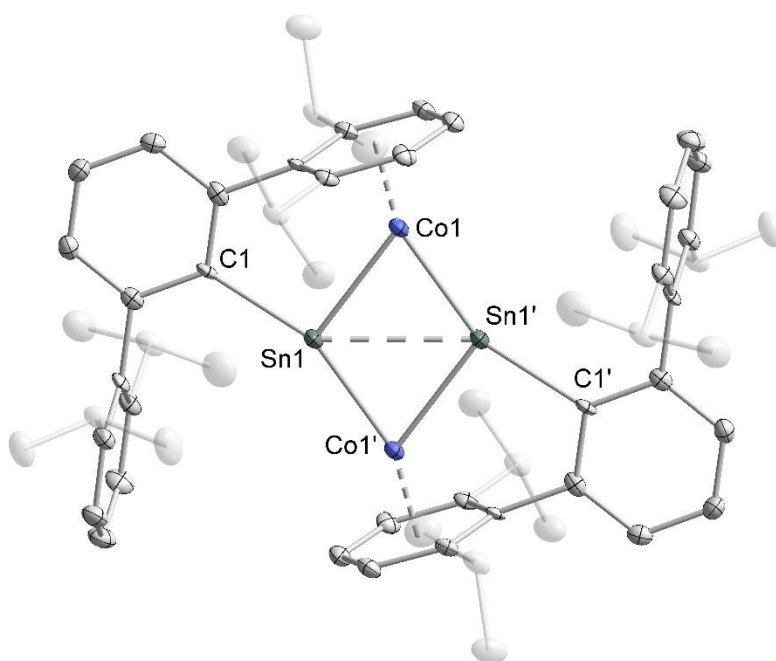
Figure 2. Displacement ellipsoid (40%) drawing of the centrosymmetric complex **1**. The co-crystallized *n*-hexane solvent molecule and the hydrogen atoms are not shown for clarity. Selected bond lengths [Å] and angles [°]: Sn1−Sn1' 2.8700(5), Sn1−Co1 2.5365(5), Sn1−Co1' 2.4071(6), Sn1−C1 2.174(3), Co−Dipp(c) 1.560(1), C1−Sn1−Sn1' 145.96(8), Co1−Sn1−Sn1' 52.43(1), Co1'−Sn1−Sn1' 56.64(1), Sn1'−Co1−Sn1 70.92(2), C1−Sn1−Co1 93.53(8), C1−Sn1−Co1' 157.38(8).

The Sn1−Co1 distance of 2.5365(5) Å resembles that predicted for a Co−Sn single bond ($\sum r_{cov}$ = 2.51 Å), whereas the Sn1−Co1′ bond length (2.4071(6) Å) is closer to that of a double bond (calculated covalent double bond radius 2.33 Å).[14] The Sn1−Sn1′ distance (2.8700(5) Å) is similar to those of Sn−Sn single bonds in bulky hexaorganodistannanes such as [tBu₃SnSntBu₃] (2.894(1) Å),[15] [(PhCH₂)₃SnSn(CH₂Ph)₃] (2.823(1) Å)[15] and [(o-Tol)₃SnSn(o-Tol)₃] (2.883(1) Å),[16] but see DFT calculations below. The cobalt atoms are η⁶-coordinated by the flanking 2,6-diisopropylphenyl rings with a very short cobalt−centroid distance (1.560(1) Å), which suggests a particularly strong cobalt-arene interaction, cf. >0.1 Å shorter than the η⁶-arene interactions in [Ar′CoCoAr′] (1.764(2) Å),[17] [(nacnac)Co(η⁶-C₇H₈)] (1.747(2) Å, nacnac = HC{C(Me)N-(2,6-Me₂C₆H₃)}₂)[18] and [(η⁶-C₇H₈)CoAr*] (1.659(1) Å, Ar* = C₆H-2,6(C₆H₂-2,4,6-iPr₃)₂-3,5-iPr₂).[19] The average C−C bond length within the metal-coordinated aryl rings is nearly 0.025 Å longer than those in the noncoordinated rings. The existence of d-π* backbonding is also underlined by the substantial upfield shift of the aryl resonances of the coordinated Dipp groups (4.76 and 4.56 ppm) in the ¹H NMR spectrum.[17] A ¹¹⁹Sn NMR signal was not detected for **1** in the range of −4200 to +4200 ppm. This is probably due to the unsymmetric electron environment at the tin atoms in **1**, which leads to fast relaxation through the anisotropy of the chemical shift tensor. The ¹J_{SnCo} coupling to the two adjacent ⁵⁷Co nuclei (I = −7/2) may additionally cause considerable broadening of the signal rendering it unobservable above the baseline. It seems noteworthy that the ¹¹⁹Sn resonance of the distannyne [Ar′SnSnAr′] could also not be detected despite extensive efforts,[3,20] but large differences were observed for the solid-state ¹¹⁹Sn NMR data of [Ar′SnSnAr′] and the closely related species [Ar*SnSnAr*] (Ar* = C₆H₃-2,6-(C₆H₂-2,4,6-iPr₃)₂)[21]

Crystallographically characterized molecular cobalt−tin clusters are rare and the known organometallic cobalt−tin complexes contain cobalt carbonyl fragments and tetravalent tin atoms.[22] The structure of **1** has a resemblance to those of ternary RECoSn stannides (RE = rare earth metal).[23,24] However, the Co₂Sn₂ units in RECoSn (2.61 and 2.67 Å Co−Sn in DyCoSn) are condensed to a ladder-like motif and the units show an inverse tilt, i.e. the tin atoms show a maximum separation of 4.04 Å. *Fässler* and co-workers described endohedral Zintl cluster anions [Co@Sn₉]⁵⁻ and [Co₂@Sn₁₇]⁵⁻ with Co⁻ anions encapsulated into Sn₉ cages.[25] A bridging μ-η¹:η⁶ coordination mode of the terphenyl ligand was observed for the doubly reduced distannyne [K₂Ar′SnSnAr′] and the digermyne silver complexes [AgAr′GeGeAr′][SbF₆] and [Ag₂Ar′GeGe(F)Ar′][SbF₆],

where the K^+ and Ag^+ cations are coordinated by two flanking Dipp substituents.[20,26] Additionally, the bonding in **1** differs markedly since these structures have relatively long Ag−Ge and K−Sn distances and short, multiple Sn−Sn and Ge−Ge bonds.

Density functional theory (DFT) studies at the B3LYP-D3/def2-TZVP level on the truncated model compound **1′** (*i*Pr substituted by H) support the presence of strong intermetallic interactions.[27–32] The HOMO and HOMO−2 (Figure 3a) and a natural bond orbital analysis (Figure S12, SI) illustrate the π-character of the shortened Sn1−Co1′ bond. Several other occupied molecular orbitals (HOMO−1, HOMO−3, HOMO−5, HOMO−10, see Figure S13, SI) also show σ-interactions between tin and cobalt. Notably, the occupied MOs do not show an interaction between the tin atoms. Sn−Sn bonding is only apparent in the LUMO.
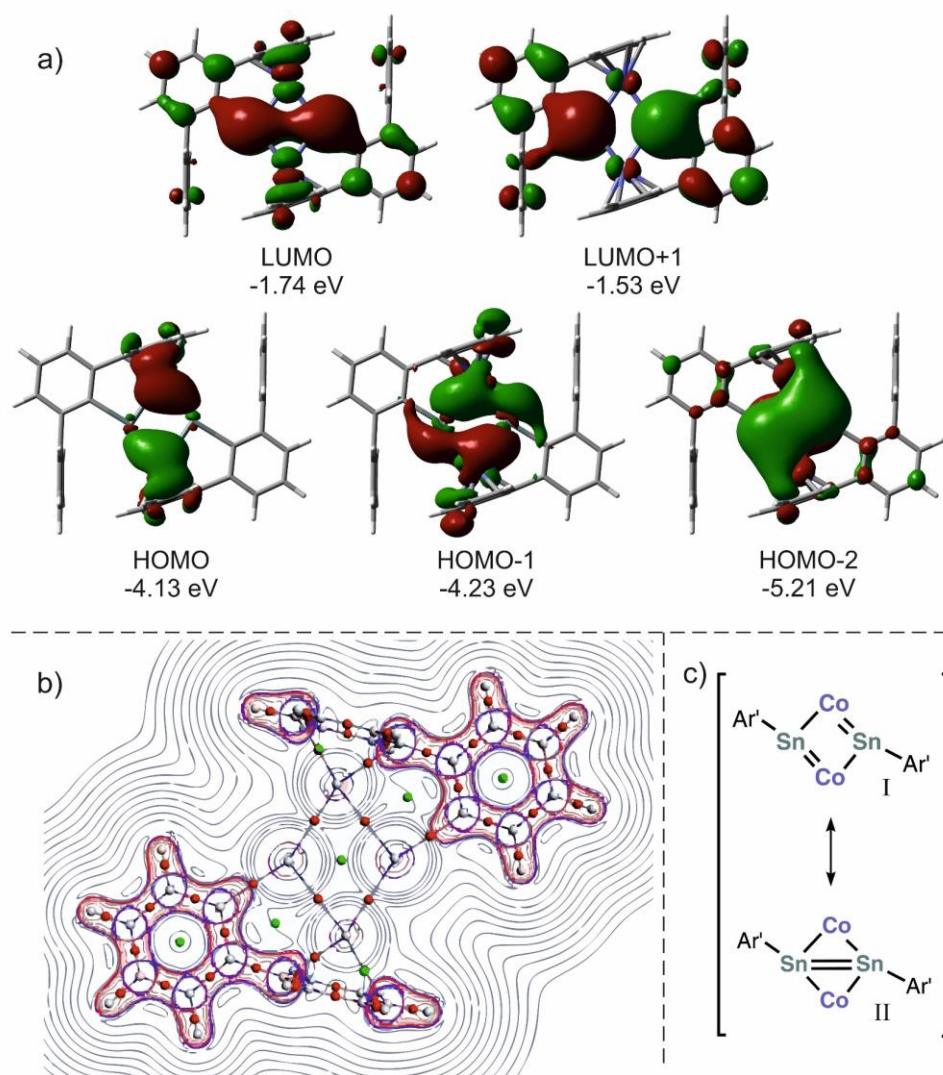
Figure 3. (a) Selected molecular orbitals of **1′** which describe the most significant interactions within the Co_2Sn_2 core; (b) AIM (Bader) analysis (bond critical points: red, ring critical points green); (c) proposed Lewis resonance structures of **1** based on DFT calculations.

A Wiberg bond index (WBI) analysis gave values of 0.68 and 0.59 for the Sn1−Co1′ and Sn1−Co1 bonds, respectively, and a WBI of 0.65 for the Sn−Sn interaction. An AIM analysis (Figure 3b) at the ZORA/ OPBE/QZ4P level[33–36] showed no bond-critical point between the two tin atoms and revealed a ring critical point at the center of the four membered ring. Taken together, these calculations suggest that the covalent Sn−Sn interaction in **1** is quite weak. In terms of Lewis representations, resonance structure I in Figure 3c representing a bis(stannylidyne) complex seems to be more important than resonance structure II describing a distannyne dicobalt complex. The ^{119}Sn Mössbauer spectrum of solid **1** recorded at 6 K (Figure S10, SI) shows a single quadrupole doublet. The isomer shift of **1** ($\delta = 2.14(1)$ mm s^{-1}) is slightly lower than that of β-Sn ($\delta = 2.6$ mm s^{-1}) and comparable to those of stannides and intermetallic tin compounds, e.g. DyCoSn ($\delta = 1.80$ mm s^{-1}, 295 K data), showing Co$_2$Sn$_2$ units similar to those of **1**.[24,37,38] Adjacent ladders in DyCoSn condense via further Co−Sn bonds, leading to a slightly distorted tetrahedral SnCo$_{4/4}$ coordination and a small electric quadrupole splitting parameter of $\Delta E_Q = 0.55$ mm s^{-1}.[24] The electric quadrupole splitting is drastically larger for the Co$_2$Sn$_2$ core in **1** ($\Delta E_Q = 2.86(1)$ mm s^{-1}). This indicates a highly anisotropic charge distribution analogous to that of the related distannyne [Ar′SnSnAr′] ($\delta = 2.658(2)$ mm s^{-1}; $\Delta E_Q = 2.995(2)$ mm s^{-1}).[21]

The cyclic voltammogram of **1** recorded in THF/[nBu$_4$N]PF$_6$ features a reversible one-electron oxidation at E$_{1/2}$ = −0.85 V (Figure 4). In order to prove the reversibility of that process we applied different scan rates, varying from 100 mV/s to 1000 mV/s. The linear plot of i_p vs. $v^{1/2}$ provided the evidence for an electrochemical reversible redox process.[39]
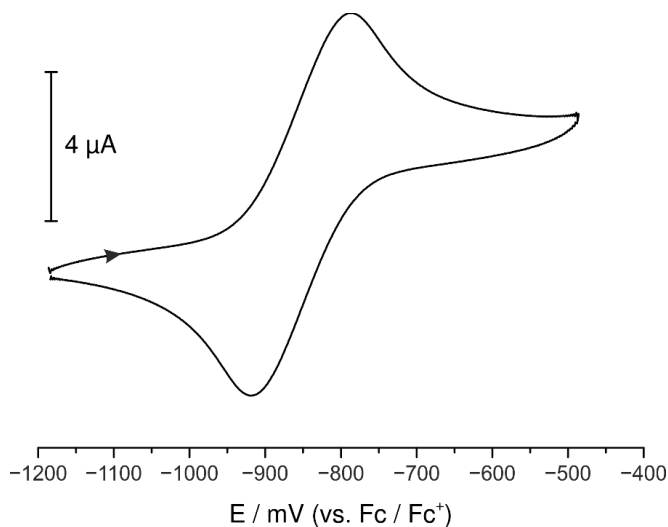
Figure 4. Cyclic voltammograms of **1** recorded in THF/[nBu₄N]PF₆ with a platinum disc working electrode, a platinum wire as counter electrode, and silver/silver nitrate as reference electrode. v = 100 mV/s; potentials are referenced to the Fc/Fc+ couple.

Encouraged by this promising CV data, we synthesized the monocationic Co_2Sn_2 cluster $[Ar'SnCo]_2^+$ (**2**) as $[BAr^F_4]^-$ salt on a preparative scale by oxidizing **1** with $[Cp_2Fe][BAr^F_4]$ ($Ar^F = 3,5-(CF_3)_2C_6H_3$) in THF. **2**$[BAr^F_4]$ was isolated as red-brown powder in up to 59% yield after removal of the ferrocene by-product by washing with *n*-hexane.
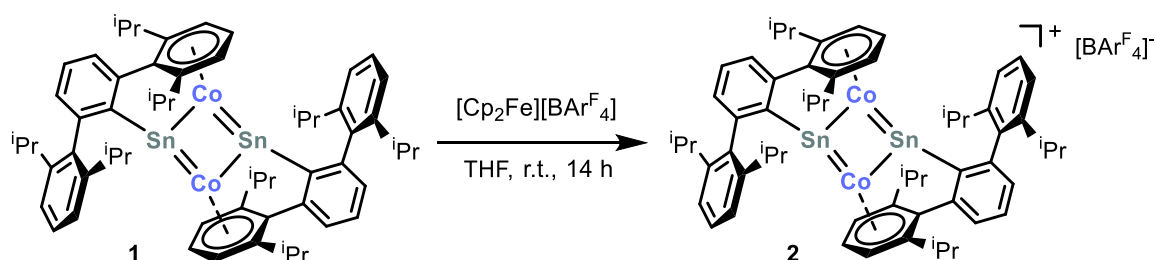
Scheme 1. Synthesis of the monocationic Co_2Sn_2 cluster **2** by oxidation of **1** with $[Cp_2Fe][BAr^F_4]$ ($Ar^F = 3,5-(CF_3)_2C_6H_3$).

Dark brown crystals of **2**$[BAr^F_4]$ were grown from a saturated toluene solution and analyzed by single-crystal XRD studies. The asymmetric unit contains two molecules of **2**$[BAr^F_4]$. However, its solid-state molecular structure reveals three crystallographically independent $[Ar'SnCo]_2^+$ cations, specifically, one whole cation, and two half cations located at an inversion center (See Figure 5). Table 1 shows the bond parameters of the three crystallographically independent cations **2**, which deviate only slightly from each other, and a comparison to the neutral starting material **1**. Generally, the molecular structure of cation **2** closely resembles the neutral precursor **1**. It features a similar rhomboidal Co_2Sn_2 cluster core, however the metal−metal bonds in **2** are overall elongated compared to those found in **1**. The Sn−Sn distance features the most significant difference and is almost 0.1 Å longer in **2** (2.9372(2) to 2.9732(2) Å) than in **1** (2.8700(5) Å). Analogously to **1**, the flanking Dipp groups of the tin bound terphenyl substituents coordinate the cobalt atoms in the η^6-fashion, though the cobalt−centroid distances are also elongated.

2$[BAr^F_4]$ is paramagnetic and shows broad ^1H NMR signals in the range of −1.4 to 12.7 ppm. (Figure S3). Although the solution effective magnetic moment [3.1(1) μ_B] (Evans Method in THF-d_8)[40] indicates the presence of two unpaired electrons per molecule, the EPR spectrum (Figure 6) clearly shows an S = ½ system. The spectrum is slightly rhombic and rather broad. It is probable that the broadening is caused by numerous overlapping hyperfine coupling interactions with two cobalt and two tin nuclei combined with g-anisotropy.
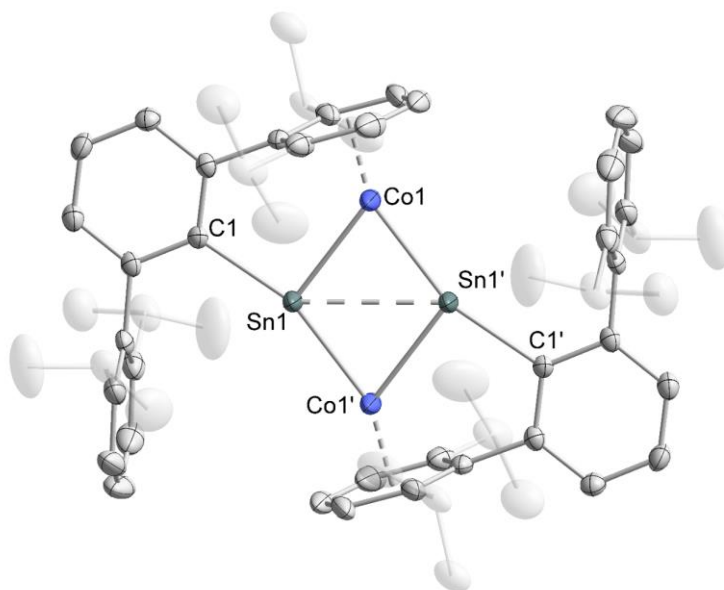
Figure 5. Displacement ellipsoid (40%) drawing of one of the centrosymmetric cations (Cation B) in the solid-state molecular structure of **2**[BAr$^F_4$]. The other two crystallographically independent **2** cations, the [BAr$^F_4$]⁻ anions, and the hydrogen atoms are not shown for clarity.

Table 1. Selected bond lengths [Å] and angles [°] of the three crystallographically independent cations of **2**[BAr$^F_4$] in comparison to those of neutral **1**.

	2			**1**[a]
	Cation A	Cation B[a]	Cation C[a]	
Sn1−Sn1′	2.9372(2)	2.9732(3)	2.9558(3)	2.8700(5)
Sn1−Co1	2.5266(4)	2.5200(4)	2.5232(5)	2.5365(5)
Sn1′−Co1′	2.5299(4)	-	-	-
Sn1−Co1′	2.4318(4)	2.4129(5)	2.4291(5)	2.4071(6)
Sn1′−Co1	2.4298(4)	-	-	-
Sn1−C1	2.151(2)	2.148(2)	2.143(2)	2.174(3)
Sn1′−C1′	2.145(2)	-	-	-
Co1−Dipp(c)	1.578(1)	1.568(1)	1.578(1)	1.560(1)
Co1′−Dipp(c)′	1.579(1)	-	-	-
C1−Sn1−Sn1′	144.72(7)	145.16(6)	145.32(7)	145.96(8)
C1′−Sn1′−Sn1	145.43(6)	-	-	-
Co1−Sn1−Sn1′	52.15(1)	51.31(1)	51.91(1)	52.43(1)
Co1′−Sn1′−Sn1	52.18(1)	-	-	-
Co1′−Sn1−Sn1′	55.26(1)	54.60(1)	54.83(1)	56.64(1)
Co1−Sn1′−Sn1	55.19(1)	-	-	-
Sn1′−Co1−Sn1	72.66(1)	74.09(1)	73.26(2)	70.92(2)
Sn1−Co1′−Sn1′	72.57(1)	-	-	-
C1−Sn1−Co1	93.71(7)	94.04(6)	93.51(7)	93.53(8)
C1′−Sn1′−Co1′	93.53(6)	-	-	-
Sn1−Co1−Sn1′−Co1′	4.73	0	0	0

[a] centrosymmetric molecules
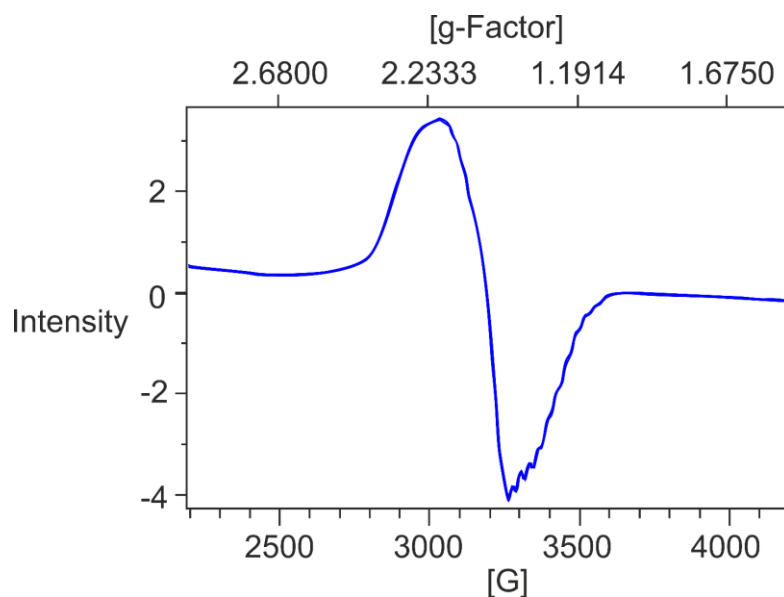
Figure 6. EPR spectrum of [Ar′₂Sn₂Co₂][BAr^F₄] (**2**[BAr^F₄]).

While reactivity studies with small molecules such as O_2 and CO gave intractable products so far, **1** reacted readily with white phosphorus in toluene to afford [Ar′₂Sn₂Co₂P₄] (**3**) as a well-defined, crystalline species in up to 76% isolated yield (Scheme 2).
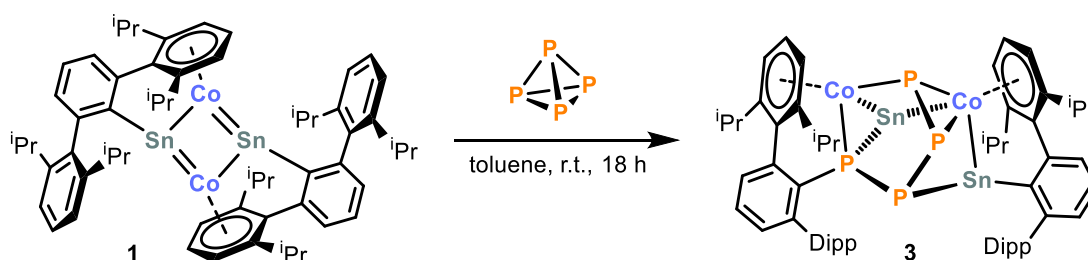
Scheme 2. Synthesis of Co₂Sn₂P₄ compound **3** by reaction of **1** with white phosphorus.

Dark-brown crystals of **3** suitable for single-crystal XRD were obtained from a concentrated cyclohexane solution. The molecular structure (Figure 7a) shows a P_4 chain resulting from the insertion of the white phosphorus molecule into the Co₂Sn₂ core of **1**. One of the terphenyl moieties has migrated from tin to phosphorus, but both cobalt atoms retain the η^6-coordination from flanking aryl rings as observed in the structure of **1**. Terphenyl migration from tin to phosphorus was previously observed by *Wesemann* and co-workers in the reaction of adamantyl phosphaalkyne with a terphenyl allyl stannylene.[41] Moreover, a similar terphenyl transfer from thallium to phosphorus was observed in the reaction of a dithallene with P_4.[42] The cobalt-centroid distances of 1.585(1) and 1.612(1) Å are slightly longer than those in **1**. The P−P bond distances ranging from 2.2005(8) to 2.1621(8) Å are typical for single bonds ($\sum r_{cov}$ = 2.22 Å).[14]

As expected, the Co−P bonds of the terminal P atoms coordinating to Co1 (Co1−P1 2.1864(6) and Co1−P4 2.2289(7) Å) are shorter than those of the side-on coordinated P−P bond coordinating to Co2 (Co2−P3 2.3350(6) and Co2−P4 2.3501(6) Å). The Co−Sn distances (Co1−Sn1 2.7380(4), Co2−Sn1 2.8263(4), and Co2−Sn2 2.6500(4) Å) are significantly longer than in **1**, while the Sn1−P2 and Sn2−P1 distances (2.6587(6) and 2.5716(6) Å, respectively) compare well with Sn−P single bonds reported for other tin−phosphorus cage compounds.[43] Weak interactions between Sn1···P3 and Sn2···P4 are also apparent, since the corresponding Sn−P distances of 2.8519(6) and 2.9277(6) Å are much smaller than the sum of van der Waals radii ($\sum r_{vdW}$ = 4.02 Å).[44]
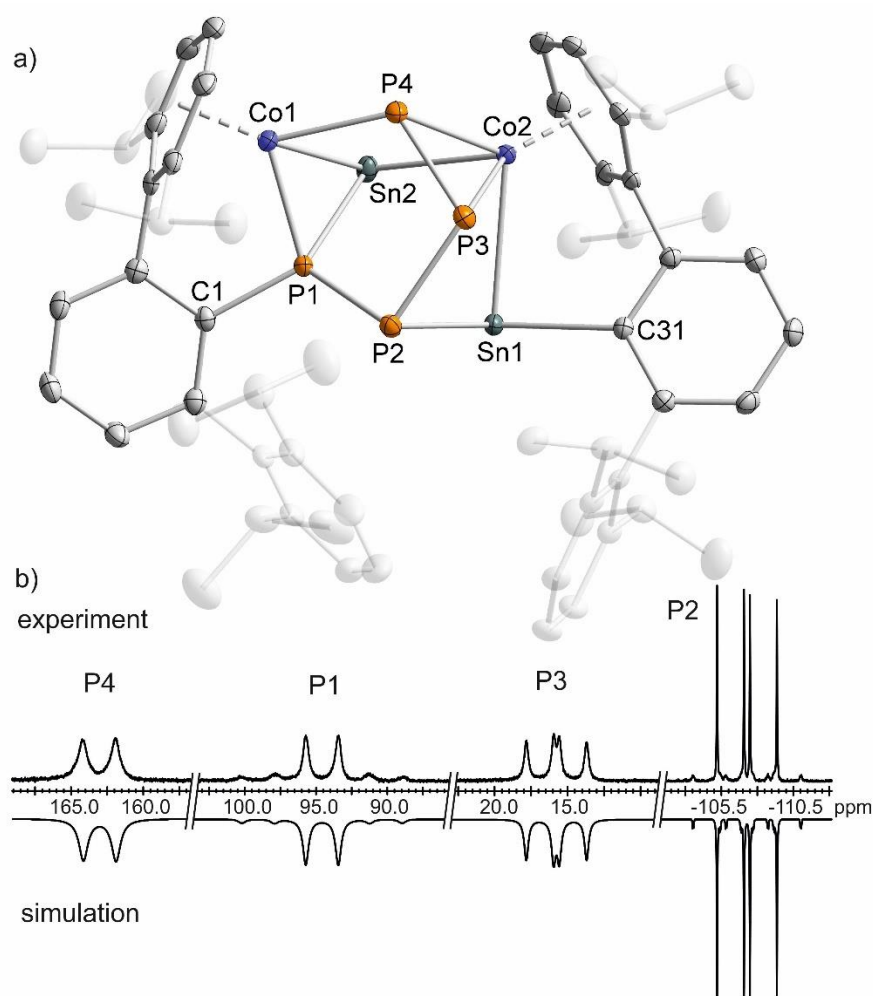
Figure 7. (a) Displacement ellipsoid (40%) drawing of the Co₂Sn₂P₄ cluster **3**. The cocrystallized cyclohexane solvent molecule and the hydrogen atoms are not shown for clarity. Selected bond lengths [Å] and angles [°]: Sn1−Co2 2.8263(4), Sn2−Co1 2.7380(4), Sn2−Co2 2.6500(4), Sn1−P2 2.6587(6), Sn2−P1 2.5716(6), Sn1···P3 2.9277(6), Sn2···P4 2.8519(6), Sn1−C31 2.279(2), Co1−P1 2.1864(6), Co1−P4 2.2289(7), Co2−P3 2.3350(6), Co2−P4 2.3501(6), P1−P2 2.2005(8), P2−P3 2.1809(8), P3−P4 2.1621(8), P1−C1 1.843(2), Co1−Dipp(c) 1.585(1), Co2−Dipp(c) 1.612(1), P1−P2−P3 93.40(3), P2−P3−P4 109.79(3), P1−P2−P3−P4 16.27(3). (b) Measured (upward) and simulated (downward) ³¹P{¹H} NMR spectra of compound **3** in THF-d_8.

The $^{31}P\{^1H\}$ NMR spectrum of **3** shows four multiplets with an integral ratio of 1:1:1:1 (Figure 7b) with additional coupling to $^{117/119}$Sn. The spectrum was successfully simulated by an iterative fitting procedure (see the SI for further details). The $^1J_{PP}$ coupling constants range from −303 to −370 Hz.[45] The proximity of P1 and P2 to adjacent tin atoms is confirmed by the observation of $^{117/119}$Sn satellites at P2 and P4 ($^1J_{P2Sn1}$ = 579 Hz, $^1J_{P1Sn2}$ = 1482 Hz). Direct bonding to quadrupolar ^{59}Co nuclei can considerably affect the line width of ^{31}P NMR resonances depending on the $^1J_{PCo}$ coupling constant and the longitudinal relaxation time.[46] Provided that there is a direct correlation of the signal width to the number of bound Co atoms, the broadened multiplets can be assigned to P1 ($\Delta v_{1/2}$ = 77 Hz), P3 ($\Delta v_{1/2}$ = 54 Hz) and P4 ($\Delta v_{1/2}$ = 121 Hz).

In agreement with the two different Sn sites in the solid-state structure, the ^{119}Sn Mössbauer spectrum of **3** (Figure S11, SI) was well reproduced with two doublets in a 1:1 ratio with isomer shifts of δ = 2.58(1) mm s⁻¹ and δ = 2.94(1) mm s⁻¹. These isomer shifts are comparable to those of other organotin(II) compounds[37,47] and metalloid tin clusters.[48,49] Both signals show similar quadrupole splittings of ΔE_Q = 1.41(1) and 1.43(1) mm s⁻¹ respectively, reflecting the noncubic site symmetries. Similar quadrupole splittings for organotin compounds with an asymmetric environment are reported in the literature.[48]

2.2.2 Synthesis of Related Heterobimetallic Clusters

2.2.2.1 Reaction of [Ar′GeCl]₂ with [K(thf)₀.₂][Co(η⁴-1,5-cod)₂]

We further investigated whether this methodology is applicable to the formation of the analogous germanium cluster [Ar′GeCo]₂ (**4**). Under the same conditions that led to **1**, an excess of [K(thf)₀.₂][Co(η⁴-1,5-cod)₂] (**D**) was reacted with [Ar′GeCl]₂ in toluene at −30 °C (Scheme 3).
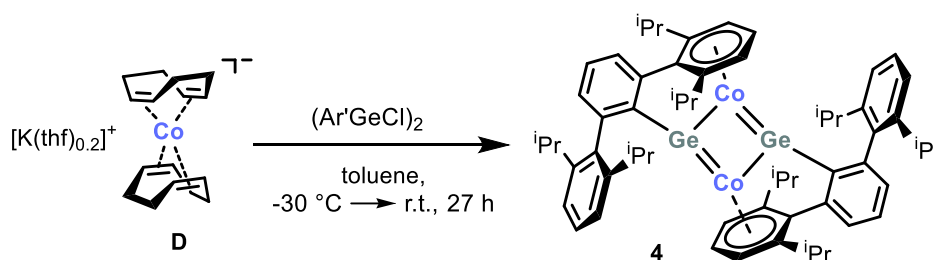
Scheme 3. Reaction of [K(thf)₀.₂][Co(η⁴-1,5-cod)₂] (**D**) with [Ar′GeCl]₂.

According to the ^{1}H NMR spectrum of the reaction mixture, the reaction is very unselective (Figure 8 bottom). Yet, several multiplets arising in the characteristic range of 4.2 to 6.0 ppm indicate the formation of **4** along with other species featuring metal coordinating arene rings. The isolation of **4** as a pure compound has been unsuccessful so far. Note that the tin analogue **1** can be purified by washing the crude product with copious amounts of Et₂O (see the Experimental Section, chapter 2.4.3.1 for details). As **4** is highly soluble in Et₂O and non-polar solvents such as *n*-hexane, this approach cannot be used to purify **4**. Nonetheless, minor amounts of dark brown crystals formed in the concentrated *n*-hexane extracts of crude **4**. Although they were unsuitable for XRD analysis, the ^{1}H NMR spectrum of the isolated crystals (Figure 8 middle) indicates that the sample is relatively pure and shows a very similar set of signals compared to the ^{1}H NMR spectrum of **1** (Figure 8 top) along with remaining *n*-hexane and some unknown impurities. The signals assigned to the coordinating Dipp groups in **4** (4.55 and 5.07 ppm) are somewhat shifted compared to **1** possibly indicating a significant difference in both the geometric and the electronic structure of the Co₂Ge₂ core.
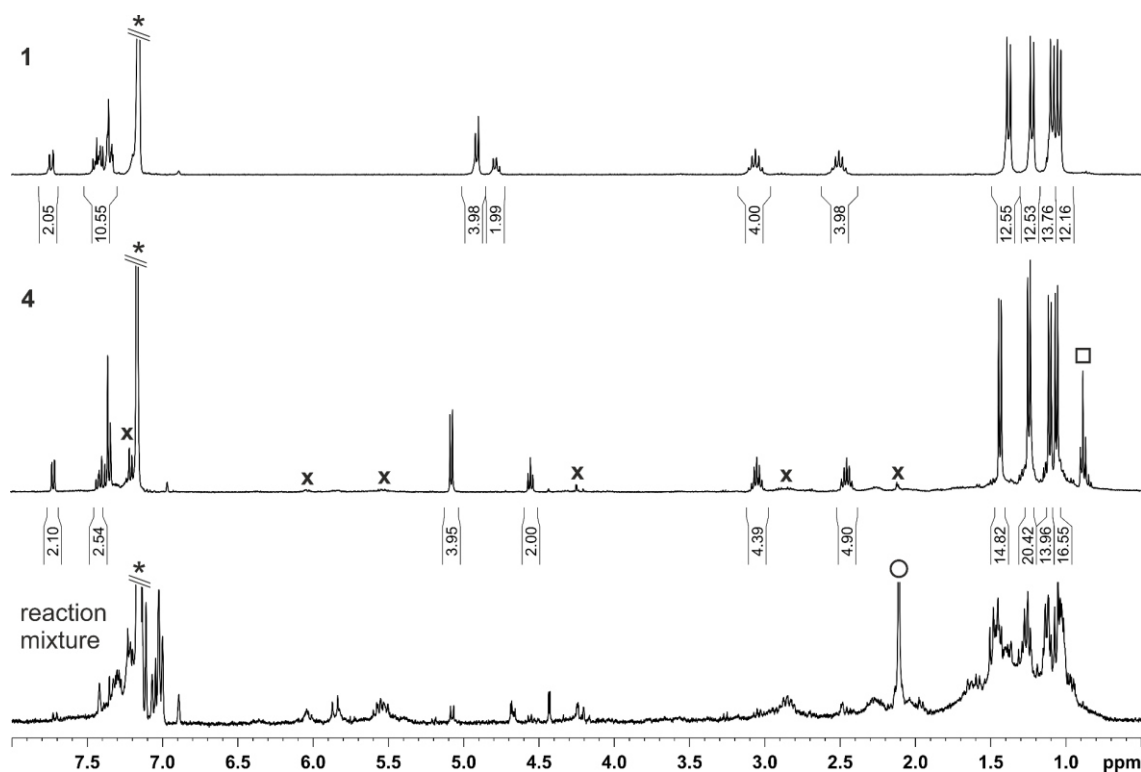
Figure 8. ^{1}H NMR spectra in C₆D₆ of *top*: [Ar'SnCo]₂ (**1**); *middle*: isolated crystals of [Ar'GeCo]₂ (**4**), *bottom*: reaction mixture of [K(thf)₀.₂][Co(η⁴-1,5-cod)₂] (**D**) with [Ar'GeCl]₂.* C₆D₆, X unknown impurities; □ *n*-hexane; ○ toluene.

2.2.2.2 Reaction of [Ar'Sn(μ-Cl)]₂ with [K(18c-6)][Fe(η⁴-1,5-cod)(η⁴-C₁₄H₁₀)]

Following the protocol that led to **1** and **4**, the formation of an analogous Fe_2Sn_2 cluster (**5**) was not observed with the Fe^- synthon $[K(18c\text{-}6)][Fe(\eta^4\text{-}1,5\text{-}cod)(\eta^4\text{-}C_{14}H_{10})]$ (3.0 equiv. with respect to **E**, 18c-6 = 18-crown-6). Only very broad signals, probably caused by residual amounts of the paramagnetic starting material or other paramagnetic by-products, are observed in the ^1H NMR spectrum of the reaction mixture. Nevertheless, a different approach, namely the reaction of $[Ar'Sn(\mu\text{-}Cl)]_2$ (**E**) with two equivalents of $[K(18c\text{-}6)][Fe(\eta^4\text{-}1,5\text{-}cod)(\eta^4\text{-}C_{14}H_{10})]$ in THF at $-90\,^\circ C$, was more promising (Scheme 4). Besides large amounts of free anthracene and [18]crown-6, the ^1H NMR spectrum of the reaction mixture (Figure 9 top) shows also minor signals (4.8 and 5.7 ppm) in the characteristic region for π-coordinating arene rings.
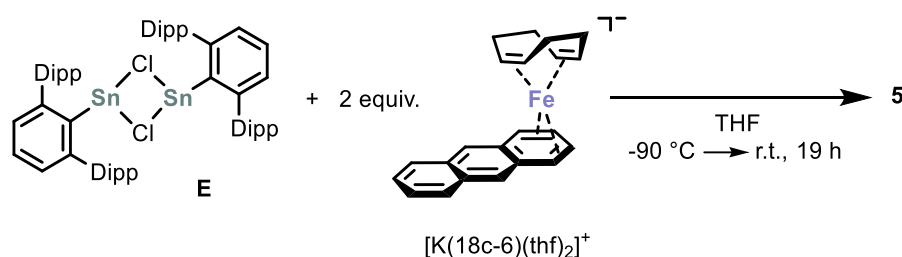
Scheme 4. Reaction of $[K(18c\text{-}6)(thf)_2][Fe(\eta^4\text{-}1,5\text{-}cod)(\eta^4\text{-}C_{14}H_{10})]$ with $\{Ar'Sn(\mu\text{-}Cl)\}_2$.
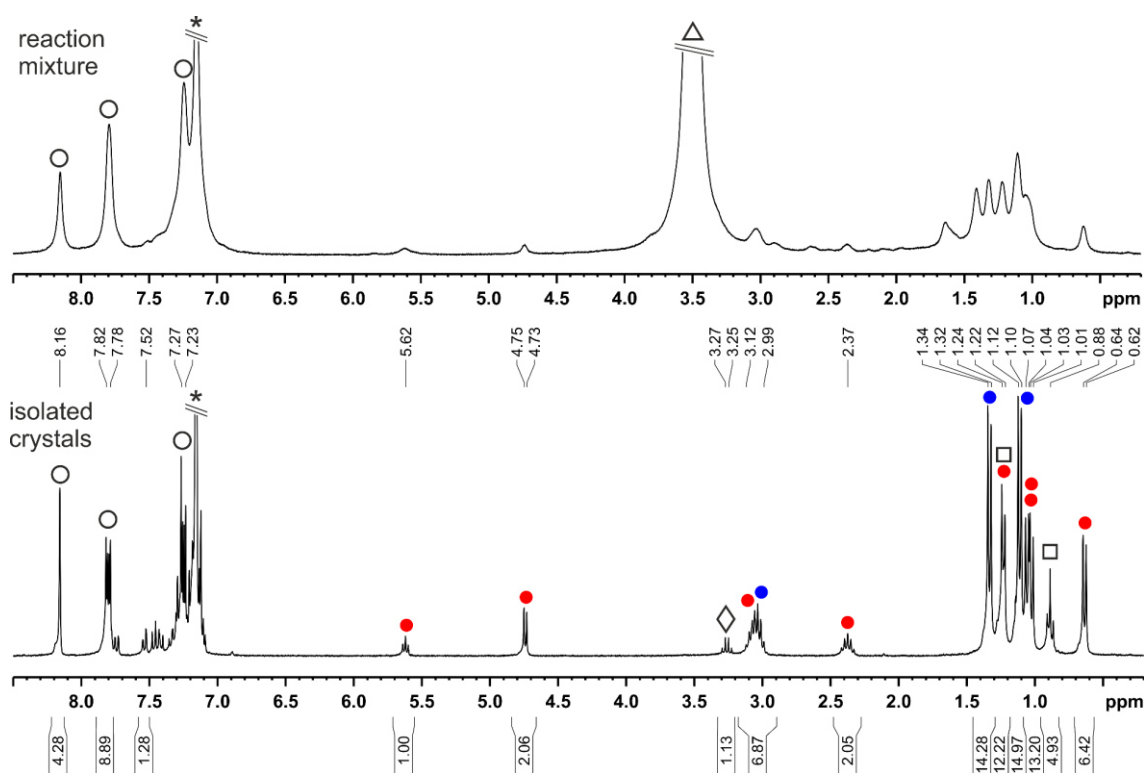
Figure 9. ^1H NMR spectra in C_6D_6 of *top*: reaction mixture of $[K(18c\text{-}6)(thf)_2][Fe(\eta^4\text{-}1,5\text{-}cod)(\eta^4\text{-}C_{14}H_{10})]$ with $\{Ar'Sn(\mu\text{-}Cl)\}_2$, *bottom*: isolated crystals of **5** with two different sets of Ar' ligand protons (● vs. ●).* C_6D_6, ○ anthracene, Δ 18c-6, ◊ Et₂O, □ *n*-hexane.

A few dark violet to red brown crystals were obtained after work-up from combined concentrated Et_2O extracts. The yield was not determined, since the isolated crystals of **5** were contaminated by considerable amounts of anthracene, Et_2O and *n*-hexane.

XRD analysis of these crystals revealed the formation of a terphenyl containing product **5** with an unclear composition. The solid-state molecular structure of compound **5** is depicted in Figure 10 center and shows a disordered centrosymmetric rhomboidal cluster core. Structural refinement revealed the presence of six metal sites with 50% occupancy each: four terphenyl-bound tin positions, and two locations for iron coordinated by the flanking Dipp groups in the η^6-fashion. Thus, the total molecular composition of the analyzed crystals is $[Ar'_2Sn_2Fe]$. Interestingly, this array can be realized in two plausible ways depending on the chemical connectivity of the metal sites. In the first scenario (Figure 10a), $[Ar'_2Sn_2Fe]$ features a triangular Sn_2Fe core **5a**, which is disordered with its symmetry generated congener. Alternatively, $[Ar'_2Sn_2Fe]$ could be described as a 1:1 co-crystallization of the distannylidyne diiron complex $[Ar'_2Sn_2Fe_2]$ (**5b**) with the well-known distannyne compound $[Ar'SnSnAr']$ (**5c**) (Figure 10b).[3] **5a** features two distinct iron−tin bonds. The Fe1−Sn2 (= Fe2−Sn3) distance of 2.621(2) Å is in the range typical for Fe−Sn single bonds ($\sum r_{cov}$ = 2.56 Å), whereas the Fe1−Sn4 (= Fe2−Sn1) bond length (2.297(1) Å) is remarkably short.[14] In fact, it is even shorter than predicted for a Fe≡Sn triple bond (calculated covalent triple bond radius 2.34 Å),[14] and also more than 0.1 Å shorter than the smallest reported Fe−Sn distance (2.408(1) Å), which was found in $[Fe(CO)_4\{Sn(OAr)_2\}]$.[50] Similar to the Co_2Sn_2 compound **1**, the elongated Sn1−Sn3 (= Sn2−Sn4) distance (3.057(2) Å), presumably indicates a weak covalent Sn−Sn interaction. The proposed distannylidyne diiron compound **5b** shows a rare linear geometry around tin (Fe1−Sn4−C2 = Fe2−Sn1−C1 176.7(1) °), that has so far only been found in some stannylidyne complexes published by *Filippou* et al.[9,51] Interactions between Sn1−Sn4 and Fe1−Sn1(= Fe2−Sn4), respectively, should be weak, since they are fairly remote (Sn1−Sn4 3.624 Å, Fe1−Sn1 3.237 Å). The bond parameters of the co-crystallized distannyne **5c** slightly differ from the original data reported by *Power* and co-workers. In **5c**, the Sn2−Sn3 bond (2.527(2) Å) is shorter, and the C1−Sn2−Sn3 angle (145.0(1) °) is wider, compared to *Power*'s data (2.6675(4) Å, 125.24(7) °).[3]

45
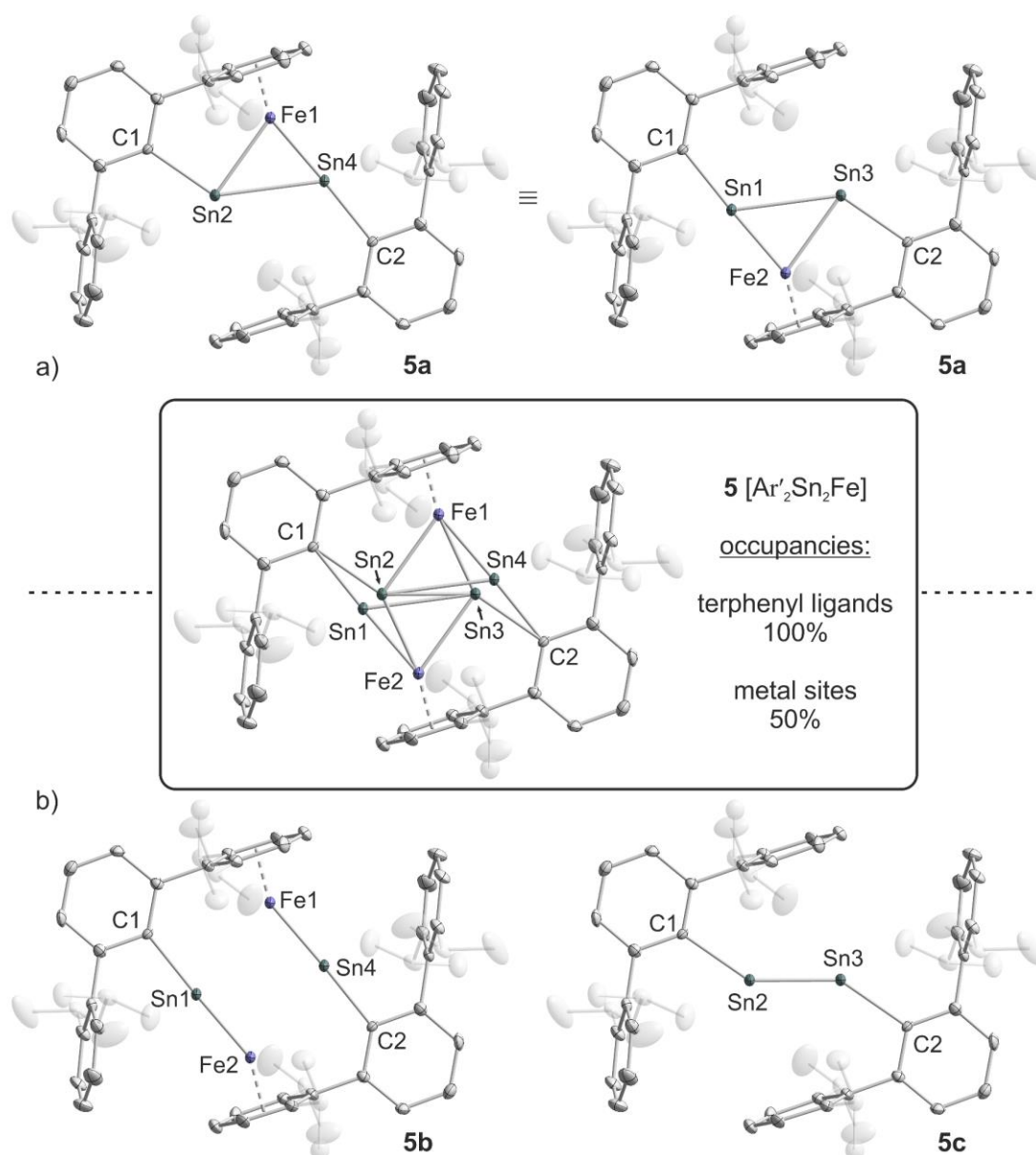
Figure 10. Displacement ellipsoid (50%) drawings of the iron tin compound **5** along with the two conceivable compositions (a and b). The metal atoms Fe1, Fe2, Sn1, Sn2, Sn3 and Sn4 feature only 50% occupancy. The Ar' ligands are fully occupied. The hydrogen atoms are not shown for clarity. Selected bond lengths [Å] and angles [°]: Sn2–Sn3 2.527(2) Sn1–Sn3 = Sn2–Sn4 3.057(2) Fe1–Sn2 = Fe2–Sn3 2.621(2), Fe1–Sn3 = Fe2–Sn2 2.349(2), Fe1–Sn4 = Fe2–Sn1 2.297(1), C1–Sn1 = C2–Sn4 2.131(4), C1–Sn2 = C2–Sn3 2.238(4), Fe1–Dipp(c) = Fe2–Dipp(c) 1.505(1), Fe1–Sn4–C2 = Fe2–Sn1–C1 176.7(1), C1–Sn2–Sn3 = C2–Sn3–Sn2 145.0(1), Sn2–Fe1–Sn4 = Sn3–Fe2–Sn1 76.55 (5), C1–Sn2–Sn4 = C2–Sn3–Sn1 137.9(1), C2–Sn4–Sn2 = C1–Sn1–Sn3 121.4(1), Fe1–Sn2–Sn4 = Fe2–Sn3–Sn1 46.96(3), Fe1–Sn4–Sn2 = Fe2–Sn1–Sn3 56.49(3).

The ^{1}H NMR spectrum of the isolated crystals recorded in C_6D_6 shows two characteristic sets of signals in an integral ratio of 1:1 that correspond to two different terphenyl substituents (Figure 9 bottom). One set (marked red) closely resembles the Ar' signal set of **1**: four doublets (0.63, 1.02, 1.06 and 1.13 ppm) and two septets (2.37 and 3.12 ppm)

for two chemically inequivalent *i*Pr groups, and the doublet and triplet at 4.74 and 5.62 ppm, respectively, that arise from the shielded arene protons of the flanking Dipp group π-coordinating to iron. The other set (marked in blue) can be assigned to a classical terphenyl ligand with two chemically and magnetically equivalent Dipp substituents. It has so far been impossible to determine whether the two different Ar′ ligands are present in the same molecule (See Figure 10, **5a**) or bound to two different symmetric species present in an equimolar ratio (**5b** = red and **5c** = blue). Notably, the ^{1}H NMR chemical shifts originally reported for the pure distannyne [Ar′SnSnAr′] in C_6D_6 solution[3] slightly differ from the experimental values assigned to **5c** (blue). According to the previous work, a septet for the methine protons of the *i*Pr groups arises at 2.87 ppm and a triplet for the *para*-protons of the terphenyl substituent resonates at 6.22 ppm.[3] Herein, the experimental chemical shift of the corresponding septet is somewhat higher (2.99 ppm) and in the range between 5.6 and 7.0 ppm, no signal was found at all.

Geometry optimizations of both possible iron tin compounds **5a** and **5b** were performed with the ORCA Program package[52] at the BP86-D3BJ/def2-TZVP+def2-ECP(Sn) level of theory.[27,28,31,32,53] While the structural parameters in the optimized structure **5a-opt** are very close to the crystallographically determined values (Figure 11), the optimized structure **5b-opt** is drastically different from **5b**. The Sn1−Fe1, Sn2−Fe2 (2.540 and 2.539 Å) and Sn1−Sn2 (3.116 Å) distances are considerably smaller, whereas the Fe1−Sn2 and Fe2−Sn1 (2.352 and 2.353 Å) bonds are longer compared to their respective equivalent in **5b** (c.f. Sn···Sn 3.624, Fe1−Sn1 3.237 and Fe2−Sn1 2.297(1) Å). Moreover, the center of symmetry is not retained and **5b-opt** features a bent "butterfly" like Sn₂Fe₂ core (Sn1−Fe1−Sn2−Fe2 torsion angle 42.0°).
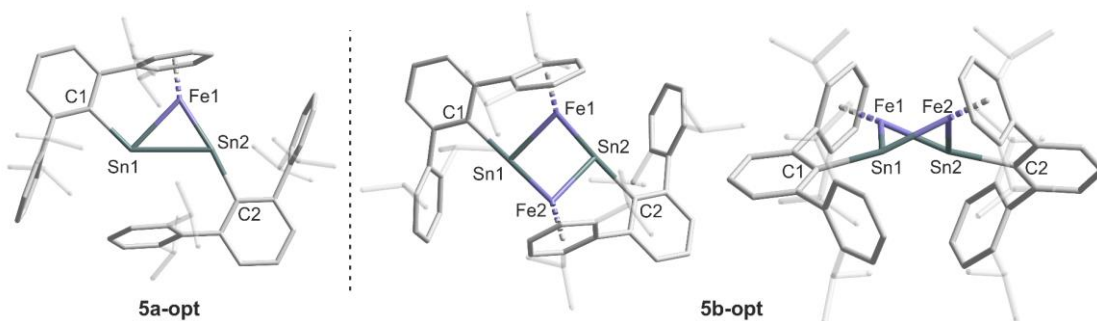
Figure 11. Geometry optimized structures of **5a-opt** (left) and **5b-opt** (center: top view, right: side view) calculated at the BP86-D3BJ/def2-TZVP+def2-ECP(Sn) level of theory. The hydrogen atoms are not shown for clarity. Selected bond lengths [Å] and angles [°] for **5a-opt**: Sn1−Sn2 3.086, Sn1−Fe1 2.660, Sn2−Fe1 2.295, C1−Sn1 2.234, C2−Sn2 2.177, C1−Sn1−Sn2 135.4, C2−Sn2−Sn1 116.8. for **5b-opt**: Sn1···Sn2 3.116, Fe1···Fe2 3.216, Sn1−Fe1 2.540, Sn2−Fe2 2.539, Sn1−Fe2 2.353, Sn2−Fe1 2.352, Sn1−C1 2.156, Sn2−C2 2.156, C1−Sn1−Fe2 168.9, C2−Sn2−Fe1 168.5, Sn1−Fe1−Sn2−Fe2 42.0.

In summary, the synthetic protocol that led to the iron tin cluster compound **5** could so far not be optimized and the separation of the by-products 18c-6 and anthracene is rather challenging due to similar solubility. The true composition of **5** remains ambiguous, since neither X-ray crystallography, nor the ^{1}H NMR spectroscopic analysis gave sufficient experimental evidence to distinguish, whether it is the disordered triangular Sn_2Fe compound **5a**, or a co-crystallized mixture of the distannylidyne complex **5b** and the distannyne **5c**. However, the latter option seems to be less likely, since both, the bond parameters and the ^{1}H NMR spectroscopic data of **5c** differ from the values originally reported of the pure distannyne. Moreover, the geometry optimizations rather support the presence of the triangular compound **5a** than the dinuclear distannylidyne compound **5b**. To better ascertain the structure of **5**, several further experiments and analyses, such as mass spectrometry, ^{119}Sn NMR and Mössbauer spectroscopy, need to be performed. Such studies have so far been hampered by the unselective synthesis **5**, which only provides access to very low amounts of product.

2.3 Conclusion

In conclusion, we successfully used the anionic cobaltate salt $[K(thf)_{0.2}][Co(\eta^4\text{-}1,5\text{-cod})_2]$ (**D**) as a Co^- source for the synthesis of the unique Co_2Sn_2 cluster **1**. We further gathered evidence for the formation of the related Co_2Ge_2 cluster **4** but its isolation as a pure compound has hitherto been unsuccessful. The reaction of the anionic ferrate salt $[K(18c\text{-}6)][Fe(\eta^4\text{-}1,5\text{-cod})(\eta^4\text{-}C_{14}H_{10})]$ with $[Ar'Sn(\mu\text{-Cl})]_2$ (**E**) gave a different outcome compared to **1**. However, it could not conclusively be determined if the product compound is the disordered triangular Sn_2Fe compound **5a** or a co-crystallized mixture of the distannylidyne complex **5b** and the distannyne **5c**.

Nevertheless, the synthesis of **1**, **4** and **5** illustrates a promising avenue to new bimetallic species with strong intermetallic bonding. The application of this synthetic strategy to a range of further other metalate anions and metal halides available across the periodic table may lead to a rich family of new heterobimetallic clusters, which may possess interesting electrochemical properties as demonstrated by the reversible oxidation of **1** with $[Cp_2Fe][BAr^F_4]$. Exemplified by the synthesis of the ternary cluster **3** from the reaction of **1** and white phosphorus, we also anticipate a rich reaction chemistry of these heterobimetallic species. Investigations in these directions are in hand.

2.4 Supporting Information

2.4.1 General Procedures

All experiments were performed under an atmosphere of dry argon, by using standard Schlenk and glovebox techniques. Solvents were purified, dried, and degassed with an MBraun SPS800 solvent purification system. NMR spectra were recorded on Bruker Avance 400 and 600 spectrometers at 300 K and internally referenced to residual solvent resonances. $^{31}P\{^{1}H\}$ and ^{31}P NMR spectra were referenced externally to 85% $H_3PO_{4(aq.)}$. The assignment of the ^{1}H and ^{13}C NMR signals was confirmed by two-dimensional (COSY, HSQC, HMBC and ROESY) experiments. Melting points were measured on samples in sealed capillaries on a Stuart SMP10 melting point apparatus. UV/vis spectra were recorded on an Ocean Optics Flame Spectrometer. Elemental analyses were determined by the analytical department of Regensburg University. The starting materials $[K(thf)_{0.2}][Co(\eta^{4}\text{-}1,5\text{-cod})_2]$,[10] $\{Ar'Sn(\mu\text{-Cl})\}_2$,[20] $(Ar'GeCl)_2$,[20] $[K(18c\text{-}6)(thf)_2][Fe(\eta^{4}\text{-}1,5\text{-cod})(\eta^{4}\text{-}C_{14}H_{10})]$,[11] were prepared according to literature procedures.

2.4.2 NMR Simulations

The $^{31}P\{^{1}H\}$ NMR spectrum of compound **3** was fitted using the full lineshape iteration of gNMR version 5.0.6.0 in order to determine the $^{31}P\text{-}^{31}P$ and $^{31}P\text{-}^{119}Sn$ coupling constants.[54] The convergence was only achieved if coupling constants close to zero (< 1 Hz) were fixed. These values are omitted in the NMR report.

2.4.3 Synthesis and Characterization

2.4.3.1 Synthesis of [Ar'SnCo]₂ (1)
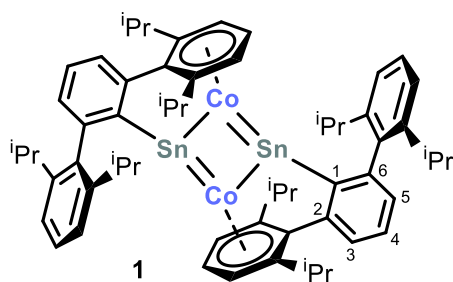
A pale yellow suspension of $[K(thf)_{0.2}][Co(\eta^{4}\text{-}1,5\text{-cod})_2]$ (379 mg, 1.15 mmol, 3.0 equiv.) in toluene (10 mL) was added dropwise to a bright orange solution of $\{Ar'Sn(\mu\text{-Cl})\}_2$ (424 mg, 0.38 mmol, 1.0 equiv.) in 10 mL toluene at −30 °C. The mixture slowly turned red and was stirred for 20 h upon warming to room temperature. The resulting dark brown reaction mixture was filtered and all volatiles were removed *in vacuo*. The dark brown residue was washed with Et₂O (23 x 1 mL) and extracted into benzene (25 x 2 mL). Concentrating the dark

green brown solution to ca. 5 mL by slow evaporation over six weeks afforded dark green to black crystals that were isolated and washed quickly with cold *n*-pentane (2 mL). Yield: 184 mg (42%).

M.p. 262 °C (decomposition to a black solid). **UV/vis** (THF, λ_{max} / nm, ε_{max} / L·mol^{-1}·cm^{-1}): 280sh (58000), 315 (41000), 415 (22000), 470sh (15000), 680 (6300). **^{1}H NMR** (600.03 MHz, 300 K, THF-d_8, in ppm): δ = 0.88 (d, $^3J_{HH}$ = 6.9 Hz, 12H, −CH(CH_3)$_2$ of C^2−Dipp), 1.00 (d, $^3J_{HH}$ = 6.7 Hz, 12H, −CH(CH_3)$_2$ of C^2−Dipp), 1.15 (d, $^3J_{HH}$ = 6.8 Hz, 12H, −CH(CH_3)$_2$ of C^6−Dipp), 1.19 (d, $^3J_{HH}$ = 6.9 Hz, 12H, −CH(CH_3)$_2$ of C^6−Dipp), 2.26 (sept, $^3J_{HH}$ = 6.8 Hz, 4H, −CH(CH$_3$)$_2$ of C^2−Dipp), 2.82 (sept, $^3J_{HH}$ = 6.8 Hz, 4H, −CH(CH$_3$)$_2$ of C^6−Dipp), 4.56 (t, $^3J_{HH}$ = 6.3 Hz, 2H, C^4−H of C^2−Dipp), 4.75 (d, $^3J_{HH}$ = 6.3 Hz, 4H, C^{3,5}−H of C^2−Dipp), 7.28 (d, $^3J_{HH}$ = 7.3 Hz, 2H, C^5−H), 7.32 (d, $^3J_{HH}$ = 7.8 Hz, 4H, C^{3,5}−H of C^6−Dipp), 7.42 (t, $^3J_{HH}$ = 7.7 Hz, 2H, C^4−H of C^6−Dipp), 7.56 (t, $^3J_{HH}$ = 7.4 Hz, 2H, C^4−H), 7.70 (d, $^3J_{HH}$ = 7.4 Hz, 2H, C^3−H). **^{13}C{^{1}H} NMR** (150.88 MHz, 300 K, THF-d_8, in ppm): δ = 23.8 (s, −CH(CH$_3$)$_2$ of C^2−Dipp), 23.9 (s, −CH(CH$_3$)$_2$ of C^6−Dipp), 29.5 (s, −CH(CH$_3$)$_2$ of C^2−Dipp), 31.3 (s, −CH(CH$_3$)$_2$ of C^6−Dipp), 84.0 (s, $C^{3,5}$ of C^2−Dipp), 87.9 (s, C^4 of C^2−Dipp), 112.0 (s, $C^{2,6}$ of C^2−Dipp), 115.1 (s, C^1 of C^2−Dipp), 123.2 (s, $C^{3,5}$ of C^6−Dipp), 126.9 (s, C^5), 127.5 (s, C^4), 128.5 (s, C^4 of C^6−Dipp), 128.6 (s, C^3), 142.1 and 142.3 (s, C^2 and C^1 of C^6−Dipp), 147.6 (s, $C^{2,6}$ of C^6−Dipp), 149.5 (s, C^6), 158.3 (s, C^1). **Elemental analysis** calcd. for C$_{60}$H$_{74}$Co$_2$Sn$_2$ (Mw = 1150.54 g·mol^{-1}) C 62.64, H 6.48; found C 62.34, H 6.13.

2.4.2.2 Synthesis of [Ar'$_2$Sn$_2$Co$_2$][BAr$^F_4$] (2[BAr$^F_4$])
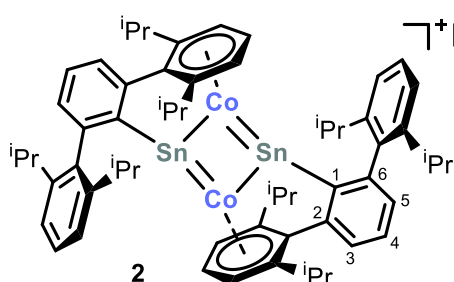
A dark blue solution of [Cp$_2$Fe][BAr$^F_4$] (46 mg, 0.044 mmol, 1.0 equiv.) in THF (2.5 mL) was added dropwise to a dark yellow suspension of **1** (50 mg, 0.043 mmol, 1.0 equiv.) in THF (2.5 mL) at room temperature. The mixture immediately turned dark red-brown and was stirred for 14 h. All volatiles were removed *in vacuo* and the dark brown residue was washed with *n*-hexane (15 x 1 mL) to remove the by-product ferrocene. The residue was extracted into Et$_2$O (6 x 1 mL) and the combined dark red brown extracts were filtered. The solvent was removed and the dark red-brown solid was carefully dried *in vacuo*. Yield: 52 mg (59%).

M.p. 219 °C. **Effective magnetic moment** (THF-d_8): μ_{eff} = 3.1(1) μ_B. **¹H NMR** (400.13 MHz, 300 K, THF-d_8, in ppm): δ = −1.36 (br s, 7H), 1.09 (s, 5H), 2.79 (s, 1H), 3.96 (br s, 3H), 7.56 (s, 4H), 7.77 (s, 6H), 8.57 (br s, 4H), 12.63 (br s, 1H). **Elemental analysis** calcd. for $C_{92}H_{86}BCo_2F_{24}Sn_2$ (Mw = 2013.76 g·mol⁻¹) C 54.87, H 4.30; found C 54.96, H 4.41.

2.4.2.3 Synthesis of [Ar′₂Sn₂Co₂P₄] (3)
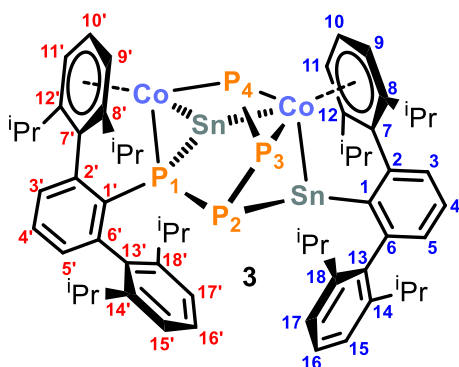
Solid P₄ (26 mg, 0.210 mmol, 1.1 equiv.) was added to a dark green brown suspension of **1** (214 mg, 0.186 mmol, 1 equiv.) in toluene (20 mL) at room temperature. The reaction mixture slowly turned dark red brown upon stirring for 18 h. The solvent was removed and the resulting residue was extracted into cyclohexane (5 x 1 mL). The dark red brown solutions were combined, filtered and reduced to ca. 2 mL. Dark brown microcrystals of **3** were isolated after storage over one day and dried *in vacuo*. Yield: 192 mg (76%).

M.p. 216 °C (decomposition to a black oil). **UV/vis** (THF, λ_{max} / nm, ε_{max} / L·mol⁻¹·cm⁻¹): 275 (32000), 350sh (18000), 390sh (13000), 430sh (9000). **¹H NMR** (400.13 MHz, 300 K, THF-d_8, in ppm): δ = 0.59 (d, ³J_{HH} = 6.8 Hz, 3H, C¹⁸′−CH(C*H*₃)₂), 0.83 (d, ³J_{HH} = 6.8 Hz, 3H, C¹⁸−CH(C*H*₃)₂), 0.93 (d, ³J_{HH} = 6.7 Hz, 3H, C¹²−CH(C*H*₃)₂), 0.97-1.01 (m, 9H, C¹⁴′−CH(C*H*₃)₂ overlapping with C¹⁴−CH(C*H*₃)₂ and C⁸′−CH(C*H*₃)₂), 1.06 and 1.08 (d, ³J_{HH} = 6.7 Hz, 6H, C⁸−CH(C*H*₃)₂), 1.13 (d, ³J_{HH} = 6.8 Hz, 3H, C¹²′−CH(C*H*₃)₂), 1.18 (d, ³J_{HH} = 6.8 Hz, 3H, C¹⁸−CH(C*H*₃)₂), 1.25 (d, ³J_{HH} = 6.8 Hz, 3H, C¹⁴′−CH(C*H*₃)₂), 1.28 (d, ³J_{HH} = 6.8 Hz, 3H, C¹⁸′−CH(C*H*₃)₂), 1.40 (d, ³J_{HH} = 6.8 Hz, 3H, C⁸′−CH(C*H*₃)₂), 1.48 (d, ³J_{HH} = 7.0 Hz, 3H, C¹⁴−CH(C*H*₃)₂), 1.57 (d, ³J_{HH} = 6.8 Hz, 3H, C¹²′−CH(C*H*₃)₂), 1.71 (d, ³J_{HH} = 6.9 Hz, 3H, C¹²−CH(C*H*₃)₂), 1.84 (sept, ³J_{HH} = 6.8 Hz, 1H, C⁸′−C*H*(CH₃)₂), 2.20 (sept, ³J_{HH} = 6.8 Hz, 1H, C¹⁸′−C*H*(CH₃)₂), 2.27 (sept, ³J_{HH} = 6.8 Hz, 1H, C¹⁴′−C*H*(CH₃)₂), 2.38 (sept, ³J_{HH} = 6.7 Hz, 1H, C⁸−C*H*(CH₃)₂), 2.46 (sept, ³J_{HH} = 6.9 Hz, 1H, C¹⁴−C*H*(CH₃)₂), 2.55 (sept, ³J_{HH} = 6.8 Hz, 1H, C¹²′−C*H*(CH₃)₂), 2.70 (sept, ³J_{HH} = 6.8 Hz, 1H, C¹⁸−C*H*(CH₃)₂), 2.77 (sept, ³J_{HH} = 6.7 Hz, 1H, C¹²−C*H*(CH₃)₂), 5.56 (t, ³J_{HH} = 6.5 Hz, 1H, C¹⁰′−*H*), 5.70 (d, ³J_{HH} = 6.4 Hz, 1H, C⁹−*H*), 5.79 (t, ³J_{HH} = 6.3 Hz, 1H, C¹⁰−*H*), 6.23 (d, ³J_{HH} = 6.6 Hz, 1H, C⁹′−*H*), 6.62 (d, ³J_{HH} = 6.2 Hz, 1H,

$C^{11}-H$), 6.65 (d, $^3J_{HH}$ = 7.3 Hz, 1H, C^5-H), 6.70 (d, $^3J_{HH}$ = 6.4 Hz, 1H, $C^{11'}-H$), 6.78 (d, $^3J_{HH}$ = 7.8 Hz, 1H, $C^{15'}-H$), 6.83-6.88 (m, 2H, $C^{17'}-H$ overlapping with $C^{5'}-H$), 7.00 (t, $^3J_{HH}$ = 7.5 Hz, 1H, C^4-H), 7.03 (t, $^3J_{HH}$ = 7.8 Hz, 1H, $C^{16'}-H$), 7.12-7.16 (m, 2H, $C^{17}-H$ overlapping with C^3-H), 7.21-7.27 (m, 2H, $C^{4'}-H$ overlapping with $C^{3'}-H$), 7.32 (d, $^3J_{HH}$ = 7.6 Hz, 1H, $C^{15}-H$), 7.43 (t, $^3J_{HH}$ = 7.7 Hz, 1H, $C^{16}-H$).

^{13}C{^{1}H} NMR (100.61 MHz, 300 K, THF-d_8): δ = 20.8-21.0 (m, $C^8-CH(CH_3)_2$ overlapping with $C^{12}-CH(CH_3)_2$), 21.7 (m, $C^{8'}-CH(CH_3)_2$ overlapping with $C^{12'}-CH(CH_3)_2$), 23.2 (s, $C^{14'}-CH(CH_3)_2$), 23.8 (d, J_{CP} = 11 Hz, $C^{18}-CH(CH_3)_2$), 24.3 (s, $C^{18'}-CH(CH_3)_2$), 24.5 (s, $C^{14}-CH(CH_3)_2$), 25.2 (d, J_{CP} = 4 Hz, $C^{12}-CH(CH_3)_2$), 25.5 (s, $C^{18'}-CH(CH_3)_2$), 25.6 (d, J_{CP} = 4 Hz, $C^{8'}-CH(CH_3)_2$), 25.9 (s, $C^{18}-CH(CH_3)_2$), 26.2 (s, $C^{12'}-CH(CH_3)_2$), 26.5 (s, $C^{14}-CH(CH_3)_2$), 26.8 (s, $C^{14'}-CH(CH_3)_2$), 27.4 (s, $C^8-CH(CH_3)_2$), 29.6 (s, $C^{12}-CH(CH_3)_2$), 30.3 (s, $C^8-CH(CH_3)_2$), 30.4 (s, $C^{8'}-CH(CH_3)_2$), 30.6-30.7 (m, $C^{18}-CH(CH_3)_2$ overlapping with $C^{18'}-CH(CH_3)_2$), 31.1 (s, $C^{12'}-CH(CH_3)_2$), 31.2 (s, $C^{14}-CH(CH_3)_2$), 31.3 (s, $C^{14'}-CH(CH_3)_2$), 87.5 (s, $C^{9'}$), 88.5 (s, C^{10}), 91.8 (s, C^{11}), 94.4 (s, $C^{10'}$), 96.8 (s, $C^{11'}$), 97.2 (s, C^9), 107.5 (s, $C^{7'}$), 114.8 (s, C^7), 117.5 (s, $C^{8'}$), 118.0 (s, C^8), 119.5 (s, $C^{12'}$), 121.0 (s, C^{12}), 122.7 (s, $C^{17'}$), 123.2, (s, C^{17}) 123.4 (s, C^{15}), 124.0 (s, $C^{15'}$), 124.6 (s, C^4), 127.3-127.4 (m, C^3 overlapping with $C^{4'}$), 128.1-128.2 (m, C^{16} overlapping with C^5 and $C^{3'}$), 129.7 (s, $C^{16'}$), 131.8 (d, $^3J_{CP}$ = 5 Hz, $C^{5'}$), 137.1 (s, $C^{13'}$), 142.6 (s, C^{13}), 142.7 (s, C^2 or C^6), 143.6 (d, $^2J_{CP}$ = 9 Hz, $C^{2'}$ or $C^{6'}$), 144.4 (d, $^2J_{CP}$ = 8 Hz, $C^{2'}$ or $C^{6'}$), 145.6 (s, $C^{18'}$), 146.3 (s, C^{14} overlapping with $C^{14'}$), 147.1 (s, C^{18}), 147.9 (s, C^2 or C^6, overlapping with d, $^1J_{CP}$ = 27 Hz, $C^{1'}$), C^1 not detected.

^{31}P{^{1}H} NMR (161.96 MHz, 300 K, THF-d_8, in ppm): δ −109.3 (1P, dd, $^1J_{P2P3}$ = −303 Hz, $^1J_{P2P1}$ = −370 Hz, ^{119}Sn satellites: $^1J_{PSn}$ = 549 Hz, P2), 15.7 (1P, br dd, Δν½ = 54 Hz, $^1J_{P2P3}$ = −303 Hz, $^1J_{P3P4}$ = −366 Hz, P3), 94.6 (1P, br d, Δν½ = 77 Hz, $^1J_{P1P2}$ = −370 Hz, ^{119}Sn satellites: $^1J_{PSn}$ = 1482 Hz, P1) 163.0 (1P, br d, Δν½ = 121 Hz, $^1J_{P4P3}$ = −366 Hz, P4). **Elemental analysis** calcd. for $C_{60}H_{74}Co_2P_4Sn_2 \cdot C_6H_{12}$ (Mw = 1358.24 g·mol^{-1}) C 58.35, H 6.38; found C 58.56, H 6.70

2.4.3.4 Synthesis of [Ar′GeCo]₂ (4)
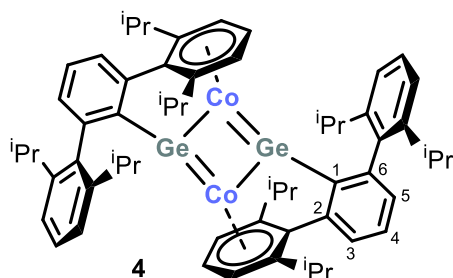
A pale yellow suspension of $[K(thf)_{0.2}][Co(\eta^4\text{-}1,5\text{-}cod)_2]$ (48 mg, 0.146 mmol, 3.0 equiv.) in toluene (1.5 mL) was added dropwise to a bright yellow solution of $(Ar′GeCl)_2$ (50 mg, 0.049 mmol, 1.0 equiv.) in 1.5 mL toluene at −30 °C. The mixture slowly turned deep yellow and was stirred for 27 h upon warming to room temperature. The resulting dark yellow green reaction mixture was filtered and all volatiles were removed *in vacuo*. The dark green brown residue was extracted into *n*-hexane (4 x 0.5 mL) and concentrated to ca. 1 mL. A few dark brown crystals were obtained after one week. The yield was not determined due to the small scale of the reaction. A ^{1}H NMR spectrum of the crystals is show in Figure 8.

^{1}H NMR (400.13 MHz, 300 K, C_6D_6, in ppm): δ = 1.06 (d, $^3J_{HH}$ = 6.8 Hz, 12H, −CH(CH_3)₂ of Dipp), 1.11 (d, $^3J_{HH}$ = 6.9 Hz, 12H, −CH(CH_3)₂ of Dipp), 1.26 (d, $^3J_{HH}$ = 6.8 Hz, 12H, −CH(CH_3)₂ of Dipp), 1.44 (d, $^3J_{HH}$ = 6.9 Hz, 12H, −CH(CH_3)₂ of Dipp), 2.45 (sept, $^3J_{HH}$ = 6.8 Hz, 4H, −CH(CH₃)₂ of Dipp), 3.05 (sept, $^3J_{HH}$ = 6.8 Hz, 4H, −CH(CH₃)₂ of Dipp), 4.55 (t, $^3J_{HH}$ = 6.4 Hz, 2H, C^4−H of C^2−Dipp), 5.07 (d, $^3J_{HH}$ = 6.4 Hz, 4H, $C^{3,5}$−H of C^2−Dipp), 7.19-7.21 (m, 4H, Ar−H), 7.34-7.43 (m, 10H, Ar−H), 7.71 (d, $^3J_{HH}$ = 7.4 Hz, 2H, Ar−H).

2.4.3.4 Reaction of {Ar′Sn(μ-Cl)}₂ (E) with [K(18c-6)(thf)₂][Fe(η^4-1,5-cod)(η^4-C₁₄H₁₀)]

A yellow solution of {Ar′Sn(μ-Cl)}₂ (50 mg, 0.045 mmol, 1.0 equiv.) in THF (2 mL) was added to a dark turquoise solution of $[K(18c\text{-}6)(thf)_2][Fe(\eta^4\text{-}1,5\text{-}cod)(\eta^4\text{-}C_{14}H_{10})]$ (72 mg, 0.091 mmol, 2.0 equiv.) in THF (2 mL) at −90 °C. The mixture slowly turned dark green and was stirred for 19 h upon warming to room temperature. The resulting dark red brown reaction mixture was evaporated to dryness and washed with *n*-hexane (10 x 1 mL). The dark brown residue was extracted into Et₂O (5 x 1 mL) and the combined dark brown extracts were filtered. Some dark red to violet crystals suitable for X-ray crystallography formed after storage for one day. The yield was not determined due to anthracene impurities and the small scale of the reaction. A ^{1}H NMR spectrum of the crystals is shown in Figure 9.

¹H NMR (300.13 MHz, 300 K, C_6D_6, in ppm): $\delta = 0.63$ (d, $^3J_{HH} = 6.9$ Hz, 6H, $-CH(CH_3)_2$ of Dipp), 1.02 (d, $^3J_{HH} = 6.9$ Hz, 6H, $-CH(CH_3)_2$ of Dipp), 1.05 (d, $^3J_{HH} = 6.8$ Hz, 6H, $-CH(CH_3)_2$ of Dipp), 1.11 (d, $^3J_{HH} = 6.8$ Hz, 12H, $-CH(CH_3)_2$ of Dipp), 1.23 (d, $^3J_{HH} = 6.7$ Hz, 6H, $-CH(CH_3)_2$ of Dipp), 1.33 (d, $^3J_{HH} = 6.7$ Hz, 6H, $-CH(CH_3)_2$ of Dipp), 2.37 (sept, $^3J_{HH} = 6.8$ Hz, 2H, $-CH(CH_3)_2$ of Dipp), 2.99-3.12 (m, 6H, $-CH(CH_3)_2$ of Dipp), 4.74 (d, $^3J_{HH} = 6.1$ Hz, 2H, Ar$-H$ of Dipp), 5.62 (t, $^3J_{HH} = 6.1$ Hz, 1H, Ar$-H$ of Dipp), 7.12-7.52 (m, Ar$-H$).

2.4.4   NMR Spectra
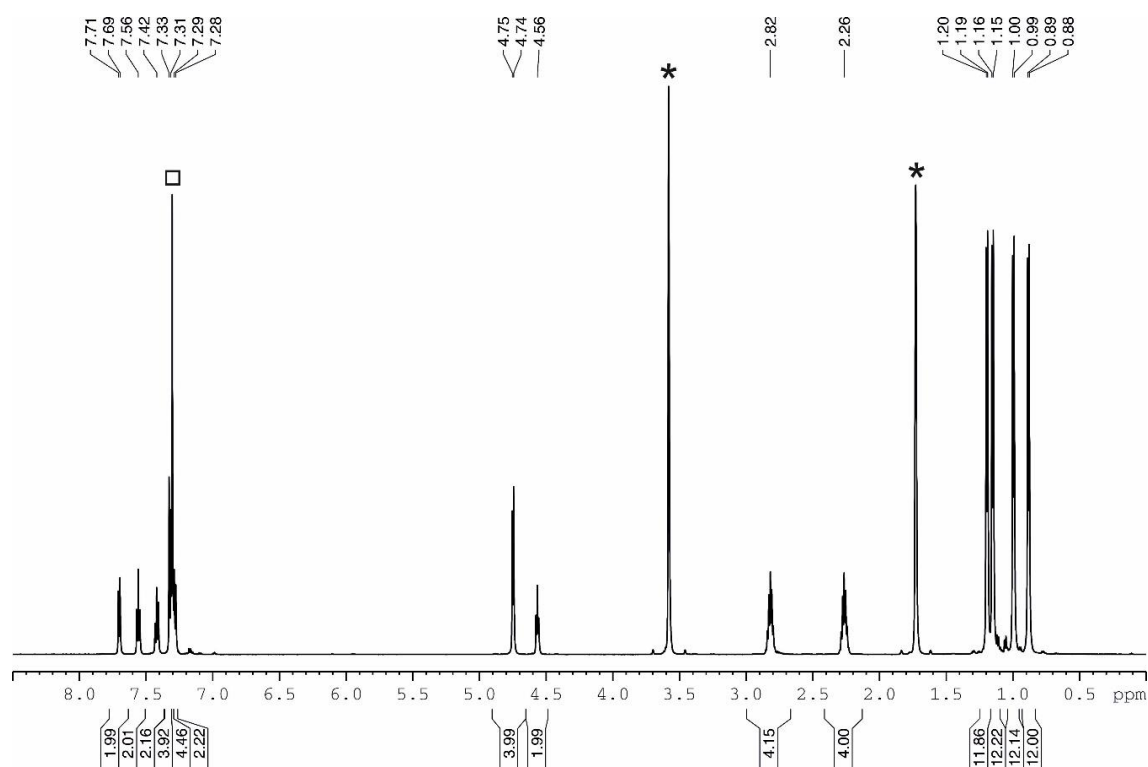
Figure S1. ^{1}H NMR spectrum (600.03 MHz, 300 K, THF-d_8) of [Ar'SnCo]$_2$ (**1**); * THF-d_8, □ benzene.
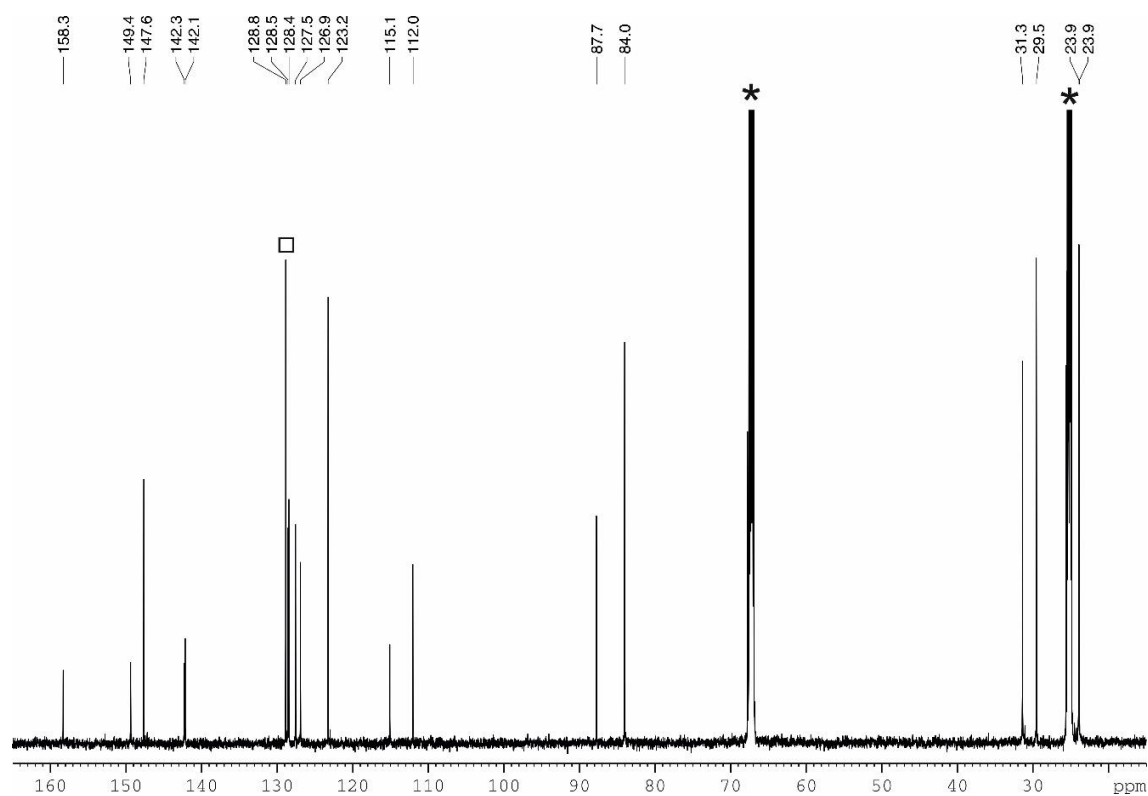
Figure S2. ^{13}C{^{1}H} NMR spectrum (150.88 MHz, 300 K, THF-d_8) of [Ar'SnCo]$_2$ (**1**); * THF-d_8, □ benzene.
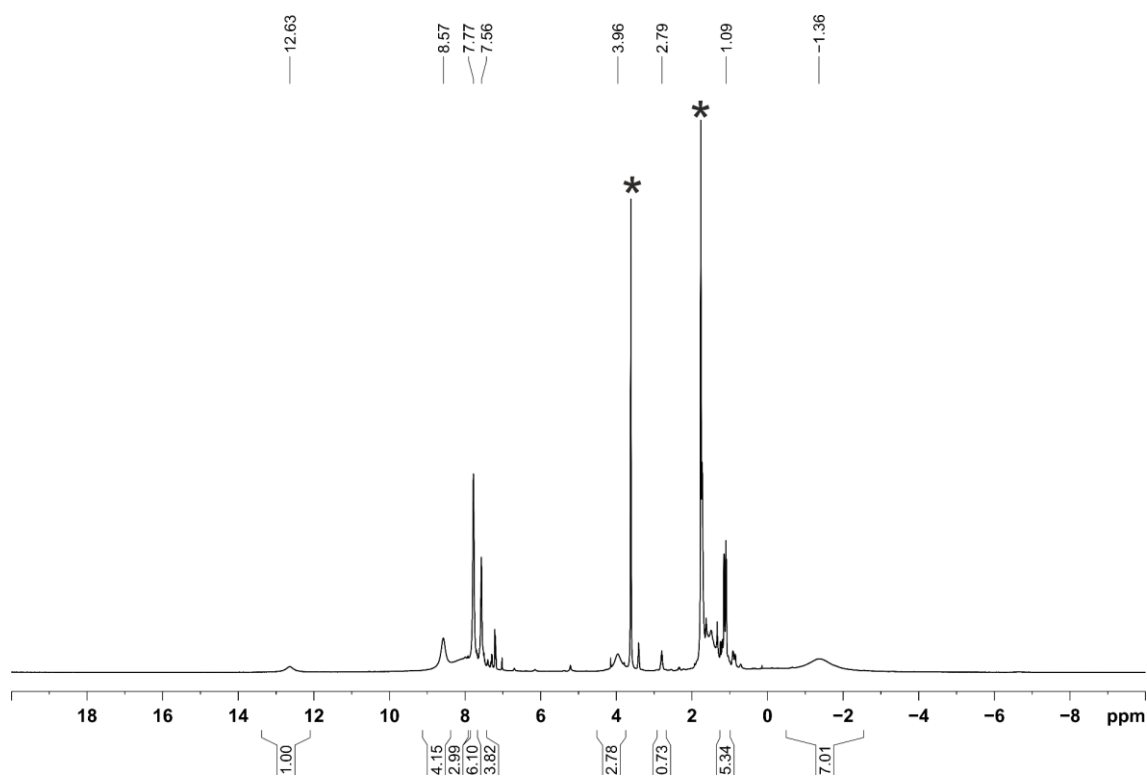
Figure S3. ¹H NMR spectrum (400.13 MHz, 300 K, THF-d_8) of [Ar'$_2$Sn$_2$Co$_2$][BAr$^F_4$] (**2**[BAr$^F_4$]); * THF-d_8.
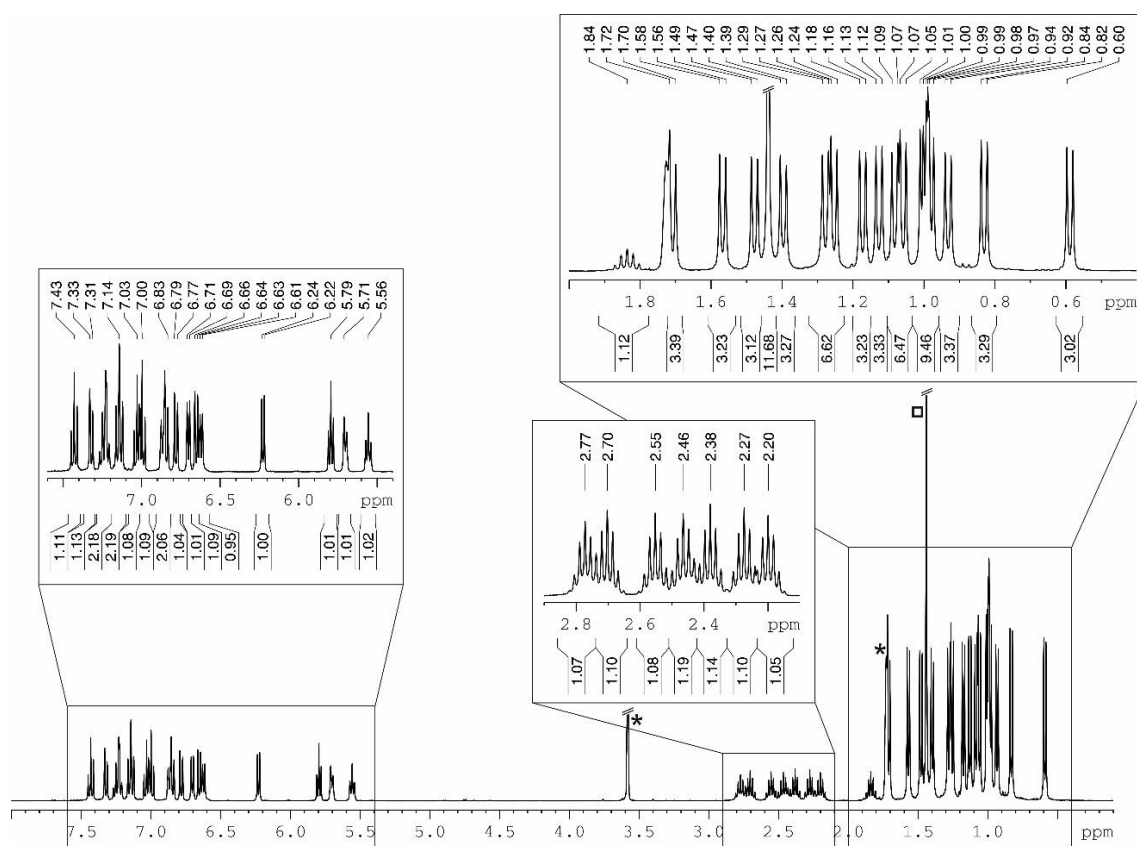
Figure S4. ¹H NMR spectrum (400.13 MHz, 300 K, THF-d_8) of [Ar'$_2$Sn$_2$Co$_2$P$_4$] (**3**); * THF-d_8, □ cyclohexane.
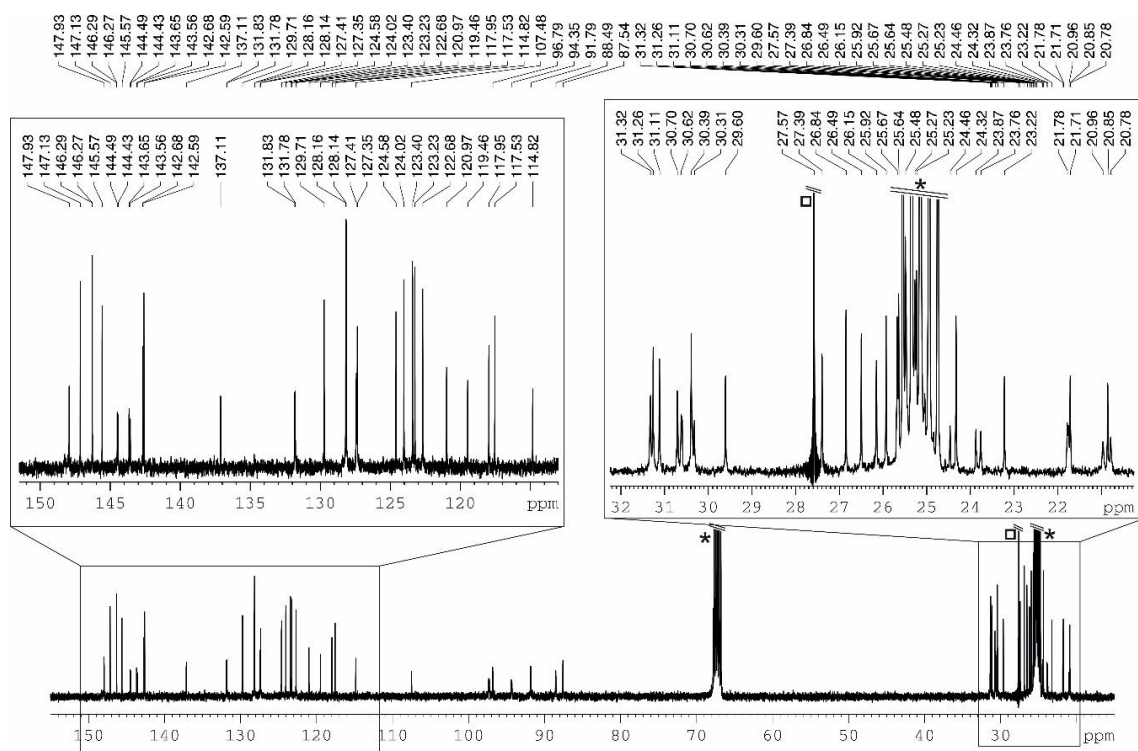
Figure S5. $^{13}C\{^1H\}$ NMR spectrum (100.61 MHz, 300 K, THF-d_8) of [Ar'$_2$Sn$_2$Co$_2$P$_4$] (**3**); * THF-d_8, □ cyclohexane.
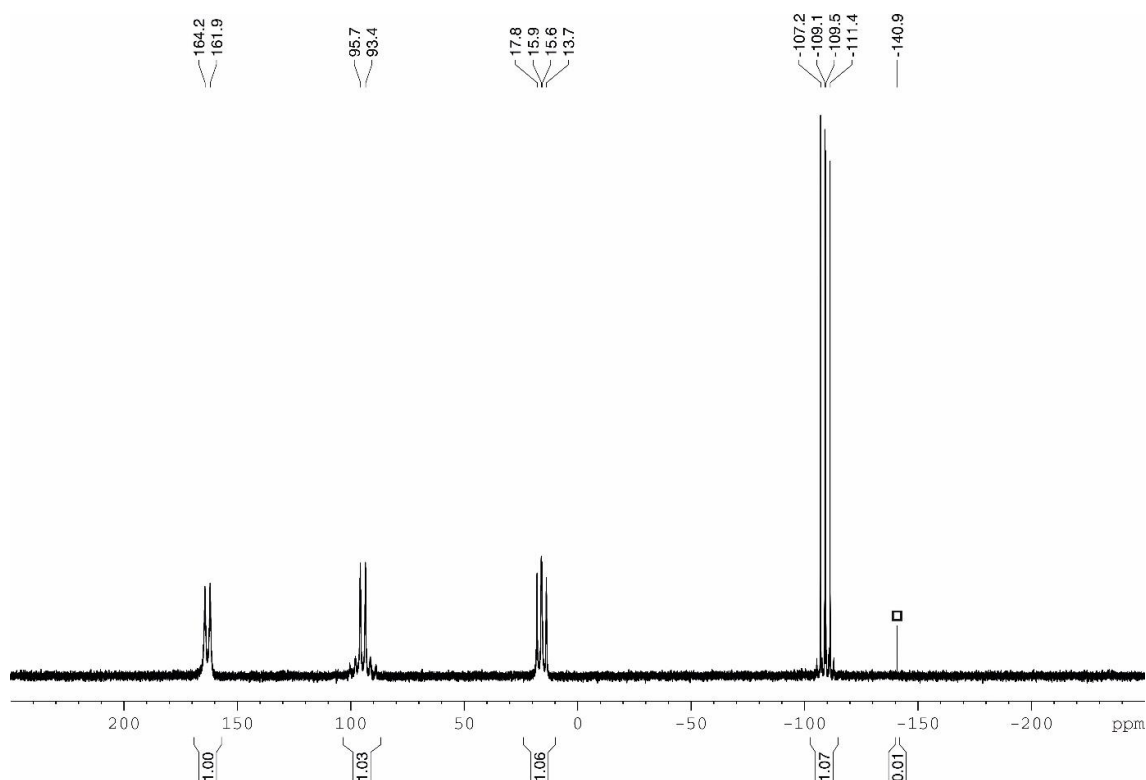
Figure S6. $^{31}P\{^1H\}$ NMR spectrum (161.98 MHz, 300 K, THF-d_8) of [Ar'$_2$Sn$_2$Co$_2$P$_4$] (**3**); □ Ar'PH$_2$.
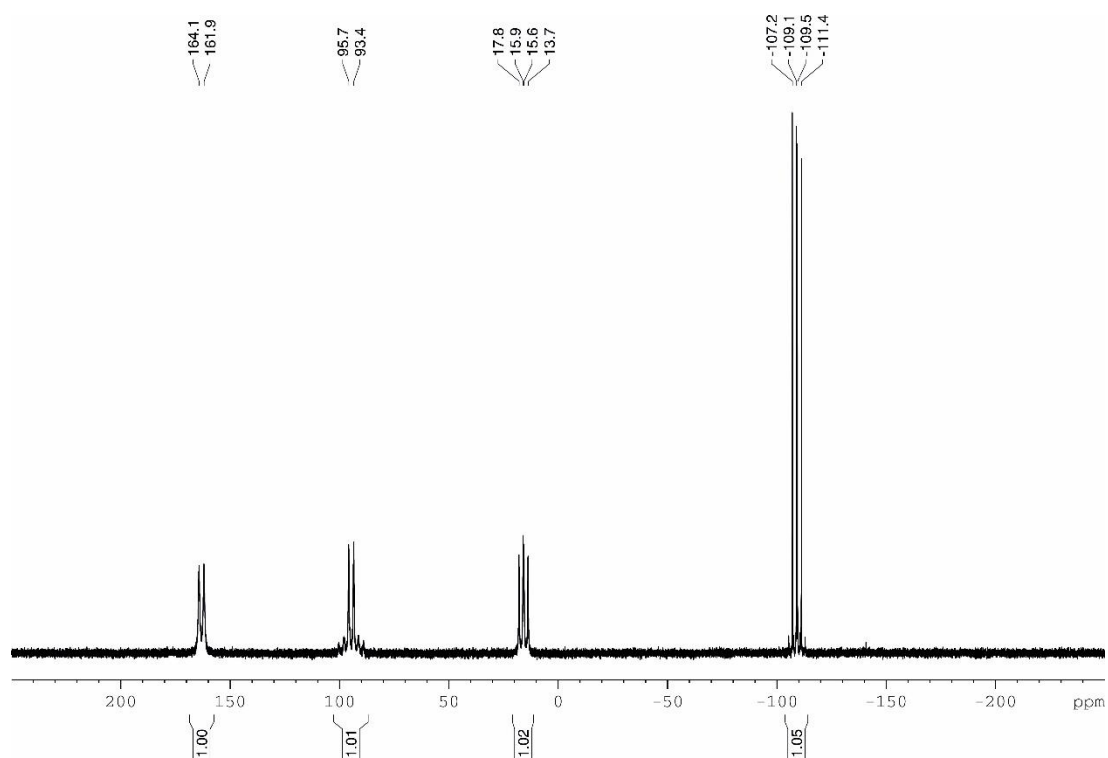
Figure S7. ^{31}P NMR spectrum (161.98 MHz, 300 K, THF-d_8) of [Ar'$_2$Sn$_2$Co$_2$P$_4$] (**3**).

2.4.5   UV/Vis Spectra
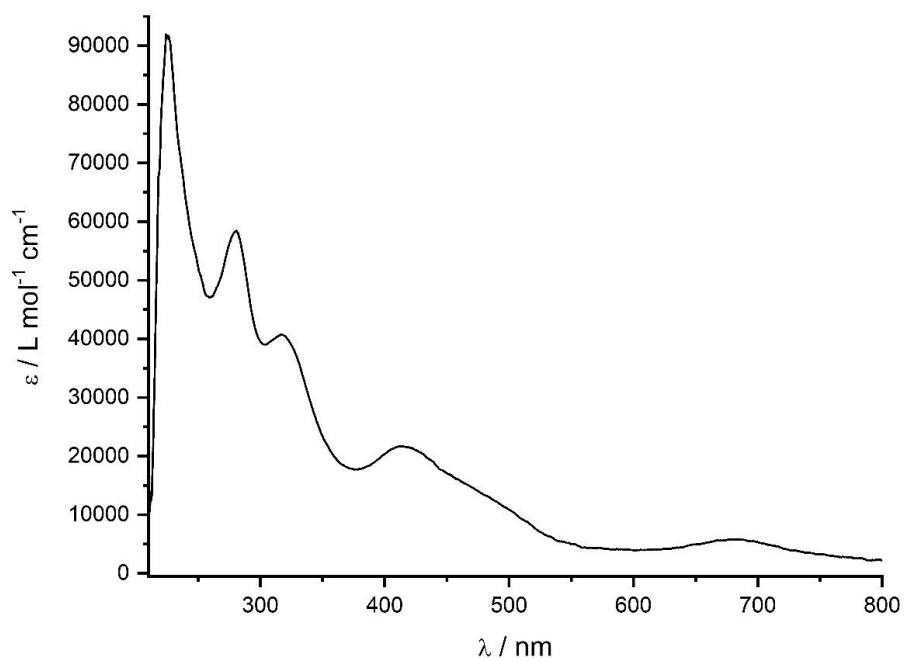
Figure S8. UV/vis spectrum of [Ar'SnCo]₂ (**1**) in THF.
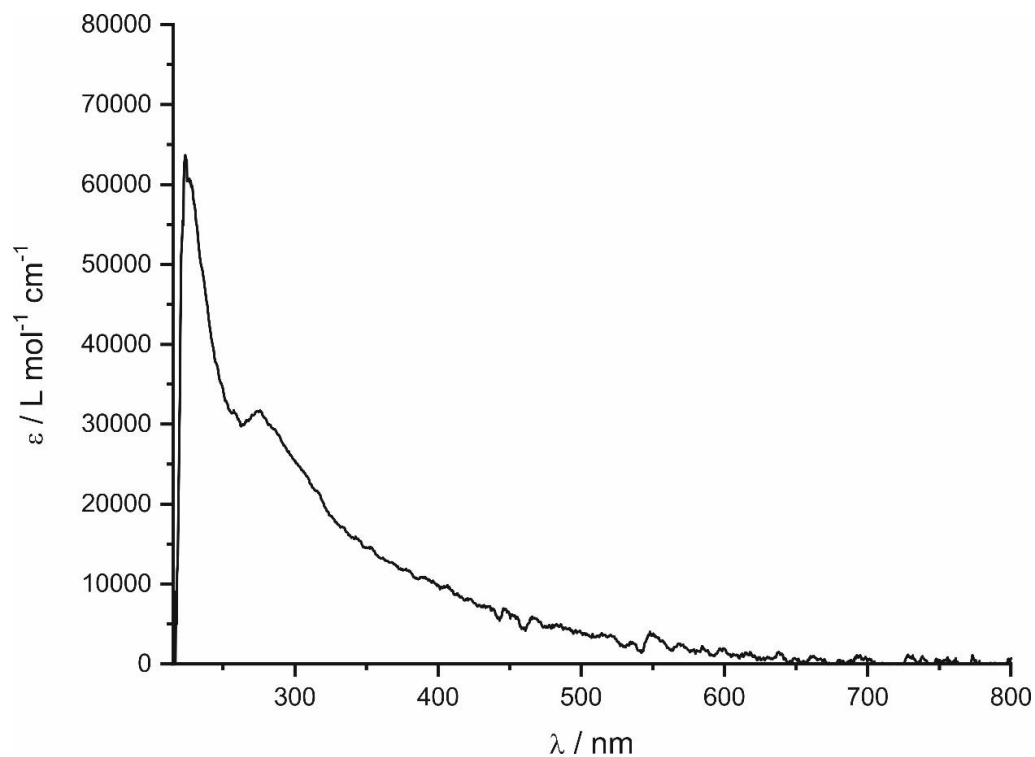
Figure S9. UV/vis spectrum of [Ar'₂Sn₂Co₂P₄] (**3**) in THF.

2.4.6 ^{119}Sn Mössbauer Spectroscopy

A Ca^{119m}SnO$_3$ source was used for the ^{119}Sn Mössbauer spectroscopic investigations. 93 mg of **1** and 170 mg of **3** were each mixed with about 500 mg KCl and were placed within two thin-walled glass containers. A palladium foil of 0.05 mm thickness was used to reduce the tin K X-rays concurrently emitted by this source. The measurements (5 d total counting time for each spectrum) were conducted in a continuous flow cryostat system (Janis Research Co LLC) at 6 K. The spectra were fitted with the WINNORMOS software package.[55]
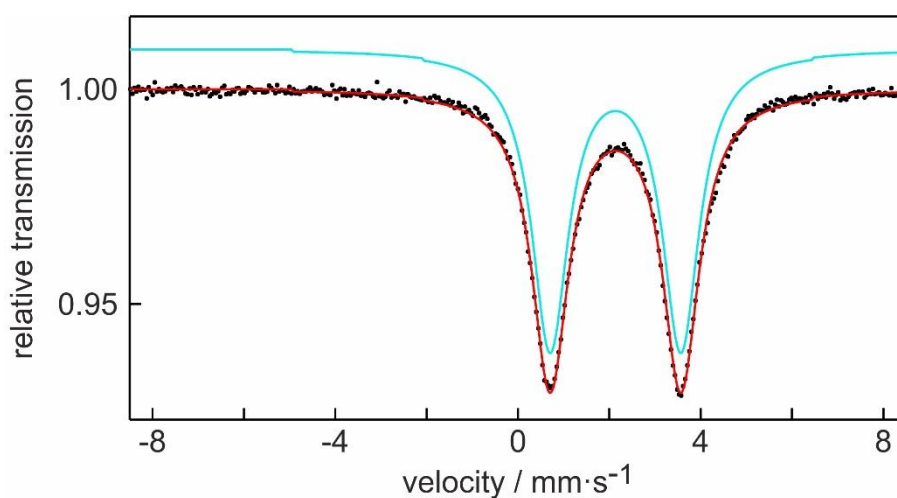
Figure S10. Experimental and simulated ^{119}Sn Mössbauer spectrum of [Ar'SnCo]₂ (**1**) at 6 K.
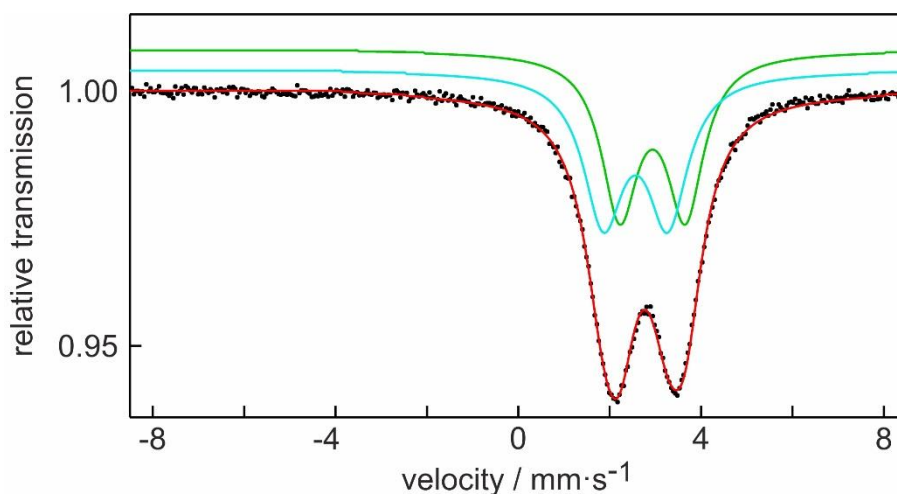
Figure S11. Experimental and simulated ^{119}Sn Mössbauer spectrum of [Ar'₂Sn₂Co₂P₄] (**3**) at 6 K.

Table S1. Fitting parameters of ^{119}Sn Mössbauer spectroscopic measurements at 5 K. δ = isomer shift, ΔE_Q = electric quadrupole splitting, Γ = experimental line width. Parameters marked with an asterisk were kept fixed during the fitting procedure.

Compound	δ (mm·s^{-1})	ΔE_Q (mm·s^{-1})	Γ (mm·s^{-1})	Area(%)
[Ar′SnCo]₂ (**1**)	2.14(1)	2.86(1)	0.98(1)	
[Ar′₂Sn₂Co₂P₄] (**3**)	2.58(1)	1.41(1)	1.07(1)	50*
	2.94(1)	1.43(1)	0.97(1)	50*

The ^{119}Sn Mössbauer spectrum of compound **3**, shown in Figure S11, was well reproduced with two doublets in a fixed ratio of 1:1 according to the two different Sn sites in this structure. The sub-signals show isomer shifts of δ = 2.58(1) mm s^{-1} (blue sub-signal) and δ = 2.94(1) mm s^{-1} (green sub-signal). Both signals show similar quadrupole splittings of ΔE_Q = 1.41(1) mm s^{-1} (blue) and ΔE_Q = 1.43(1) mm s^{-1} (green), reflecting the non-cubic site symmetries. The experimental line widths of Γ = 1.07(1) mm s^{-1} (blue) and Γ = 0.97(1) mm s^{-1} (green) are in the usual range for ^{119}Sn Mössbauer spectroscopic investigations.

2.4.7   X-Ray Crystallography

The single-crystal X-ray diffraction data were recorded on a Bruker APEX-II CCD diffractometer with Mo-K_α radiation (λ = 0.71073 Å) and an Agilent Technologies SuperNova and GV1000, TitanS2 diffractometer with Cu-K_α radiation (λ = 1.54184 Å). Either semi-empirical multi-scan absorption corrections[56] or analytical ones[57] were applied to the data. The structures were solved with SHELXT[58] and least-square refinements on F^2 were carried out with SHELXL.[59] The hydrogen atoms were located in idealized positions and refined isotropically with a riding model.

CCDC 1858481 (**1**) and 1858482 (**3**) contain the supplementary crystallographic data for this paper. These data are provided free of charge by The Cambridge Crystallographic Data Centre (https://www.ccdc.cam.ac.uk/).

Table S2. Crystallographic data and structure refinement of **1** and **2**[BAr$^F_4$].

	1	**2**[BAr$^F_4$]
Empirical formula	$C_{66}H_{88}Co_2Sn_2$	$C_{92}H_{86}BCo_2F_{24}Sn_2$
Formula weight / g·mol^{-1}	1236.60	2013.65
Temperature / K	90.15(1)	123.0(1)
Crystal system	monoclinic	triclinic
Space group	$P2_1/n$	$P\bar{1}$
a / Å	12.072(2)	12.6510(2)
b / Å	20.119(2)	25.0940(4)
c / Å	12.565(2)	29.7812(4)
α /°	90	73.280(1)
β /°	99.727(2)	82.432(1)
γ /°	90	80.904(1)
V / Å^3	3007.8(6)	8903.6(2)
Z	2	4
ρ_{calc} / g cm^{-1}	1.37	1.502
μ / mm^{-1}	1.4	8.101
F(000)	1276.0	4052.0
Crystal size / mm^3	$0.501 \times 0.482 \times 0.408$	$0.323 \times 0.158 \times 0.091$
Radiation / Å	MoK$_\alpha$ ($\lambda = 0.71073$)	CuK$_\alpha$ ($\lambda = 1.54184$)
2Θ range for data collection /°	4.778 – 54.886	6.224 – 147.87
Diffractometer	Bruker APEX-II CCD	GV1000, TitanS2
Index ranges	$-15 \leq h \leq 15$	$-14 \leq h \leq 15$
	$-26 \leq k \leq 25$	$-30 \leq k \leq 30$
	$-16 \leq l \leq 16$	$-37 \leq l \leq 37$
Reflections collected	36305	99842
Independent reflections	6867 [R$_{int}$ = 0.0351, R$_{sigma}$ = 0.0251]	34819 [R$_{int}$ = 0.0363, R$_{sigma}$ = 0.0355]
Data/restraints/parameters	6867/0/451	34819/118/2276
Goodness-of-fit on F^2	1.311	1.010
Final R indexes [I>=2σ (I)]	R$_1$ = 0.0392, wR$_2$ = 0.0936	R$_1$ = 0.0340, wR$_2$ = 0.0821
Final R indexes [all data]	R$_1$ = 0.0457, wR$_2$ = 0.0957	R$_1$ = 0.0396, wR$_2$ = 0.0854
Largest diff. peak/hole / e Å^{-3}	1.02/−1.06	0.87/−0.92
CCDC	**1858481**	**-**

Table S3. Crystallographic data and structure refinement of **3** and **5**.

	3	**5**
Empirical formula	$C_{66}H_{88}Co_2P_4Sn_2$	$C_{60}H_{74}FeSn_2$
Formula weight / g·mol⁻¹	1358.46	1088.42
Temperature / K	123.0(2)	275.6(1)
Crystal system	monoclinic	orthorhombic
Space group	$P2_1/c$	$Pccn$
a / Å	17.3183(2)	15.5450(1)
b / Å	16.6352(2)	20.5720(1)
c / Å	22.9521(2)	16.5464(1)
α /°	90	90
β /°	104.327(1)	90
γ /°	90	90
V / Å³	6406.7(1)	5291.40(5)
Z	4	4
ρ_{calc} / g cm⁻¹	1.41	1.366
μ / mm⁻¹	11.3	9.876
F(000)	2784.0	2240.0
Crystal size / mm³	$0.297 \times 0.077 \times 0.042$	$0.275 \times 0.124 \times 0.053$
Radiation / Å	CuK_α ($\lambda = 1.54184$)	CuK_α ($\lambda = 1.54184$)
2Θ range for data collection /°	6.636 – 148.166	7.128 – 152.24
Diffractometer	GV1000, TitanS2	Agilent Technologies Supernova
Index ranges	$-21 \le h \le 19$ $-20 \le k \le 20$ $-25 \le l \le 28$	$-19 \le h \le 19$ $-25 \le k \le 25$ $-20 \le l \le 20$
Reflections collected	36498	150461
Independent reflections	12629 [$R_{int} = 0.0351$, $R_{sigma} = 0.0335$]	5549 [$R_{int} = 0.0480$, $R_{sigma} = 0.0117$]
Data/restraints/parameters	12629/0/683	5549/0/306
Goodness-of-fit on F^2	1.024	1.353
Final R indexes [I>=2σ (I)]	$R_1 = 0.0265$, $wR_2 = 0.0637$	$R_1 = 0.0589$, $wR_2 = 0.1268$
Final R indexes [all data]	$R_1 = 0.0302$, $wR_2 = 0.0658$	$R_1 = 0.0593$, $wR_2 = 0.1270$
Largest diff. peak/hole / e Å⁻³	0.91/−0.66	0.72/−0.76
CCDC	**1858482**	**-**

2.4.8   Quantum Chemical Calculations

Geometry optimization of **1′** (iPr substituted by H) was performed with the Gaussian09 program package (Revision E.01).[60] The B3LYP density functional[61] and the Ahlrichs def2-TZVP basis set[29,30] were employed for all atoms. Atom-pairwise dispersion correction to the DFT energy with Becke–Johnson damping (D3BJ) was applied.[31,32] The nature of the stationary points was verified by numerical frequency analyses. Scalar relativistic effects were taken into account for tin by means of Stuttgart effective core potential.[62] Natural bond orbital (NBO) analysis was performed using NBO6 implemented in Gaussian09.[63] Molecular orbitals were visualized with the program GaussView5.[64] The isosurface value is set to 0.02 for all figures.

NBO-145
ε = -0.19544 H

NBO-146
ε = -0.19544 H
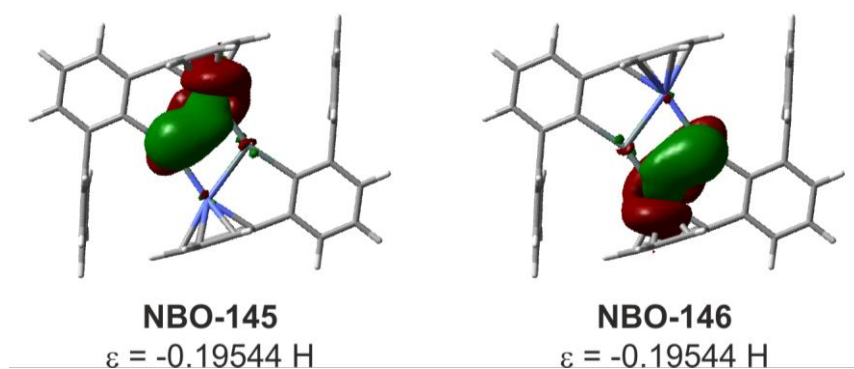
Figure S12. Natural bond orbital plots of **1′** calculated at B3LYP-D3/def2TZVP level of theory.

66
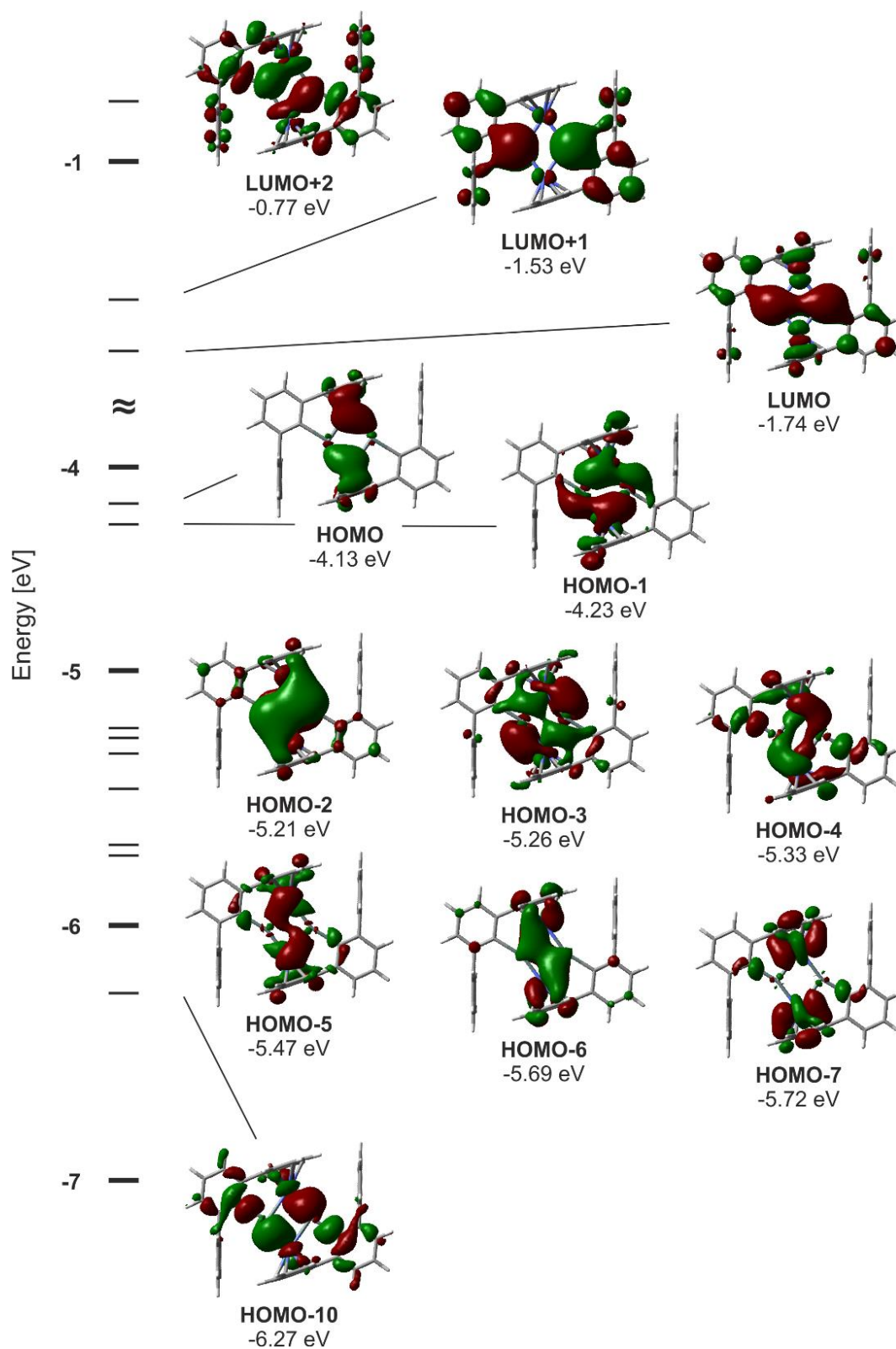
Figure S13. Kohn-Sham frontier orbitals of **1'** calculated at B3LYP-D3/def2TZVP level of theory.

Cartesian coordinates of $[\text{ArSnCo}]_2$ (**1′**, Ar = $C_6H_3\text{-}2,6\text{-}\{C_6H_5\}_2$) optimized with Gaussian09 at the BP86-D3/def2-TZVP level of theory

Energy = -4582.32441818

Sn	1.42197600	0.12046600	-0.05771900		C	-4.72751200	0.37545400	0.11762800
Sn	-1.42211000	-0.12021500	-0.06293400		C	5.11346300	3.44099000	0.08337800
Co	-0.28772500	1.97238500	-0.08269500		H	3.50729500	4.91626200	0.00999100
Co	0.28748500	-1.97196300	-0.07734400		H	6.50889500	1.76495200	0.16047300
C	3.09121400	1.50613900	0.01468800		C	4.84672300	-1.10261100	-1.09887200
C	-3.09123700	-1.50640900	0.01195100		C	4.76579900	-1.04703600	1.36911500
C	1.29125700	3.24695000	-0.04602900		C	-5.11339300	-3.44165500	0.07898100
C	0.55021600	3.35280600	1.19829100		H	-3.50700400	-4.91657500	0.00499000
C	-0.85306600	3.62581700	1.13187400		H	-6.50896600	-1.76586400	0.15781800
C	-1.51337000	3.76565700	-0.11860900		C	-4.76345400	1.04333900	1.37213000
C	-0.78918800	3.61757000	-1.33291200		C	-4.85030900	1.10467900	-1.09559800
H	-1.33192000	3.65093800	-2.28890000		H	5.90993200	4.20152500	0.10873100
C	0.61614600	3.34897800	-1.32665000		C	5.06487300	-2.49328200	-1.03937000
H	-1.44497100	3.66692300	2.05786100		C	4.98016500	-2.43943100	1.38596400
C	-1.29102500	-3.24711400	-0.04627300		H	-5.90975400	-4.20233400	0.10327900
C	-0.61328300	-3.34633400	-1.32567700		C	-4.97694200	2.43578100	1.39272400
C	0.79230200	-3.61367700	-1.32948700		C	-5.06774700	2.49530400	-1.03232200
C	1.51405600	-3.76375400	-0.11400100		C	5.14302100	-3.15793900	0.19286300
C	0.85098700	-3.62721000	1.13540600		H	5.16623500	-3.06706500	-1.97447700
H	1.44117500	-3.66925700	2.06232500		H	5.01449900	-2.97174000	2.35011600
C	-0.55269100	-3.35572300	1.19949800		C	-5.14217500	3.15715900	0.20165000
H	1.33703100	-3.64474300	-2.28443200		H	-5.00896600	2.96596800	2.35812000
C	2.74466800	2.87608700	-0.00435900		H	-5.17160900	3.07130100	-1.96578700
C	4.43913300	1.09509400	0.07691500		H	5.31958100	-4.24507700	0.22359600
C	-2.74455300	-2.87636100	-0.00676500		H	-5.31804300	4.24432400	0.23536000
C	-4.43929100	-1.09569100	0.07464500		H	4.63463800	-0.50469300	2.28211100
H	-2.60599100	3.88312800	-0.14594900		H	-1.15088200	-3.22274300	-2.24252600
H	2.60681300	-3.88026900	-0.13942300		H	-1.04571000	-3.23579400	2.14154300
C	3.76661200	3.84559400	0.02731600		H	-4.77895800	0.60685500	-2.04004500
C	5.45307100	2.07596400	0.11080900		H	-4.63085500	0.49871300	2.28355700
C	4.72702800	-0.37616100	0.11639300		H	1.15550200	3.22648600	-2.24261400
C	-3.76643900	-3.84596800	0.02347400		H	1.04100700	3.22978300	2.14110000
C	-5.45311500	-2.07672100	0.10770800		H	4.77254400	-0.60267000	-2.04198200

The Topological Analysis of the Electron Density[65] has been performed[66] using the OPBE[34–36] functional, which is the combination of Handy's optimized exchange (OPTX) with the PBE correlation functional. Relativistic effects have been included using the Zero Order Regular Approximation (Zora)[33].

BE(ZORA/OPBE/QZ4P)= -11.14091748 hartree

1 Sn	1.409504458000	0.034863146680	-0.052722804470
2 Sn	-1.408784201000	-0.032929665850	-0.055634672480
3 Co	-0.126835782000	2.004569705000	-0.051841959870
4 Co	0.127501674900	-2.002645582000	-0.060619003460
5 C	3.215123686000	1.240395787000	-0.043572606760
6 C	-3.214455154000	-1.238398184000	-0.055019153430
7 C	1.536715599000	3.088283215000	-0.046035342230
8 C	0.832995149600	3.276528124000	1.182006389000
9 C	-0.535847240900	3.626165573000	1.170408635000
10 C	-1.213284620000	3.802651373000	-0.055977866460
11 C	-0.527237693500	3.624677741000	-1.277458758000
12 H	-1.064006141000	3.710454462000	-2.220151812000
13 C	0.841872448500	3.276043818000	-1.279185742000

14 H	-1.079156664000	3.713030985000	2.109231780000
15 C	-1.536073360000	-3.086317977000	-0.061857735480
16 C	-0.838775841000	-3.269308509000	-1.294379992000
17 C	0.530269360800	-3.618405692000	-1.291370451000
18 C	1.213910952000	-3.800639082000	-0.069157035330
19 C	0.534091685900	-3.628481602000	1.156509242000
20 H	1.075639003000	-3.718673999000	2.096039196000
21 C	-0.834823528800	-3.279288556000	1.166823774000
22 H	1.068832587000	-3.700867441000	-2.233331178000
23 C	2.951196925000	2.617358518000	-0.041389709110
24 C	4.537553408000	0.793516252300	-0.039586049690
25 C	-2.950564011000	-2.615362241000	-0.058061447880
26 C	-4.536876891000	-0.791487616000	-0.052223723980
27 H	-2.280879725000	4.010255050000	-0.059872804000
28 H	2.281508902000	-4.008256643000	-0.071667734550
29 C	4.009909618000	3.528484990000	-0.035210513490
30 C	5.589701024000	1.704956403000	-0.033218755980
31 C	-4.009308345000	-3.526469704000	-0.057869708150
32 C	-5.589062792000	-1.702912230000	-0.052107441230
33 C	5.323664320000	3.070846703000	-0.031035598420
34 H	3.805775497000	4.598282500000	-0.033835605610
35 H	6.619536584000	1.350102346000	-0.029896444760
36 C	-5.323060560000	-3.068808722000	-0.055102790350
37 H	-3.805209962000	-4.596269581000	-0.060269331180
38 H	-6.618890364000	-1.348034313000	-0.049712421680
39 H	6.144129097000	3.786490400000	-0.026094833950
40 H	-6.143543336000	-3.784445488000	-0.055057634160
41 H	-4.757395440000	0.275746041100	-0.049918611490
42 H	4.758118753000	-0.273707959000	-0.041134955220
43 H	1.347896361000	3.106102127000	2.124672685000
44 H	1.363405918000	3.105422469000	-2.218163258000
45 H	-1.351496960000	-3.112357922000	2.109143731000
46 H	-1.358526460000	-3.095166988000	-2.233706882000

CP #   52
(RANK,SIGNATURE):   (3,+1)

CP COORDINATES: 0.000361   0.000892   -0.054245

EIGENVALUES OF HESSIAN MATRIX:

   -0.2452467E-01   0.3318050E-02   0.7886420E-01

EIGENVECTORS (ORTHONORMAL) OF HESSIAN MATRIX (COLUMNS):

   -0.1008269E-02   0.1295212E-01 -0.9999156E+00
   -0.2315022E-02   0.9999134E+00   0.1295443E-01
    0.9999968E+00   0.2327888E-02 -0.9781973E-03

VALUES OF SOME FUNCTIONS AT CP(a.u.):

        Rho =   0.4510789E-01
    |GRAD(Rho)| =   0.1701624E-10
     GRAD(Rho)x = -0.1582282E-10
     GRAD(Rho)y = -0.6260159E-11
     GRAD(Rho)z = -0.3314393E-13
      Laplacian =   0.5765758E-01
 (-1/4)Del**2(Rho)) = -0.1441440E-01

HESSIAN MATRIX:

```
      0.7885142E-01  -0.9786394E-03   0.1019657E-03
              0.3330579E-02   0.6349898E-04
                      -0.2452442E-01
 --------------------------------------------------------
```

CP # 53
(RANK,SIGNATURE):   (3,-1)

CP COORDINATES: -0.616323 -1.026005 -0.058104

EIGENVALUES OF HESSIAN MATRIX:

   -0.4686240E-01 -0.4472208E-01   0.1276168E+00

EIGENVECTORS (ORTHONORMAL) OF HESSIAN MATRIX (COLUMNS):

   -0.3991380E-02   0.7863784E+00   0.6177322E+00
   -0.5619524E-02   0.6177097E+00 -0.7863861E+00
    0.9999762E+00   0.6610127E-02 -0.1953558E-02

VALUES OF SOME FUNCTIONS AT CP(a.u.):

          Rho =   0.6829727E-01
     |GRAD(Rho)| =   0.1368282E-08
      GRAD(Rho)x = -0.8080071E-09
      GRAD(Rho)y =   0.1104224E-08
      GRAD(Rho)z =   0.3090547E-11
       Laplacian =   0.3603230E-01
 (-1/4)Del**2(Rho)) = -0.9008076E-02

HESSIAN MATRIX:

    0.2104120E-01 -0.8371813E-01 -0.1994317E-03
            0.6185274E-01   0.2767831E-03
                    -0.4686164E-01

CP # 54
(RANK,SIGNATURE):   (3,-1)

CP COORDINATES: 0.617010   1.027928 -0.052220

EIGENVALUES OF HESSIAN MATRIX:

   -0.4686109E-01 -0.4471967E-01   0.1276101E+00

EIGENVECTORS (ORTHONORMAL) OF HESSIAN MATRIX (COLUMNS):

    0.5542972E-03   0.7863754E+00   0.6177487E+00
    0.7174925E-05   0.6177488E+00 -0.7863755E+00
    0.9999998E+00 -0.4403180E-03 -0.3367742E-03

VALUES OF SOME FUNCTIONS AT CP(a.u.):

          Rho =   0.6829549E-01
     |GRAD(Rho)| =   0.7169555E-11
      GRAD(Rho)x = -0.6233198E-11
      GRAD(Rho)y = -0.3542233E-11
      GRAD(Rho)z = -0.4838404E-13
       Laplacian =   0.3602934E-01
 (-1/4)Del**2(Rho)) = -0.9007336E-02

HESSIAN MATRIX:

```
 0.2104369E-01  -0.8371478E-01  -0.3703879E-04
               0.6184672E-01   0.4562291E-04
                             -0.4686107E-01
```

CP # 55
(RANK,SIGNATURE):   (3,+1)

CP COORDINATES: 1.750173   1.668031   -0.047604

EIGENVALUES OF HESSIAN MATRIX:

  -0.1518558E-01   0.3533225E-01   0.5239890E-01

EIGENVECTORS (ORTHONORMAL) OF HESSIAN MATRIX (COLUMNS):

```
  -0.3342891E-02   0.9897294E+00  -0.1429142E+00
  -0.2066460E-02   0.1429079E+00   0.9897338E+00
   0.9999923E+00   0.3603899E-02   0.1567510E-02
```

VALUES OF SOME FUNCTIONS AT CP(a.u.):

```
        Rho =   0.2318493E-01
   |GRAD(Rho)| =   0.5604616E-13
    GRAD(Rho)x =   0.2382221E-13
    GRAD(Rho)y =   0.5073131E-13
    GRAD(Rho)z =  -0.8871919E-16
    Laplacian =   0.7254557E-01
(-1/4)Del**2(Rho)) =  -0.1813639E-01
```

HESSIAN MATRIX:

```
 0.3568026E-01  -0.2414377E-02   0.1650510E-03
               0.5205007E-01   0.1308698E-03
                             -0.1518476E-01
```

CP # 79
(RANK,SIGNATURE):   (3,-1)

CP COORDINATES: -0.713816   1.045750   -0.053626

EIGENVALUES OF HESSIAN MATRIX:

  -0.4655771E-01 -0.4359977E-01   0.1898259E+00

EIGENVECTORS (ORTHONORMAL) OF HESSIAN MATRIX (COLUMNS):

```
  -0.1341524E-02   0.8220933E+00  -0.5693512E+00
  -0.1080356E-02  -0.5693526E+00  -0.8220928E+00
   0.9999985E+00   0.4877549E-03  -0.1651954E-02
```

VALUES OF SOME FUNCTIONS AT CP(a.u.):

```
        Rho =   0.7086502E-01
   |GRAD(Rho)| =   0.2436568E-11
    GRAD(Rho)x =  -0.2282871E-11
    GRAD(Rho)y =  -0.6918435E-12
    GRAD(Rho)z =  -0.4967054E-12
    Laplacian =   0.9966842E-01
```

(-1/4)Del**2(Rho)) =   -0.2491710E-01

HESSIAN MATRIX:

    0.3206767E-01   0.1092571E+00   0.2235147E-03
            0.1141578E+00   0.3202015E-03
                    -0.4655707E-01

CP #   89
(RANK,SIGNATURE):   (3,-1)

CP COORDINATES: 0.714497   -1.043823   -0.056913

EIGENVALUES OF HESSIAN MATRIX:

   -0.4655154E-01   -0.4359315E-01   0.1898030E+00

EIGENVECTORS (ORTHONORMAL) OF HESSIAN MATRIX (COLUMNS):

   -0.1185463E-03   0.8220813E+00   -0.5693701E+00
   -0.3782700E-02   -0.5693664E+00   -0.8220752E+00
    0.9999928E+00   -0.2056303E-02   -0.3177184E-02

VALUES OF SOME FUNCTIONS AT CP(a.u.):

        Rho =   0.7085915E-01
   |GRAD(Rho)| =   0.2242213E-15
    GRAD(Rho)x =   0.1695864E-15
    GRAD(Rho)y =   0.1466562E-15
    GRAD(Rho)z =   0.2758800E-17
     Laplacian =   0.9965832E-01
(-1/4)Del**2(Rho)) =   -0.2491458E-01

HESSIAN MATRIX:

    0.3206976E-01   0.1092446E+00   0.4225628E-03
            0.1141377E+00   0.6207943E-03
                    -0.4654915E-01

Coordinates of **5a-opt**-

 C   10.76836927986383   11.82494145138815   4.14634314482429
 H   11.55347446177596   11.20735845973226   3.70478772752813
 C   8.76006513474169   13.41416772713868   5.30675165429788
 C   10.34355113637864   10.03934043284365   5.87683821549812
 C   9.48810816651058   13.88078459384152   4.20072120425849
 H   9.27800854477144   14.87594127771838   3.80263187849368
 C   8.13234433857788   15.17661291302378   6.97838862190544
 C   10.47918004814168   13.08623779053372   3.61830251795542
 H   11.03612899664462   13.45717031491734   2.75637482533375
 C   11.26061330933964   9.97506328762947   6.98429457251897
 C   7.73533551237157   14.29793496522503   5.94501153739129
 C   10.04962903389746   11.35885914414420   5.25376142685383
 C   5.47075086655538   15.14312589850394   6.08659550937406
 H   4.43108452353530   15.12820185721821   5.75399053123613
 C   8.60741439526898   8.95625171495944   4.31735667543122
 H   8.34681237759427   10.01900398872158   4.19908393888642
 C   11.97294092133854   11.22209184322274   7.47603150890224
 H   11.37196043668960   12.08053991237939   7.14087782948419

```
C   6.39282878761060    14.25850522123853    5.51285882599465
C   9.03020601060891    12.13578847707490    5.82906788667015
C   9.60802050670533     8.87445895372557    5.45636463373104
C   5.93822384879628    13.26975883873812    4.45131000992253
H   6.80017454291737    12.62950340817540    4.21198149677815
C  13.35710450541002    11.33086504775955    6.81581695707848
H  13.98996311512161    10.47431731505703    7.09434816766184
H  13.86917433710340    12.25142769054965    7.13268896352031
H  13.27111227300147    11.34739754879943    5.72054191625186
C  10.81108015333597     7.54982965894972    7.16399592427685
H  10.92075847463692     6.61740117004228    7.71661659491536
C   9.55045479755783    15.13929725174815    7.52851161486849
H  10.16563859266884    14.57764542419283    6.81050719295223
C   9.86200897533476     7.63661318813274    6.11592924567523
H   9.26677553176529     6.76003633284102    5.86446462953299
C   5.86260237199224    16.04202437757237    7.07670538579615
H   5.13523112273337    16.73163623940859    7.50872938575387
C   7.18188826167871    16.04484323950888    7.52903277107772
H   7.47522286455792    16.73300815306048    8.32364126434307
C  11.49157617938640     8.71208960343600    7.60064322556053
H  12.13293485829143     8.65184899055046    8.47868748802845
C   4.82303310728544    12.35696424436857    4.98305630850140
H   5.14373221878487    11.86320895589260    5.91322409463299
H   4.56946233919711    11.58137614303334    4.24548889333598
H   3.90622383965705    12.92500579296506    5.20238202344844
C  12.07011419404228    11.29586792202612    9.00263335442119
H  11.08039645045179    11.15342493035967    9.45825426417074
H  12.46185225624475    12.27584355713316    9.31075689024410
H  12.74726555465403    10.53093031511792    9.41139137264969
C   7.30870260204205     8.19125616088305    4.58866576418864
H   7.47156179987012     7.10444325937594    4.63826909274202
H   6.58365173086356     8.37722516176876    3.78334760304669
H   6.86555230722853     8.50925353288318    5.54298083515282
C   5.51827789543021    13.98538707290350    3.15872767180649
H   4.66158715359493    14.65294377501707    3.33630126086742
H   5.22581824353500    13.25724483519995    2.38749266796865
H   6.34229718194309    14.59491442749956    2.76173852336299
C   9.27366285413732     8.49057892435613    3.01212271469322
H  10.17093987555504     9.08592824949966    2.79310323443840
H   8.58133841400748     8.58887137347175    2.16314271794395
H   9.57742620239682     7.43505127416148    3.08554653778679
C  10.17409569445113    16.53298879571772    7.67986211905026
H  10.15124612151976    17.08205145793491    6.72809794805704
H  11.22180923406860    16.44940992426441    8.00391076536434
H   9.64503224668676    17.13789515814710    8.43115962705068
C   9.58188676280903    14.36934154144815    8.85826863235775
H   8.98281048009922    14.88560283411348    9.62353684679731
H  10.61032964374071    14.26807075555169    9.23432368197862
H   9.16062296818303    13.35810431846187    8.74311011488859
Fe  9.43754545791580     9.13879685213763    7.49596568056295
Sn  7.98943344159604     8.71042444822715    9.22375122529514
C   4.43851025218935     8.99154000906209   11.96397247774276
H   3.69476175591186     9.73476584445894   12.25796463456822
C   6.36090052182572     7.09844619501422   11.22765613052825
C   5.44309609857923    10.71673416588180   10.43486172257755
C   5.37256285011572     6.76406231234469   12.15847347749268
H   5.36291065722894     5.76596975883483   12.60022109927640
C   7.27540722471716     5.36410799647396    9.64501955816502
C   4.41336962896691     7.71289287296538   12.52487112001258
H   3.64566276318209     7.45623465017218   13.25623548958413
C   4.52572809725361    11.06740237860217    9.41403009249450
C   7.44015242961211     6.14722605277838   10.81379697556895
```

C	5.41576452085478	9.34381051168400	11.01962072705007
C	9.71135491673424	5.33542072012427	11.04882454713752
H	10.66586856181489	5.32865810076455	11.57785474185845
C	7.36436060792016	11.30464952927113	12.02445458473091
H	7.40982892007004	10.20786974748048	12.09563863134831
C	3.57806297579446	10.02538159047073	8.83493098090280
H	3.30980918023888	9.33602298713785	9.65070899208161
C	8.67013521495559	6.14853997676443	11.51502640688657
C	6.37901308668537	8.38684768940804	10.65173148762690
C	6.38827171965071	11.65476045545797	10.91052817069176
C	8.88243536301200	7.02635602649780	12.73903709209178
H	7.96894753273585	7.62213304750636	12.87985596111896
C	2.27673611857764	10.61791211927541	8.28250288650490
H	2.45457187433749	11.21658328393183	7.37699189084615
H	1.58406943224110	9.81003476443229	8.00617441099013
H	1.77865898554211	11.25997876945298	9.02269998602633
C	5.46716955243076	13.30874579288908	9.38641727952516
H	5.49172514655178	14.31003463059577	8.95851099041391
C	5.97256598149944	5.38574732461617	8.86101990521235
H	5.37345370566604	6.22466920599140	9.24518137036579
C	6.37730046132832	12.94949925705514	10.37483094102757
H	7.09700503671564	13.68596661545403	10.73285433126975
C	9.54944064520689	4.54617373613740	9.91214224236714
H	10.37178119052844	3.92052181644057	9.56106742095716
C	8.34182712079112	4.56351084944701	9.21671081288714
H	8.22966003158171	3.95523974440458	8.31802870542764
C	4.55410700086909	12.37154388229275	8.90809526957882
H	3.86771236820569	12.66032370806612	8.11291765693805
C	10.04655441162565	8.00874660642318	12.53771931868532
H	9.89598517436104	8.62728711774401	11.63952226654469
H	10.13759991935038	8.68003006332624	13.40395207587592
H	11.00424143708147	7.48063504214367	12.41846821569015
C	4.28771992549274	9.19002145032726	7.75375481040724
H	5.16886852657573	8.67322445915818	8.15825316676119
H	3.60795804558809	8.43013266150322	7.33984315302320
H	4.63270067042388	9.83388163136611	6.93149395049270
C	8.78781400223641	11.80185853899634	11.74292236975338
H	8.84636817330931	12.89968943635323	11.72861920975924
H	9.47809053096277	11.44370834095261	12.52012279735970
H	9.14681386232246	11.43211320385176	10.77094492258110
C	9.07797694443995	6.17500529647378	14.00346156821887
H	9.98149065785770	5.55171013121403	13.92691651056279
H	9.18504146105702	6.81759076233979	14.88968947587329
H	8.22112035722053	5.50586753918362	14.16466027151594
C	6.84135844593624	11.82518470636872	13.37390515094958
H	5.84795017378438	11.41063142721736	13.59603372209676
H	7.52288123256621	11.54473754647045	14.19104043129138
H	6.75453400486972	12.92207177172548	13.36057495953739
C	5.17124738735874	4.09676815301255	9.10574394319457
H	4.96228338197965	3.95916272442534	10.17601776229261
H	4.21189512269093	4.12852616544741	8.56854802387369
H	5.72935077126877	3.21539918260584	8.75526714665805
C	6.20197423650595	5.63359771585757	7.36326438266122
H	6.73006678599181	4.79351746167919	6.88779148773182
H	5.24118253179828	5.75821883070009	6.84388828133697
H	6.79908201025523	6.54352250780240	7.20222674219139
Sn	7.77873041576254	11.21726170806813	7.43604331383631

Coordinates of **5b-opt**

C	11.18976920434641	11.99474249554165	4.61279485505085
H	12.20908462618683	11.61486977322391	4.52152198510445

C	8.56604003716743	12.99037480449661	4.83886425964690
C	10.91918512589819	10.75987185910229	6.82194510950968
C	9.34836298407531	13.31080632380787	3.72041382117902
H	8.93728197532266	13.95012544270835	2.93681699804137
C	6.95771360178544	14.64866218448355	5.82340603181206
C	10.65276720695539	12.81670842435739	3.61537650803120
H	11.25821352317184	13.07338234354818	2.74472126532230
C	11.44505979749437	11.34328984139525	8.03516747939045
C	7.17319430303286	13.48457629712510	5.05278486174751
C	10.41389951908393	11.65002049090618	5.72634781997559
C	4.78575209899156	13.10526795601711	4.93441944760902
H	3.93549785317574	12.50427770504842	4.60853649785217
C	10.11231600394153	8.72000741432686	5.48173416611458
H	9.52318667626868	9.51324219578273	4.99593098725536
C	11.59962510709617	12.85008525558700	8.16577069973209
H	10.86821963253111	13.31236400008413	7.48399446363223
C	6.08539512741983	12.70078300485428	4.60670124554502
C	9.10846258854453	12.16090411039968	5.82945961785018
C	10.73415249333621	9.33721188098094	6.72285758863138
C	6.31817487493775	11.40380563910784	3.84641401914285
H	7.36378800462945	11.40583319573059	3.50454657207603
C	13.00012475780017	13.26484756097651	7.68493292544757
H	13.77681953276774	12.80569158637957	8.31522721127440
H	13.12097409224864	14.35713507999850	7.73328573043566
H	13.17266841785619	12.94624602916332	6.64753318857306
C	11.69793661751192	9.08096412251780	8.99864006408538
H	11.93617784026075	8.44051872004078	9.84771551813957
C	8.12066766926681	15.48725580936911	6.33176543259783
H	9.04746233225673	14.94914303243766	6.08373161702081
C	11.14882089707213	8.51943062740158	7.81757258627252
H	10.93846063064617	7.45119642330097	7.78916050681080
C	4.56255238785228	14.25883463246026	5.68426911133601
H	3.54336787906734	14.55806623543374	5.93383398280774
C	5.64133283841790	15.02328807070985	6.12258926020286
H	5.45922031283654	15.92162957089886	6.71525668361637
C	11.82668832450201	10.48429337479555	9.10914156433207
H	12.16661393047143	10.91937693313278	10.04791498446557
C	6.14124819271264	10.19395712297806	4.77819184050086
H	6.84844880285897	10.22867284868880	5.62115538147499
H	6.31493043091607	9.25237267184085	4.23651288937271
H	5.12567054886654	10.16762799152415	5.19877870093500
C	11.30897110047645	13.37663935308522	9.57496553250234
H	10.33610088306655	13.00624443004732	9.93022573408805
H	11.28631564120559	14.47580791201547	9.56722804950466
H	12.08320785211728	13.07125873508283	10.29454067185253
C	9.16218700501712	7.55596461949548	5.77731606966864
H	9.68842658573291	6.68282655314577	6.18958988324164
H	8.66602697969418	7.23013142842394	4.85166507462934
H	8.39236765652751	7.85095526115803	6.50305893868608
C	5.42469972760384	11.27750713960963	2.60446380491195
H	4.36137134294210	11.19690194221318	2.87427000846808
H	5.68853064161408	10.37402682028022	2.03563518789417
H	5.53939267854508	12.14729007376068	1.94250063444443
C	11.22359810091714	8.29290452131527	4.50729623371042
H	11.86975286137379	9.14170141257129	4.24454319138777
H	10.79464263174166	7.88826774991644	3.57881372826042
H	11.85579399155041	7.51386187158530	4.95997039662799
C	8.17111844430949	16.84690538717226	5.61164464028994
H	8.24671817808679	16.71656065219772	4.52789392273750
H	9.03866008729661	17.43250045793845	5.95537813007533
H	7.26389265693170	17.43480071921241	5.82218972439417
C	8.03308407455757	15.65644879605510	7.85823660566411

H	7.19604007441646	16.22264372597135	8.17952642932246
H	8.97262982741280	16.20102987617580	8.20726548560712
H	8.05871013657351	14.67819041978621	8.36304938311632
Fe	9.89107616842846	10.03138470853175	8.45652837242232
Sn	7.93010523567570	9.12386841190555	9.38729635140374
C	4.86408457393495	8.87622872980130	12.45716974940764
H	4.44845901778099	9.59490989349372	13.16595439257913
C	5.93463439967179	7.00882137306663	10.64246097966559
C	6.26039526610045	10.71993104688213	11.39423901948520
C	4.98604261395619	6.60526766478841	11.59271713325710
H	4.66467775696732	5.56258248511744	11.62872853265558
C	5.98876992208336	5.93702342135544	8.37489085676931
C	4.46029680593257	7.53666559159554	12.49426133933895
H	3.72545760825479	7.21555692676043	13.23411832741513
C	5.53824828413677	11.64262970899162	10.56066104233681
C	6.57115834908752	6.08865891900808	9.65340469219008
C	5.79619348733350	9.29838384291390	11.50123745412915
C	8.46579025013577	4.75005381417115	8.96252946013599
H	9.43078924311686	4.28872535509504	9.18021832771126
C	8.30098198319288	10.12993583993349	12.85247880008045
H	8.02934098211131	9.11653204099268	12.51689112623152
C	4.25905113391986	11.21794713735997	9.85996494036042
H	4.28381455806206	10.11916462162206	9.79493796151490
C	7.82074852634230	5.50192759068046	9.95316450029240
C	6.32705455317032	8.35354755878400	10.60628073136286
C	7.51125935265115	11.11242321954362	12.00226411117900
C	8.46974423239375	5.67637874767797	11.31797074997481
H	7.85426294104097	6.38909229696211	11.88646769411719
C	3.04642936652219	11.61277873349678	10.72065476174359
H	2.99104752995235	12.70645319309979	10.83160966526432
H	2.11010248356750	11.26833702670441	10.25758372736059
H	3.11278024282264	11.17466472623732	11.72602763385704
C	7.26079810583393	13.37094294106649	11.02906445233972
H	7.66773408792143	14.36353082329285	10.83664324381775
C	4.68260440180066	6.63447107681434	8.02551870465823
H	4.21722186348662	6.95310589491329	8.97003383602126
C	7.99134885793668	12.44170930361302	11.80435566641322
H	8.96205151096305	12.72616670652790	12.20806444673136
C	7.89831880787492	4.59307061531254	7.70017009699967
H	8.41775677149031	4.01311130819018	6.93571403739667
C	6.67011935702885	5.18505810248005	7.41032783278699
H	6.24055806666292	5.06921242601820	6.41418519659593
C	6.05062697418061	12.96696730220535	10.40929797362019
H	5.55913006066826	13.64832288670573	9.71613237585161
C	9.88178562869942	6.27217478985473	11.21230728682269
H	9.86796836413797	7.22697138596968	10.66406164730289
H	10.29723298785013	6.45728039806435	12.21370641081705
H	10.56791069836901	5.59244696054882	10.68520787681596
C	4.12234855634441	11.76033133047861	8.43441537095412
H	5.00181109105214	11.50153460202458	7.82960128094624
H	3.22857208112259	11.33678627023638	7.95379884450178
H	4.01684869062524	12.85464430294350	8.41267005035141
C	9.81928553596133	10.27004786193010	12.70308905067910
H	10.19004679786368	11.20759714970097	13.14352705090314
H	10.32487184508055	9.44352178853890	13.22268872403648
H	10.10490189414992	10.24611167849275	11.64115871763494
C	8.47650914220897	4.35052390084254	12.09569671402688
H	9.07522395937830	3.58941829960640	11.57302295963710
H	8.90645967515054	4.49024284166490	13.09865599957947
H	7.45715001721165	3.95548790054488	12.20928817166025
C	7.86298151245060	10.25867241136759	14.32093690989160
H	6.78317229537809	10.08534870064474	14.42808258985320

```
H   8.39217883740922      9.52849419266838     14.95086810849107
H   8.08508095086476     11.26644059831024     14.70357916502706
C   3.68985090480481      5.70830345604177      7.30907821564882
H   3.50554344113296      4.79553273162991      7.89281481800530
H   2.72909820691918      6.22231212011235      7.16013974894977
H   4.05750393016993      5.40606215231585      6.31738867252011
C   4.95234669237264      7.90012483852351      7.19566176827122
H   5.46963417092878      7.65152202517090      6.25781706520764
H   4.01214358695545      8.41359750698524      6.94561146528209
H   5.58558342040342      8.61393251006648      7.74469858520659
Fe  7.49999524140433     11.55768195155710      9.97243372897607
Sn  8.16995614811254     11.74968838857088      7.72618976348556
```

2.5   References

[1]   S. T. Liddle (Ed.) *Molecular Metal-Metal Bonds*, *Compounds, Synthesis, Properties*, Wiley-VCH Verlag GmbH & Co. KGaA, Weinheim, Germany, **2015**.

[2]   a) P. J. Davidson, M. F. Lappert, *J. Chem. Soc., Chem. Commun.* **1973**, 317a; b) D. E. Goldberg, D. H. Harris, M. F. Lappert, K. M. Thomas, *J. Chem. Soc., Chem. Commun.* **1976**, 261.

[3]   A. D. Phillips, R. J. Wright, M. M. Olmstead, P. P. Power, *J. Am. Chem. Soc.* **2002**, *124*, 5930–5931.

[4]   a) R. Jambor, B. Kasná, K. N. Kirschner, M. Schürmann, K. Jurkschat, *Angew. Chem. Int. Ed.* **2008**, *47*, 1650–1653, *Angew. Chem.* **2008**, *120*, 1674–1677; b) T. J. Hadlington, C. Jones, *Chem. Commun.* **2014**, *50*, 2321–2323.

[5]   a) T. F. Fässler, *Coord. Chem. Rev.* **2001**, *215*, 347–377; b) S. Scharfe, F. Kraus, S. Stegmaier, A. Schier, T. F. Fässler, *Angew. Chem. Int. Ed.* **2011**, *50*, 3630–3670, *Angew. Chem.* **2011**, *123*, 3712–3754.

[6]   a) N. Wiberg, P. P. Power in *Molecular clusters of the main group elements* (Eds.: M. Driess, H. Nöth), Wiley-VCH, Weinheim, **2004**, 188–208; b) N. Wiberg, *Coord. Chem. Rev.* **1997**, *163*, 217–252.

[7]   A. Schnepf, *Chem. Soc. Rev.* **2007**, *36*, 745–758.

[8]   a) D. Agustin, G. Rima, H. Gornitzka, J. Barrau, *Eur. J. Inorg. Chem.* **2000**, *2000*, 693–702; b) B. E. Eichler, A. D. Phillips, S. T. Haubrich, B. V. Mork, P. P. Power, *Organometallics* **2002**, *21*, 5622–5627; c) H. Lei, J.-D. Guo, J. C. Fettinger, S. Nagase, P. P. Power, *Organometallics* **2011**, *30*, 6316–6322; d) M. Wagner, V. Deáky, C. Dietz, J. Martincová, B. Mahieu, R. Jambor, S. Herres-Pawlis, K. Jurkschat, *Chem. Eur. J.* **2013**, *19*, 6695–6708.

[9]   A. C. Filippou, P. Portius, A. I. Philippopoulos, H. Rohde, *Angew. Chem. Int. Ed.* **2003**, *42*, 445–447, *Angew. Chem.* **2003**, *115*, 461–464.

[10]   K. Jonas, R. Mynott, C. Krüger, J. C. Sekutowski, Y.-H. Tsay, *Angew. Chem. Int. Ed. Engl.* **1976**, *15*, 767–768, *Angew. Chem.* **1976**, *88*, 808–809.

[11]   W. W. Brennessel, R. E. Jilek, J. E. Ellis, *Angew. Chem. Int. Ed.* **2007**, *46*, 6132–6136, *Angew. Chem.* **2007**, *119*, 6244–6248.

[12]   W. W. Brennessel, J. E. Ellis, *Inorg. Chem.* **2012**, *51*, 9076–9094.

[13] J. E. Ellis, *Inorg. Chem.* **2006**, *45*, 3167–3186.

[14] P. Pyykkö, M. Atsumi, *Chem. Eur. J.* **2009**, *15*, 12770–12779.

[15] H. Puff, B. Breuer, G. Gehrke-Brinkmann, P. Kind, H. Reuter, W. Schuh, W. Wald, G. Weidenbrück, *J. Organomet. Chem.* **1989**, *363*, 265–280.

[16] C. Schneider-Koglin, K. Behrends, M. Dräger, *J. Organomet. Chem.* **1993**, *448*, 29–38.

[17] T. Nguyen, W. A. Merrill, C. Ni, H. Lei, J. C. Fettinger, B. D. Ellis, G. J. Long, M. Brynda, P. P. Power, *Angew. Chem. Int. Ed.* **2008**, *47*, 9115–9117, *Angew. Chem.* **2008**, *120*, 9255–9257.

[18] X. Dai, P. Kapoor, T. H. Warren, *J. Am. Chem. Soc.* **2004**, *126*, 4798–4799.

[19] H. Lei, B. D. Ellis, C. Ni, F. Grandjean, G. J. Long, P. P. Power, *Inorg. Chem.* **2008**, *47*, 10205–10207.

[20] L. Pu, A. D. Phillips, A. F. Richards, M. Stender, R. S. Simons, M. M. Olmstead, P. P. Power, *J. Am. Chem. Soc.* **2003**, *125*, 11626–11636.

[21] G. H. Spikes, J. R. Giuliani, M. P. Augustine, I. Nowik, R. H. Herber, P. P. Power, *Inorg. Chem.* **2006**, *45*, 9132–9136.

[22] a) J. Weaver, P. Woodward, *J. Chem. Soc., Dalton Trans.* **1973**, 1060–1064; b) O. J. Curnow, B. K. Nicholson, *J. Organomet. Chem.* **1984**, *267*, 257–263; c) O. J. Curnow, B. K. Nicholson, M. J. Severinsen, *J. Organomet. Chem.* **1990**, *388*, 379–390.

[23] a) A. E. Dwight, P. P. Vaishnava, C. W. Kimball, J. L. Matykiewicv, *J. Less Common Metals* **1986**, *119*, 319–326; b) E. A. Gorlich, R. Kmiec, K. Latka, A. Szytula, A. Zygmunt, *J. Phys.: Condens. Matter* **1994**, *6*, 11127.

[24] P. Salamakha, O. Sologub, L. Righi, G. Bocelli, *J. Alloys Compd.* **2000**, *302*, L3-L5.

[25] a) V. Hlukhyy, H. He, L.-A. Jantke, T. F. Fässler, *Chem. Eur. J.* **2012**, *18*, 12000–12007; b) H. He, W. Klein, L.-A. Jantke, T. F. Fässler, *Z. anorg. allg. Chem.* **2014**, *640*, 2864–2870.

[26] X. Wang, Y. Peng, M. M. Olmstead, H. Hope, P. P. Power, *J. Am. Chem. Soc.* **2010**, *132*, 13150–13151.

[27] A. D. Becke, *Phys. Rev. A* **1988**, *38*, 3098–3100.

[28] J. P. Perdew, *Phys. Rev. B* **1986**, *33*, 8822–8824.

[29] A. Schäfer, C. Huber, R. Ahlrichs, *J. Chem. Phys.* **1994**, *100*, 5829–5835.

[30] F. Weigend, *Phys. Chem. Chem. Phys.* **2006**, *8*, 1057–1065.

[31] S. Grimme, J. Antony, S. Ehrlich, H. Krieg, *J. Chem. Phys.* **2010**, *132*, 154104.

[32] S. Grimme, S. Ehrlich, L. Goerigk, *J. Comp. Chem.* **2011**, *32*, 1456–1465.

[33] E. van Lenthe, A. Ehlers, E.-J. Baerends, *J. Chem. Phys.* **1999**, *110*, 8943–8953.

[34] N. C. Handy, A. J. Cohen, *Mol. Phys.* **2001**, *99*, 403–412.

[35] J. P. Perdew, K. Burke, M. Ernzerhof, *Phys. Rev. Lett.* **1996**, *77*, 3865.

[36] M. Swart, A. W. Ehlers, K. Lammertsma, *Mol. Phys.* **2004**, *102*, 2467–2474.

[37] P. E. Lippens, *Phys. Rev. B* **1999**, *60*, 4576–4586.

[38] R. Pöttgen, *Z. Naturforsch. B* **2006**, *61*.

[39] a) P. Zanello, *Inorganic Electrochemistry*, *theory, practice and application*, The Royal Society of Chemistry, Cambridge, UK, **2003**; b) A. J. Bard, L. R. Faulkner, *Electrochemical Methods*, *Fundamentals and Applications*, John Wiley & Sons, Inc., New York, **2001**.

[40] D. F. Evans, *J. Chem. Soc.* **1959**, 2003.

[41] K. M. Krebs, J. Jamin, L. Wesemann, *Dalton. Trans.* **2016**, *45*, 5933–5936.

[42] A. R. Fox, R. J. Wright, E. Rivard, P. P. Power, *Angew. Chem. Int. Ed.* **2005**, *44*, 7729–7733, *Angew. Chem.* **2005**, *117*, 7907–7911.

[43] a) D. Nikolova, C. von Hänisch, A. Adolf, *Eur. J. Inorg. Chem.* **2004**, *2004*, 2321–2325; b) F. García, A. D. Hopkins, R. A. Kowenicki, M. McPartlin, C. M. Pask, M. L. Stead, A. D. Woods, D. S. Wright, *Organometallics* **2005**, *24*, 1813–1818; c) M. McPartlin, R. L. Melen, V. Naseri, D. S. Wright, *Chem. Eur. J.* **2010**, *16*, 8854–8860; d) S. Almstätter, M. Eberl, G. Balázs, M. Bodensteiner, M. Scheer, *Z. anorg. allg. Chem.* **2012**, *638*, 1739–1745; e) A. Velian, B. M. Cossairt, C. C. Cummins, *Dalton. Trans.* **2016**, *45*, 1891–1895.

[44] A. Bondi, *J. Phys. Chem.* **1964**, *68*, 441–451.

[45] a) F. Dielmann, A. Timoshkin, M. Piesch, G. Balázs, M. Scheer, *Angew. Chem. Int. Ed.* **2017**, *56*, 1671–1675, *Angew. Chem.* **2017**, *129*, 1693–1698; b) F. Hennersdorf, J. Frötschel, J. J. Weigand, *J. Am. Chem. Soc.* **2017**, *139*, 14592–14604.

[46] a) M. Di Vaira, M. P. Ehses, M. Peruzzini, P. Stoppioni, *Polyhedron* **1999**, *18*, 2331–2336; b) K. Heinze, G. Huttner, L. Zsolnai, A. Jacobi, P. Schober, *Chem. Eur. J.* **1997**, *3*, 732–743.

[47] a) N. Rinn, L. Guggolz, J. Lange, S. Chatterjee, T. Block, R. Pöttgen, S. Dehnen, *Chem. Eur. J.* **2018**, *24*, 5840–5848; b) K. M. Krebs, S. Freitag, H. Schubert, B. Gerke, R. Pöttgen, L. Wesemann, *Chem. Eur. J.* **2015**, *21*, 4628–4638.

[48] M. Binder, C. Schrenk, T. Block, R. Pöttgen, A. Schnepf, *Chem. Commun.* **2017**, *53*, 11314–11317.

[49] a) M. Binder, C. Schrenk, T. Block, R. Pöttgen, A. Schnepf, *Molecules* **2018**, *23*; b) C. Schrenk, F. Winter, R. Pöttgen, A. Schnepf, *Inorg. Chem.* **2012**, *51*, 8583–8588.

[50] P. B. Hitchcock, M. F. Lappert, S. A. Thomas, A. J. Thorne, A. J. Carty, N. J. Taylor, *J. Organomet. Chem.* **1986**, *315*, 27–44.

[51] a) A. C. Filippou, A. I. Philippopoulos, G. Schnakenburg, *Organometallics* **2003**, *22*, 3339–3341; b) A. C. Filippou, P. Ghana, U. Chakraborty, G. Schnakenburg, *J. Am. Chem. Soc.* **2013**, *135*, 11525–11528; c) A. C. Filippou, D. Hoffmann, G. Schnakenburg, *Chem. Sci.* **2017**, *8*, 6290–6299.

[52] F. Neese, *WIREs Comput Mol Sci* **2018**, *8*, e1327.

[53] a) B. Metz, H. Stoll, M. Dolg, *J. Chem. Phys.* **2000**, *113*, 2563–2569; b) F. Weigend, R. Ahlrichs, *Phys. Chem. Chem. Phys.* **2005**, *7*, 3297–3305.

[54] *IvorySoft: gNMR for Windows*, *NMR Simulation Program,* P. H. M. Budzelaar, **2006**.

[55] *University of Duisburg: Normos Mössbauer Fitting Program,* R. A. Brand, **2002**.

[56] a) SCALE3ABS, CrysAlisPro, Aglient Technologies Inc., Oxford, GB, 2012, b) G. M. Sheldrick, SADABS, Bruker AXS, Madison, USA, **2007**.

[57] R. C. Clark, J. S. Reid, *Acta Cryst. A* **1995**, *51*, 887–897.

[58] G. M. Sheldrick, *Acta Cryst. A* **2015**, *71*, 3–8.

[59] G. M. Sheldrick, *Acta Cryst. A* **2008**, *64*, 112–122.

[60] *Gaussian Inc.,* M. J. Frisch, G. W. Trucks, H. B. Schlegel, G. E. Scuseria, M. A. Robb, J. R. Cheeseman, G. Scalmani, V. Barone, G. A. Petersson, H. Nakatsuji et al., Wallingford CT, **2016**.

[61] a) C. Lee, W. Yang, R. G. Parr, *Phys. Rev. B* **1988**, *37*, 785–789; b) P. J. Stephens, F. J. Devlin, C. F. Chabalowski, M. J. Frisch, *J. Phys. Chem.* **1994**, *98*, 11623–11627.

[62] D. Andrae, U. Huermann, M. Dolg, H. Stoll, H. Preu, *Theoret. Chim. Acta* **1990**, *77*, 123–141.

[63] *NBO 6.0,* E. D. Glendening, J. K. Badenhoop, A. E. Reed, J. E. Carpenter, J. A. Bohmann, C. M. Morales, C. R. Landis, F. Weinhold, Theoretical Chemistry Institute, University of Wisconsin, Madison, **2013**.

[64] *Semichem Inc.,* R. Dennington, T. A. Keith, J. M. Millam, Shawnee Mission, KS, **2016**.

[65] a) R. F. W. Bader, *Atoms in molecules*, *A quantum theory*, Oxford University Press, Oxford, **1994**, pp. 438; b) R. F. W. Bader, *Chem. Rev.* **1991**, *91*, 893–928; c) J. I. Rodríguez, *J. Comp. Chem.* **2013**, *34*, 681–686.

[66] G. te Velde, F. M. Bickelhaupt, E. J. Baerends, C. Fonseca Guerra, S. J. A. van Gisbergen, J. G. Snijders, T. Ziegler, *J. Comp. Chem.* **2001**, *22*, 931–967.

3 [3+2] FRAGMENTATION OF A PENTAPHOSPHIDO LIGAND BY

CYANIDE[a,b]

CHRISTIAN M. HOIDN, THOMAS M. MAIER, KAROLINA TRABITSCH, JAN J. WEIGAND AND

ROBERT WOLF

3.1 Introduction

Over the past decades, studies of the activation of white phosphorus have produced numerous early and late transition metal polyphosphido complexes.[1] The functionalization of the polyphosphorus ligands in such compounds with electrophiles and/or nucleophiles is potentially an elegant and atom economical route to unique phosphorus compounds. However, such transition metal-mediated P_4 functionalizations and, in particular, the release of useful phosphorus building blocks from the metal center are generally difficult to achieve due to the low reactivity of many known polyphosphido compounds toward electrophiles.[2] Rare examples of successful electrophilic functionalization reactions are shown in Scheme 1a.
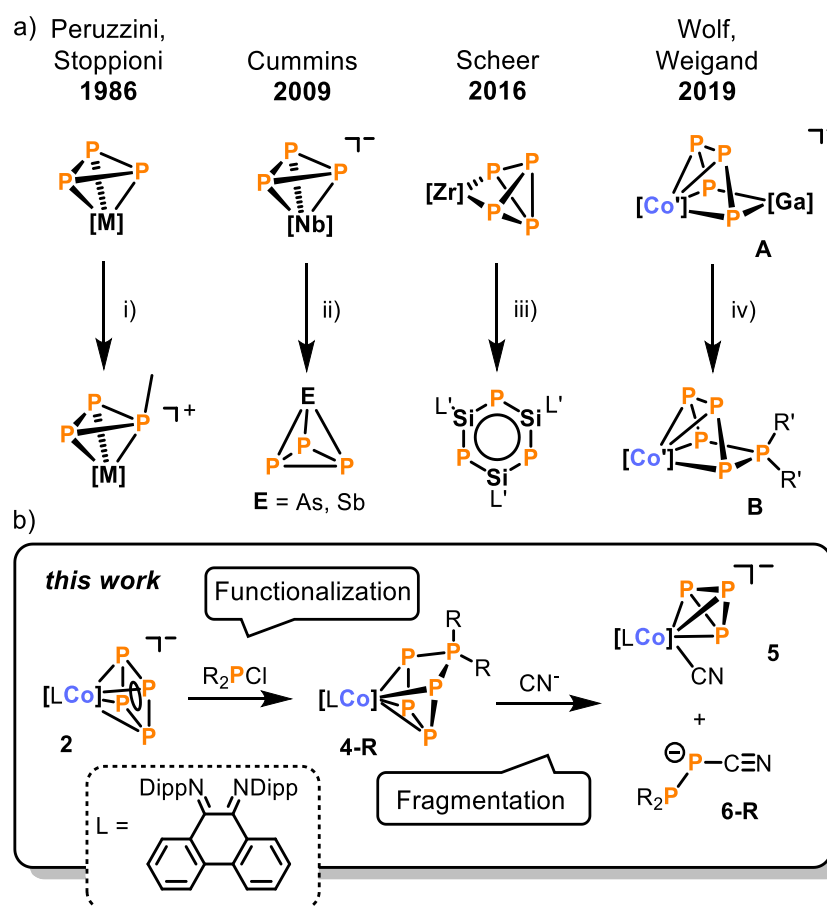
Scheme 1. (a) Examples for established functionalizations of polyphosphorus ligands (i) +CF₃SO₃Me or +[Me₃O]BF₄/−Me₂O; [M] = [M(triphos)] (M = Co, Rh, Ir, triphos = CH₃C(CH₂PPh₂)₃); (ii) +AsCl₃ or +SbCl₃/−NaCl, −[Nb]Cl₂(thf); [Nb] = [Nb(ODipp)₃] (Dipp = 2,6-*i*Pr₂C₆H₃); (iii) +[(L')SiCl]/−[Zr]Cl₂, L' = PhC(N*t*Bu)₂; [Zr] = [(C₅H₃*t*Bu₂)₂Zr] (iv) +R'₂PCl/−KCl, −[Ga]; [Ga] = [Ga(CH(CMeNDipp)₂)], [Co'] = [(ᴹᵉˢBIAN)Co], BIAN = 1,2-bis(arylimino)acenaphthene; R' = Cy, *i*Pr, *t*Bu; (b) ligand functionalization and subsequent fragmentation reactions afford new phosphorus compounds (L = PHDI = bis(2,6-diisopropylphenyl)phenanthrene-9,10-diimine; R = Cy, *t*Bu, Ph, Mes, N(*i*Pr)₂).

Peruzzini and *Stoppioni* reported the methylation of a *cyclo*-P$_3$ ligand at group 9 metal cations,[3] *Cummins* described the remarkable synthesis of EP$_3$ (E = As, Sb) molecules from [Nb(ODipp)$_3$(η^3-P$_3$)]$^-$ (Dipp = 2,6-*i*Pr$_2$C$_6$H$_3$) and ECl$_3$,[4] and quite recently *Scheer* disclosed the synthesis of a phosphorus-silicon analogue of benzene from a tetraphosphido zirconium complex.[5] Recent work from our group has shown that the heterodinuclear cobalt-gallium species **A** can be successfully applied for the construction of novel alkyl-substituted pentaphosphido complexes **B**.[6] However, the synthesis of **A** is cumbersome, and the reaction properties of **B**-type species have therefore not been explored.

Herein we present a much more facile synthesis of pentaphosphido ligands and an unprecedented fragmentation reaction of such ligands into a P$_2$ and a P$_3$ moiety (Scheme 1b). The new bis(2,6-diisopropylphenyl)phenanthrene-9,10-diimine (PHDI) complex **1** enables the straightforward, high yielding synthesis of an anionic *cyclo*-P$_4$ cobalt complex **2**, which is readily functionalized with dialkyl, diaryl- and diaminylposhphino groups. Cyanide anions induce a unique fragmentation reaction of the resulting pentaphosphorus unit into a unique *cyclo*-P$_3$ complex **5** and rare examples of 1-cyano-diphosphan-1-ide anions [R$_2$PPCN]$^-$ (**6-R**).[7]

3.2   Results and Discussion

3.2.1   Synthesis and Characterization of *cyclo*-P$_4$ Cobalt Complexes

Our investigation commenced with the synthesis of the new α-diimine complex [K(18c-6)(thf)$_{1.5}$][(PHDI)Co(η^4-1,5-cod)] ([K(18c-6)]**1**, 18c-6 = 18-crown-6, cod = cyclooctadiene). [K(18c-6)]**1** can be synthesized in good yield by ligand exchange of 1,5-cod in [K(thf)$_{0.2}$][Co(η^4-1,5-cod)$_2$] with PHDI followed by the addition of 18-crown-6 (Scheme 2a).
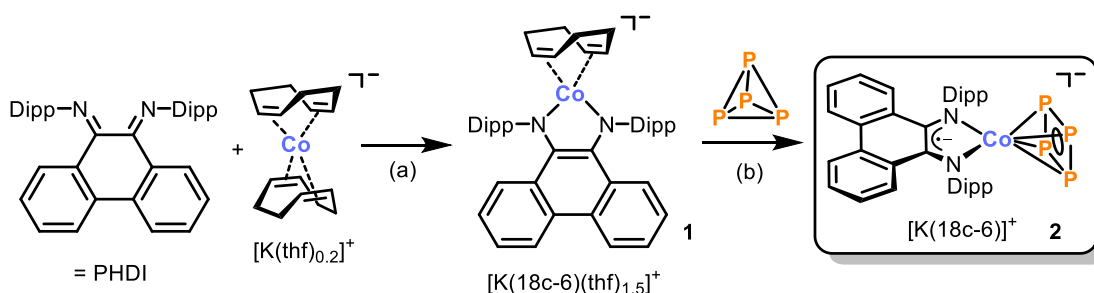
Scheme 2. Synthesis of compounds [K(18c-6)]**1** and [K(18c-6)]**2** (18c-6 = 18-crown-6); reagents and by-products: (a) +18c-6/−1,5-cod; (b) +P$_4$/−1,5-cod.

Filtration and crystallization from THF/*n*-hexane affords analytically pure, dark-green crystals of [K(18c-6)]**1**. The NMR spectroscopic properties of diamagnetic **1** compare well with those of related BIAN complexes K[Co(η^4-1,5-cod)(^{Ar}BIAN)] (Ar = Dipp, Mes, BIAN = 1,2-bis(arylimino)acenaphthene).[6,8] Next, the reaction of [K(18c-6)]**1** with white phosphorus was examined (Scheme 2b). ^{31}P{^{1}H} NMR spectroscopic monitoring shows quantitative conversion to [K(18c-6)][(PHDI)Co(η^4-*cyclo*-P$_4$)] ([K(18c-6)]**2**) at room temperature. Crystallization from toluene/*n*-hexane gave [K(18c-6)]**2** as dark turquoise crystals in up to 80% yield (corresponding to >1.5 g of product). The ^{31}P{^{1}H} NMR spectrum of [K(18c-6)]**2** in THF-*d$_8$* shows a sharp singlet at 136.5 ppm (*cf.* the chemical shifts of 175.2 ppm observed for [(η^5-Cp^{tBu3})Co(η^4-P$_4$)][9] and 114.1 ppm for [(η^5-Cp^{Ar})Fe(η^4-P$_4$)]$^-$ (Cp^{Ar} = C$_5$(C$_6$H$_4$-4-Et)$_5$).[10] A single-crystal X-ray diffraction (XRD) analysis clearly revealed the presence of a bidentate PHDI ligand and a terminal η^4-coordinated *cyclo*-P$_4$ unit, but a more detailed interpretation of the structure was prevented by heavy disorder within the *cyclo*-P$_4$ unit (see Fig. S59, SI, for further details). Fortunately, the tungsten pentacarbonyl adduct [K(18c-6)][(PHDI)Co(μ^2:η^1,η^4-P$_4$)W(CO)$_5$] ([K(18c-6)]**3**), obtained quantitatively from [K(18c-6)]**2** and [W(CO)$_5$(thf)], shows an ordered structure (Scheme 3, Figure 1a).
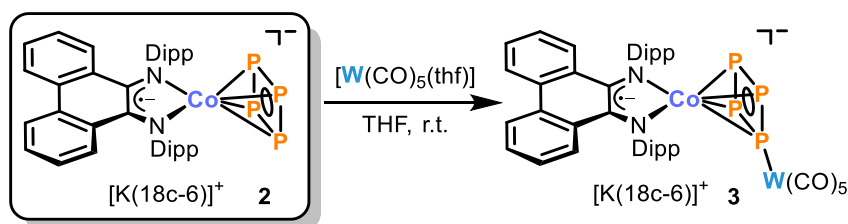
Scheme 3. Synthesis of the tungsten pentacarbonyl complex [K(18c-6)]**3**.

The almost square *cyclo*-P$_4$ unit shows P−P bond lengths in the range of 2.132(4) to 2.173(5) Å (mean: 2.147(7) Å) in between the values expected for P−P single (2.22 Å) and P=P double bonds (2.04 Å))[11] and similar to those found in other *cyclo*-P$_4$ complexes.[12]–[12]
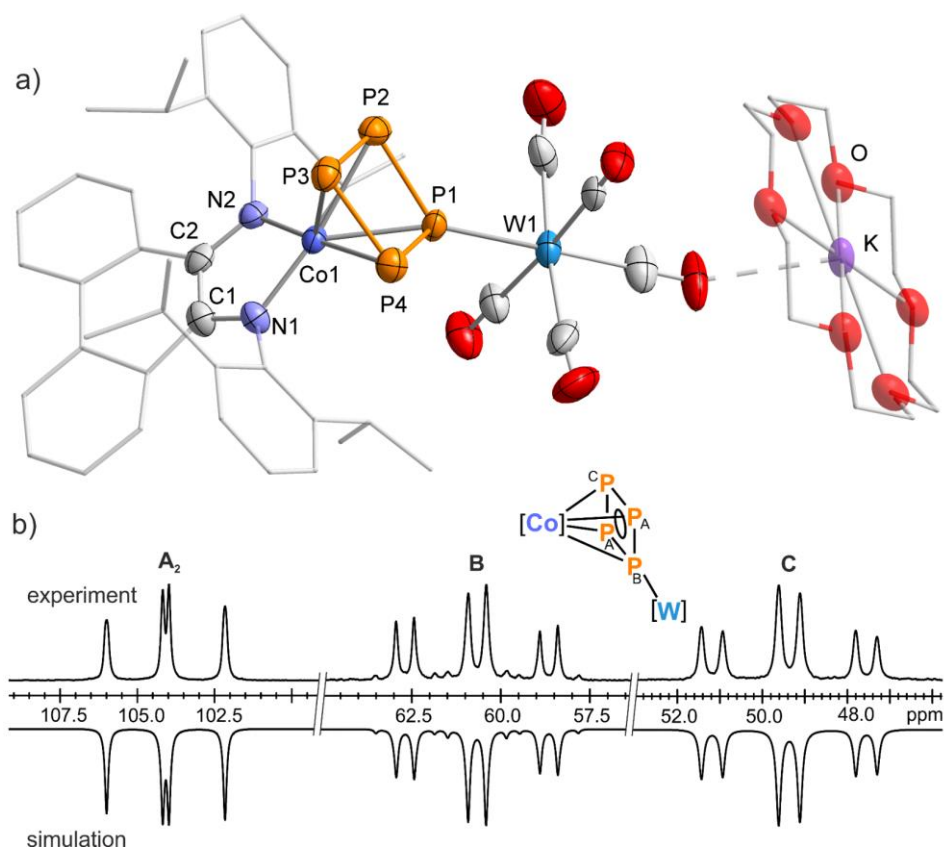

Figure 1. (a) Solid-state molecular structure of [K(18c-6)][(PHDI)Co(μ^2:η^1,η^4-P$_4$)W(CO)$_5$] ([K(18c-6)]**3**). Hydrogen atoms and disorder in the PHDI ligand are omitted for clarity and thermal ellipsoids are drawn at the 40% probability level. The asymmetric unit contained a second crystallographically independent molecule and one molecule of Et$_2$O, which are not shown. Selected bond lengths [Å] and angles [°]: W1−P1 2.521(2), 2.527(3), P1−P2 2.151(3), 2.173(5), P1−P4 2.134(3), 2.132(4), P2−P3 2.155(3), 2.133(6), P3−P4 2.153(3), 2.144(7), Co1−P1 2.314(2), 2.297(3), Co1−P2 2.394(2), 2.419(4), Co1−P3 2.313(2), 2.313(4), Co1−P4 2.405(2), 2.392(3), Co1−N1 1.880(6), 1.888(7), Co1−N2 1.888(6), 1.884(8), C1−N1 1.36(1), 1.36(1), C2−N2 1.35(1), 1.36(1), C1−C2 1.42(1), 1.42(1), P1−P2−P3 87.9(1), 87.4(2), P2−P3−P4 91.4(1), 92.5(2), P3−P4−P1 88.4(1), 88.2(2), P2−P1−P4 92.0(1), 91.7(2). (b) Section of the ^{31}P{^{1}H} NMR spectrum of **3** at −80 °C with nuclei assigned to an A$_2$BC spin system; experimental (upwards); simulation (downwards): δ(P$_A$) = 104.0 ppm, δ(P$_B$) = 60.7 ppm, δ(P$_C$) = 49.4 ppm, $^1J_{AB}$ = −326.9 Hz, $^1J_{AC}$ = −294.3 Hz, $^2J_{BC}$ = 81.0 Hz, $^1J_{PW}$ = −186.3 Hz. [Co] = [(PHDI)Co], [W] = [W(CO)$_5$].

The C−C and C−N distances in the PHDI backbone (C−C 1.42(1) Å; C−N 1.36(1) Å) indicate the presence of PHDI in its radical anionic form.[13] The $^{31}P\{^1H\}$ NMR spectrum (THF-d_8) shows an extremely broad singlet at 83.6 ppm ($\Delta v_{1/2}$ = 2400 Hz) at room temperature due to rapid migration of the [W(CO)$_5$] unit around the *cyclo*-P$_4$ ring, while three well-resolved doublets of triplets with an integral ratio of 2:1:1 appear upon cooling (Figure 2). Similar dynamic behaviour has been reported for other W(CO)$_5$ complexes.[14,15] Iterative fitting of the $^{31}P\{^1H\}$ NMR spectrum (Figure 1b) at −80 °C gave P−P coupling constants ($^1J_{PP}$ = −326.9 and −294.3 Hz) and ancillary ^{183}W-satellites ($^1J_{PW}$ = −186.3 Hz) typical for tungsten pentacarbonyl complexes of polyphosphides.[15,16]
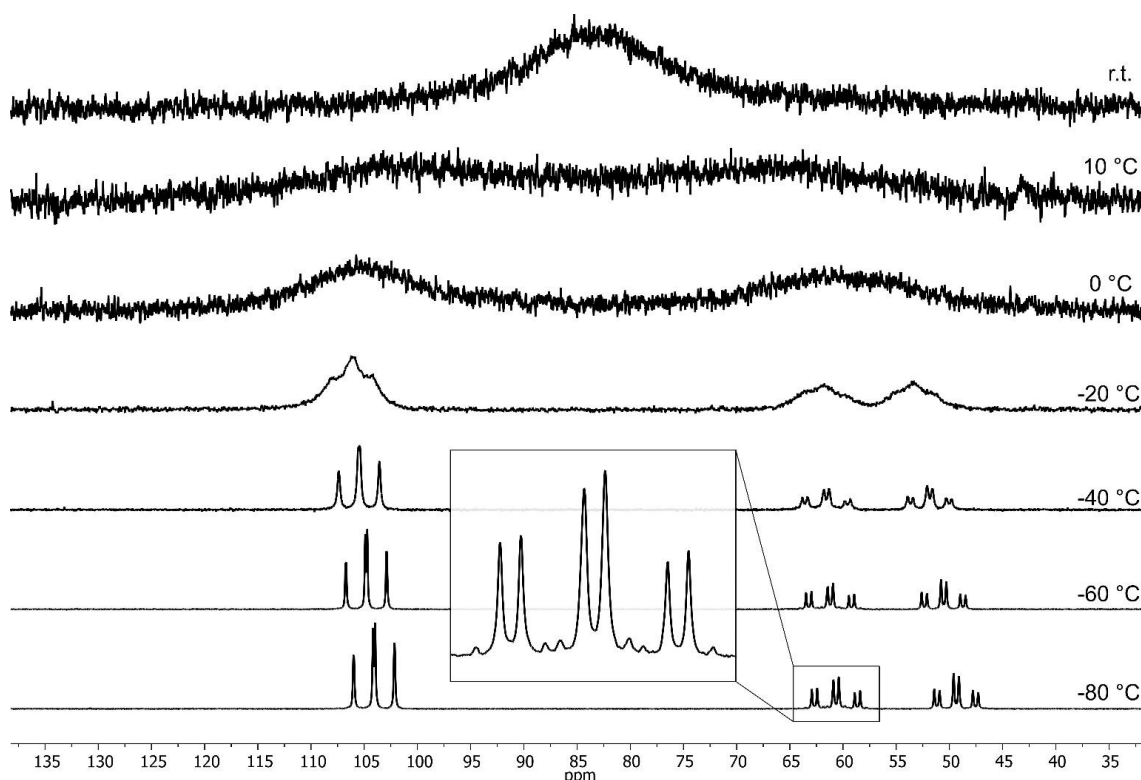
Figure 2. $^{31}P\{^1H\}$ NMR monitoring (161.98 MHz, 300 K, THF-d_8) [K(18c-6)][(PHDI)Co(μ^2:η^1,η^4-P$_4$)W(CO)$_5$] ([K(18c-6)]**3**).

In general, mononuclear *cyclo*-P$_4$ complexes are still rare in the literature. Besides two recently published iron complexes,[10,12] only examples with early transition metals (e.g. V, Nb, Ta, Mo) are known to date.[17] A recently reported, neutral *cyclo*-P$_4$ cobalt sandwich complex [(η^5-Cp^{tBu3})Co(η^4-P$_4$)] (Cp^{tBu3} = C$_5$H$_2$tBu$_3$) described by *Scheer* and co-workers is unstable at room temperature and only accessible in low yields after column chromatography.[9] By contrast, [K(18c-6)]**2** is indefinitely stable at room temperature both as a solid and in solution.

3.2.2 Synthesis and Characterization of Pentaphosphido Complexes 4-R

Due to the ease of synthesis and high yield, [K(18c-6)]**2** could be an excellent precursor for P–P bond formation reactions with diorganochlorophosphanes. Reactions with R_2PCl (R = Cy, tBu, Ph, Mes, N(iPr)$_2$, Scheme 4) proceed quantitatively (^{31}P NMR monitoring) to afford pentaphosphido complexes [(PHDI)Co(η^4-P$_5$R$_2$)] (**4-R**), which are isolated as dark blue crystals in up to 77% yield by a simple work-up procedure. Analogous reactions with $K_2[Co_2(\mu^2{:}\eta^4,\eta^4$-P$_4)(^{Dipp}$BIAN)$_2]$ are observed to lead only to unproductive outer sphere electron transfer reactions.
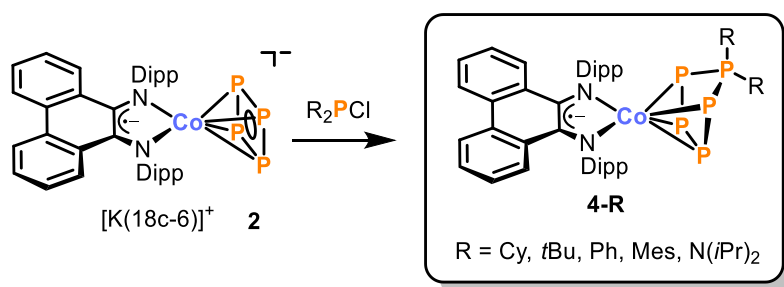
Scheme 4. Functionalization of the P$_4$ unit in **2** by several chlorophosphanes affording the pentaphosphido complexes **4-R**; reagents and by-products +R$_2$PCl/−KCl, −18c-6.

Complexes **4-R** are isostructural and resemble those of the recently reported species [(^{Mes}BIAN)Co(η^4-P$_5$R$_2$)] (**B**, R= iPr, tBu, Cy, see Scheme 1a).[6] The molecular structure of **4-tBu** is shown as an example in Figure 3a, while the remaining structures with R = Cy, Ph, Mes, NiPr$_2$ are given in the Supporting Information. The η^4-$cyclo$-P$_5$R$_2$ ligands show an envelope conformation with P−P distances ranging from 2.1197(2) to 2.182(1) Å that indicate some delocalized character.[11] The C−C and C−N distances in **4-R** suggest the presence of PHDI$^{\bullet-}$ radical anions.[6,13] The ^{31}P{^{1}H} NMR spectra recorded in C$_6$D$_6$ shows an AMM′XX′ spin system in each case (see Figure 3b for the spectrum of **4-tBu** as an example).[6] The chemical shift of the tetracoordinate phosphorus atoms P$_A$ varies with the substituent (e.g. 161.7 ppm for **4-tBu** vs. 84.3 ppm for **4-Mes**), while the remaining data is similar to those observed for complexes **B**.
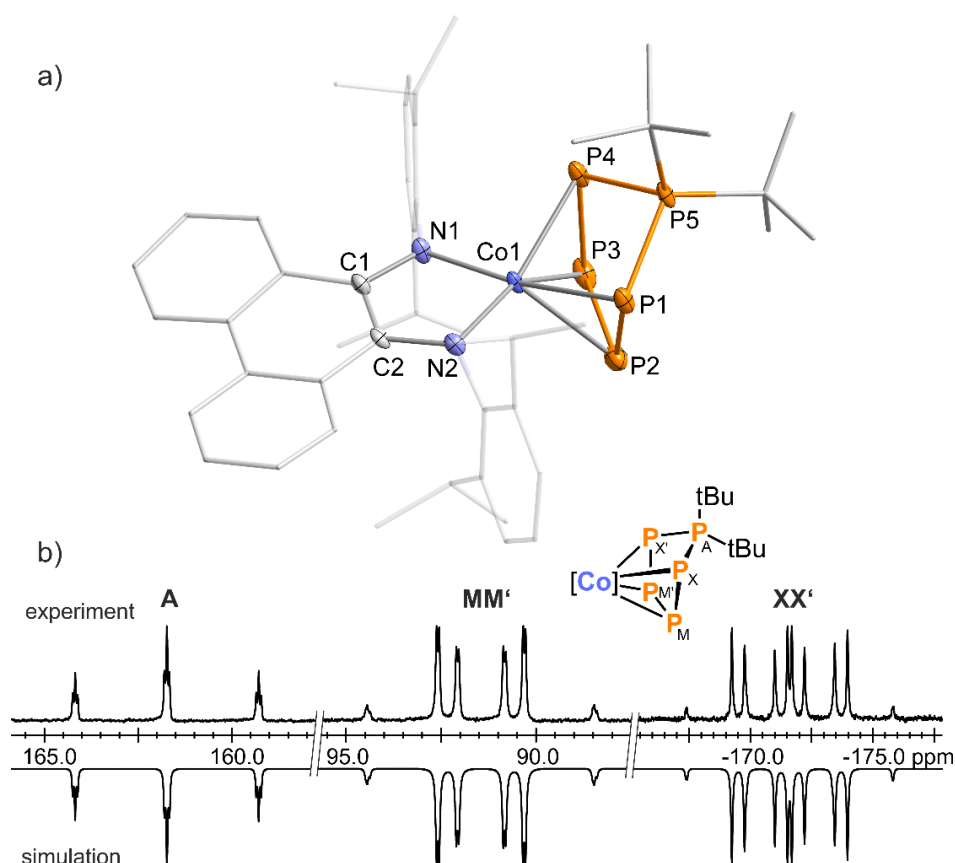
Figure 3. a) Solid-state molecular structure of [(PHDI)Co(η^4-P$_5t$Bu$_2$)] (**4-*t*Bu**). Hydrogen atoms are omitted for clarity and thermal ellipsoids are drawn at the 60% probability level. Selected bond lengths [Å] and angles [°]: P1–P2 2.1410(9), P1–P5 2.1596(8), P2–P3 2.132(1), P3–P4 2.1394(9), P4–P5 2.1487(9), Co1–P1 2.3687(7), Co1–P2 2.3463(7), Co1–P3 2.3236(7), Co1–P4 2.3928(7), Co1–N1 1.893(2), Co1–N2 1.896(2), C1–N1 1.360(3), C2–N2 1.360(3), C1–C2 1.427(3), P1–P2–P3 103.63(3), P2–P3–P4 105.11(4), P3–P4–P5 100.41(4), P4–P5–P1 95.69(3), P5–P1–P2 100.63(3). b) Section of the ^{31}P{^{1}H} NMR spectrum of **4-*t*Bu** with nuclei assigned to an AMM'XX' spin system; experimental (upwards); simulation (downwards): δ(P$_A$) = 161.7 ppm, δ(P$_{MM'}$) = 91.4 ppm, δ(P$_{XX'}$) = −171.6 ppm, $^1J_{AX}$ = $^1J_{AX'}$ = −396.3 Hz, $^1J_{MX}$ = $^1J_{M'X'}$ = −404.1 Hz, $^1J_{MM'}$ = −383.6 Hz, $^2J_{MX'}$ = $^2J_{M'X}$ = 35.9 Hz, $^2J_{AM}$ = $^2J_{AM'}$ = 10.9 Hz, $^2J_{XX'}$ = −4.9 Hz; the spectra of the residual compounds **4-R** are very similar (see supporting information for further details); [Co] = (PHDI)Co.

3.2.3 [3+2] Fragmentation of 4-R by Cyanides

Having substantial quantities of *cyclo*-P$_5$R$_2$ complexes **4-R** (R = Cy, *t*Bu, Ph, Mes, N(*i*Pr)$_2$) in hand, reactions with [M]CN ([M] = [*n*Bu$_4$N]$^+$, [Et$_4$N]$^+$, [K(18c-6)]$^+$, Scheme 5a) were examined with the aim of releasing the functionalized polyphosphorus ligand. An immediate color change from dark blue to dark purple-blue occurs upon addition of the cyanide salt. ^{31}P{^{1}H} NMR reaction monitoring revealed the clean formation of [(PHDI)Co(η^3-P$_3$)(CN)]$^-$ (**5**, singlet at 193.2 ppm), which can be isolated as the tetra-*n*-butylammonium salt [*n*Bu$_4$N]**5** in 40–64% yield by crystallization from toluene. In addition, the formation of the new cyanodiphosphanide anions [R$_2$PPCN]$^-$ (**6-R**, R = Cy, *t*Bu, Ph, N(*i*Pr)$_2$) is observed, which are identified by the characteristic set of doublets ($^1J_{PP}$ = 261 to 278 Hz) in the ^{31}P{^{1}H} NMR. The reaction thus results in an unprecedented fragmentation of the polyphosphide ligand into a P$_3$ and a P$_2$ unit. To our knowledge, there is only one related reaction involving the [3+2] fragmentation of a P$_5$ species in the literature, which has a completely different outcome. As reported by *Weigand* and co-workers, the reaction of [P$_5$DippCl]$^+$ cation (Dipp = 2,6-*i*Pr$_2$C$_6$H$_3$) with *N,N'*-bis(2,6-diisopropylphenyl)-4,5-dichloro-imidazol-2-ylidene (^{Cl}Im^{Dipp}) affords a triphosphaallyl cation [(^{Cl}Im^{Dipp})P$_3$(IPrCl$_2$)]$^+$ and an inversely polarized phosphaalkene [(^{Cl}Im^{Dipp})P=P(Cl)Dipp].[18]
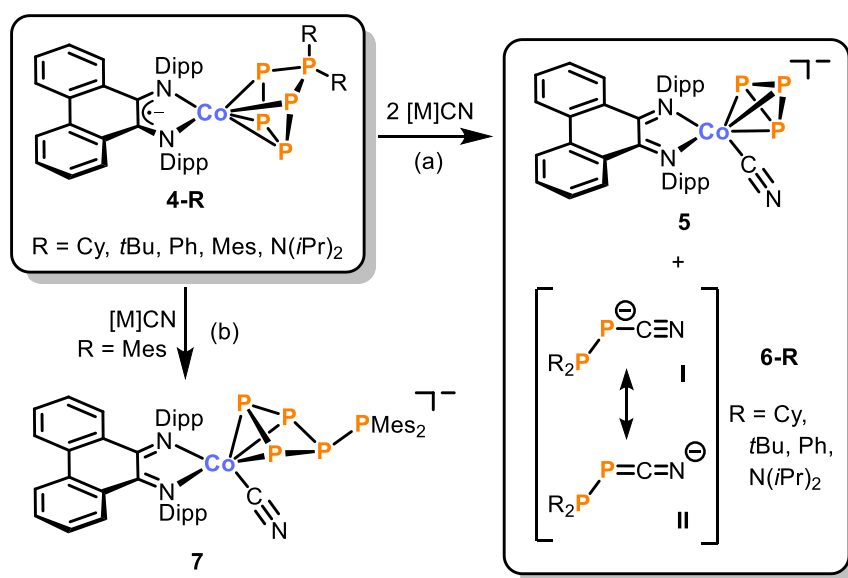
Scheme 5. Fragmentation (a) and rearrangement (b) of the pentaphosphido ligand in **4-R** depending on the substituent R. Reagents and by-products (a) for R = Cy, *t*Bu, Ph, N(*i*Pr)$_2$, + 2 equiv. [M]CN; (b) only for R = Mes, + 1 equiv. [M]CN ([M] = [*n*Bu$_4$N]$^+$, [Et$_4$N]$^+$, [K(18c-6)]$^+$). **I** and **II** are two conceivable resonance structures of anions **6-R**.

[*n*Bu$_4$N]**5** is a rare example of an anionic *cyclo*-P$_3$ cobalt complex.[19] Compared to related neutral species such as [(ArNC)$_3$Co(η^3-P$_3$)] (Ar = 2,6-(Mes)$_2$C$_6$H$_3$, δ = −276 ppm),[20] and [(CH$_3$C(CH$_2$PPh$_2$)$_3$)Co(η^3-P$_3$)] (δ = −278 ppm),[21] the ^{31}P{^{1}H} NMR resonance of [*n*Bu$_4$N]**5** (δ = −193.2 ppm) is shifted downfield. [*n*Bu$_4$N]**6-*t*Bu** can be isolated as a light purple solid in 40% yield by extracting the crude reaction mixture with cyclohexane:*n*-hexane (3:2 v/v).

While X-ray quality crystals of [*n*Bu$_4$N]**5** and [*n*Bu$_4$N]**6-*t*Bu** could not be obtained so far, crystal structures of both potassium salts [K(18c-6)]**5** and [K(18c-6)]**6-*t*Bu** have been obtained from separate single crystals grown from same the reaction mixture (attempts to separate these compounds in a preparative manner have thus far been unsuccessful). The molecular structure of [K(18c-6)]**5** features a cobalt atom coordinated by a cyanide anion, a formally neutral PHDI ligand [C1−N1 1.338(2), C2−N2 1.344(2), and C1−C2 1.453(2) Å],[22–25] and a η^3-coordinated *cyclo*-P$_3$ ring (Figure 4).
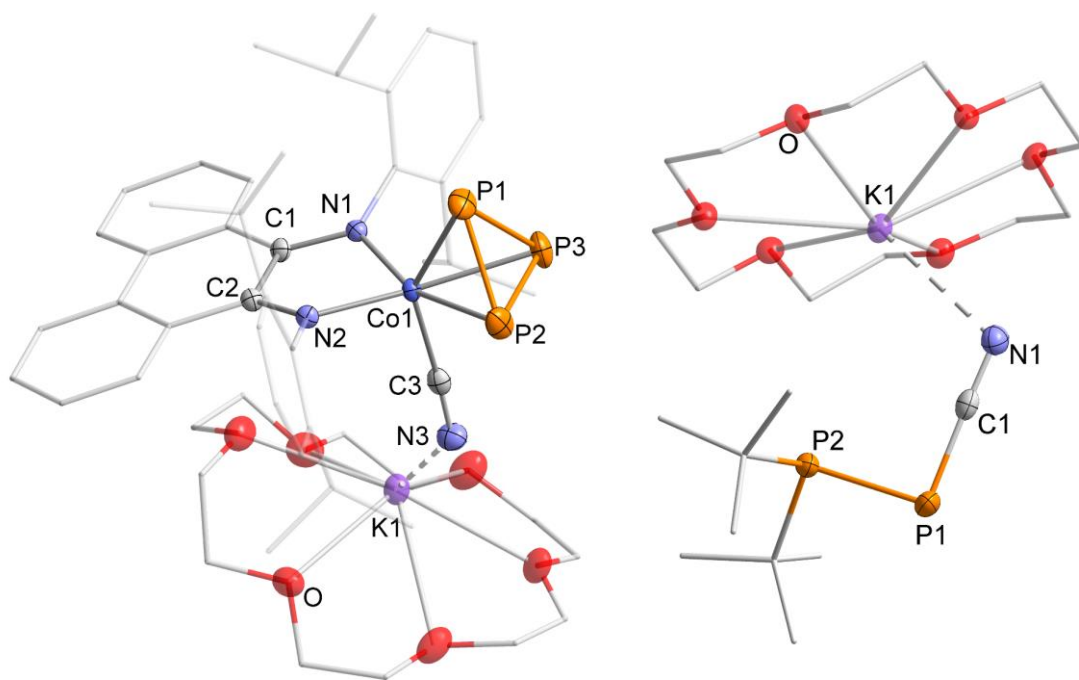

Figure 4. Solid-state molecular structures of [K(18c-6)][(PHDI)Co(η^3-P$_3$)(CN)] (left, [K(18c-6)]**5**) and [K(18c-6)][*t*Bu$_2$PPCN] (right, [K(18c-6)]**6-*t*Bu**). Hydrogen atoms, solvent molecules and disorder are omitted for clarity and thermal ellipsoids are drawn at the 50% probability level. Selected bond lengths [Å] and angles [°]: [K(18c-6)]**5**: P1−P2 2.1256(8), P1−P3 2.1228(7), P2−P3 2.1599(7), Co1−P1 2.2780(5), Co1−P2 2.3200(5), Co1−P3 2.3027(5), Co1−N1 1.908(1), Co1−N2 1.906(2), Co1−C3 1.909(2), C1−N1 1.338(2), C2−N2 1.344(2), C3−N3 1.153(2), C1−C2 1.453(2), K1···N3 2.714(2), P1−P2−P3 59.38(2), P1−P3−P2 59.51(2), P2−P1−P3 61.12(2), Co1−C3−N3 177.0(2); [K(18c-6)]**6-*t*Bu**: P1−P2 2.1895(4), P1−C1 1.763(1), C1−N1 1.160(2), K1···N1 2.828(1), P1−C1−N1 178.4(1), C1−P1−P2 92.43(4).

The mean P−P (2.1361(8) Å) and Co−P (2.300(5) Å) distances in [K(18c-6)]**5** are similar to neutral CoP$_3$ complexes.[20,26] The Co−C (1.909(2) Å) and C≡N (1.153(2) Å)) bond lengths as well as the ν_{CN} stretching frequency (2068 cm^{-1}) are typical for cyanide cobalt complexes.[27] The solid-state molecular structure of [K(18c-6)]**6-*t*Bu** shows an almost linear, phosphanyl-substituted PCN moiety (P1−C1−N1 178.4(1)°) with a P−P distance of 2.1895(4) Å, i.e. close to a typical single bond.[11] The structural motif is reminiscent of *Schmidpeter*'s [RPCN]$^-$ (R = CN, Ph) anions.[28–30] The IR spectrum shows the characteristic ν_{CN} stretch at 2049 cm^{-1}, which is smaller than those of known dicyanophosphanides [P(CN)$_2$]$^-$ (2120, 2113 cm^{-1})[28,29] and other trivalent monocyanophosphanes (~2160 cm^{-1}).[31]

Recently, *Borger* and *Grützmacher* described related cyanophosphanides [(NHP)PCN] with bulky *N*-heterocyclic phosphenium (NHP) substituents. These species feature a similar CN stretching frequency (2087 to 2046 cm^{-1}) and similar bond parameters as [K(18c-6)]**6-*t*Bu**.[7,28–30] Similar to that compound, the electronic structure of **6-R** may be described as a cyanophosphanide ($^-$P−C≡N, **I**) and a phosphaketeneimide (P=C=N$^-$, **II**) resonance structure (c.f. Scheme 5a). A natural resonance analysis at the B3LYP/6-31G+* level shows that the phosphaketeneimide form plays only a minor role in the electronic ground state on **6-*t*Bu** (**I**: 69% vs. **II**: 23%). Analogous calculations for related cyanate and phosphaethynolate anions (O$^-$−C≡X vs. O=C=X$^-$, X = N, P) gave much higher contributions of the ketene form in NCO$^-$ (33%) and PCO$^-$ (40%).[32]

Remarkably, a different product [Et$_4$N][(PHDI)Co(η^3-P$_4$PMes$_2$)(CN)] ([Et$_4$N]**7**) is isolated when mesityl-substitued **4-Mes** is reacted with [Et$_4$N]CN (one equiv., Scheme 5b). According to ^{31}P{^{1}H} NMR monitoring, the reaction reaches full conversion within two hours at −30 °C in MeCN; the main product, [Et$_4$N]**7** is identified by an AB$_2$CD spin system (δ = 32.8, 59.2, 94.0 and 193.7 ppm). Deep purple crystals can be isolated in 38% yield from toluene/THF after work-up at low temperature (<–30 °C).[33] The single-crystal XRD structure (Figure 5) shows a bent P$_4$ ring coordinating to cobalt via three P atoms with P3–P4 and P4–P5 distances of 2.1667(9) and 2.172(1) Å respectively, indicating some delocalized character. The remaining P–P bond lengths (2.2416(9), 2.241(1), and 2.2381(9) Å) are typical of single bonds.[34] The structural parameters of the PHDI ligand (C1−N1 1.328(4), C2−N2 1.335(3), and C1−C2 1.457(4) Å) are similar to those of [K(18c-6)]**5**, which suggests the presence of a neutral PHDI molecule.[22–25]
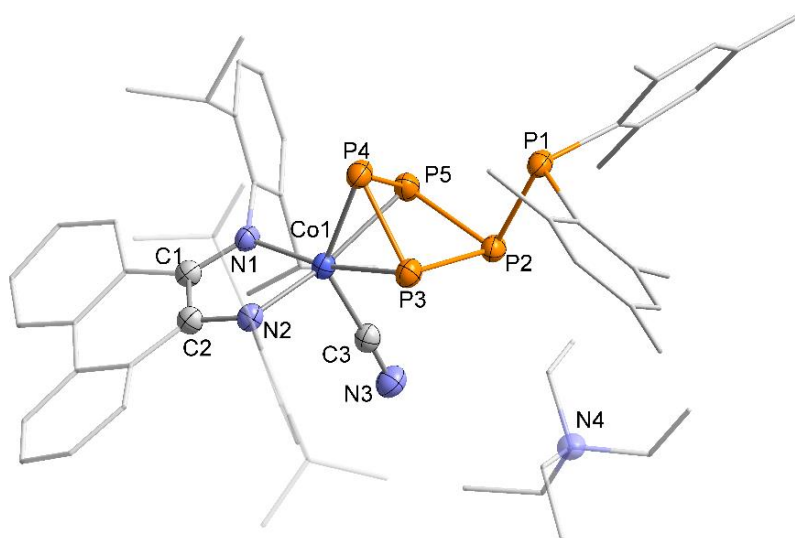
Figure 5. Solid-state molecular structure of [Et$_4$N][(PHDI)Co(η^3-P$_4$PMes$_2$)(CN)] ([Et$_4$N]**7**). Hydrogen atoms are omitted for clarity and thermal ellipsoids are drawn at the 50% probability level. Selected bond lengths [Å] and angles [°]: P1–P2 2.2416(9), P2–P3 2.241(1), P2–P5 2.2381(9), P3–P4 2.1667(9), P4–P5 2.172(1), Co1–P3 2.3356(8), Co1–P4 2.2671(8), Co1–P5 2.3174(8), Co1–N1 1.921(2), Co1–N2 1.927(2), Co1–C3 1.925(3), C1–N1 1.328(4), C2–N2 1.335(3), C3–N3 1.144(4), C1–C2 1.457(4), P1–P2–P3 94.77(4), P1–P2–P5 98.13(3), P2–P3–P4 90.36(4), P3–P4–P5 83.68(4), P4–P5–P2 90.28(4), P5–P2–P3 80.52(3).

The mechanism of the formation of [Et$_4$N]**7** is proposed to involve an attack of the cyanide anion at cobalt, which induces a rearrangement to a phosphanyl-substituted *cyclo*-P$_4$ ring. It is noteworthy to add that [Et$_4$N]**7** is not converted into P$_3$ and P$_2$ products (**5** and hypothetical **6-Mes**) by addition with a second equivalent of cyanide. Presumably, the sterically encumbering nature of the mesityl substituents prevents the CN$^-$ anion from approaching P2. Nevertheless, it is likely that intermediates similar to [Et$_4$N]**7** are formed in the fragmentation reactions of **4-R** with smaller substituents.

3.3   Conclusion

In conclusion, neutral pentaphosphido complexes **4-R** are readily accessible from [K(18c-6)]**1**, P_4 and R_2PCl in two steps with an considerable range of alkyl, aryl and amino substituents. Remarkably, the pentaphosphorus ligands of **4-R** undergo an unprecedented [3+2] fragmentation upon reaction with two equiv. of cyanide, forming an anionic cyclotriphosphido cobalt complex **5** and rare phosphanyl substituted cyanophosphanides **6-R**. Reaction of **4-Mes** with cyanide affords [Et$_4$N]**7**, which contains a rearranged P_5Mes_2 ligand. The structure of this complex suggests that tetraphosphido complexes are key intermediates *en route* to anions **5** and **6-R**. The results of this work show for the first time that diimine cobalt complexes are an excellent platform for studying the degradation of polyphosphorus ligands with inorganic nucleophiles. An extension of this approach to a wider range of polyphosphides and other nucleophiles should give rise to further unique phosphorus compounds. Furthermore, reactions of [K(18c-6)]**2** and [nBu$_4$N]**5** with electrophiles will likely give rise to novel polyphosphanes and polyphosphido complexes. Investigations into this research area are currently underway.

.

## 3.4   Supporting Information

3.4.1   General Procedures

All experiments were performed under an atmosphere of dry argon, by using standard Schlenk and glovebox techniques. Solvents were purified, dried, and degassed with an MBraun SPS800 solvent purification system. NMR spectra were recorded on Bruker Avance 400 spectrometers at 300 K. ^{1}H and ^{13}C{^{1}H} spectra were referenced internally to residual solvent resonances. ^{31}P{^{1}H} and ^{31}P NMR spectra were referenced externally to 85% $H_3PO_{4(aq.)}$. The assignment of the ^{1}H and ^{13}C NMR signals was confirmed by two-dimensional (COSY, HSQC, HMBC and ROESY) experiments. Melting points were measured on samples in sealed capillaries on a Stuart SMP10 melting point apparatus. UV/vis spectra were recorded on an Ocean Optics Flame Spectrometer. Elemental analyses were determined by the analytical department of the University of Regensburg. IR spectra were recorded with a Bruker ALPHA spectrometer equipped with a diamond ATR unit. The starting materials PHDI,[35] Cy_2PCl,[36] and tBu$_2$PCl[37] were prepared according to literature procedures. Literature protocols were slightly modified for [K(thf)$_{0.2}$][Co(η^4-1,5-cod)$_2$][38] (usage of potassium instead of lithium) and Mes$_2$PCl[39] (usage of 0.5 equiv. of PCl_3 instead of one equivalent). [18]c-6, Ph$_2$PCl, [nBu$_4$N]CN, [Et$_4$N]CN were purchased from Sigma Aldrich; [W(CO)$_6$], KCN from Merck; and (iPr$_2$N)$_2$PCl from Acros and all were used as received.

2.4.2   NMR Simulations

For compounds which give rise to a higher order spin system in the ^{31}P{^{1}H} NMR spectrum, the resolution enhanced ^{31}P{H} NMR spectrum was transferred to the software gNMR, version 5.0.6.0, by Cherwell Scientific.[40] The full line shape iteration procedure of gNMR was applied to obtain the best match of the fitted to the experimental spectrum. $^1J(^{31}$P^{31}P) coupling constants were set to negative values and all other signs of the coupling constants were obtained accordingly.[41]

3.4.3 Synthesis and Characterization

3.4.3.1 Synthesis of [K(18c-6)][(PHDI)Co(η^4-1,5-cod)] ([K(18c-6)]1)

[K(18c-6)(thf)$_{1.4}$]$^+$
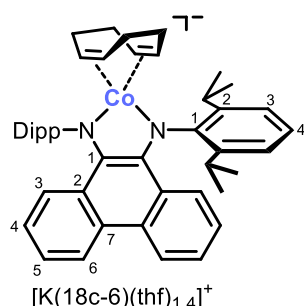
A deep yellowish green solution of [K(thf)$_{0.2}$][Co(η^4-1,5-cod)$_2$] (2.4 g, 7.28 mmol, 1.0 equiv.) and 18c-6 (1.94 g, 7.32 mmol, 1.0 equiv.) in THF (80 mL) was added to a deep red solution of PHDI (4.0 g, 7.62 mmol, 1.05 equiv.) in THF (80 mL) at −30 °C. The resulting deep green mixture was stirred overnight upon warming to room temperature and filtered through a P4 glass frit. The filtrate was concentrated to ca. ½ and layered with *n*-hexane (80 mL). After one week, deep green crystals were isolated by filtration, washed with *n*-pentane (2 x 70 mL) and dried *in vacuo*. Yield: 6.04 g (76%)

M.p. 180 °C (decomposition to a black oil). **UV/vis** (THF, λ_{max} / nm, ε_{max} / L·mol^{-1}·cm^{-1}): 360 (15000), 440 (18500), 560 (3800). **^{1}H NMR** (400.30 MHz, THF-d_8, 300 K): δ/ppm = 0.64 (d, $^3J_{HH}$ = 6.9 Hz, 12H, −CH(CH_3)$_2$ of Dipp), 0.98-1.03 (m, 4H, CH_2 of COD), 1.39 (d, $^3J_{HH}$ = 6.9 Hz, 12H, −CH(CH_3)$_2$ of Dipp), 2.29-2.31 (m, 4H, CH_2 of COD), 2.79 (s, 4H, CH of COD), 3.34 (s, 24H, 18c-6), 4.51 (sept, $^3J_{HH}$ = 6.9 Hz, 4H, −CH(CH$_3$)$_2$ of Dipp), 6.40-6.44 (m, 2H, C^4−H of PHDI), 6.62 (t, 2H, $^3J_{HH}$ = 7.2 Hz, C^5−H of PHDI), 7.79 (d, $^3J_{HH}$ = 8.8 Hz, 2H, C^3−H of PHDI), 7.04-7.06 (m, 6H, C^{3,4}−H of Dipp), 8.20 (d, $^3J_{HH}$ = 8.1 Hz, 2H, C^6−H of PHDI). **^{13}C{^{1}H} NMR** (100.61 MHz, THF-d_8, 300 K): δ /ppm = 25.0 (s, −CH(CH$_3$)$_2$ of Dipp overlapping with THF-d_8 signal), 28.2 (s, −CH(CH$_3$)$_2$ of Dipp), 31.9 (s, CH$_2$ of COD), 68.4 (s, CH of COD), 70.8 (s, 18c-6), 117.1 (s, C^5 of PHDI), 122.2 (s, C^4 of PHDI overlapping with C^6 of PHDI), 122.7 and 123.2 (s, $C^{3,4}$ of Dipp), 124.5 (s, C^7 of PHDI), 125.8 (s, C^3 of PHDI), 127.9 (s, C^2 of PHDI), 140.0 (s, C^1 of PHDI), 145.5 (s, C^2 of Dipp), 157.1 (s, C^1 of Dipp). **Elemental analysis** calcd. for $C_{58}H_{78}CoKN_2O_6$(THF)$_{1.4}$ (Mw = 1098.25 g·mol^{-1}) C 69.56, H 8.19 N 2.55; found C 68.97, H 8.09, N 2.29.H 6.13.

3.4.2.2 Synthesis of [K(18c-6)][(PHDI)Co(η^4-P$_4$)] ([K(18c-6)]2)
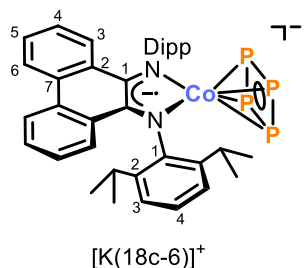
[K(18c-6)]$^+$

A 500 mL Schlenk flask was filled with P$_4$ (250 mg, 2.02 mmol, 1.0 equiv.), [K(18c-6)]**1**·(thf)$_{1.2}$ (2.189 g, 2.02 mmol, 1.0 equiv.) and THF (200 mL). The resulting deep green mixture was stirred for 15 h. The solvent was removed and the dark green residue was extracted into toluene (400 mL) and filtered through a P4 glass frit. The volume of the solvent was

reduced to 200 mL and the deep turquoise solution was layered with n-hexane (ca. 1.1 L). After ten days, dark pink shimmering crystals were isolated by decantation of the supernatant. The crystals were washed with *n*-pentane (2 x 40 mL) and dried *in vacuo*. Yield: 1.65 g (80%)

M.p. 240 °C (decomposition to a black solid). **UV/vis** (THF, λ_{max} / nm, ε_{max} / L·mol^{-1}·cm^{-1}): 260 (62000), 365 (35000), 425sh (20000), 660 (37000). **^{1}H NMR** (400.13 MHz, THF-d_8, 300 K): δ/ppm = 0.74 (d, $^3J_{HH}$ = 6.9 Hz, 12H, −CH(CH_3)$_2$ of Dipp), 1.06 (d, $^3J_{HH}$ = 6.9 Hz, 12H, −CH(CH_3)$_2$ of Dipp), 3.58 (s, 24H, 18c-6), 4.30 (sept, $^3J_{HH}$ = 6.9 Hz, 4H, −CH(CH$_3$)$_2$ of Dipp), 6.74-6.79 (m, 2H, C^4−H of PHDI), 7.01-7.03 (m, 4H, C^3−H of Dipp), 7.06-7.10 (m, 2H, C^4−H of Dipp), 7.20-7.24 (m, 2H, C^5−H of PHDI), 7.36 (d, $^3J_{HH}$ = 8.8 Hz, 2H, C^3−H of PHDI), 8.36 (d, $^3J_{HH}$ = 7.6 Hz, 2H, C^6−H of PHDI). **^{13}C{^{1}H} NMR** (100.61 MHz, THF-d_8, 300 K): δ /ppm = 24.7 (s, −CH(CH_3)$_2$ of Dipp), 29.0 (s, −CH(CH$_3$)$_2$ of Dipp), 71.1 (s, 18c-6), 122.0 (s, C^5 of PHDI), 123.0 (s, C^3 of Dipp), 123.6 (s, C^6 of PHDI), 124.3 (s, C^4 of Dipp), 125.3 (s, C^4 of PHDI), 127.5 (s, C^3 of PHDI), 128.6 (s, C^7 of PHDI), 130.1 (s, C^2 of PHDI), 140.0 (s, C^2 of Dipp), 145.0 (s, C^1 of PHDI), 164.4 (s, C^1 of Dipp). **^{31}P{^{1}H} NMR** (161.98 MHz, THF-d_8, 300 K): δ / ppm = 136.5 (s). **Elemental analysis** calcd. for C$_{50}$H$_{66}$CoKN$_2$O$_6$P$_4$(toluene)$_{0.1}$ (Mw = 1022.23 g·mol^{-1}) C 59.57, H 6.59 N 2.74; found C 59.68, H 6.46, N 2.54.

.

3.4.2.3 Synthesis of [K(18c-6)][(PHDI)Co(μ^2:η^1,η^4-P$_4$)W(CO)$_5$] ([K(18c-6)3)

[K(18c-6)]$^+$

A stirred, colorless solution of [W(CO)$_6$] (34 mg, 0.097 mmol, 1.0 equiv.) in THF (4 mL) was irradiated with UV-light (365 nm) for 4 h. The solution turned deep yellow and was added dropwise to a dark green solution of [K(18c-6)]**2** (100 mg, 0.097 mmol, 1.0 equiv.) in THF (20 mL). After stirring overnight all volatiles were removed and the resulting dark green residue was extracted into Et$_2$O (2 x 40 mL). The dark green filtrate was concentrated to one fourth of the original volume and layered with *n*-pentane (50 mL). Dark green crystals formed upon storage for one week, which were isolated by decantation of the supernatant and dried *in vacuo*. Yield: 41 mg (32%)

M.p. 186 °C (decomposition to a black oil). **UV/vis** (THF, λ_{max} / nm, ε_{max} / L·mol^{-1}·cm^{-1}): 370 (28000), 415sh (18000), 660 (25000). **^{1}H NMR** (400.13 MHz, THF-d_8, 300 K): δ/ppm = 0.69 (d, $^3J_{HH}$ = 6.9 Hz, 12H, −CH(CH_3)$_2$ of Dipp), 1.19 (d, $^3J_{HH}$ = 6.9 Hz, 12H,

−CH(CH_3)$_2$ of Dipp), 3.58 overlapping with THF-d_8 solvent signal (s, 24H, 18c-6,), 4.24 (sept, $^3J_{HH}$ = 6.9 Hz, 4H, −CH(CH$_3$)$_2$ of Dipp), 6.72-6.76 (m, 2H, C^4−H of PHDI), 7.06-7.10 (m, 6H, C^3−H of Dipp overlapping with C^3−H of PHDI), 7.12-7.16 (m, 2H, C^4−H of Dipp), 7.23-7.27 (m, 2H, C^5−H of PHDI), 8.32 (d, $^3J_{HH}$ = 7.7 Hz, 2H, C^6−H of PHDI). ^{13}C{^{1}H} NMR (100.61 MHz, THF-d_8, 300 K): δ/ppm = 24.3 (s, −CH(CH_3)$_2$ of Dipp), 29.3 (s, −CH(CH$_3$)$_2$ of Dipp), 71.0 (s, 18c-6), 123.2 (s, C^5 of PHDI), 123.6 (s, C^3 of Dipp), 123.7 (s, C^6 of PHDI), 125.0 (s, C^4 of Dipp), 125.6 (s, C^4 of PHDI), 127.7 (s, C^3 of PHDI), 129.3 (s, C^7 of PHDI), 129.9 (s, C^2 of PHDI), 139.4 (s, C^2 of Dipp), 146.7 (s, C^1 of PHDI), 164.2 (s, C^1 of Dipp), 199.2 (s, C≡O). ^{31}P{^{1}H} NMR (161.98 MHz, THF-d_8, 300 K): δ / ppm = 83.6 (br s, Δν$_½$ = 2400 Hz). IR (solid state): ν/ cm^{-1} = 2952w, 2899w, 2862w, 2057s (C≡O), 1971w (C≡O), 1921vs (C≡O), 1885vs (C≡O), 1495m, 1434m, 1350m, 1235m, 1103s, 961m-s, 834w-m, 7914m-w, 754m-s, 722m, 591s, 575s. Elemental analysis calcd. for C$_{55}$H$_{66}$CoKN$_2$O$_{11}$P$_4$W (Mw = 1336.90 g·mol^{-1}) C 49.41, H 4.98 N 2.10; found C 49.76, H 49.1, N 2.04.

3.4.3.4 Synthesis of [(PHDI)Co(η^4-P$_5$Cy$_2$)] (4-Cy)
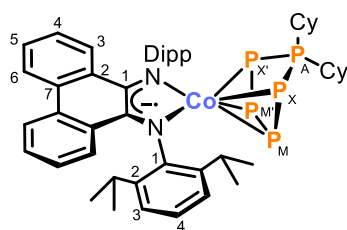
A stock solution of Cy$_2$PCl (2 mL, c = 0.112 M in n-hexane, 0.224 mmol, 1.0 equiv.) was added to a deep turquoise suspension of [K(18c-6)]**2** (228 mg, 0.224 mmol, 1.0 equiv.) in toluene (20 mL) at room temperature. The reaction mixture turned dark blue immediately and was stirred for 13 h. The mixture was filtered through a pad of silica gel (1.5 x 3 cm) and washed with toluene (ca. 10 mL). The solvent was removed and the dark blue residue was extracted into n-hexane (5 x 10 mL). The deep blue filtrate was concentrated to one fifth of the original volume until incipient crystallization. Numerous purple shimmering crystals were formed upon storage at −18 °C for six days, which were isolated by decantation of the mother liquor and subsequently dried *in vacuo*. Yield: 159 mg (77%)

M.p. 244 °C (decomposition to a black oil). UV/vis (THF, λ$_{max}$ / nm, ε$_{max}$ / L·mol^{-1}·cm^{-1}): 345 (14000), 520sh (6000), 600 (21000). ^{1}H NMR (400.13 MHz, C$_6$D$_6$, 300 K): δ /ppm = 0.55-0.74 (m, 4H, Cy−H), 0.77 (d, $^3J_{HH}$ = 6.8 Hz, 12H, −CH(CH_3)$_2$ of Dipp), 0.82-0.95 (m, 7H, Cy−H overlapping with CH_3 of n-hexane), 1.20-1.37 (m, 5H, Cy−H overlapping with CH_2 of n-hexane), 1.51-1.59 (m, 3H, Cy−H), 1.67 (d, $^3J_{HH}$ = 6.8 Hz, 12H, −CH(CH_3)$_2$ of Dipp), 1.83-1.86 (m, 2H, Cy−H), 1.97-2.04 (m, 1H, Cy−H), 3.69 (sept,

$^3J_{HH}$ = 6.8 Hz, 4H, $-CH(CH_3)_2$ of Dipp), 6.84-6.88 (m, 2H, C^4-H of PHDI), 7.24-7.27 (m, 4H, C^3-H and C^5-H of PHDI), 7.41-7.43 (m, 4H, C^3-H of Dipp), 7.48-7.52 (m, 2H, C^4-H of Dipp), 8.01 (d, $^3J_{HH}$ = 7.6 Hz, 2H, C^6-H of PHDI). **$^{13}C\{^1H\}$ NMR** (100.61 MHz, C_6D_6, 300 K): δ /ppm = 25.2 (s, $-CH(CH_3)_2$ of Dipp), 25.6 (s, Cy-C), 25.8 (s, $-CH(CH_3)_2$ of Dipp), 26.0 (s, Cy-C), 26.6 (s, Cy-C), 26.7 (s, Cy-C), 26.8 (s, Cy-C), 29.7 (s, $-CH(CH_3)_2$ of Dipp), 30.7 (s, Cy-C), 31.2 (s, Cy-C), 37.8-38.0 (m, Cy-C), 38.9 (m, Cy-C), 124.3 (s, C^6 of PHDI), 125.1 (s, C^3 of Dipp), 125.4 (s, C^3 or C^5 of PHDI), 126.7 (s, C^4 of PHDI), 127.2 (s, C^4 of Dipp), 128.4 (s, C^3 or C^5 of PHDI), 130.1 (s, C^2 of PHDI), 130.6 (s, C^7 of PHDI), 140.3 (s, C^2 of Dipp), 148.0 (s, C^1 of PHDI), 159.9 (s, C^1 of Dipp). **$^{31}P\{^1H\}$ NMR** (161.98 MHz, 300 K, C_6D_6): (AMM'XX') spin system δ / ppm = −127.0 - −118.7 (m, 2P, $P_{XX'}$), 94.0-100.0 (m, 2P, $P_{MM'}$), 146.0 (t, 1P, P_A). **Elemental analysis** calcd. for $(C_{50}H_{64}CoN_2P_5)(n\text{-hexane})_{0.5}$ (Mw = 949.97 g·mol^{-1}) C 67.01, H 7.53, N 2.95; found C 66.97, H 7.29, N 2.78.

3.4.3.5 Synthesis of [(PHDI)Co(η^4-P$_5$*t*Bu$_2$)] (4-*t*Bu)
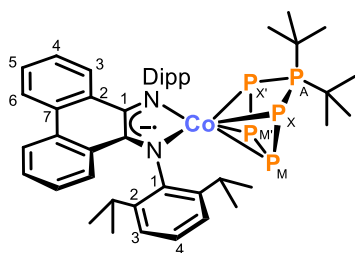
Neat tBu_2PCl (0.1 mL, 95 mg, 0.526 mmol, 1.0 equiv.) was added dropwise via syringe to a deep turquoise suspension of [K(18c-6)]**2** (536 mg, 0.526 mmol, 1.0 equiv.) in toluene (100 mL) at room temperature. The reaction mixture was stirred for three days while the color changed to dark blue. The mixture was filtered through a pad of silica gel (3 x 3 cm) and washed with toluene (ca. 20 mL). The volume of the dark blue filtrate was reduced to one third of the original volume and layered with *n*-pentane (ca. 300 mL). After two weeks, purple shimmering crystals have formed, which were isolated by decantation of the mother liquor and dried *in vacuo* Yield: 232 mg (52%)

M.p. 240 °C (decomposition to a black oil). **UV/vis** (THF, λ_{max} / nm, ε_{max} / L·mol^{-1}·cm^{-1}): 340 (27000), 430sh (8000), 580 (17000), 660 (28000). **^1H NMR** (400.13 MHz, C_6D_6, 300 K): δ /ppm =0.39 (d, $^3J_{HP}$ = 14.3 Hz, 9H, $-C(CH_3)_3$), 0.77 (d, $^3J_{HH}$ = 6.7 Hz, 12H, $-CH(CH_3)_2$ of Dipp), 1.54 (d, $^3J_{HP}$ = 12.8 Hz, 9H, $-C(CH_3)_3$), 1.75 (d, $^3J_{HH}$ = 6.7 Hz, 12H, $-CH(CH_3)_2$ of Dipp), 3.69 (sept, $^3J_{HH}$ = 6.7 Hz, 4H, $-CH(CH_3)_2$ of Dipp), 6.83-6.87 (m, 2H, C^4-H of PHDI), 7.18-7.20 (m, 2H, C^3-H of PHDI), 7.22-7.26 (m, 2H, C^5-H of PHDI), 7.42-7.44 (m, 4H, C^3-H of Dipp), 7.48-7.52 (m, 2H, C^4-H of Dipp), 8.06 (d, $^3J_{HH}$ = 7.7 Hz, 2H, C^6-H of PHDI). **$^{13}C\{^1H\}$ NMR** (100.61 MHz, C_6D_6, 300 K): δ /ppm =25.4

and 25.8 (s, −CH(CH$_3$)$_2$ of Dipp), 29.4 (s, −C(CH$_3$)$_3$), 29.9 (s, −CH(CH$_3$)$_2$ of Dipp), 31.8 (s, −C(CH$_3$)$_3$), 42.4 (s, −C(CH$_3$)$_3$), 124.1 (s, C^6 of PHDI), 124.7 (s, C^3 of Dipp), 125.4 (s, C^5 of PHDI), 126.5 (s, C^4 of PHDI), 127.3 (s, C^4 of Dipp), 128.8 (s, C^3 of PHDI), 130.1 (s, C^2 of PHDI), 130.6 (s, C^7 of PHDI), 141.7 (s, C^2 of Dipp), 147.9 (s, C^1 of PHDI), 154.3 (s, C^1 of Dipp). ^{31}P{^{1}H} NMR (161.98 MHz, 300 K, C$_6$D$_6$): (AMM'XX') spin system δ / ppm = −175.8 - −167.4 (m, 2P, P$_{XX'}$), 88.5-94.4 (m, 2P, P$_{MM'}$), 116.7 (tt, 1P, P$_A$). **Elemental analysis** calcd. for (C$_{46}$H$_{60}$CoN$_2$P$_5$) (Mw = 854.80 g·mol^{-1}) C 64.64, H 7.08, N 3.28; found C 65.08, H 7.00, N 3.08.

3.4.3.6 Synthesis of [(PHDI)Co(η^4-P$_5$Ph$_2$)] (4-Ph)
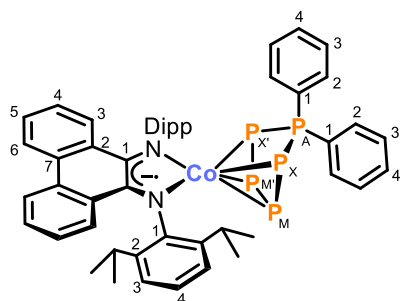
A stock solution of Ph$_2$PCl (3 mL, c = 0.08 M in toluene, 0.240 mmol, 1.0 equiv.) was added to a deep turquoise suspension of [K(18c-6)]**2** (245 mg, 0.240 mmol, 1.0 equiv.) in toluene (25 mL) at room temperature. The reaction mixture was stirred for 15 hours while the color changed to dark blue. The mixture was filtered through a pad of silica gel (3 x 2.5 cm) and washed with toluene (3 x ca. 10 mL). The solvent was removed in vacuo and the dark blue residue was extracted into cyclohexane (2 x 10 mL). The dark blue extract was concentrated to ca. one fourth of the original volume and stored at 7 °C. After three days, dark blue crystals were formed, which were isolated by decantation and dried *in vacuo*. Yield: 83 mg (33%)

M.p. 219 °C (decomposition to a black oil). **UV/vis** (THF, λ$_{max}$ / nm, ε$_{max}$ / L·mol^{-1}·cm^{-1}): 335 (25000), 600sh (25000), 630 (29000). ^{1}H NMR (400.13 MHz, C$_6$D$_6$, 300 K): δ /ppm = 0.77 (d, $^3J_{HH}$ = 6.7 Hz, 12H, −CH(CH$_3$)$_2$ of Dipp), 1.52 (d, $^3J_{HH}$ = 6.7 Hz, 12H, −CH(CH$_3$)$_2$ of Dipp), 3.78 (sept, $^3J_{HH}$ = 6.7 Hz, 4H, −CH(CH$_3$)$_2$ of Dipp), 6.57-6.66 (m, 3H, C^4−H and C^3−H of Ph), 6.76-6.86 (m, 4H, C^2−H of Ph and C^4−H of PHDI), 7.76-7.86 (m, 4H, C^2−H of Ph and C^4−H of PHDI), 6.88-6.92 (m, 2H, C^3−H of Ph), 6.96-7.00 (m, 1H, C^4−H of Ph), 7.22-7.26 (m, 4H, C^3−H and C^5−H of PHDI), 7.39-7.41 (m, 4H, C^3−H of Dipp), 7.48-7.51 (m, 2H, C^4−H of Dipp), 7.55-7.59 (m, 2H, C^2−H of Ph), 7.98 (d, $^3J_{HH}$ = 8.3 Hz, 2H, C^6−H of PHDI). ^{13}C{^{1}H} NMR (100.66 MHz, C$_6$D$_6$, 300 K): δ /ppm =25.1 and 25.2 (s, −CH(CH$_3$)$_2$ of Dipp), 29.8 (s, −C(CH$_3$)$_3$), 124.3 (s, C^6 of PHDI), 125.0 (s, C^3 of Dipp), 125.7 (s, C^3 or C^5 of PHDI), 126.8 (s, C^4 of PHDI), 127.3 (s, C^4 of Dipp), 129.0 (d, $^3J_{CP}$ = 9.6 Hz, C^3 of Ph), 129.9 (d, $^2J_{CP}$ = 8.8 Hz, C^2 of Ph), 130.1 (s, C^2

of PHDI), 130.7 (s, C^7 of PHDI), 131.0 (s, C^4 of Ph), 131.9 (s, C^4 of Ph), 133.0 (s, C^2 of Ph), 140.3 (s, C^2 of Dipp), 148.3 (s, C^1 of PHDI), 157.1 (s, C^1 of Dipp), C^1 of Ph: not detected, C^3 or C^5 of PHDI and C^3 of Ph: overlapping with C_6D_6 solvent signal. **^{31}P{^{1}H} NMR** (161.98 MHz, 300 K, C_6D_6): (AMM'XX') spin system δ / ppm = −161.8 - −153.5 (m, 2P, $P_{XX'}$), 76.6-82.6 (m, 2P, $P_{MM'}$), 95.1 (t, 1P, P_A). **Elemental analysis** calcd. for $(C_{50}H_{52}CoN_2P_5)$(cyclohexane)$_{0.1}$ (Mw = 903.20 g·mol^{-1}) C 67.29, H 5.94, N 3.10; found C 67.63, H 5.68, N 3.09.

3.4.3.7 Synthesis of [(PHDI)Co(η^4-P$_5$Mes$_2$)] (4-Mes)
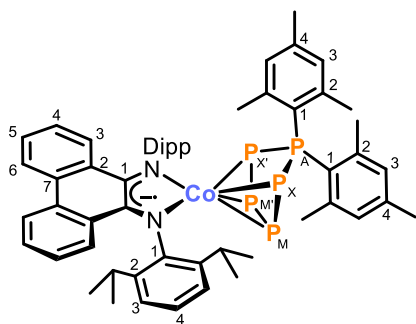
A 100 mL Schlenk flask was filled with Mes$_2$PCl (75 mg, 0.246 mmol, 1.0 equiv.), [K(18c-6)]**2** (250 mg, 0.242 mmol, 1.0 equiv.) and toluene (ca. 50 mL). The blue mixture was stirred overnight, filtered through a pad of silica gel (2.5 x 2.5 cm), and washed with toluene (2 x ca. 15 mL). The solvent was removed *in vacuo* and the dark blue residue was extracted into *n*-hexane (80 mL). The extract was concentrated to one fourth of the original volume until crystals began to form. After four days, the supernatant was decanted and the dark blue crystals with a purple shimmer were dried *in vacuo*. Yield: 166 mg (70%)

M.p. 228 °C (decomposition to a black solid). **UV/vis** (THF, λ_{max} / nm, ε_{max} / L·mol^{-1}·cm^{-1}): 340 (19000), 375sh (15000), 590sh (14000), 650 (21000). **^{1}H NMR** (400.30 MHz, C_6D_6, 300 K): δ /ppm = 0.79 (d, $^3J_{HH}$ = 6.7 Hz, 12H, −CH(CH_3)$_2$ of Dipp), 1.52 (d, $^3J_{HH}$ = 6.8 Hz, 12H, −CH(CH_3)$_2$ of Dipp), 1.73 (s, 3H, C^4−CH_3 of Mes), 1.96 (s, 3H, C^4−CH_3 of Mes), 2.24 (s, 6H, C^2−CH_3 of Mes), 2.66 (s, 6H, C^2−CH_3 of Mes), 3.73 (s br, 4H, −CH(CH$_3$)$_2$ of Dipp), 6.10 (s, 2H, C^3−H of Mes), 6.58 (s, 2H, C^3−H of Mes), 6.82-6.86 (m, 2H, C^4−H of PHDI), 7.17-7.22 (m, 4H, C^3−H and C^5−H of PHDI), 7.35-7.37 (m, 4H, C^3−H of Dipp), 7.42-7.46 (m, 2H, C^4−H of Dipp), 8.00 (d, $^3J_{HH}$ = 7.9 Hz, 2H, C^6−H of PHDI). **^{13}C{^{1}H} NMR** (100.66 MHz, C_6D_6, 300 K): δ /ppm = 20.5 (s, C^4−CH_3 of Mes), 20.7 (s, C^4−CH_3 of Mes), 22.9 (s, C^2−CH_3 of Mes), 25.0 (s, −CH(CH_3)$_2$ of Dipp overlapping with C^2−CH_3 of Mes), 124.2 (s, C^6 of PHDI), 124.7 (s, C^3 of Dipp), 125.4 (s, C^3 or C^5 of PHDI), 126.6 (s, C^4 of PHDI), 127.2 (s, C^4 of Dipp), 129.9 (s, C^2 of PHDI), 130.5 (s, C^7 of PHDI), 131.2 (d, $^3J_{CP}$ = 8.3 Hz, C^3 of Mes), 131.5 (d, $^3J_{CP}$ = 8.2 Hz, C^3 of Mes), 139.9 (d, $^2J_{CP}$ = 7.0 Hz, C^2 of Mes), 140.6 (s, C^4 of Mes), 140.7 (s, C^2 of

Dipp), 141.0 (s, C^4 of Mes), 143.6 (d, $^2J_{CP}$ = 7.9 Hz, C^2 of Mes), 148.2 (s, C^1 of PHDI), 155.5 (s, C^1 of Dipp), C^1 of Mes: not detected, C^3 or C^5 of PHDI: overlapping with C_6D_6 solvent signal. **^{31}P{^{1}H} NMR** (161.98 MHz, 300 K, C_6D_6): (AMM'XX') spin system δ / ppm = −106.7 - −98.2 (m, 2P, $P_{XX'}$), 64.4-70.6 (m, 2P, $P_{MM'}$), 84.3 (t, 1P, P_A). **Elemental analysis** calcd. for $(C_{56}H_{64}CoN_2P_5)$(n-hexane)$_{0.7}$ (M_w = 1039.27 g·mol^{-1}) C 69.57, H 7.16, N 2.70; found C 70.07, H 7.15, N 2.44.

3.4.3.8 Synthesis of [(PHDI)Co(η^4-P_5(N(iPr$_2$)$_2$)] (4-NiPr)
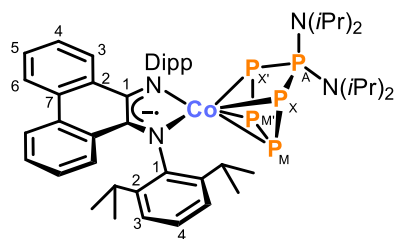
(iPr$_2$N)$_2$PCl (50 mg, 0.187 mmol, 1.0 equiv.), [K(18c-6)]**2** (200 mg, 0.187 mmol, 1.0 equiv.) and toluene (ca. 25 mL) were added to a 100 mL Schlenk flask. The resulting dark turquoise mixture turned dark blue upon stirring for 24 h. The mixture was filtered through a pad of silica gel (3 x 1 cm) and was washed with toluene (ca. 10 mL) until the washings were colorless. The solvent was removed *in vacuo* and the dark blue residue was extracted into n-hexane (110 mL). The dark blue filtrate was concentrated to one fourth of the original volume. Dark violet microcrystals formed upon storage for one week at room temperature, which were isolated by decantation of the mother liquor and dried *in vacuo*. (Further product can be isolated by concentrating the mother liquor). Yield: 89 mg (51%); including a 2nd crop: 114 mg (65%).

M.p. 231 °C (decomposition to a black solid). **UV/vis** (THF, λ_{max} / nm, ε_{max} / L·mol^{-1}·cm^{-1}): 340 (22000), 425sh (8000), 590 (17000), 660 (22000). **^{1}H NMR** (400.13 MHz, C_6D_6, 300 K): δ /ppm = 0.67 (d, $^3J_{HH}$ = 6.9 Hz, 12H, −N(CH(CH_3)$_2$)$_2$), 0.78 (d, $^3J_{HH}$ = 6.8 Hz, 12H, −CH(CH_3)$_2$ of Dipp), 1.27 (d, $^3J_{HH}$ = 6.9 Hz, 12H, −N(CH(CH_3)$_2$)$_2$), 1.77 (d, $^3J_{HH}$ = 6.8 Hz, 12H, −CH(CH_3)$_2$ of Dipp), 3.19 (sept, $^3J_{HH}$ = 6.5 Hz, 2H, −N(CH(CH$_3$)$_2$)$_2$), 3.79 (sept, $^3J_{HH}$ = 6.8 Hz, 4H, −CH(CH$_3$)$_2$ of Dipp), 3.86 (sept, $^3J_{HH}$ = 6.9 Hz, 2H, −N(CH(CH$_3$)$_2$)$_2$), 6.83-6.87 (m, 2H, C^4−H of PHDI), 7.19 (d, $^3J_{HH}$ = 8.9 Hz, 2H, C^3−H of PHDI), 7.22-7.27 (m, 2H, C^5−H of PHDI), 7.47-7.54 (m, 6H, C^3−H and C^4−H of Dipp), 8.00 (d, $^3J_{HH}$ = 8.0 Hz, 2H, C^6−H of PHDI). **^{13}C{^{1}H} NMR** (100.61 MHz, C_6D_6, 300 K): δ /ppm = 23.7 (s, −N(CH(CH_3)$_2$)$_2$), 24.1 (s, −N(CH(CH_3)$_2$)$_2$), 25.2 (s, −CH(CH_3)$_2$ of Dipp), 25.9 (s, −CH(CH_3)$_2$ of Dipp), 30.2 (s, −CH(CH$_3$)$_2$ of Dipp), 48.1 (s, −N(CH(CH$_3$)$_2$)$_2$), 50.4 (s, −N(CH(CH$_3$)$_2$)$_2$), 124.2 (s, C^6 of PHDI), 125.0 (s, C^3 of Dipp), 125.3 (s, C^5 of PHDI), 126.6 (s, C^4 of PHDI), 127.3 (s, C^4

of Dipp), 128.7 (s, C^3 of PHDI), 130.4 (s, C^2 of PHDI), 130.6 (s, C^7 of PHDI), 141.0 (s, C^2 of Dipp), 148.1 (s, C^1 of PHDI), 155.0 (s, C^1 of Dipp). **^{31}P{^{1}H} NMR** (162.04 MHz, 300 K, C$_6$D$_6$): (AMM'XX') spin system δ / ppm = −142.2 - −133.8 (m, 2P, P$_{XX'}$), 60.5-66.5 (m, 2P, P$_{MM'}$), 126.5 (t, 1P, P$_A$). **Elemental analysis** calcd. for (C$_{50}$H$_{70}$CoN$_4$P$_5$) (Mw = 940.94 g·mol^{-1}) C 63.82, H 7.50, N 5.95; found C 64.22, H 7.10, N 5.88.

3.4.3.9 Synthesis of [*n*Bu₄N][(PHDI)Co(η³-P₃)(CN)] ([*n*Bu₄N]5) and [*n*Bu₄N][*t*Bu₂PPCN] ([*n*Bu₄N]6-*t*Bu)

A suspension of [*n*Bu₄N]CN (63 mg, 0.234 mmol, 2.0 equiv.) in toluene (10 mL) was added dropwise to a suspension of **4-*t*Bu** (101 mg, 0.117 mmol, 1.0 equiv.) in toluene (10 mL) at room temperature. The mixture turned dark purple blue and was stirred for 4 h. The solvent was removed, and the diphosphanide [*n*Bu₄N]**6-*t*Bu** was separated by extracting the dark purple residue with a cyclohexane/*n*-hexane mixture (3:2 *v/v*, 5 x 10 mL). The combined dark purple/blue extract was concentrated to ca. 25 mL. A purple oily precipitate containing a crude mixture of [*n*Bu₄N]**5** and [*n*Bu₄N]**6-*t*Bu** was obtained upon storage at 4 °C for one week, which was separated by filtration. Pure [*n*Bu₄N]**6-*t*Bu** (21 mg, 40%) was isolated by evaporation of this filtrate and drying *in vacuo*. The dark purple residue of the cyclohexane/*n*-hexane extraction was extracted into toluene (3 x 15 mL) and concentrated to one fourth of the original volume. Storage at −30 °C for four days gave numerous dark purple crystals of [*n*Bu₄N]**5**, which were isolated by filtration, washing with cyclohexane (ca. 1 mL) and drying *in vacuo* (57 mg, 51%).
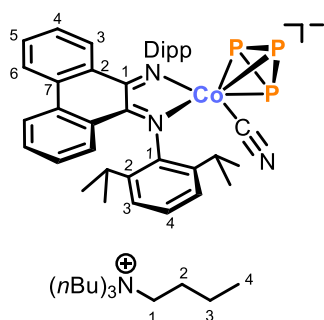

M.p. 216 °C. **UV/vis** (THF, λ$_{max}$ / nm, ε$_{max}$ / L·mol^{-1}·cm^{-1}): 380sh (13500), 410 (14500), 555 (17000). **^{1}H NMR** (400.13 MHz, 300 K, THF-*d*$_8$): δ /ppm = 0.20 (d, $^3J_{HH}$ = 6.9 Hz, 6H, −CH(CH_3)$_2$ of Dipp), 0.93 (t, $^3J_{HH}$ = 7.4 Hz, 12H, −CH_3 of [*n*Bu₄N]$^+$), 1.18 (d, $^3J_{HH}$ = 6.9 Hz, 12H, −CH(CH_3)$_2$ of Dipp), 1.39 (sext, $^3J_{HH}$ = 7.4 Hz, 8H, C$^3H_2$ of [*n*Bu₄N]$^+$), 1.53 (d, $^3J_{HH}$ = 6.6 Hz, 12H, −CH(CH_3)$_2$ of Dipp), 1.59-1.71 (m, 10H, −CH(CH$_3$)$_2$ of Dipp overlapping with C$^2H_2$ of [*n*Bu₄N]$^+$), 3.29-3.34 (m, 8H, C$^1H_2$ of [*n*Bu₄N]$^+$), 5.03 (sept, $^3J_{HH}$ = 6.8 Hz, 2H, −CH(CH$_3$)$_2$ of Dipp), 6.82-6.86 (m, 4H, C^4−H of PHDI overlapping with C^5−H of Dipp), 7.10 (t, $^3J_{HH}$ = 7.7 Hz, 2H, C^4−H of Dipp), 7.24 (d, $^3J_{HH}$ = 7.7 Hz, 2H, C^3−H of Dipp), 7.39-7.43 (m, 2H, C^5−H of PHDI), 7.78 (d, $^3J_{HH}$ =

8.7 Hz, 2H, C^3−H of PHDI), 8.32 (d, $^3J_{HH}$ = 7.7 Hz, 2H, C^6−H of PHDI). **^{13}C{^{1}H} NMR** (100.61 MHz, 300 K, THF-d_8): δ /ppm = 14.1 (s, C^4 of [nBu$_4$N]$^+$), 20.7 (s, C^3 of [nBu$_4$N]$^+$), 24.4 (s, −CH(CH$_3$)$_2$ of Dipp), 26.2 (s, −CH(CH$_3$)$_2$ of Dipp), 26.3 (s, −CH(CH$_3$)$_2$ of Dipp), 27.2 (s, −CH(CH$_3$)$_2$ of Dipp), 28.4 (s, −CH(CH$_3$)$_2$ of Dipp), 28.5 (s, −CH(CH$_3$)$_2$ of Dipp), 59.4 (s, C^1 of [nBu$_4$N]$^+$), 124.0 (s, C^5 of Dipp), 124.7, 124.9 (s, $C^{3,4}$ of Dipp and C^6 of PHDI), 125.5 (s, C^5 of PHDI), 127.2 (s, C^4 of PHDI), 128.1 (s, C^3 of PHDI), 129.2 (s, C^7 of PHDI), 130.6 (s, C^2 of PHDI), 135.6 (s, C^6 of Dipp), 140.1 (s, C^2 of Dipp), 156.2 (s, C^1 of PHDI), 156.7 (s, C^1 of Dipp), $C \equiv N$: not detected; C^2 of [nBu$_4$N]$^+$: overlapping with THF-d_8 solvent signal. **^{31}P{^{1}H} NMR** (161.98 MHz, 300 K, THF-d_8): δ / ppm = −193.2 (s). **IR** (solid state): ν/ cm^{-1} = 2958m, 2924m-sh, 2862w, 2068m (C≡N), 1487m, 1455s, 1436s, 1378m, 1357m, 1319m, 1253m, 1174w, 1158w, 1095w, 1051m, 790s, 753vs, 722s, 596m, 425m. **Elemental analysis** calcd. for (C$_{55}$H$_{78}$CoN$_4$P$_3$) (Mw = 947.11 g·mol^{-1}) C 69.75, H 8.30, N 5.92; found C 69.90, H 8.35, N 5.65.
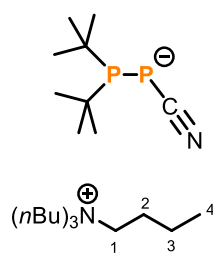
^{1}H NMR (400.13 MHz, 300 K, C$_6$D$_6$): δ /ppm = 1.01 (t, $^3J_{HH}$ = 7.2 Hz, 12H, −CH$_3$ of [nBu$_4$N]$^+$), 1.40-1.53 (m, 16H, C^2H_2 and C^3H_2 of [nBu$_4$N]$^+$), 1.57 (d, $^3J_{HP}$ = 10.4 Hz, 18H, −C(CH$_3$)$_3$), 3.25-3.29 (m, 8H, C^1H_2 of [nBu$_4$N]$^+$). **^{13}C{^{1}H} NMR** (100.61 MHz, 300 K C$_6$D$_6$): δ /ppm = 14.1 (s, C^4 of [nBu$_4$N]$^+$), 20.2 (s, C^3 of [nBu$_4$N]$^+$), 24.5 (s, C^2 of [nBu$_4$N]$^+$), 31.7 (dd, $^2J_{CP}$ = 14.0 Hz, $^3J_{CP}$ = 6.0 Hz, −C(CH$_3$)$_3$) 33.6 (dd, $^1J_{CP}$ = 30.0 Hz, $^2J_{CP}$ = 9.8 Hz, −C(CH$_3$)$_3$), 58.8 (s, C^1 of [nBu$_4$N]$^+$), 144.6 (dd, $^1J_{CP}$ = 116.0 Hz, $^2J_{CP}$ = 22.0 Hz, −C≡N). **^{31}P{^{1}H} NMR** (161.98 MHz, 300 K, C$_6$D$_6$): δ / ppm = −194.4 (d, $^1J_{PP}$ = −261.3 Hz, 1P, PCN), 50.2 (d, $^1J_{PP}$ = −261.2 Hz, 1P, tBu$_2$$P$). **IR** (solid state): ν/ cm^{-1} = 2960s, 2929s, 2874s, 2853s, 2049vs (C≡N), 1466s, 1378m, 1356m, 1257w, 1172m, 1016w, 880m, 806m, 739m, 511w. **HRMS** (ESI, MeCN): m/z(%) calculated for C$_9$H$_{18}$NP$_2$$^-$ [M$^-$]: 202.0915; found: 202.0923.

Elemental analysis, UV/Vis spectrum, and the melting point were not recorded due to the waxy nature of the isolated solid that prevented precise weighing on a milligram scale.

3.4.3.9 Synthesis of [Et₄N][(PHDI)Co(η³-P₅Mes₂)(CN)] ([Et₄N]7)
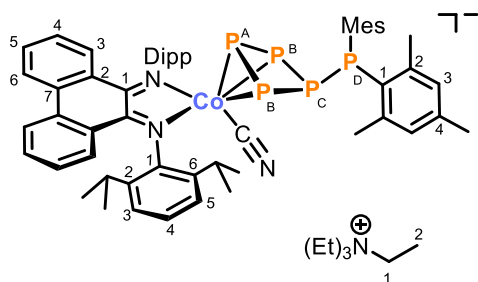
[Et₄N]CN (8.3 mg, 0.053 mmol, 1.0 equiv.) and **4-Mes** (52 mg, 0.053 mmol, 1.0 equiv.) were suspended in MeCN (5 mL) and stirred at r.t. for 2 h. The color changed from dark blue to deep purple. The solvent was removed, and the dark purple/blue residue was washed with Et₂O (20 x 1 mL) and subsequently with toluene (6 x 1 mL). The dark purple residue was subsequently extracted with a toluene/THF mixture (1:1 *v/v*, 17 x 1 mL). Concentration of the deep purple filtrate to one fourth of the original volume and storage at −30 °C gave very small, deep purple crystals after two days. The crystals were isolated by decantation of the supernatant and washed with cold toluene (−30 °C, 1 mL). Drying *in vacuo* gave satisfactorily pure product (23 mg, 38%). The compound decomposes at ambient temperature over the course of days.

UV/vis (THF, λ_{max} / nm, ε_{max} / L·mol⁻¹·cm⁻¹): 360 (28000), 400sh (24000), 545 (39000), 635sh (15000). **¹H NMR** (400.13 MHz, THF-d_8, 263 K): δ /ppm = 0.18 (d, $^3J_{HH}$ = 6.8 Hz, 6H, C⁶−CH(CH₃)₂ of Dipp), 0.93 (d, $^3J_{HH}$ = 6.7 Hz, 6H, C⁶−CH(CH₃)₂ of Dipp), 1.13-1.16 (m, 18H, C²−CH(CH₃)₂ of Dipp overlapping with −C²H₃ of [Et₄N]⁺), 1.48 (d, $^3J_{HH}$ = 6.5 Hz, 6H, C²−CH(CH₃)₂ of Dipp), 1.87-1.93 (m, 2H, C⁶−CH(CH₃)₂ of Dipp), 2.13 (s, 6H, C⁴−CH₃ of Mes), 2.34 (s, 12H, C²−CH₃ of Mes), 3.28-3.33 (m, 8H, C¹H₂ of [Et₄N]⁺), 5.14 (sept, $^3J_{HH}$ = 6.7 Hz, 2H, C²−CH(CH₃)₂ of Dipp), 6.61 (s, 4H, C³−H of Mes), 6.80-6.87 (m, 4H, C⁵−H of Dipp overlapping with C⁴−H of PHDI), 7.04 (t, $^3J_{HH}$ = 7.8 Hz, 2H, C⁴−H of Dipp), 7.19-7.21 (m, 2H, C³−H of Dipp), 7.41-7.45 (m, 2H, C⁵−H of PHDI), 7.62-7.64 (m, 2H, C³−H of PHDI), 8.37 (d, $^3J_{HH}$ = 7.9 Hz, 2H, C⁶−H of PHDI). **¹³C{¹H} NMR** (100.61 MHz, THF-d_8, 263 K): δ /ppm = 7.6 (s, C^2 of [Et₄N]⁺), 20.8 (s, −C⁴−CH₃ of Mes), 23.7 (m, −C²−CH₃ of Mes), 24.5 (s, −CH(CH₃)₂ of Dipp), 27.4 (s, −CH(CH₃)₂ of Dipp), 28.1 (s, −CH(CH₃)₂ of Dipp), 28.6 (s, −CH(CH₃)₂ of Dipp), 52.6 (s, C^1 of [Et₄N]⁺), 123.5 (s, C^5 of Dipp), 124.5 (s, C^3 of Dipp and C^6 of PHDI), 125.2 (s, C^4 of Dipp), 125.9 (s, C^5 of PHDI), 127.1 (s, C^4 of PHDI), 128.5 (s, C^3 of PHDI), 129.6 (s, C^7 of PHDI), 129.7 (s, C^3 of Mes), 130.6 (s, C^2 of PHDI), 136.5 (s, C^4 of Mes), 137.3 (s, C^6 of Dipp), 137.7 (d, $^1J_{CP}$ = 42.0 Hz, C^1 of Mes), 141.0 (s, C^2 of Dipp), 142.8 (d, $^2J_{CP}$ = 13.3 Hz, C^2 of Mes), 153.2 (s, C^1 of Dipp), 154.2 (s, C^1 of PHDI), C≡N: not detected. **³¹P{¹H} NMR** (161.98 MHz, THF-d_8, 263 K): (AB₂CD) spin system δ / ppm = 32.8 (dq, 1P, P_D), 59.2 (dt, 1P, P_C), 94.0 (ddd, 2P, P_B), 193.7 (dt, 1P, P_A). **IR** (solid state):

ν/ cm^{-1} = 2957m, 2919m-sh, 2860w, 2058m (C≡N), 1600w, 1439s, 1379m, 1318m, 1051m, 848m, 790s, 754vs, 722s, 554m. **Elemental analysis** calcd. for $(C_{65}H_{84}CoN_4P_5)\cdot(toluene)_{0.8}$ (Mw = 1208.93 g·mol^{-1}) C 70.14, H 7.54, N 4.63; found C 70.50, H 7.56, N 4.53.
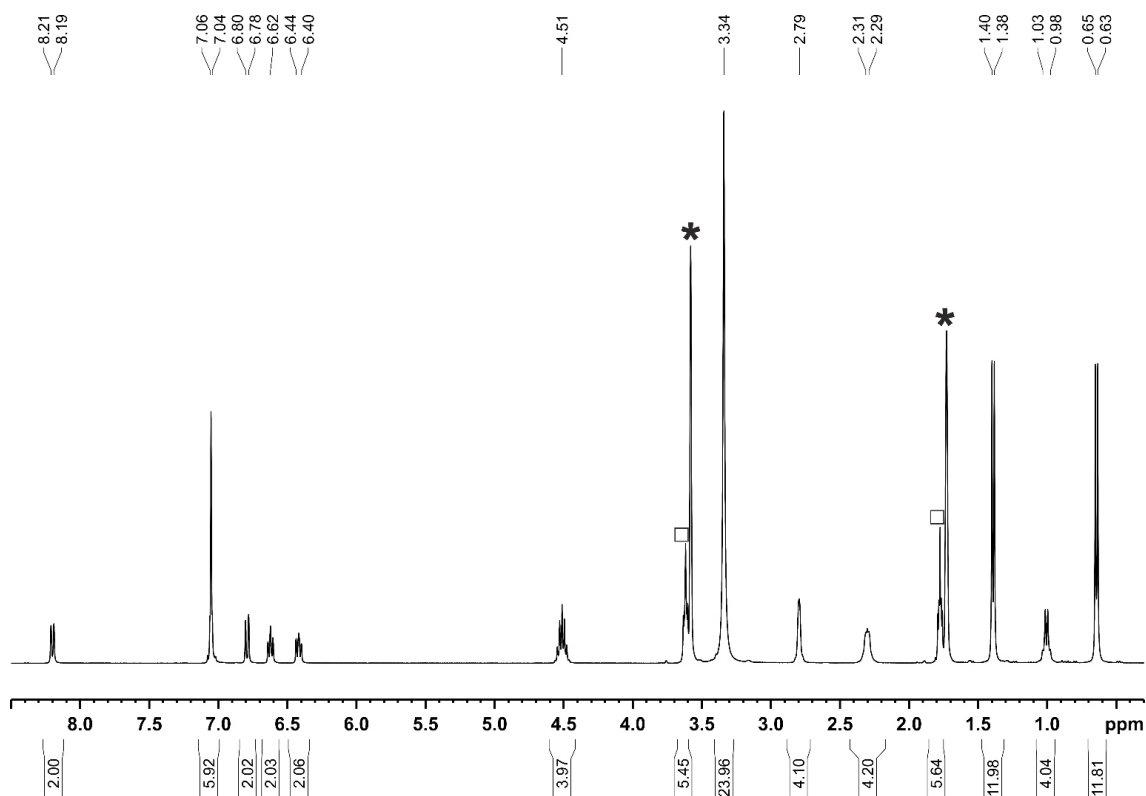
3.4.4 NMR Spectra

Figure S1. ^{1}H NMR spectrum (400.13 MHz, THF-d_8, 300 K) of [K(18c-6)][(PHDI)Co(η^4-1,5-cod)] ([K(18c-6)]**1**)·(THF)$_{1.4}$; * THF-d_8, □ THF.
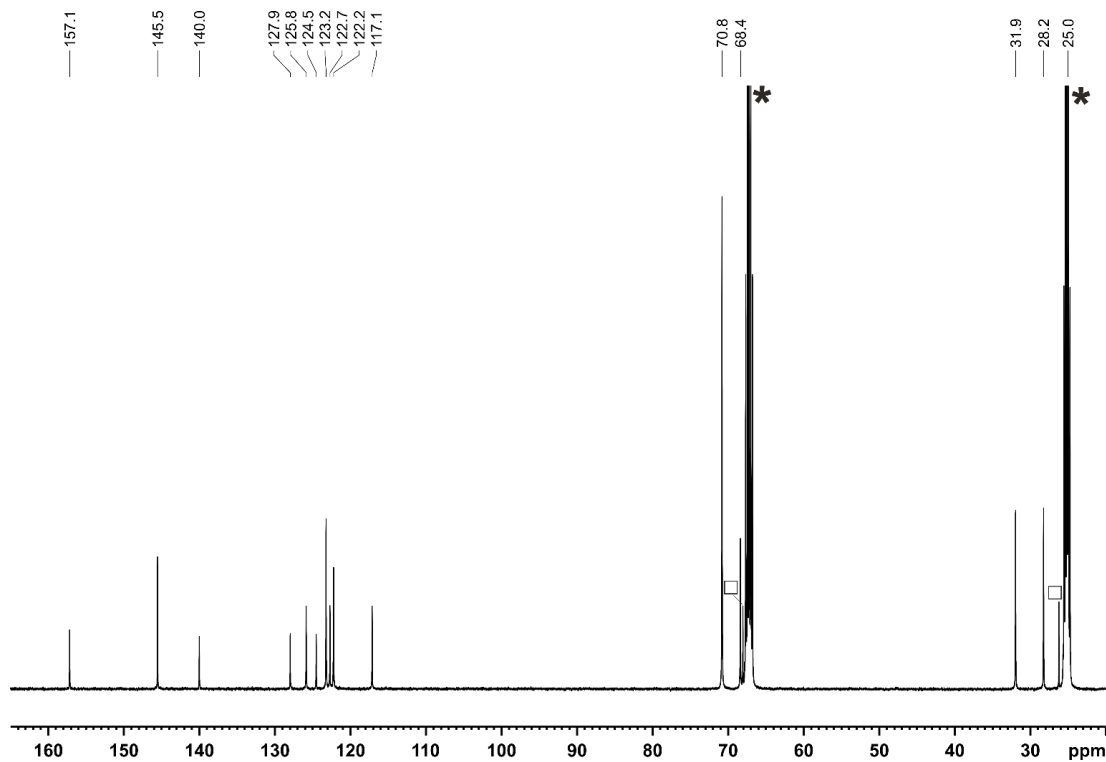
Figure S2. ^{13}C{^{1}H} NMR spectrum (100.61 MHz, THF-d_8, 300 K) of [K(18c-6)][(PHDI)Co(η^4-1,5-cod)] ([K(18c-6)]**1**)·(thf)$_{1.4}$; * THF-d_8, □ THF.
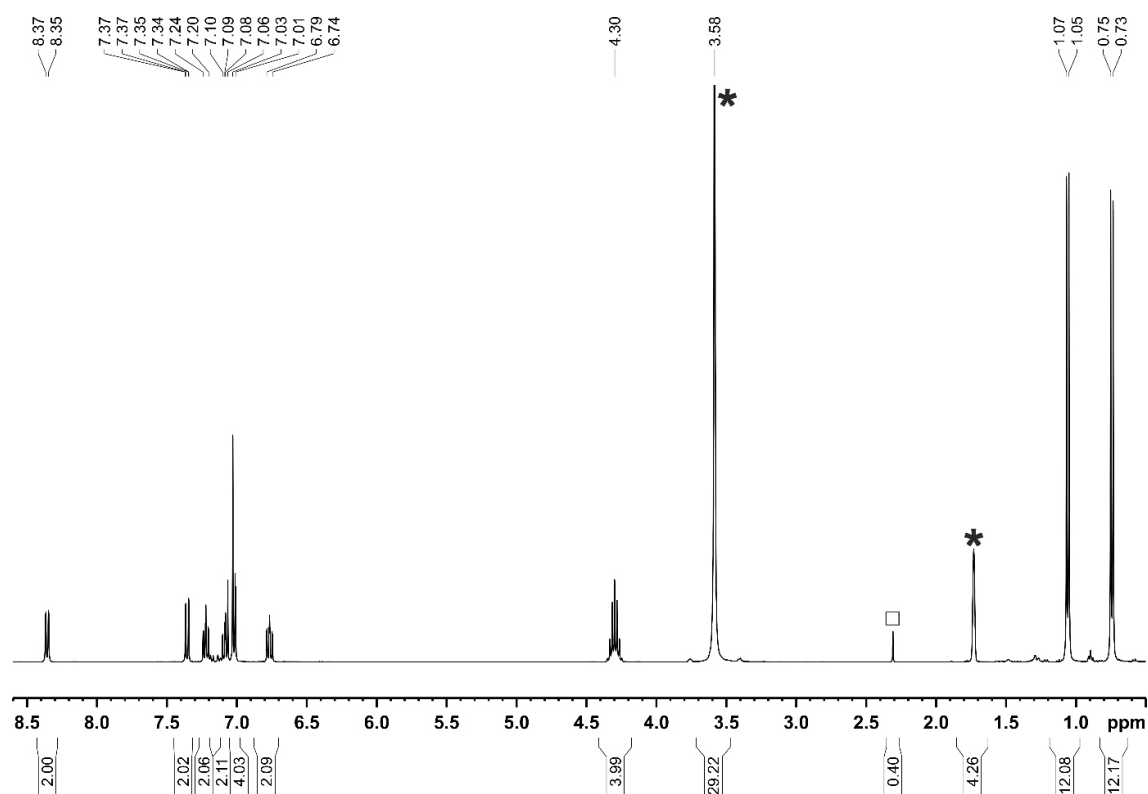
Figure S3. ^{1}H NMR spectrum (400.13 MHz, THF-d_8, 300 K) of [K(18c-6)][(PHDI)Co(η^4-P$_4$)] ([K(18c-6)]**2**)·(toluene)$_{0.1}$; * THF-d_8, □ toluene.
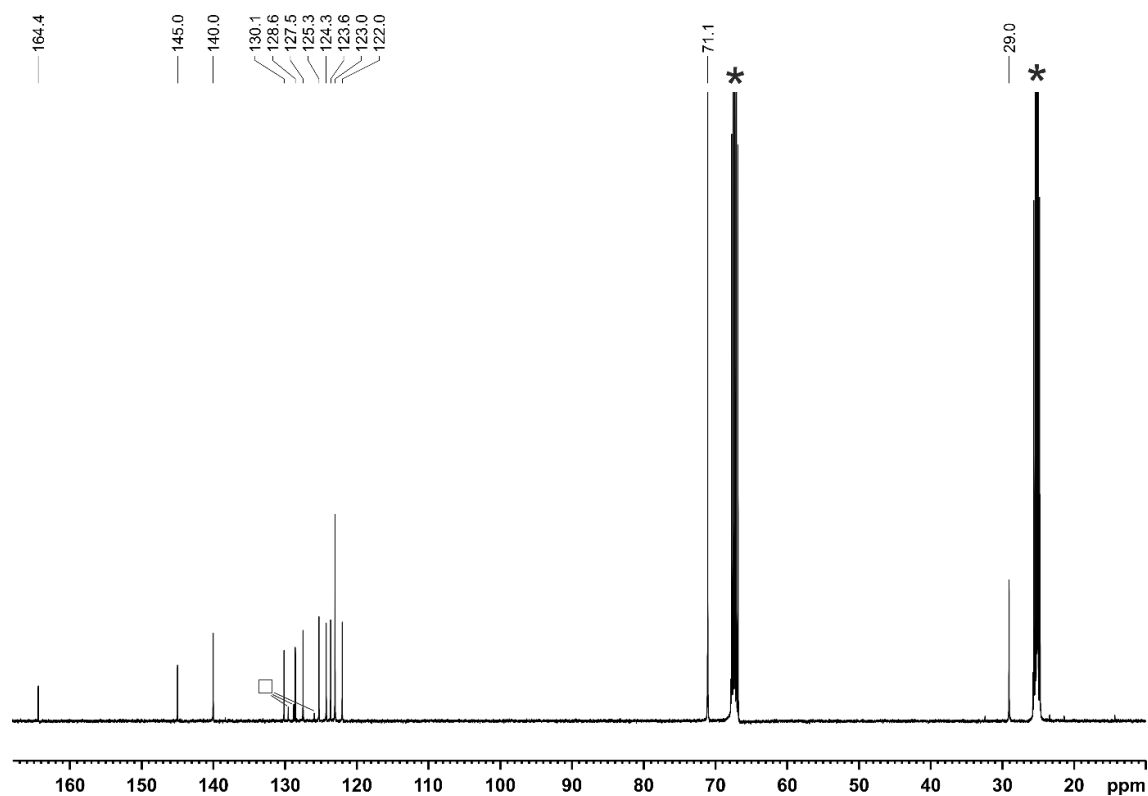
Figure S4. ^{13}C{^{1}H} NMR spectrum (100.61 MHz, THF-d_8, 300 K) of [K(18c-6)][(PHDI)Co(η^4-P$_4$)] ([K(18c-6)]**2**)·(toluene)$_{0.1}$; * THF-d_8, □ toluene.
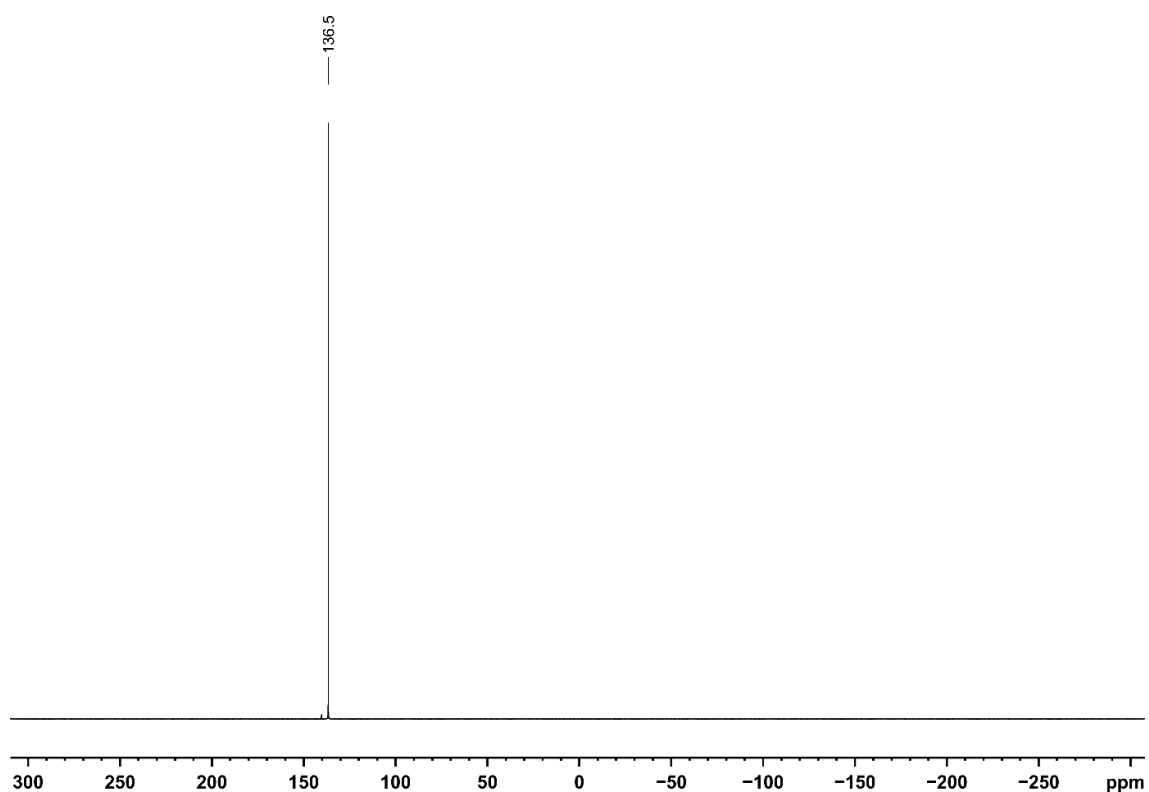
Figure S5. $^{31}P\{^1H\}$ NMR spectrum (161.98 MHz, 300 K, THF-d_8) of [K(18c-6)][(PHDI)Co(η^4-P$_4$)] ([K(18c-6)]**2**)·(toluene)$_{0.1}$.
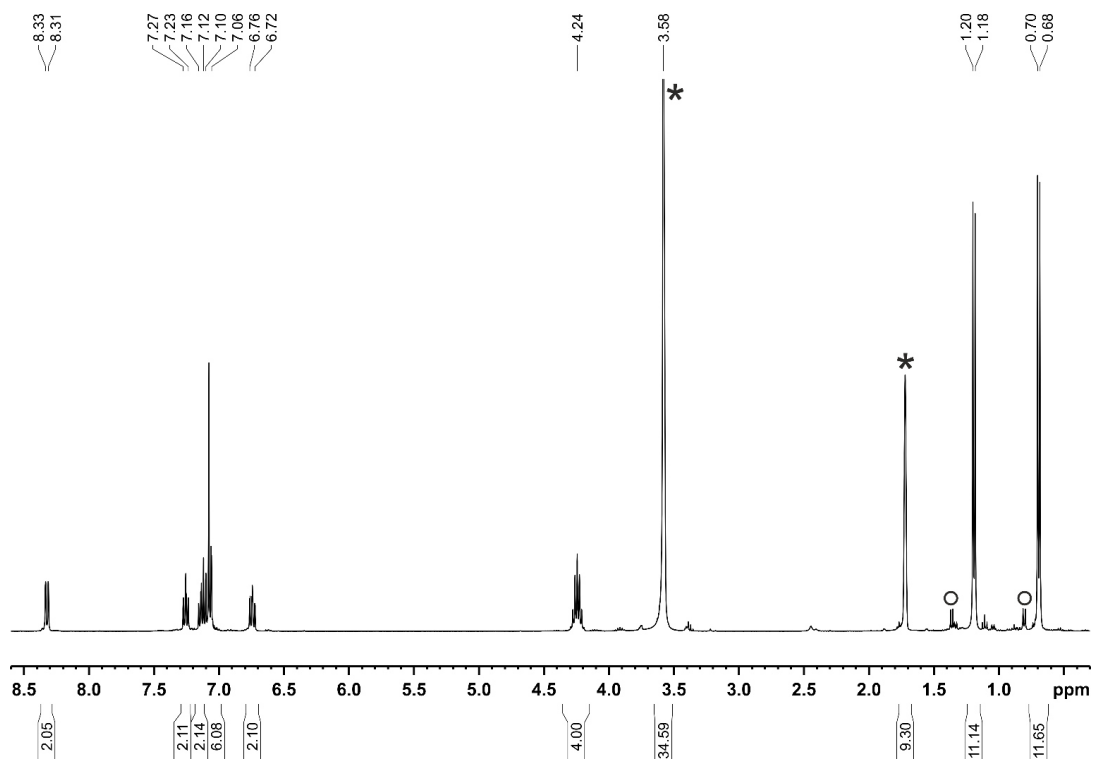
Figure S6. ^1H NMR spectrum (400.13 MHz, THF-d_8, 300 K) of [K(18c-6)][(PHDI)Co(μ^2:η^1,η^4-P$_4$)W(CO)$_5$] ([K(18c-6)]**3**); * THF-d_8, ○ minor unknown impurity.
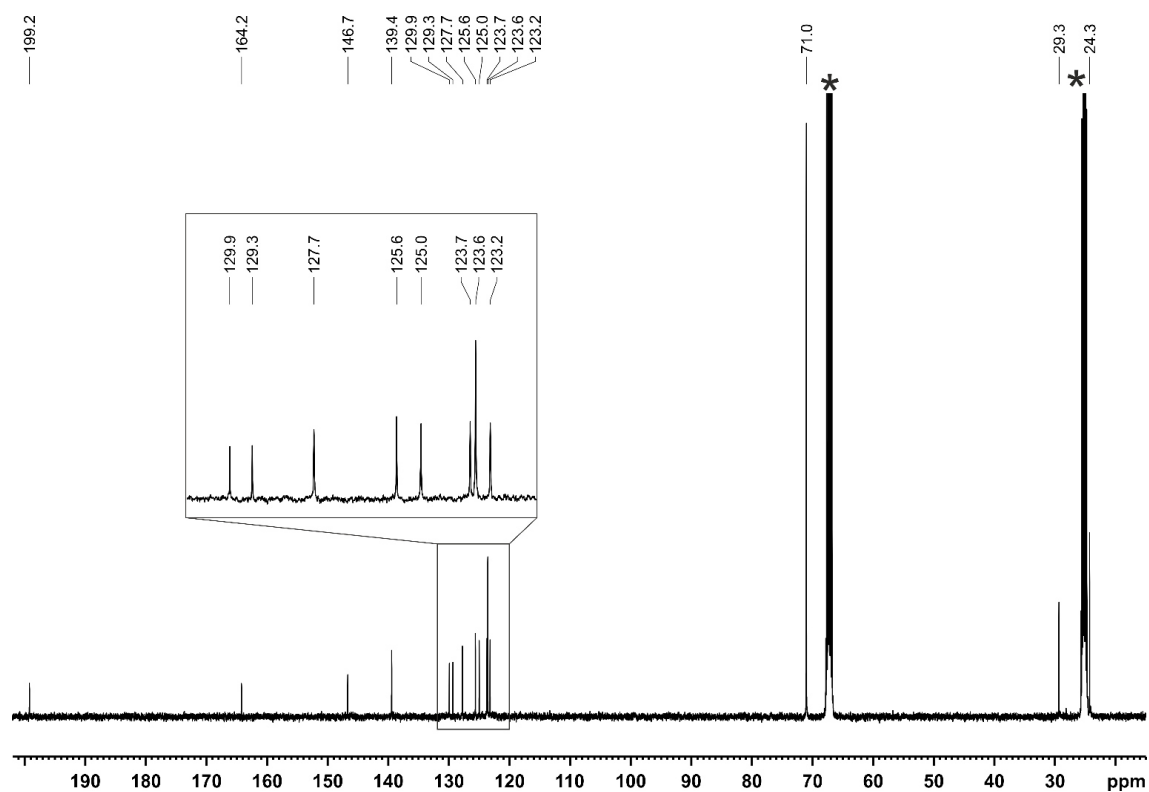
Figure S7. ^{13}C{^{1}H} NMR spectrum (100.61 MHz, THF-d_8, 300 K) of [K(18c-6][(PHDI)Co(μ^2:η^1,η^4-P$_4$)W(CO)$_5$] ([K(18c-6)]3); * THF-d_8.
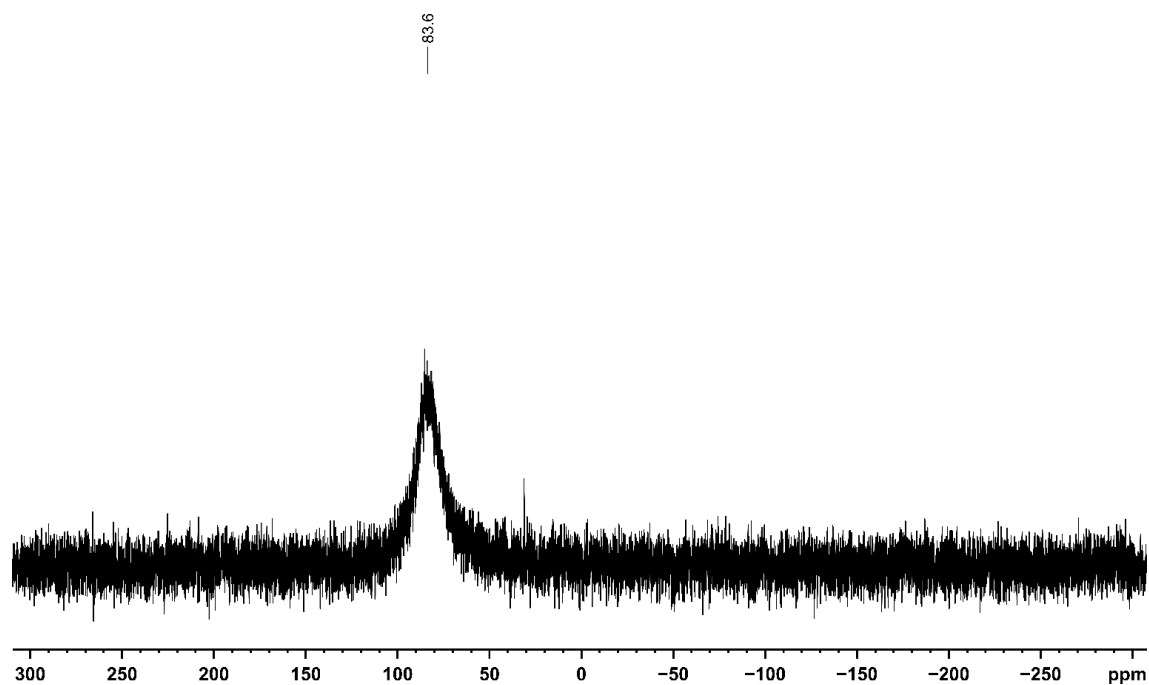
Figure S8. ^{31}P{^{1}H} NMR spectrum (161.98 MHz, 300 K, THF-d_8) [K(18c-6][(PHDI)Co(μ^2:η^1,η^4-P$_4$)W(CO)$_5$] ([K(18c-6)]3.
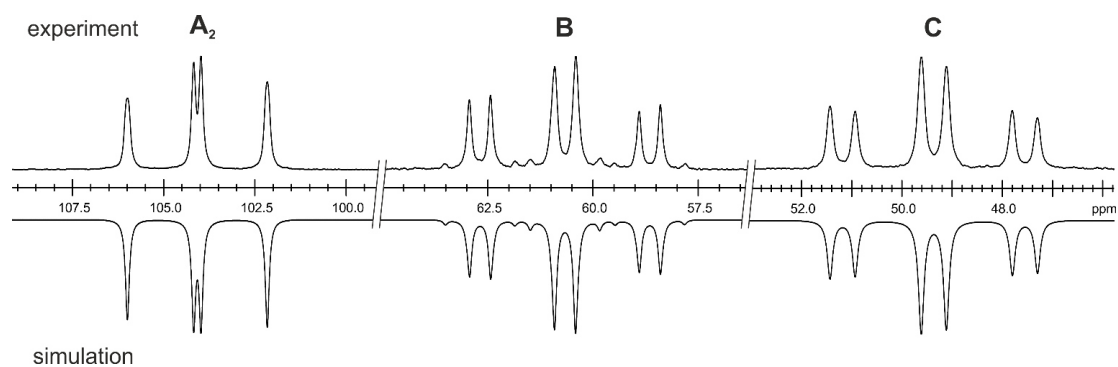
Figure S9. Section of the $^{31}P\{^1H\}$ NMR (161.98 MHz, 300 K, THF-d_8) of [K(18c-6][(PHDI)Co(μ^2:η^1,η^4-P$_4$)W(CO)$_5$] ([K(18c-6)]**3**); experimental (upwards) and simulation (downwards).

Table S1. Coupling constants from the iterative fit of the A$_2$BC spin system and schematic representation of the CoP$_4$W core of [K(18c-6][(PHDI)Co(μ^2:η^1,η^4-P$_4$)W(CO)$_5$] ([K(18c-6)]**3**).

$^1J_{AB} = -326.9$ Hz
$^1J_{AC} = -294.3$ Hz
$^2J_{BC} = 81.0$ Hz

^{183}W satellites:
$^1J_{PW} = -186.3$ Hz
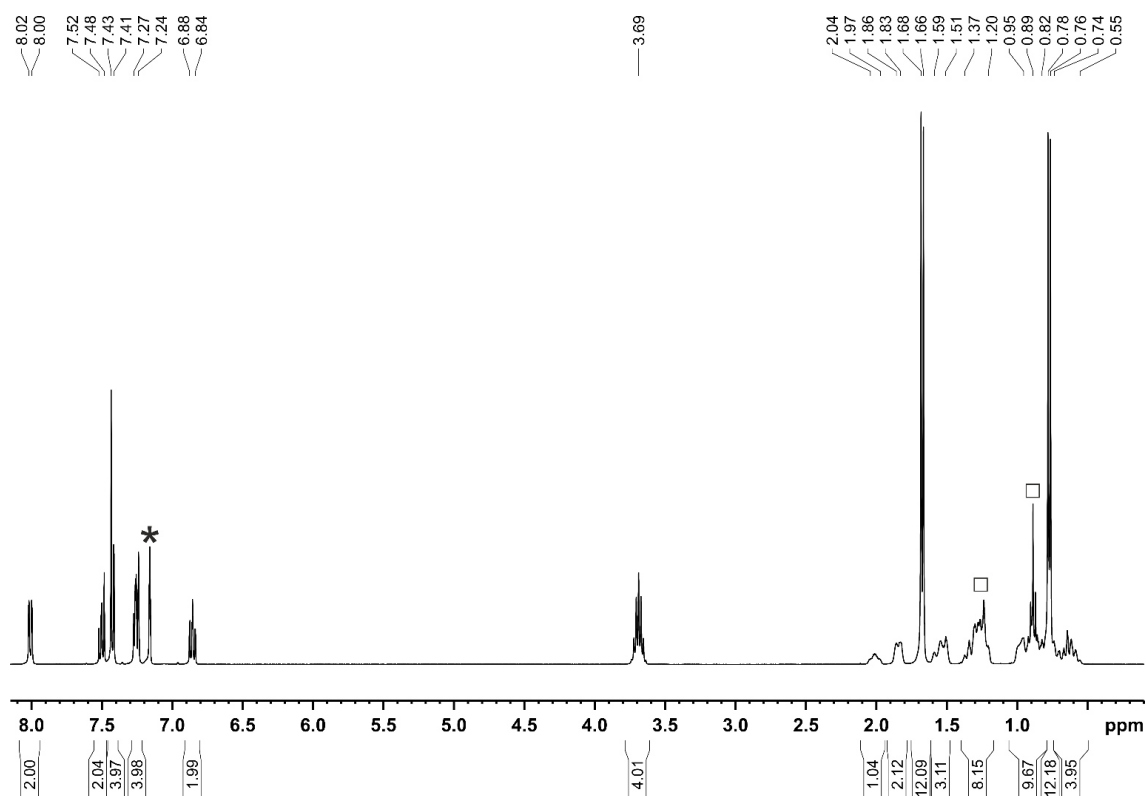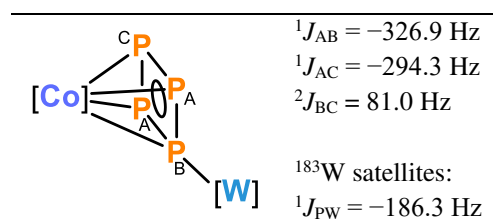
Figure S10. ^1H NMR spectrum (400.13 MHz, C$_6$D$_6$, 300 K) of [(PHDI)Co(η^4-P$_5$Cy$_2$)] **(4-Cy)**·(n-hexane)$_{0.5}$; * C$_6$D$_6$, □ n-hexane.
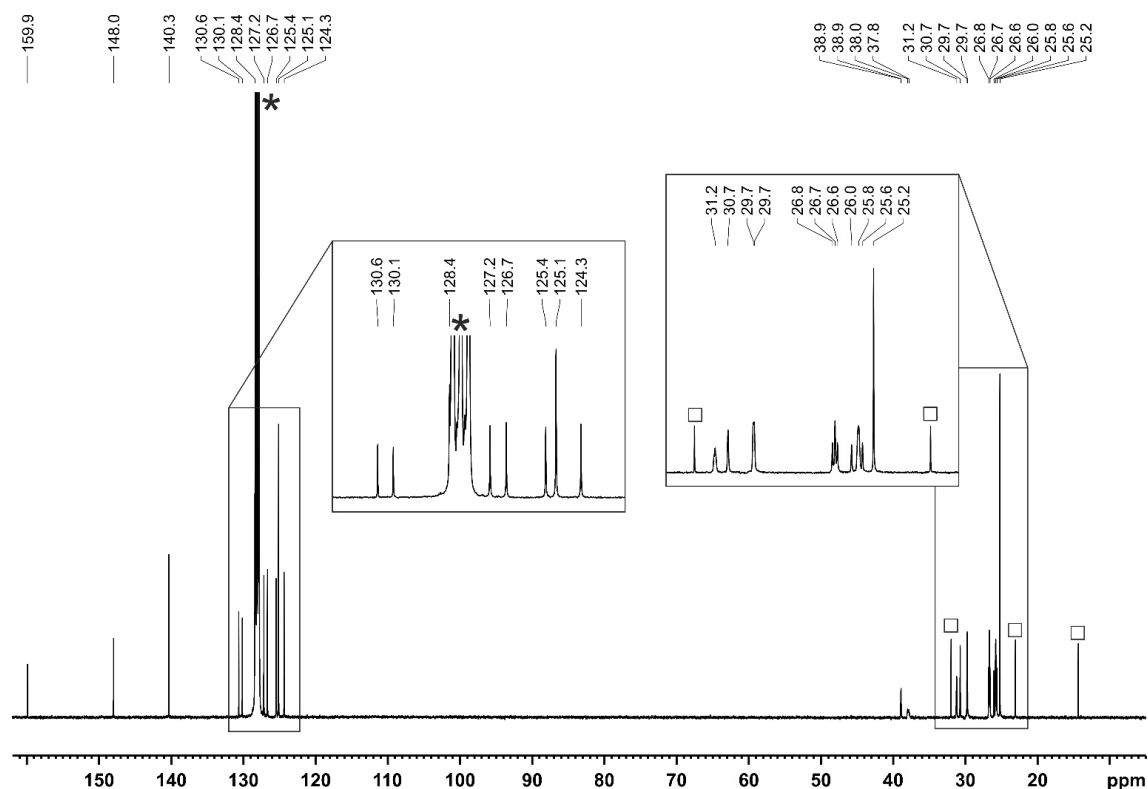
Figure S11. $^{13}C\{^1H\}$ NMR spectrum (100.61 MHz, C_6D_6, 300 K) of [(PHDI)Co(η^4-P$_5$Cy$_2$)] (4-Cy)·(n-hexane)$_{0.5}$; * C_6D_6, □ n-hexane.
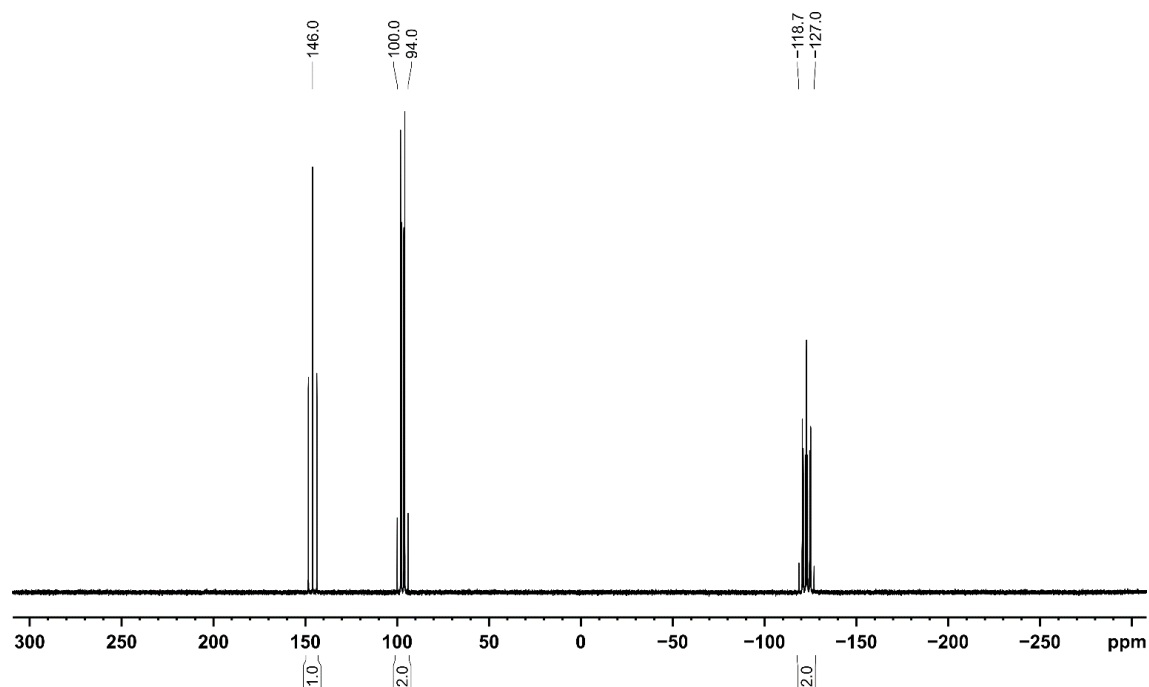
Figure S12. $^{31}P\{^1H\}$ NMR spectrum (161.98 MHz, 300 K, C_6D_6, 300 K) of [(PHDI)Co(η^4-P$_5$Cy$_2$)] (4-Cy)·(n-hexane)$_{0.5}$.

Figure S13. Section of the ^{31}P{^{1}H} NMR (161.98 MHz, C$_6$D$_6$, 300 K) of [(PHDI)Co(η^4-P$_5$Cy$_2$)] (**4-Cy**); experimental (upwards) and simulation (downwards).

Table S2. Coupling constants from the iterative fit of the AMM'XX' spin system and schematic representation of the CoP$_5$Cy$_2$ core of [(PHDI)Co(η^4-P$_5$Cy$_2$)] (**4-Cy**).

$^1J_{AX} = {}^1J_{AX'} = -373.5$ Hz

$^1J_{MX} = {}^1J_{M'X'} = -399.8$ Hz

$^1J_{MM'} = -384.4$ Hz

$^2J_{MX'} = {}^2J_{M'X} = 4.2$ Hz

$^2J_{AM} = {}^2J_{AM'} = 33.7$ Hz

$^2J_{XX'} = -0.3$ Hz

Figure S14. ^{1}H NMR spectrum (400.13 MHz, C$_6$D$_6$, 300 K) of [(PHDI)Co(η^4-P$_5$tBu$_2$)] (**4-tBu**); * C$_6$D$_6$.
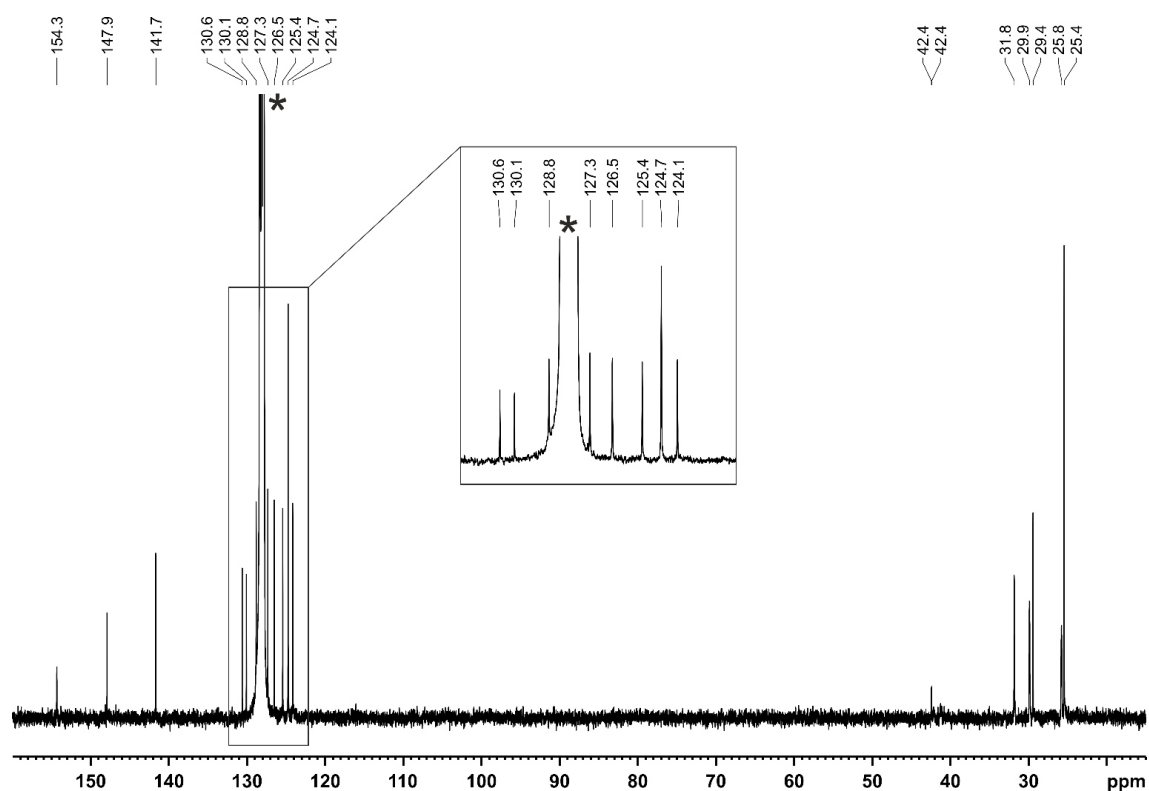
Figure S15. $^{13}C\{^1H\}$ NMR spectrum (100.61 MHz, C_6D_6, 300 K) of [(PHDI)Co(η^4-P_5tBu_2)] (**4-tBu**); * C_6D_6.
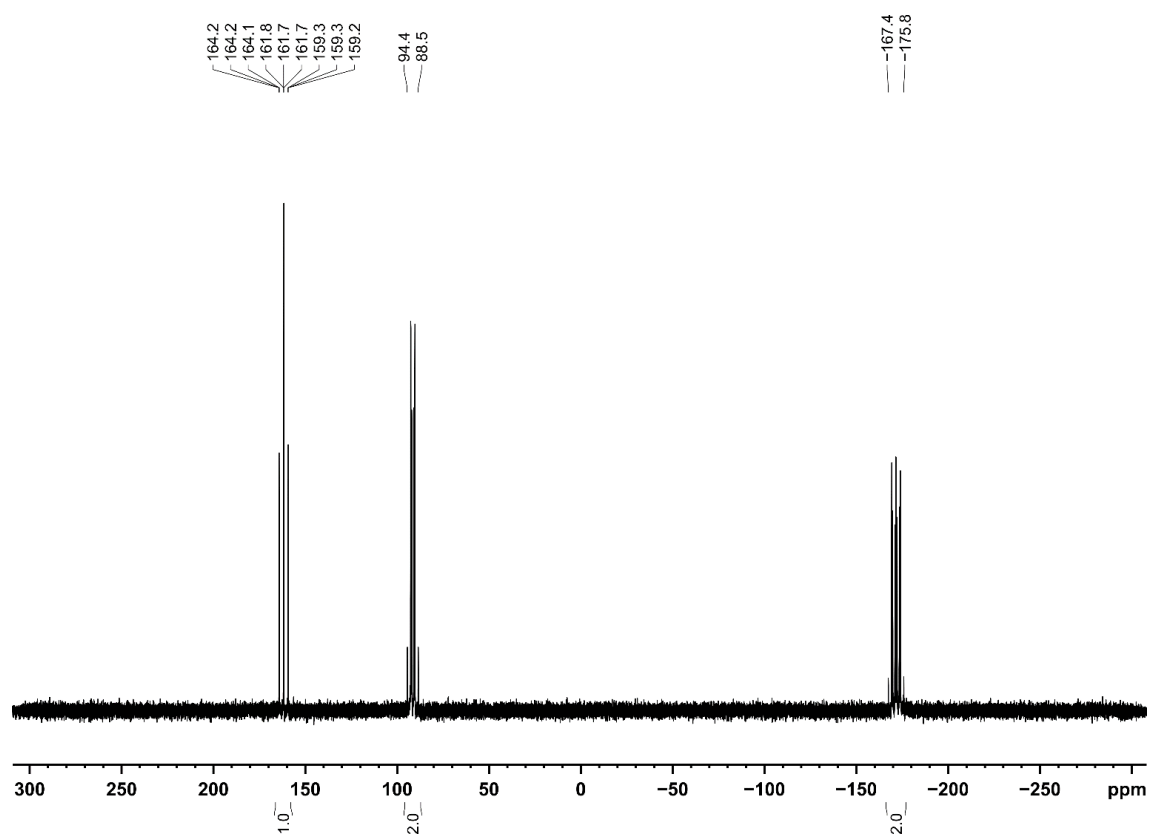
Figure S16. $^{31}P\{^1H\}$ NMR spectrum (161.98 MHz, 300 K, C_6D_6, 300 K) of [(PHDI)Co(η^4-P_5tBu_2)] (**4-tBu**).
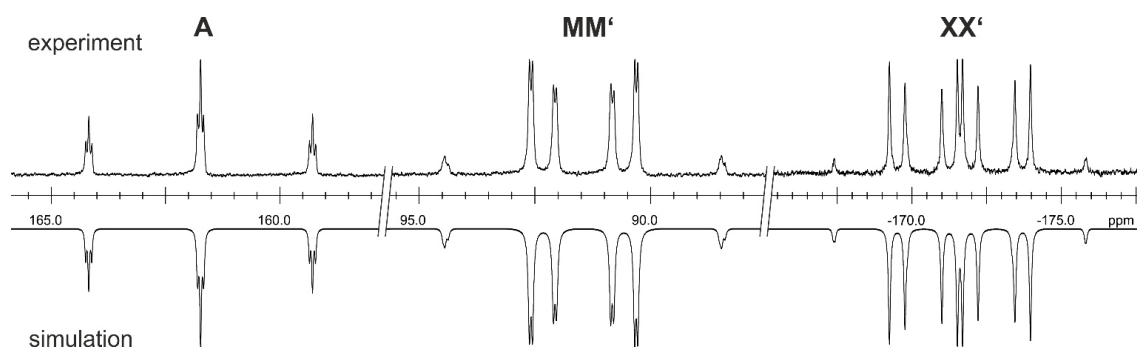
Figure S17. Section of the $^{31}P\{^1H\}$ NMR (161.98 MHz, C_6D_6, 300 K) of [(PHDI)Co(η^4-P_5tBu_2)] (4-tBu); experimental (upwards) and simulation (downwards).
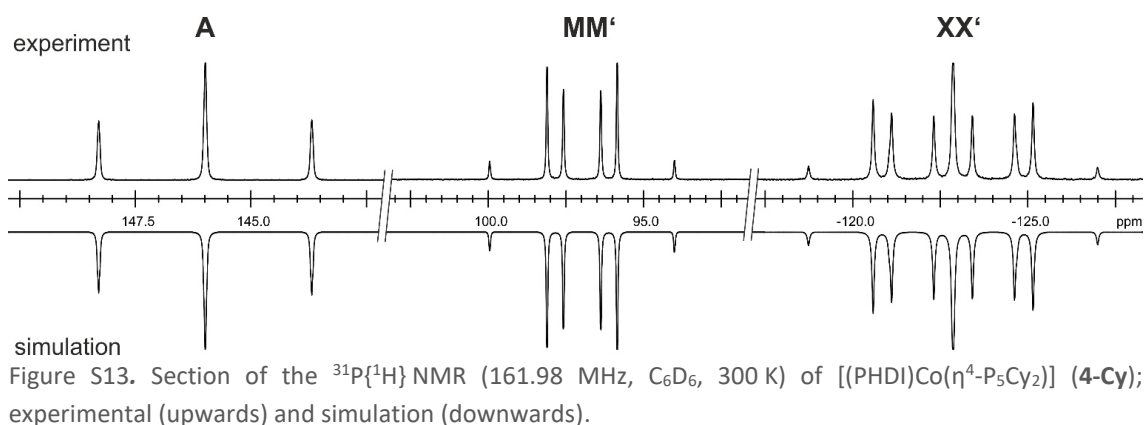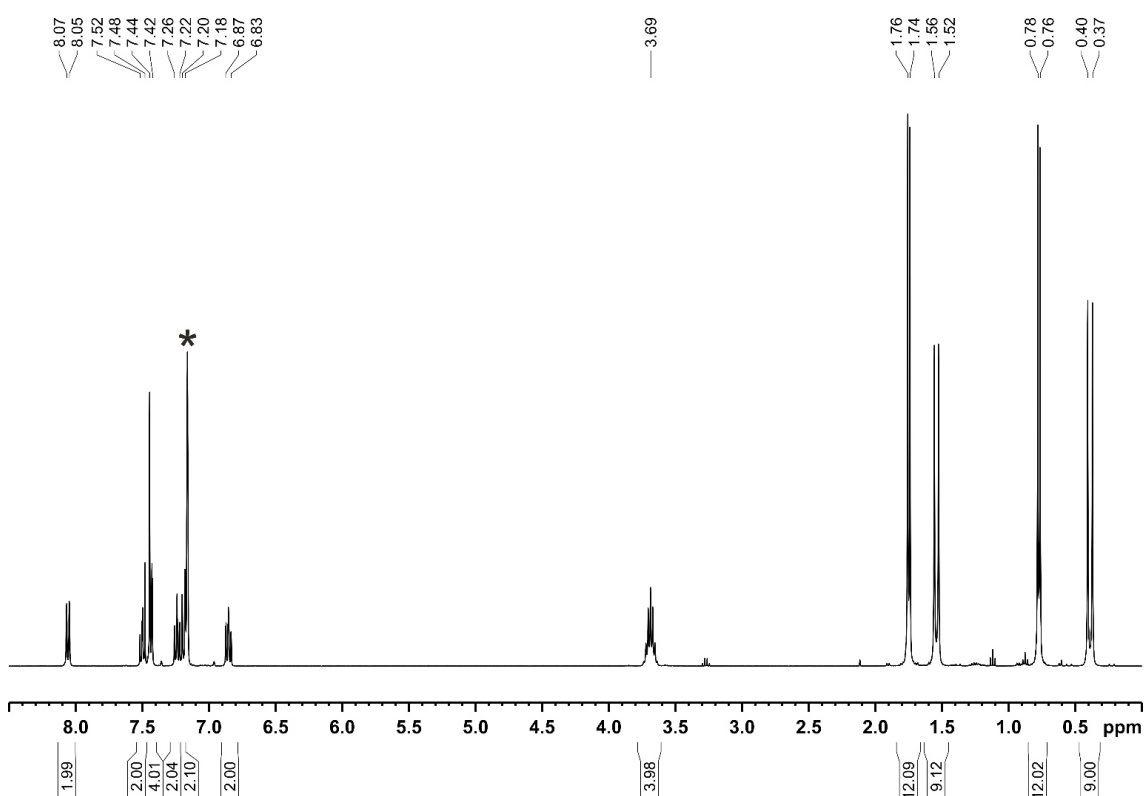
Table S3. Coupling constants from the iterative fit of the AMM'XX' spin system and schematic representation of the CoP$_5$tBu$_2$ core of [(PHDI)Co(η^4-P_5tBu_2)] (4-tBu).

$^1J_{AX} = {}^1J_{AX'} = -396.3$ Hz
$^1J_{MX} = {}^1J_{M'X'} = -404.1$ Hz
$^1J_{MM'} = -383.6$ Hz
$^2J_{MX'} = {}^2J_{M'X} = 35.9$ Hz
$^2J_{AM} = {}^2J_{AM'} = 10.9$ Hz
$^2J_{XX'} = -4.9$ Hz
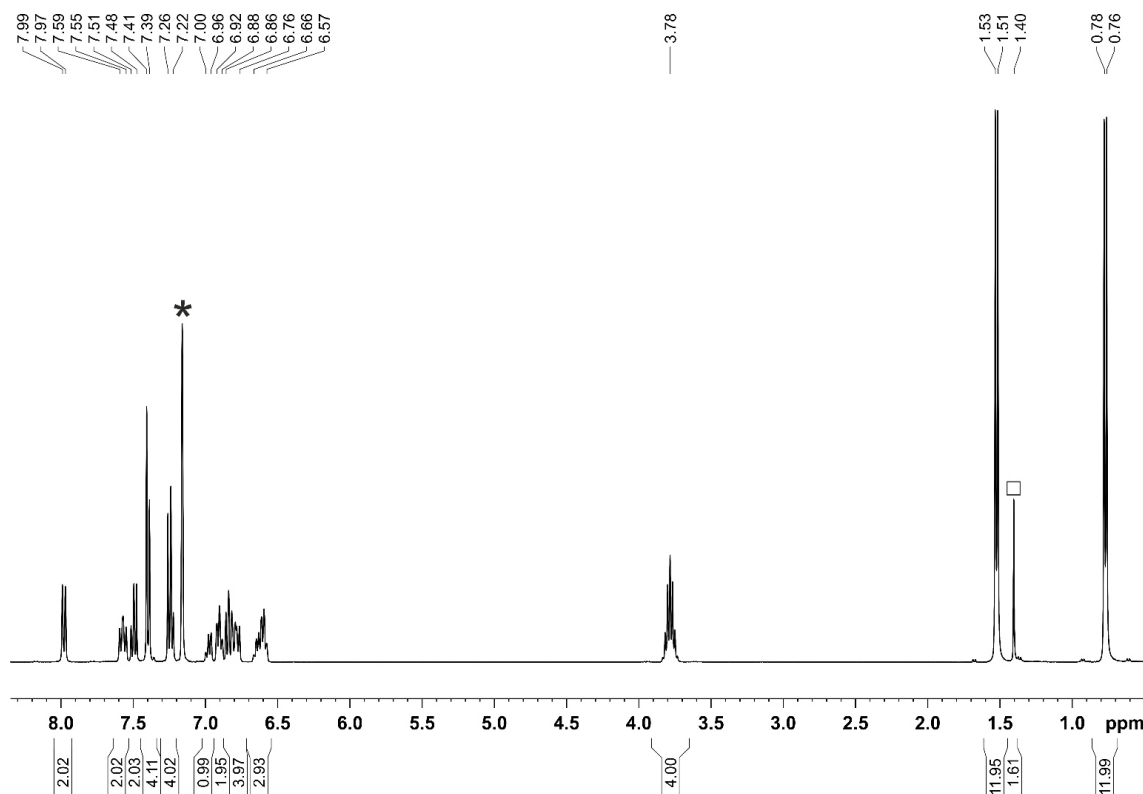
Figure S18. ^1H NMR spectrum (400.13 MHz, C_6D_6, 300 K) of [(PHDI)Co(η^4-P_5Ph_2)] (4-Ph)·(cyclohexane)$_{0.1}$; * C_6D_6, □ cyclohexane.

117
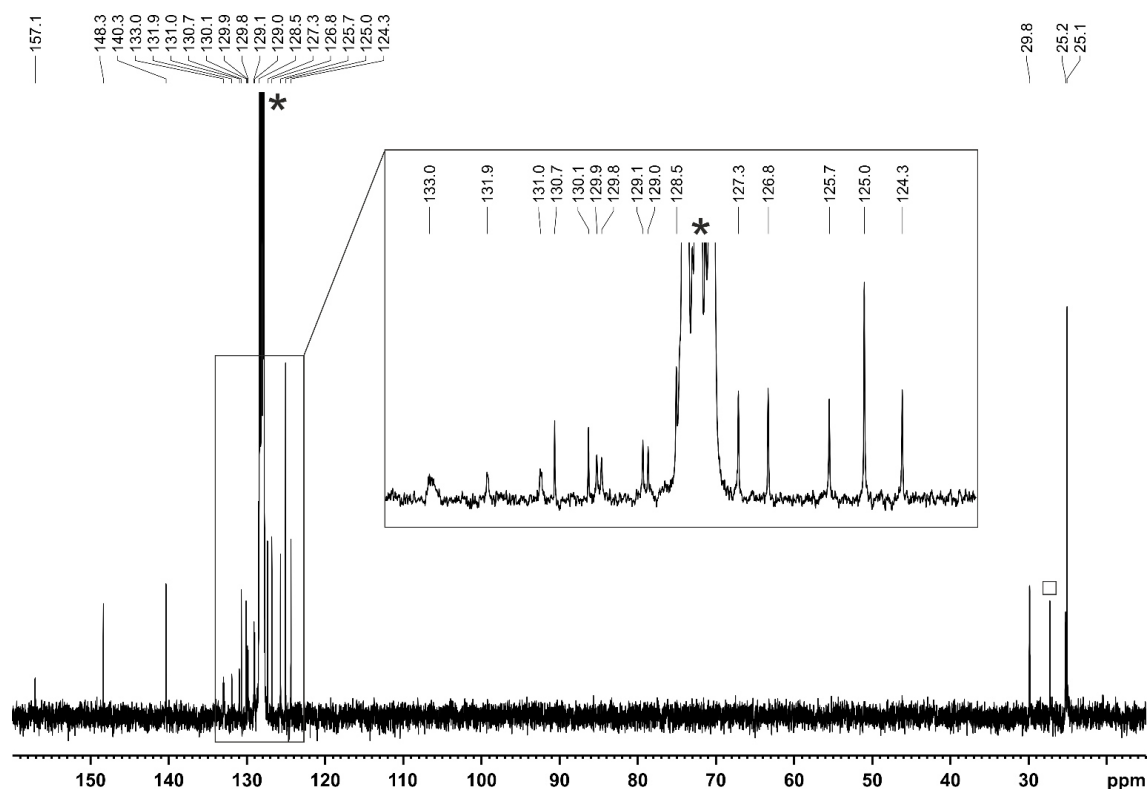
Figure S19. $^{13}C\{^1H\}$ NMR spectrum (100.61 MHz, C$_6$D$_6$, 300 K) of [(PHDI)Co(η^4-P$_5$Ph$_2$)] (4-Ph)·(cyclohexane)$_{0.1}$; * C$_6$D$_6$, □ cyclohexane.
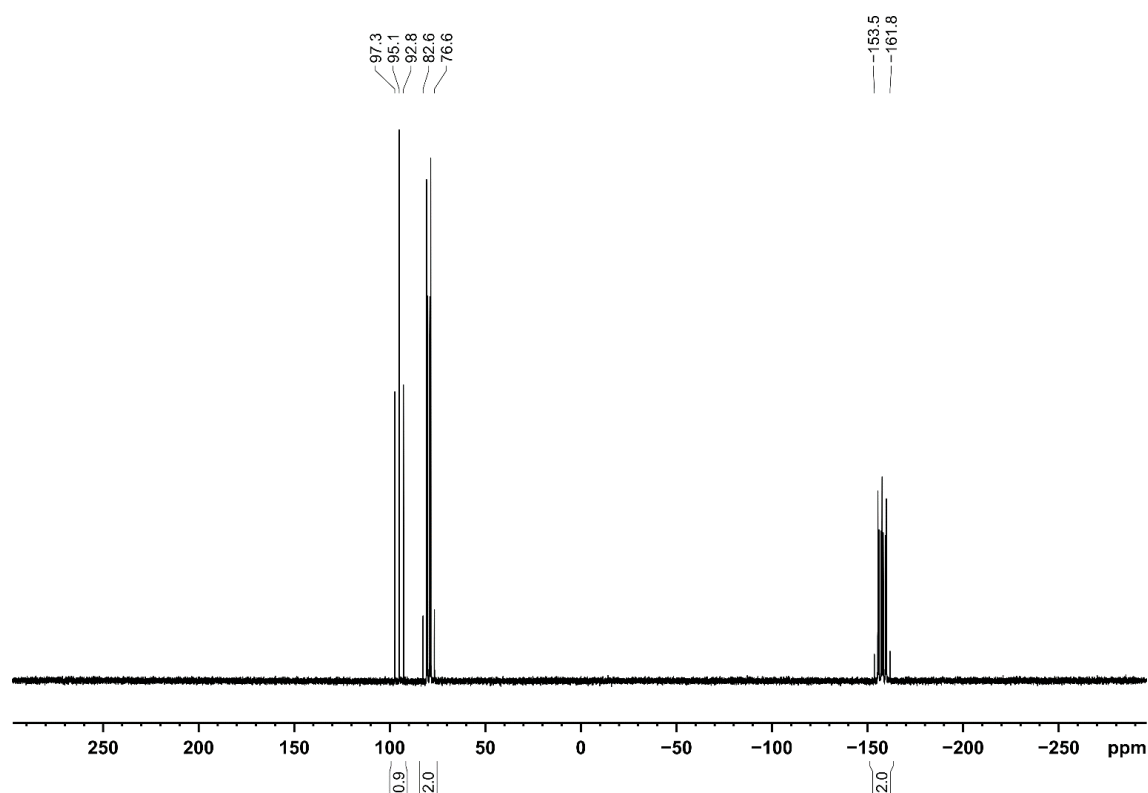
Figure S20. $^{31}P\{^1H\}$ NMR spectrum (161.98 MHz, 300 K, C$_6$D$_6$, 300 K) of [(PHDI)Co(η^4-P$_5$Ph$_2$)] (4-Ph)·(cyclohexane)$_{0.1}$.

118
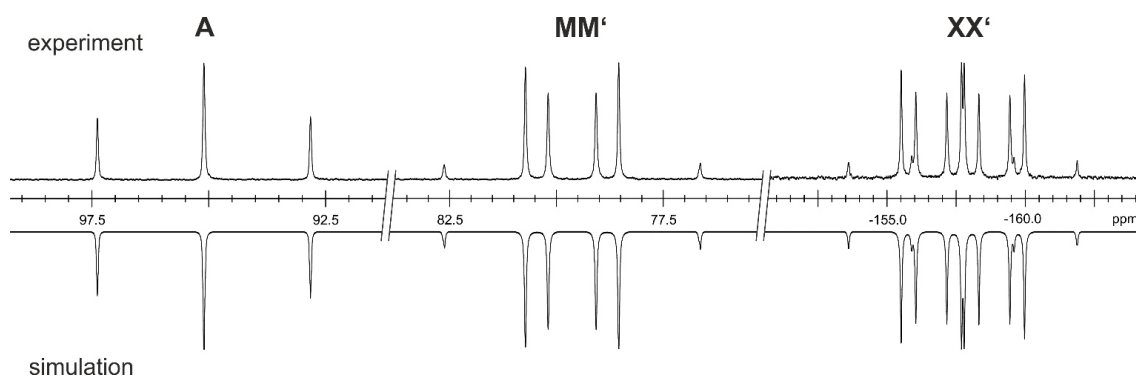
Figure S21. Section of the $^{31}P\{^1H\}$ NMR (161.98 MHz, C$_6$D$_6$, 300 K) of [(PHDI)Co(η^4-P$_5$Ph$_2$)] (**4-Ph**); experimental (upwards) and simulation (downwards).

Table S4. Coupling constants from the iterative fit of the AMM'XX' spin system and schematic representation of the CoP$_5$Ph$_2$ core of [(PHDI)Co(η^4-P$_5$Ph$_2$)] (**4-Ph**).

$^1J_{AX} = {}^1J_{AX'} = -369.5$ Hz

$^1J_{MX} = {}^1J_{M'X'} = -386.9$ Hz

$^1J_{MM'} = -394.2$ Hz

$^2J_{MX'} = {}^2J_{M'X} = 33.1$ Hz

$^2J_{AM} = {}^2J_{AM'} = 2.9$ Hz

$^2J_{XX'} = 2.0$ Hz
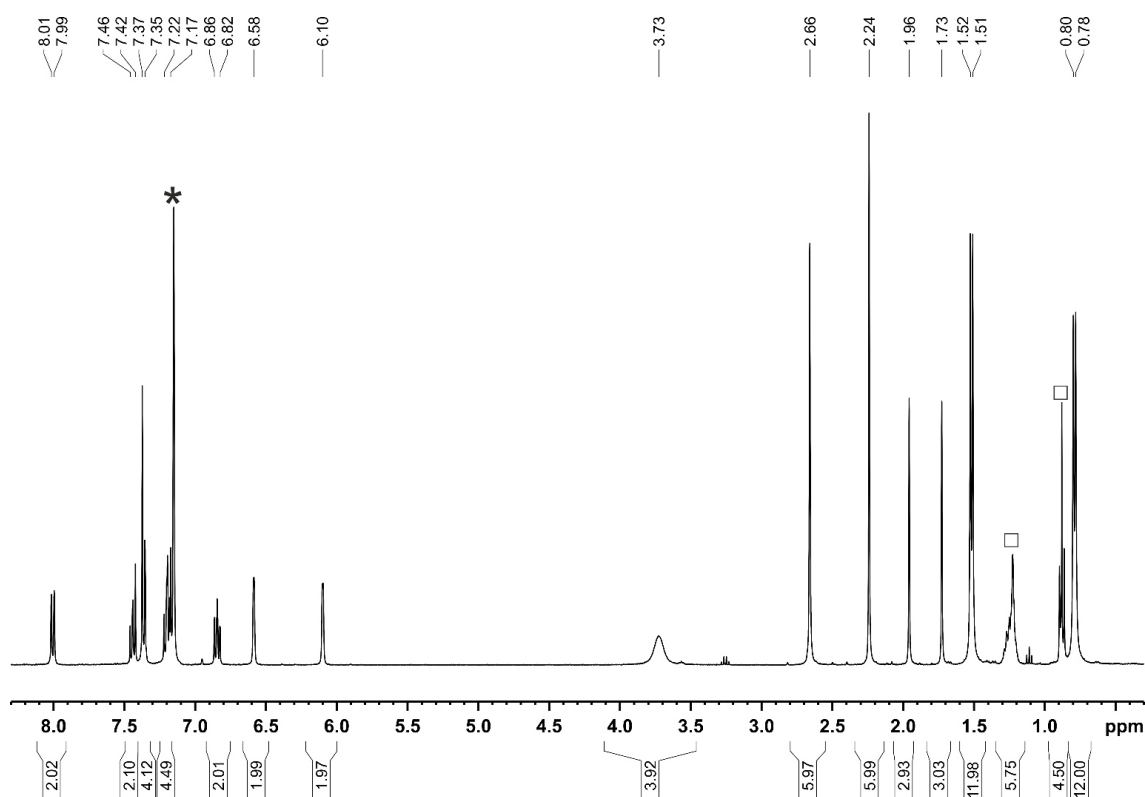
Figure S22. ^{1}H NMR spectrum (400.13 MHz, C$_6$D$_6$, 300 K) of [(PHDI)Co(η^4-P$_5$Mes$_2$)] (**4-Mes**)·(*n*-hexane)$_{0.7}$; * C$_6$D$_6$, □ *n*-hexane.
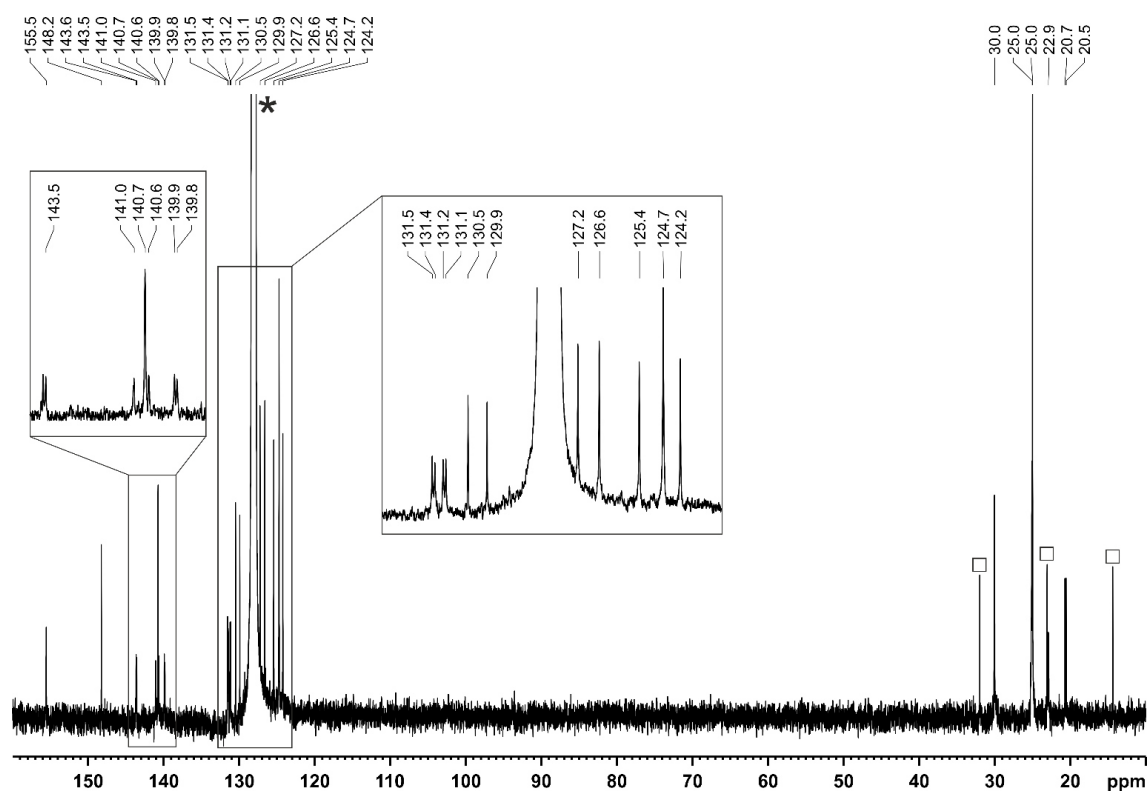
Figure S23. $^{13}C\{^1H\}$ NMR spectrum (100.61 MHz, C_6D_6, 300 K) of [(PHDI)Co(η^4-P_5Mes_2)] (**4-Mes**)·(n-hexane)$_{0.7}$; * C_6D_6, □ n-hexane.
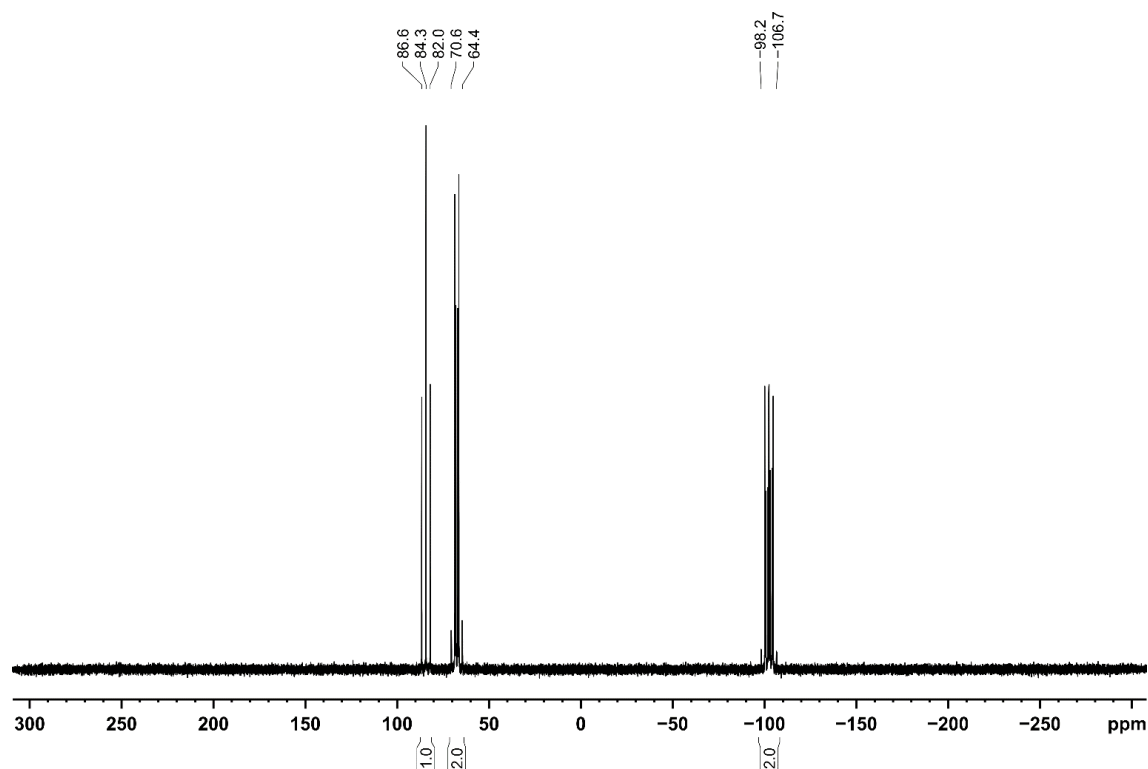
Figure S24. $^{31}P\{^1H\}$ NMR spectrum (161.98 MHz, 300 K, C_6D_6, 300 K) of [(PHDI)Co(η^4-P_5Mes_2)] (**4-Mes**)·(n-hexane)$_{0.7}$.
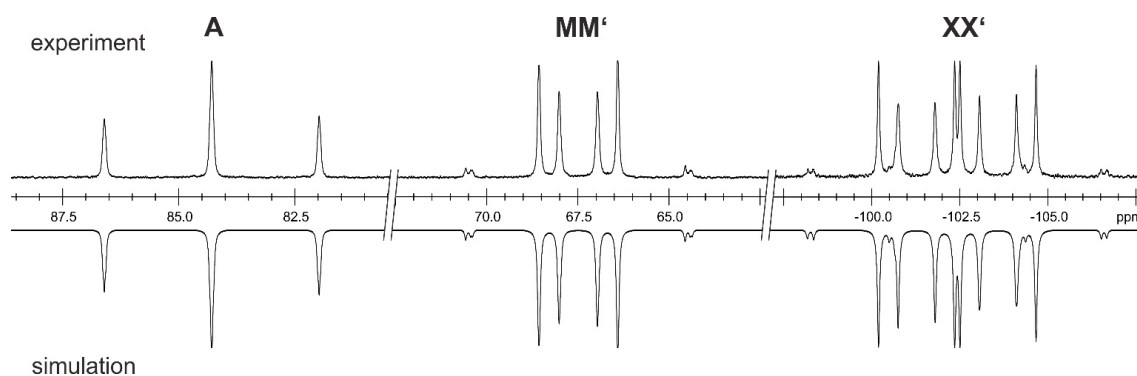
Figure S25. Section of the $^{31}P\{^1H\}$ NMR (161.98 MHz, C$_6$D$_6$, 300 K) of [(PHDI)Co(η^4-P$_5$Mes$_2$)] (**4-Mes**); experimental (upwards) and simulation (downwards)).

Table S5. Coupling constants from the iterative fit of the AMM'XX' spin system and schematic representation of the CoP$_5$Mes$_2$ core of [(PHDI)Co(η^4-P$_5$Mes$_2$)] (**4-Mes**).

$^1J_{AX} = {}^1J_{AX'} = -374.5$ Hz

$^1J_{MX} = {}^1J_{M'X'} = -378.6$ Hz

$^1J_{MM'} = -402.6$ Hz

$^2J_{MX'} = {}^2J_{M'X} = 28.6$ Hz

$^2J_{AM} = {}^2J_{AM'} = 5.3$ Hz

$^2J_{XX'} = -15.7$ Hz

Figure S26. ^1H NMR spectrum (400.13 MHz, C$_6$D$_6$, 300 K) of [(PHDI)Co(η^4-P$_5$(N(*i*Pr$_2$)$_2$)] (**4-N*i*Pr**); * C$_6$D$_6$.
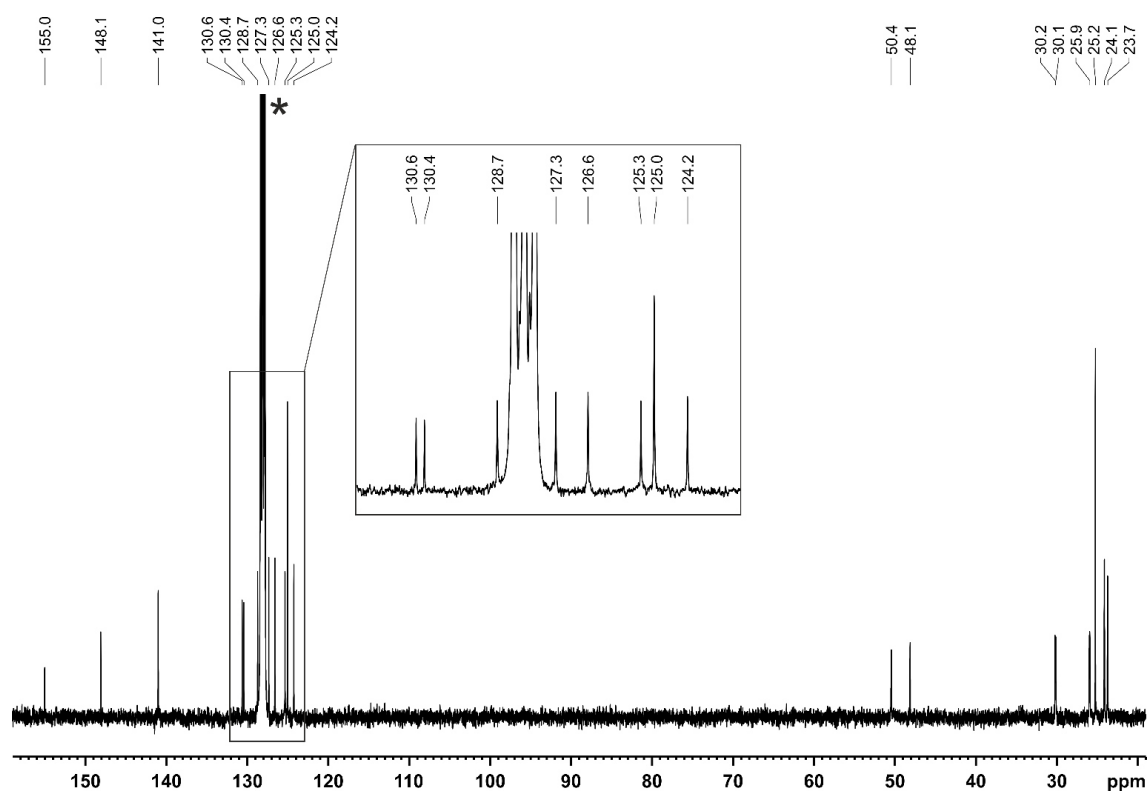
Figure S27. $^{13}C\{^{1}H\}$ NMR spectrum (100.61 MHz, C$_6$D$_6$, 300 K) of [(PHDI)Co(η^4-P$_5$(N(iPr$_2$)$_2$))] (**4-NiPr**); * C$_6$D$_6$.
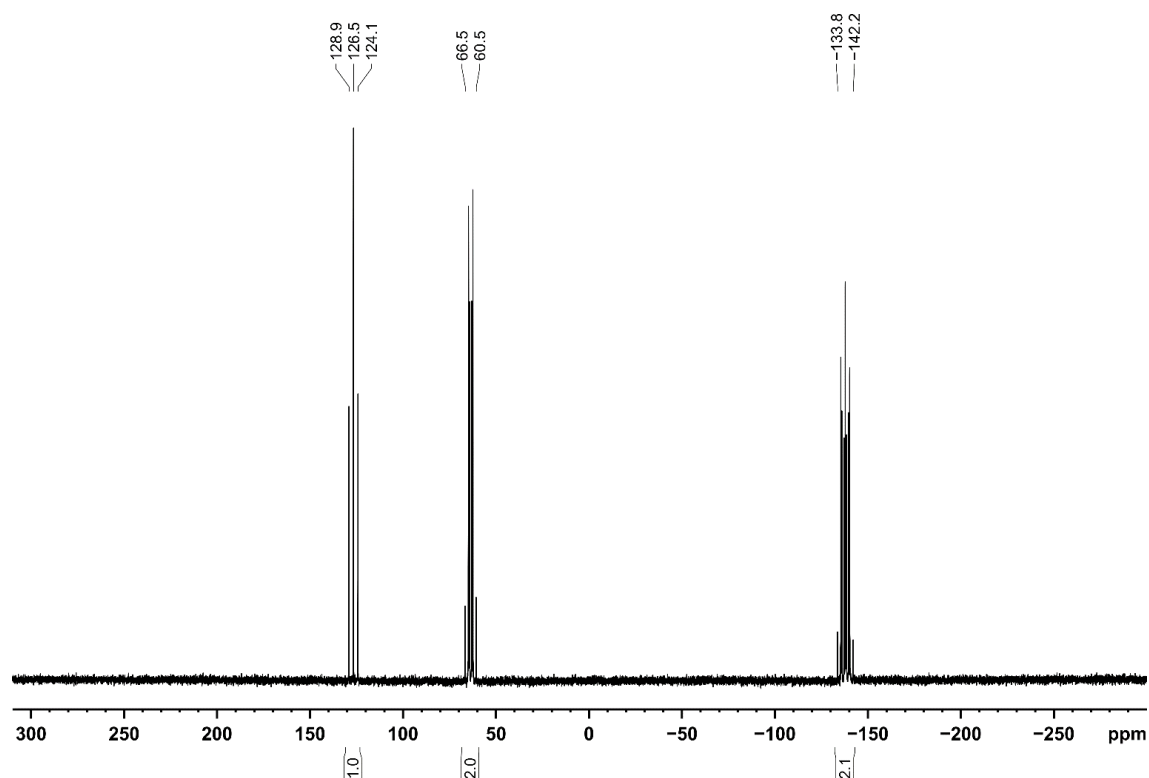
Figure S28. $^{31}P\{^{1}H\}$ NMR spectrum (161.98 MHz, 300 K, C$_6$D$_6$, 300 K) of [(PHDI)Co(η^4-P$_5$(N(iPr$_2$)$_2$))] (**4-NiPr**).
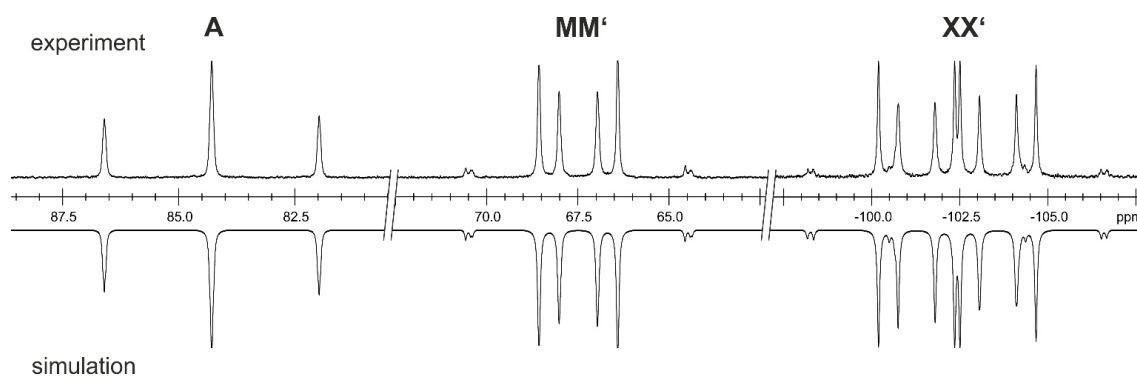
Figure S29. Section of the $^{31}P\{^1H\}$ NMR (161.98 MHz, C_6D_6, 300 K) of [(PHDI)Co(η^4-P_5Mes_2)] (**4-Mes**); experimental (upwards) and simulation (downwards).

Table S6. Coupling constants from the iterative fit of the AMM'XX' spin system and schematic representation of the CoP_5Mes_2 core of [(PHDI)Co(η^4-P_5Mes_2)] (**4-Mes**).

$^1J_{AX} = {}^1J_{AX'} = -374.5$ Hz
$^1J_{MX} = {}^1J_{M'X'} = -378.6$ Hz
$^1J_{MM'} = -402.6$ Hz
$^2J_{MX'} = {}^2J_{M'X} = 28.6$ Hz
$^2J_{AM} = {}^2J_{AM'} = 5.3$ Hz
$^2J_{XX'} = -15.7$ Hz

Figure S30. ^1H NMR spectrum (400.13 MHz, C_6D_6, 300 K) of [(PHDI)Co(η^4-$P_5(N(iPr_2)_2)$)] (**4-NiPr**); * C_6D_6.
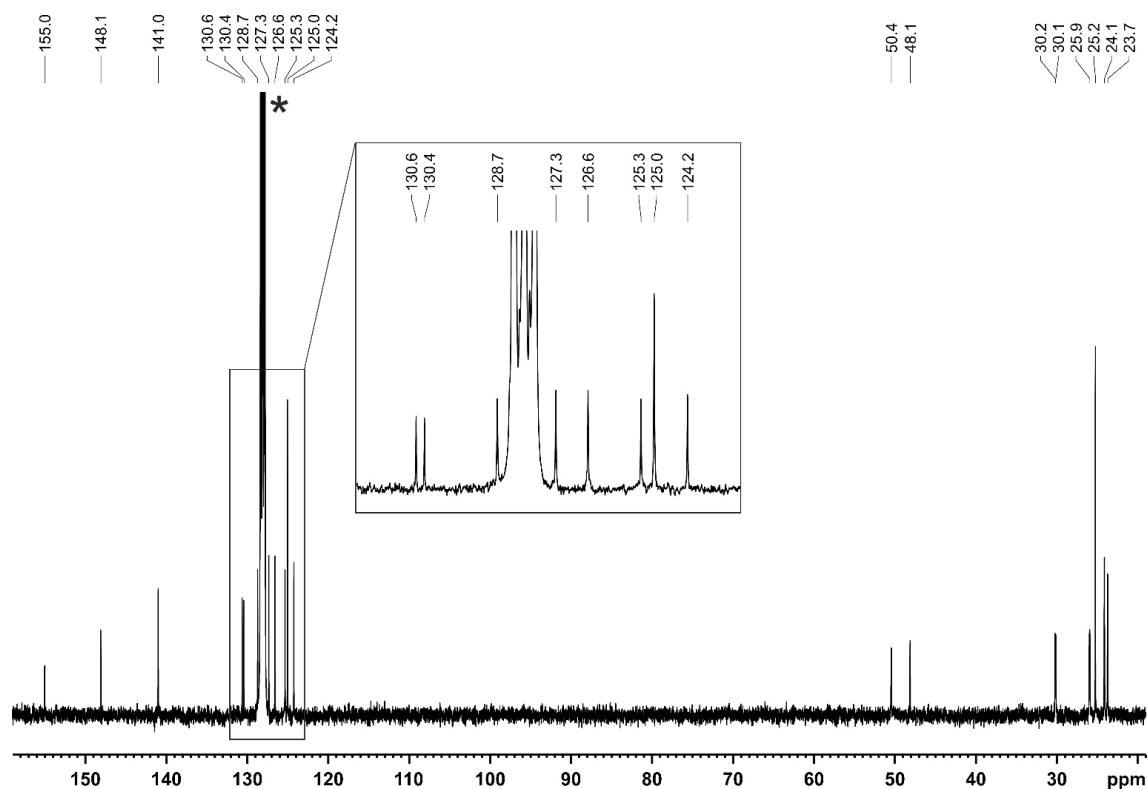
Figure S31. $^{13}C\{^1H\}$ NMR spectrum (100.61 MHz, C_6D_6, 300 K) of [(PHDI)Co(η^4-P_5(N(iPr_2)$_2$))] (**4-N*i*Pr**); * C_6D_6.
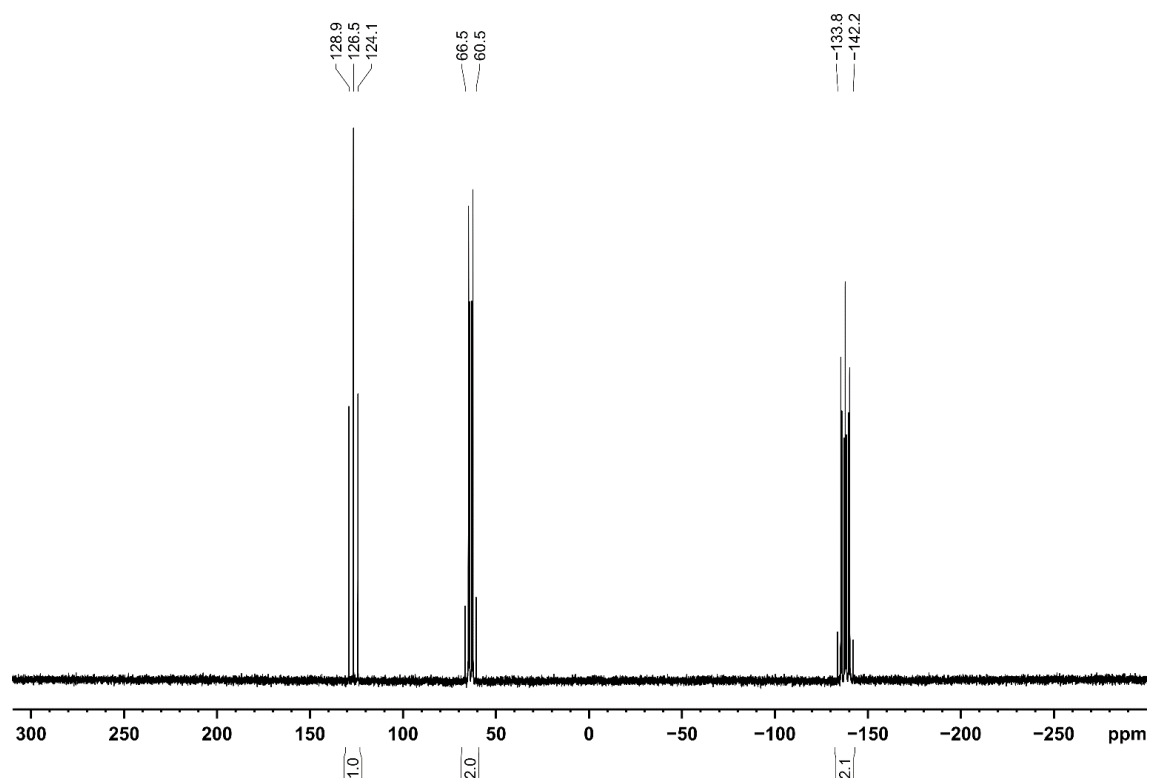
Figure S32. $^{31}P\{^1H\}$ NMR spectrum (161.98 MHz, 300 K, C_6D_6, 300 K) of [(PHDI)Co(η^4-P_5(N(iPr_2)$_2$))] (**4-N*i*Pr**).
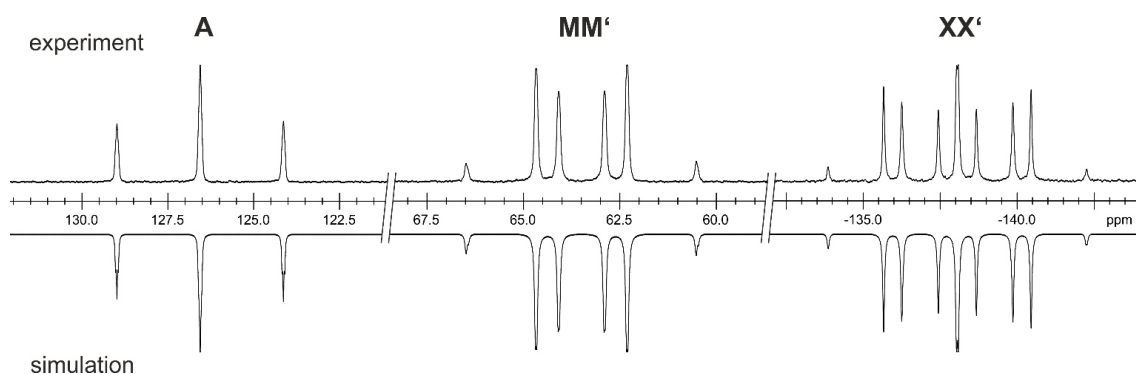
Figure S33. Section of the $^{31}P\{^1H\}$ NMR (161.98 MHz, C_6D_6, 300 K) of [(PHDI)Co(η^4-P_5(N(iPr$_2$)$_2$)] (**4-NiPr**); experimental (upwards) and simulation (downwards).

Table S7. Coupling constants from the iterative fit of the AMM'XX' spin system and schematic representation of the CoP$_5$N(iPr$_2$)$_2$ core of [(PHDI)Co(η^4-P_5(N(iPr$_2$)$_2$)] (**4-NiPr**).

$^1J_{AX} = {}^1J_{AX'} = -392.7$ Hz

$^1J_{MX} = {}^1J_{M'X'} = -407.1$ Hz

$^1J_{MM'} = -386.6$ Hz

$^2J_{MX'} = {}^2J_{M'X} = 24.5$ Hz

$^2J_{AM} = {}^2J_{AM'} = -6.6$ Hz

$^2J_{XX'} = 3.5$ Hz
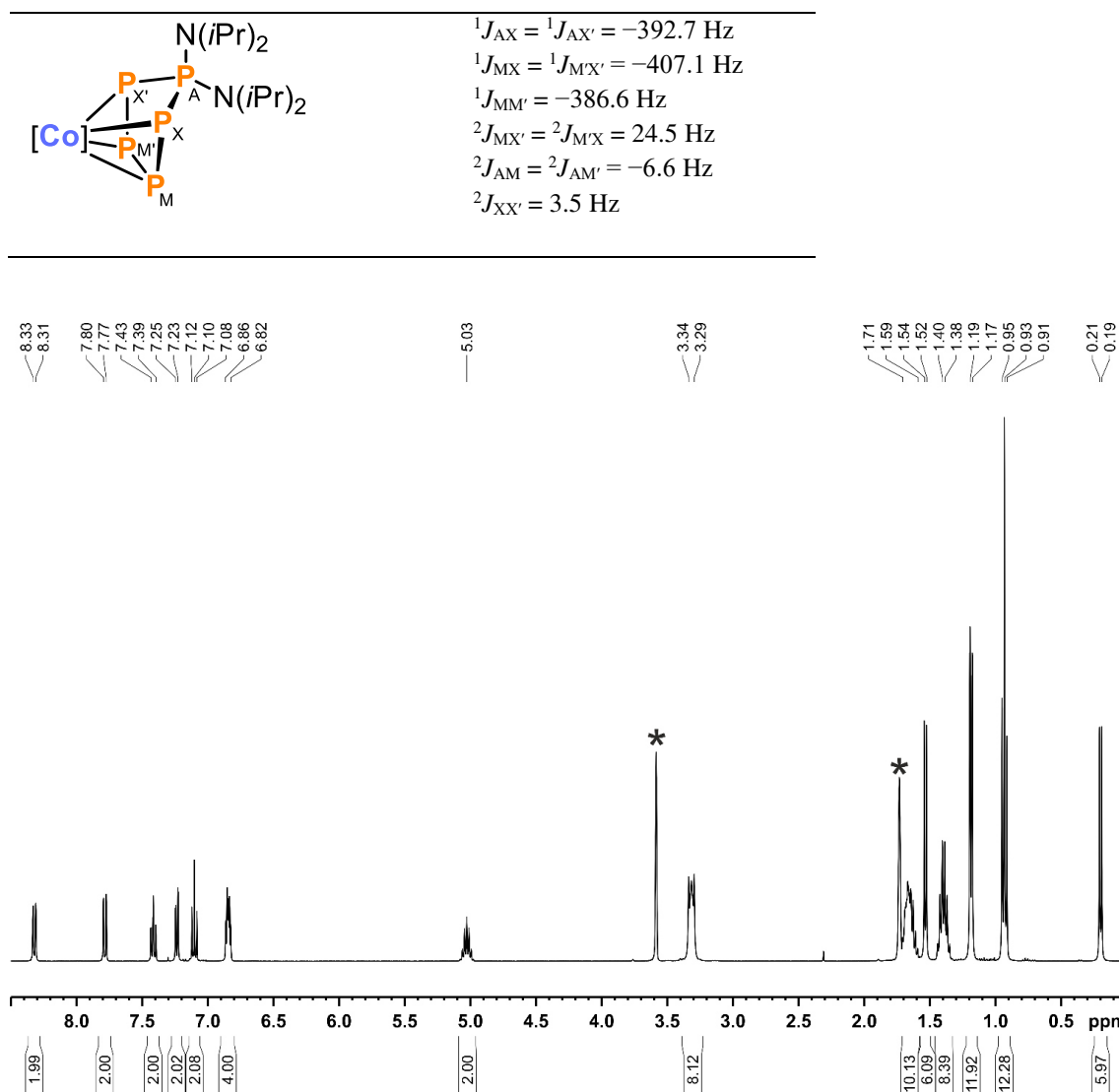
Figure S34. ^1H NMR spectrum (400.13 MHz, THF-d_8, 300 K) of [nBu$_4$N][(PHDI)Co(η^3-P_3)(CN)] ([nBu$_4$N]**5**); * THF-d_8.
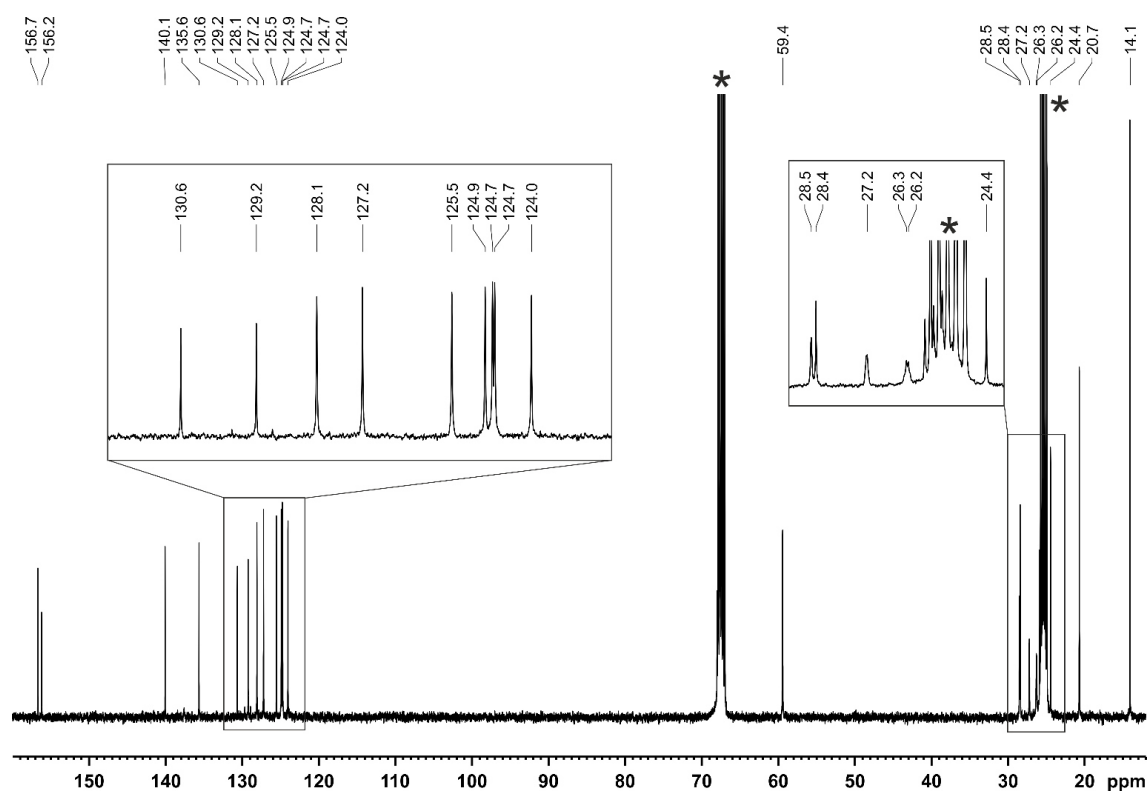
Figure S35. ^{13}C{^{1}H} NMR spectrum (100.61 MHz, THF-d_8, 300 K) of [nBu$_4$N][(PHDI)Co(η^3-P$_3$)(CN)] ([nBu$_4$N]5); * THF-d_8.
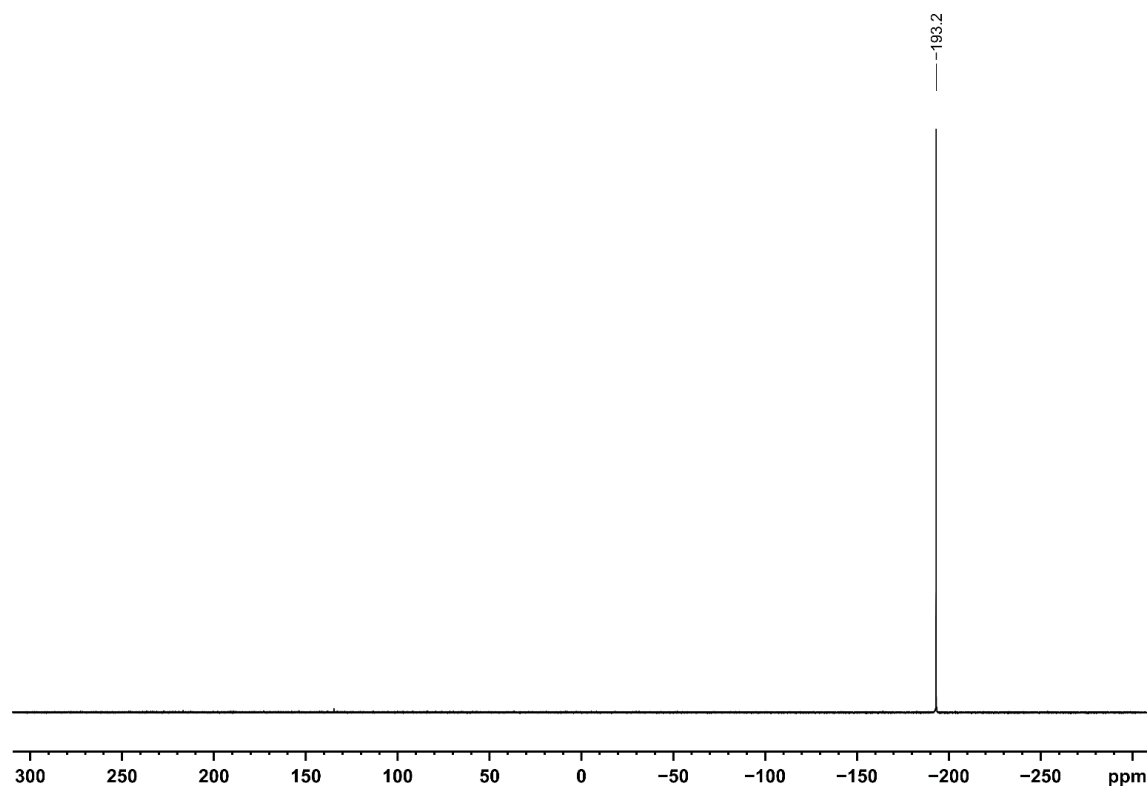
Figure S36. ^{31}P{^{1}H} NMR spectrum (161.98 MHz, THF-d_8, 300 K) of [nBu$_4$N][(PHDI)Co(η^3-P$_3$)(CN)] ([nBu$_4$N]5).

126
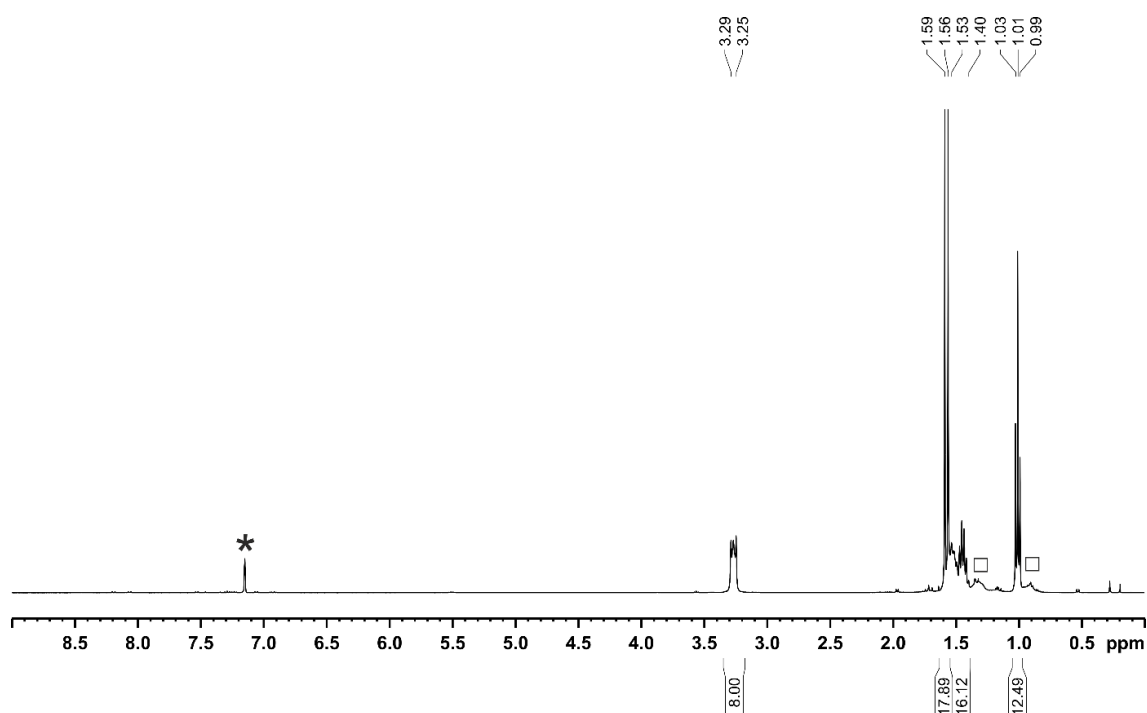
Figure S37. ^{1}H NMR spectrum (400.13 MHz, C$_6$D$_6$, 300 K) of [nBu$_4$N][tBu$_2$P(PCN)] ([nBu$_4$N]**6-tBu**); * C$_6$D$_6$, □ n-hexane.
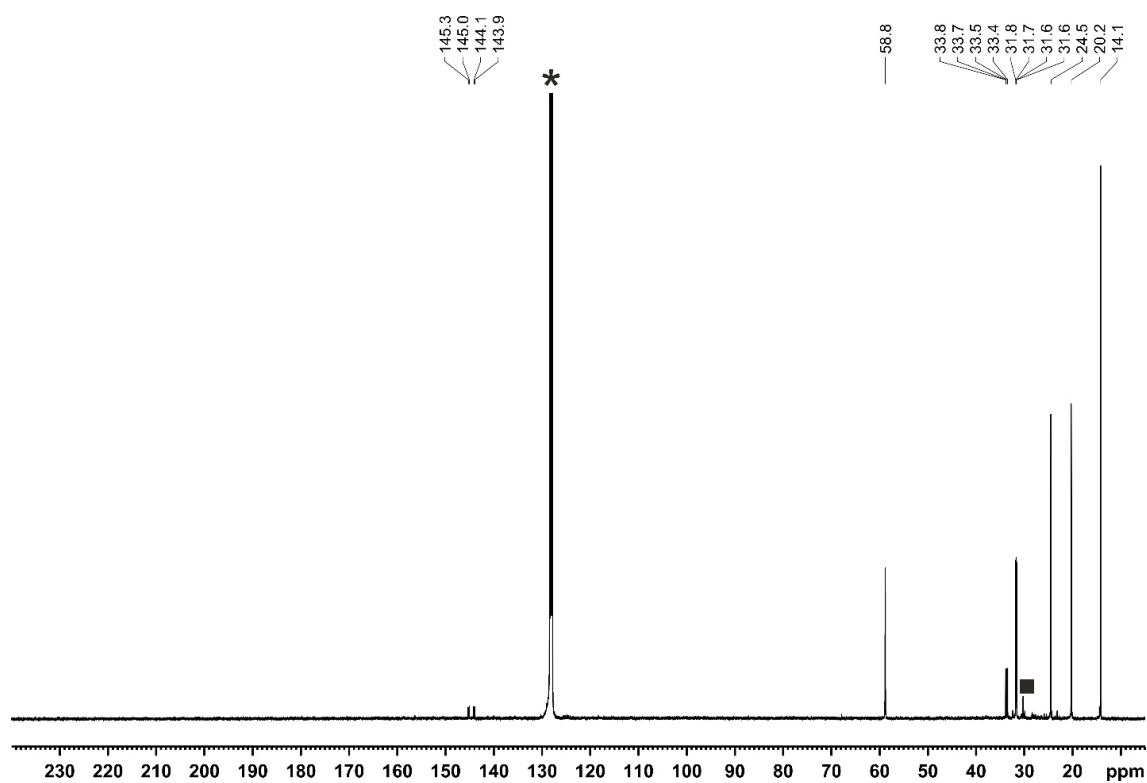
Figure S38. ^{13}C{^{1}H} NMR spectrum (100.61 MHz, C$_6$D$_6$, 300 K) of [nBu$_4$N][tBu$_2$P(PCN)] ([nBu$_4$N]**6-tBu**); * C$_6$D$_6$, ■ unknown impurity.
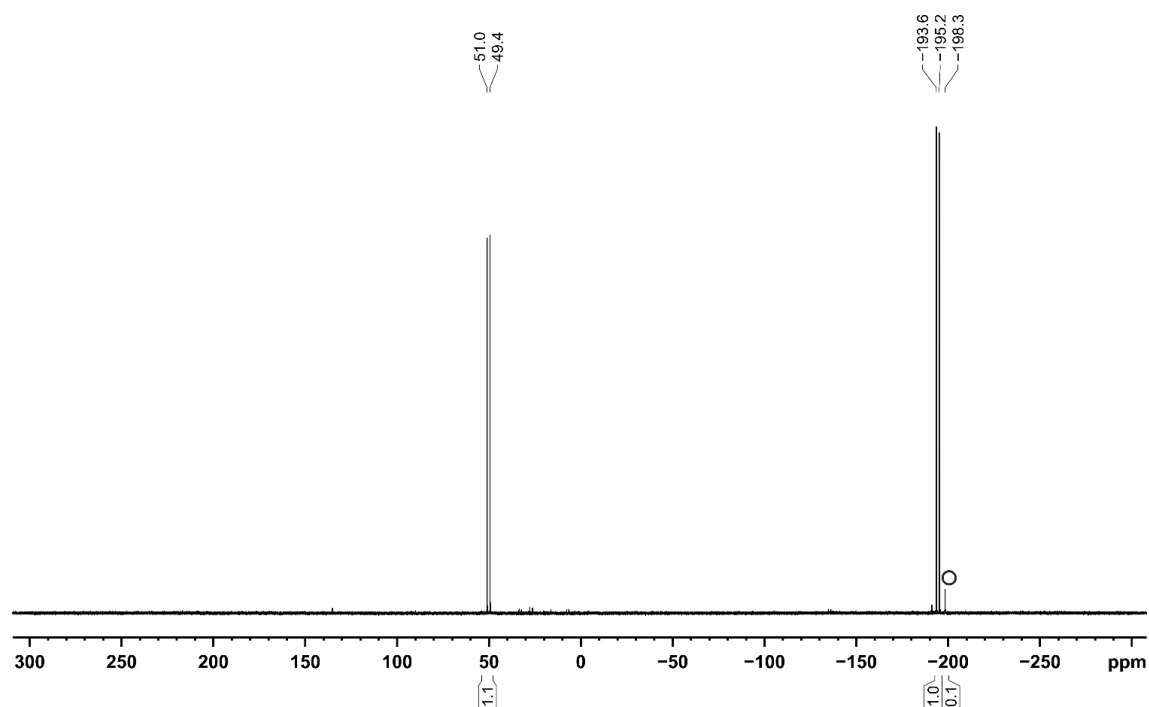
Figure S39. $^{31}P\{^1H\}$ NMR spectrum (161.98 MHz, C_6D_6, 300 K) of [nBu$_4$N][tBu$_2$P(PCN)] ([nBu$_4$N]**6-tBu**); ○ minor impurity of [nBu$_4$N]**5**.
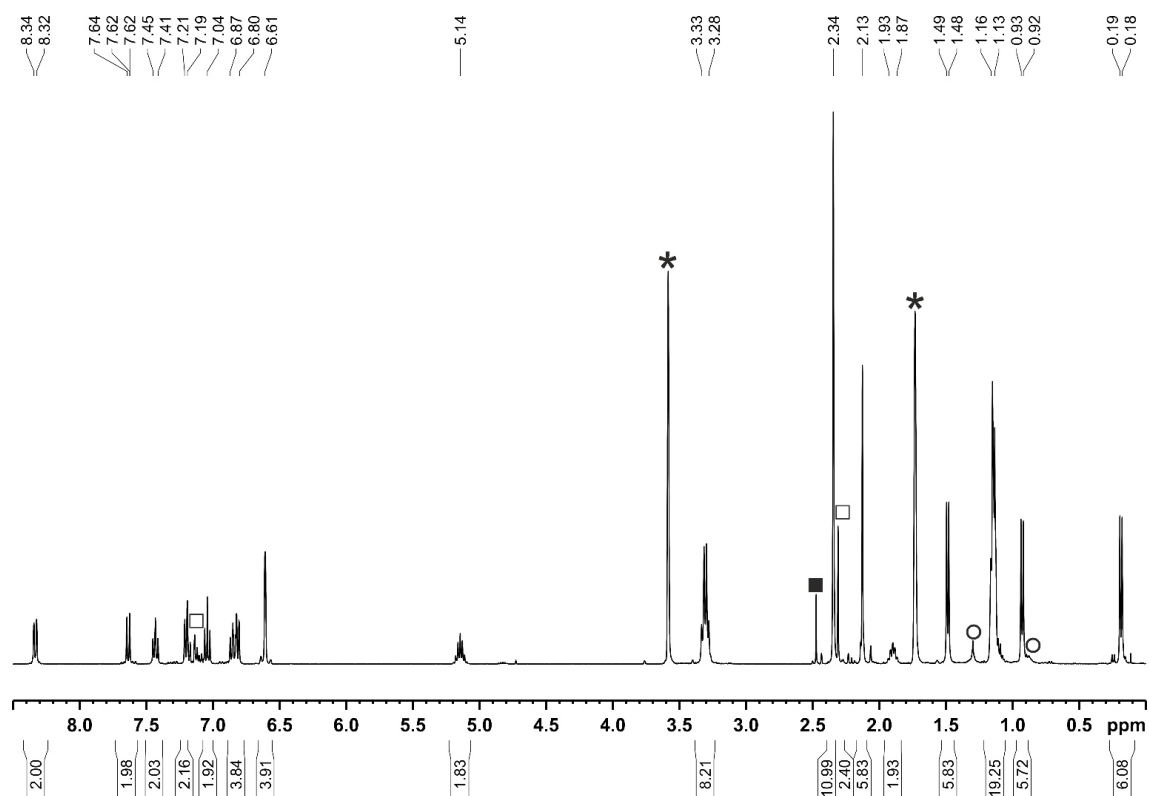
Figure S40. ^1H NMR spectrum (400.13 MHz, THF-d_8, 263 K) of [Et$_4$N][(PHDI)Co(η^3-P$_5$Mes$_2$)(CN)] ([Et$_4$N]**7**)·(toluene)$_{0.8}$; * THF-d_8, □ toluene, ○ n-hexane, ■ unknown impurity.
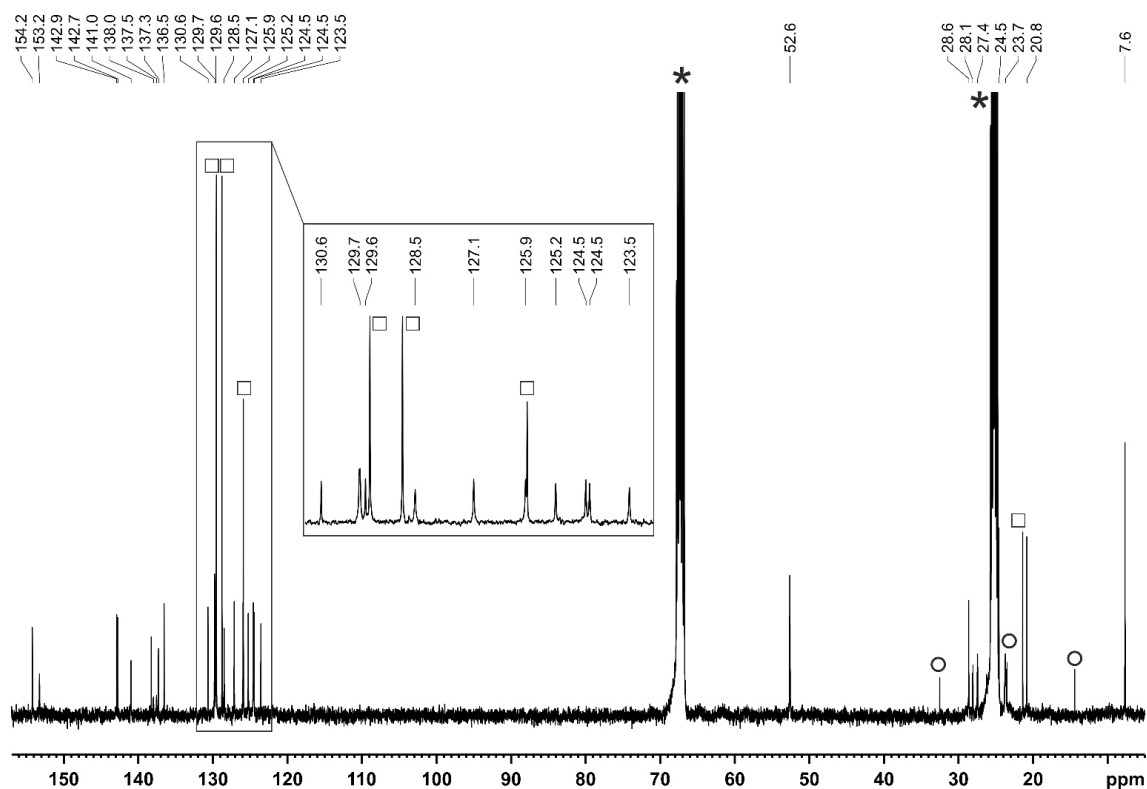
Figure S41. $^{13}C\{^1H\}$ NMR spectrum (100.61 MHz, THF-d_8, 263 K) of [Et$_4$N][(PHDI)Co(η^3-P$_5$Mes$_2$)(CN)] ([Et$_4$N]7)·(toluene)$_{0.8}$; * THF-d_8, □ toluene, ○ n-hexane.
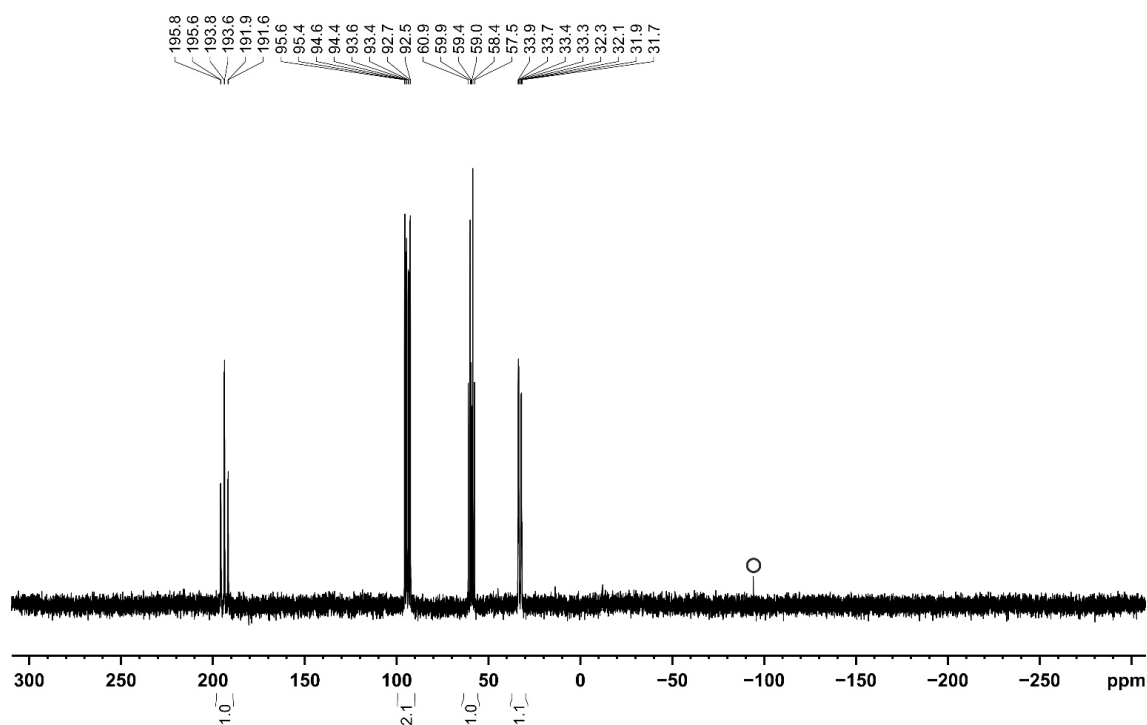
Figure S42. $^{31}P\{^1H\}$ NMR spectrum (161.98 MHz, THF-d_8, 263 K) of [Et$_4$N][(PHDI)Co(η^3-P$_5$Mes$_2$)(CN)] ([Et$_4$N]7)·(toluene)$_{0.8}$; ○ minor impurity of Mes$_2$PH.[33]

129

experiment
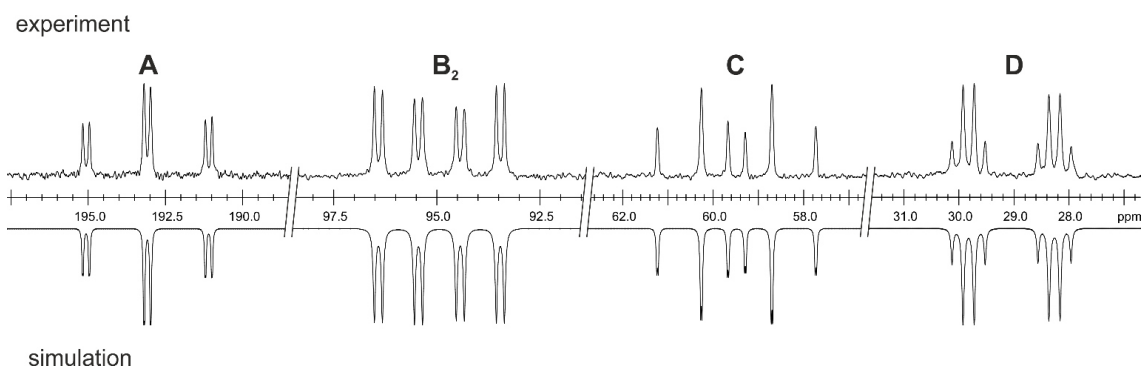
simulation

Figure S43. Section of the $^{31}P\{^1H\}$ NMR (161.98 MHz, THF-d_8, 263 K) of [Et$_4$N][(PHDI)Co(η^3-P$_5$Mes$_2$)(CN)] ([Et$_4$N]**7**); experimental (upwards) and simulation (downwards).

Table S8. Coupling constants from the iterative fit of the AB$_2$CD spin system and schematic representation of the CoP$_5$Mes$_2$ core of [Et$_4$N][(PHDI)Co(η^3-P$_5$Mes$_2$)(CN)] ([Et$_4$N]**7**)..

$^1J_{AB} = -321.$ Hz
$^1J_{BC} = -157.3$ Hz
$^1J_{CD} = -252.8$ Hz
$^2J_{AC} = -5.2$ Hz
$^2J_{BD} = 31.6$ Hz
$^3J_{AD} = -34.3$ Hz

3.4.5   UV/Vis Spectra
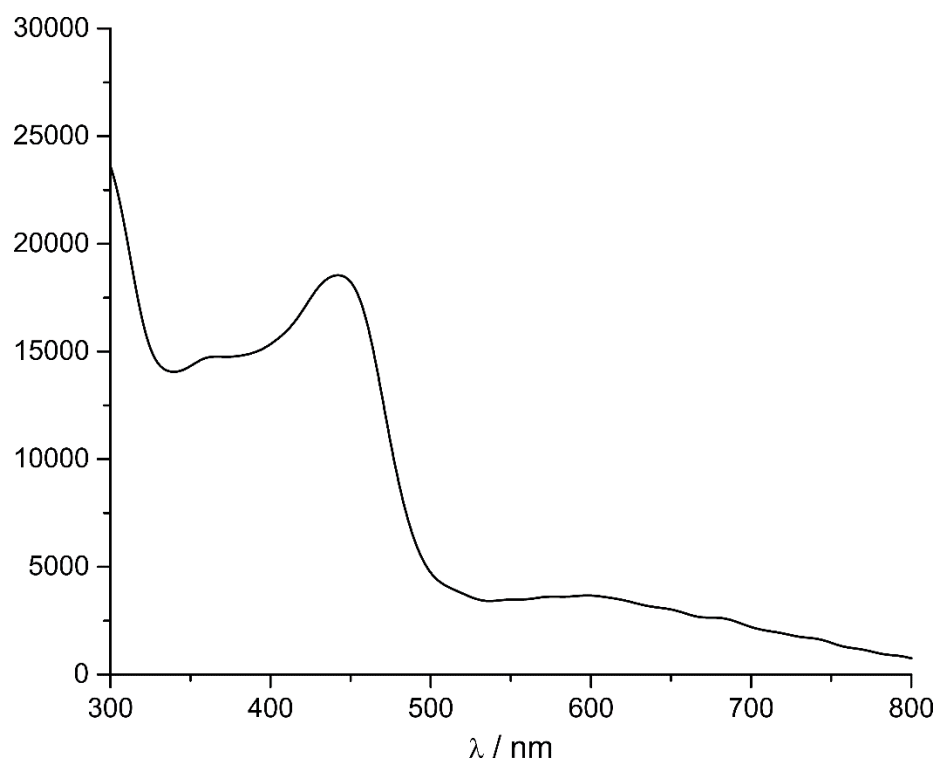
Figure S44. UV/vis spectrum of [K(18c-6)][(PHDI)Co(η^4-1,5-cod)]·(THF)$_{1.4}$ ([K(18c-6)]**1**) in THF.
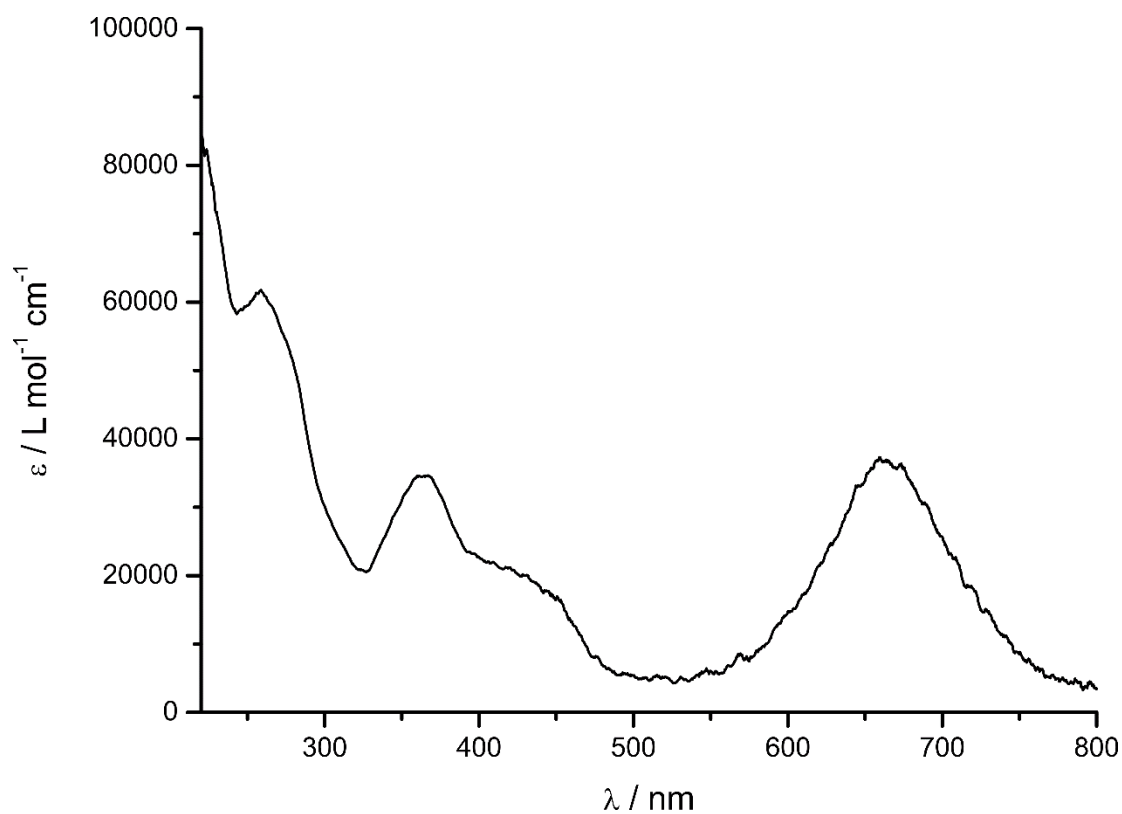
Figure S45. UV/vis spectrum of [K(18c-6)][(PHDI)Co(η^4-P$_4$)] ([K(18c-6)]**2**) in THF.
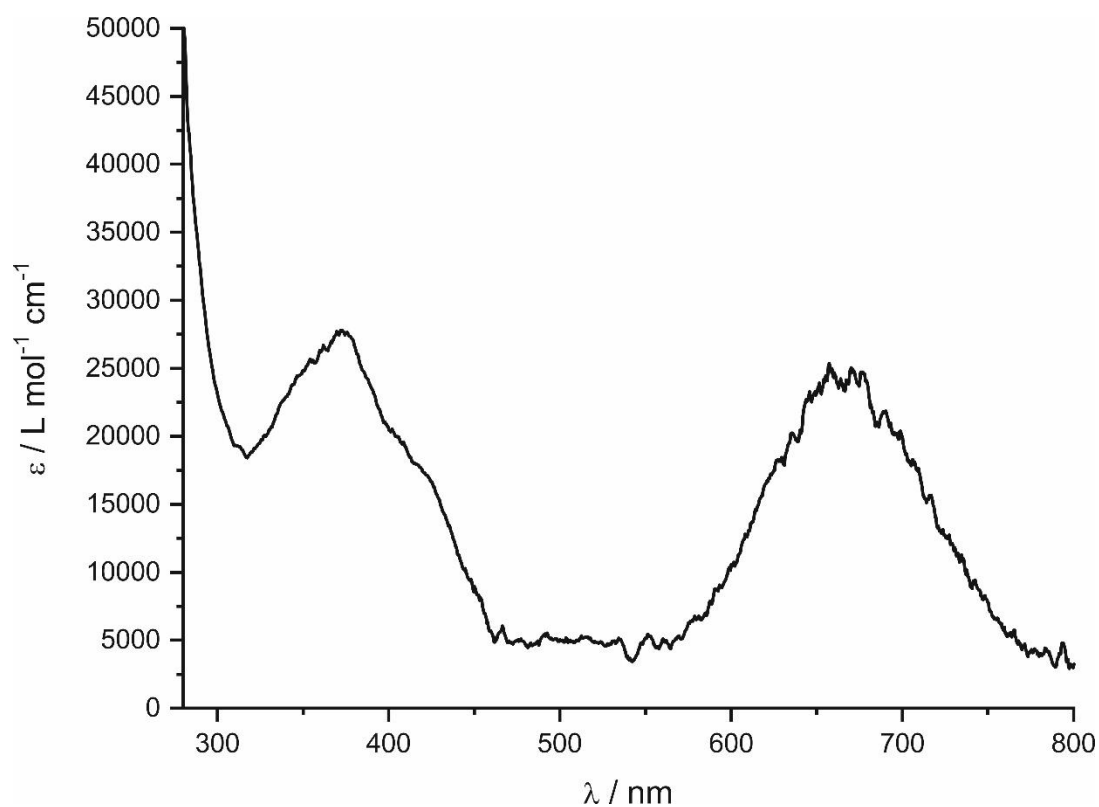
Figure S46. UV/vis spectrum of [K(18c-6)][(PHDI)Co(μ^2:η^1,η^4-P$_4$)W(CO)$_5$] ([K(18c-6)]**3**) in THF.
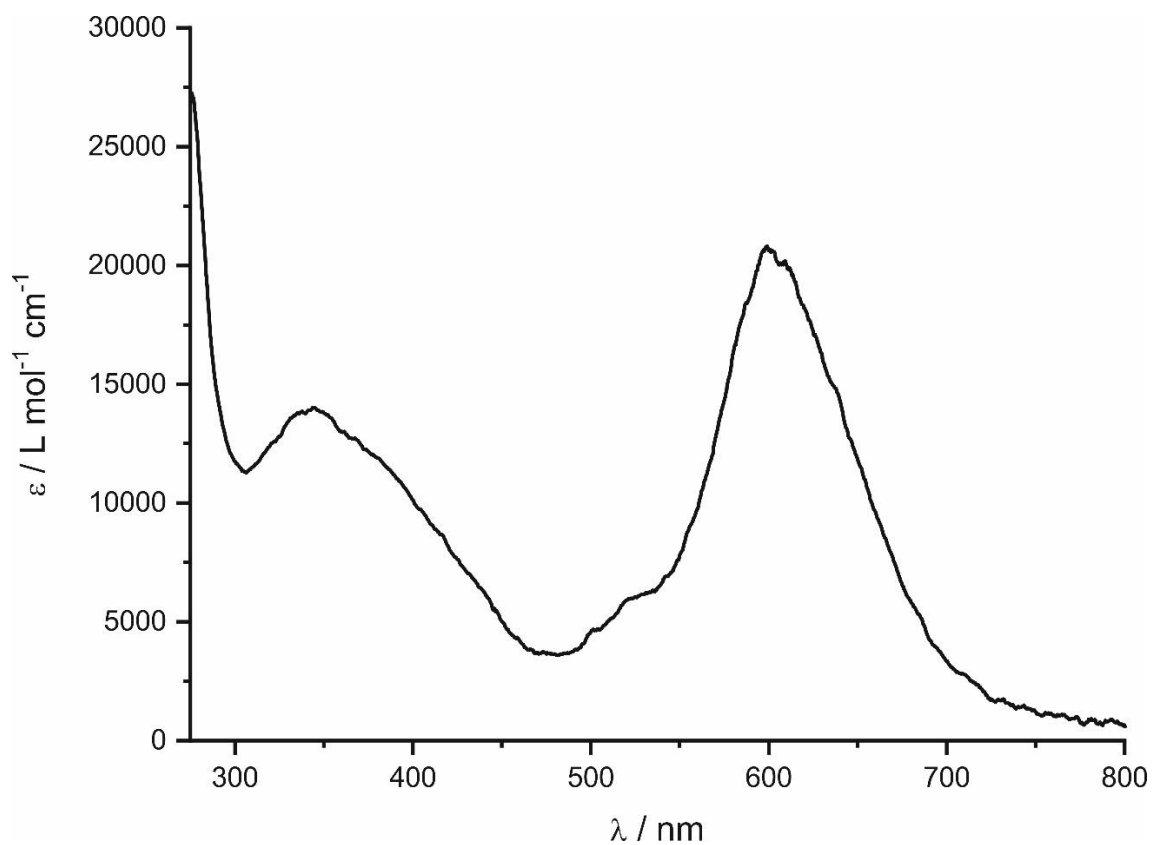
Figure S47. UV/vis spectrum of [(PHDI)Co(η^4-P$_5$Cy$_2$)] (**4-Cy**) in THF.
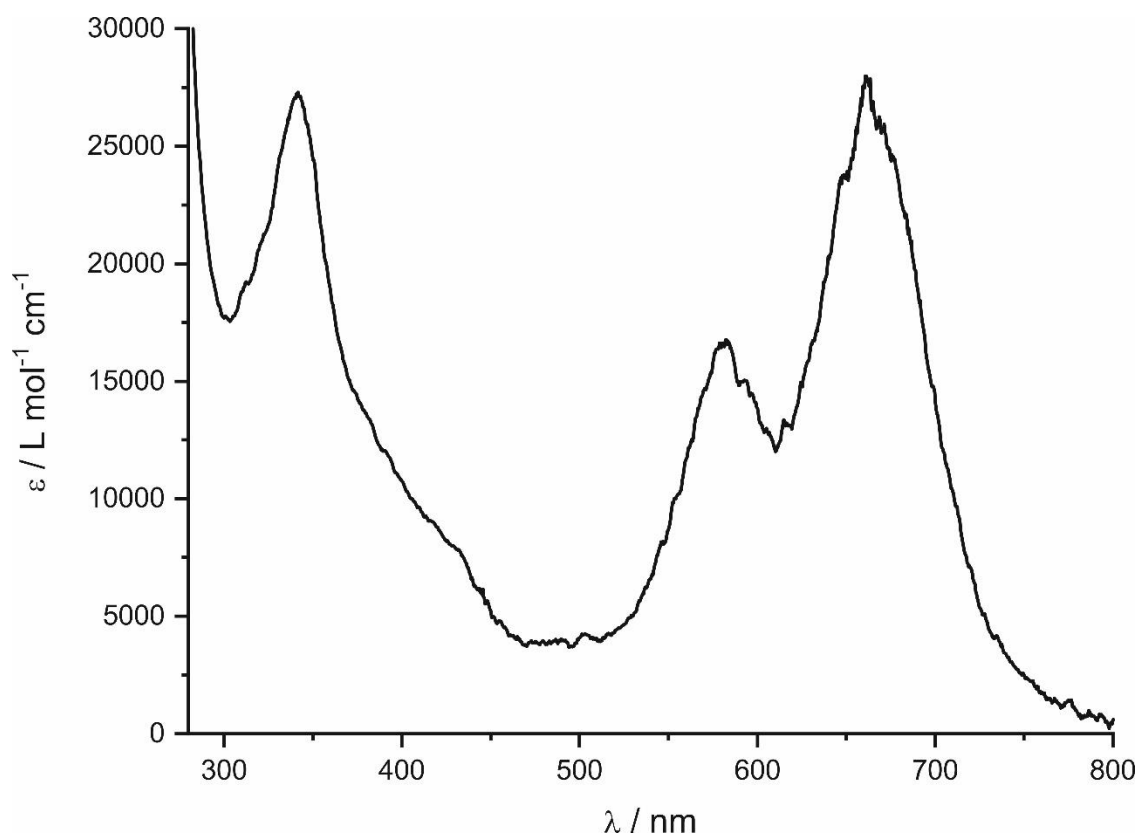
Figure S48. UV/vis spectrum of [(PHDI)Co(η^4-P$_5t$Bu$_2$)] (**4-*t*Bu**) in THF.
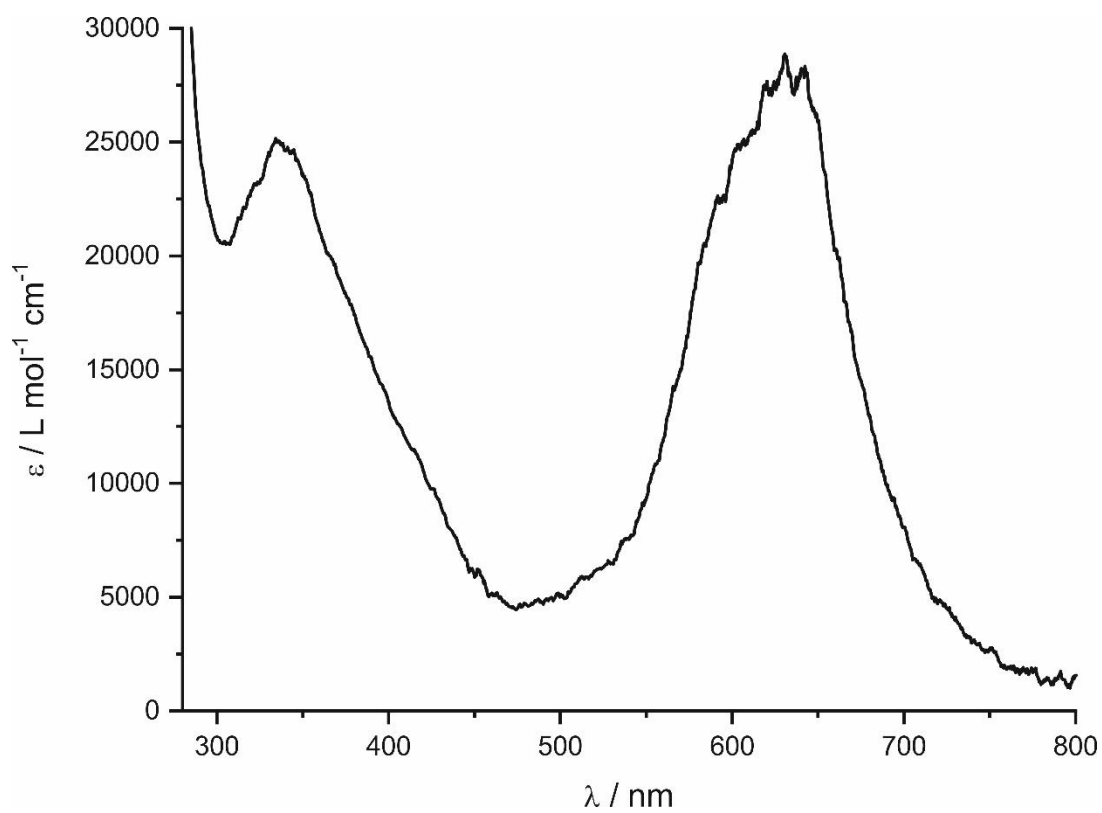
Figure S49. UV/vis spectrum of [(PHDI)Co(η^4-P$_5$Ph$_2$)] (**4-Ph**) in THF.

133
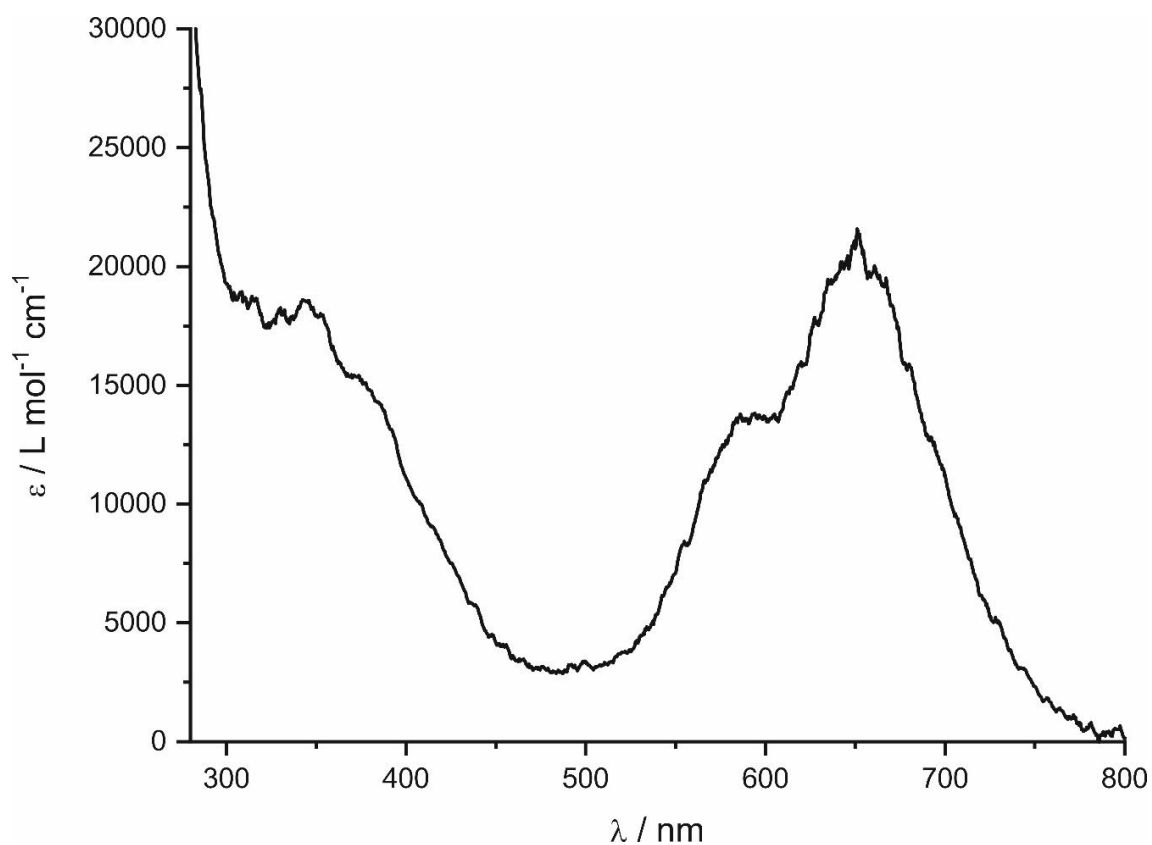
Figure S50. UV/vis spectrum of [(PHDI)Co(η^4-P$_5$Mes$_2$)] (**4-Mes**) in THF.
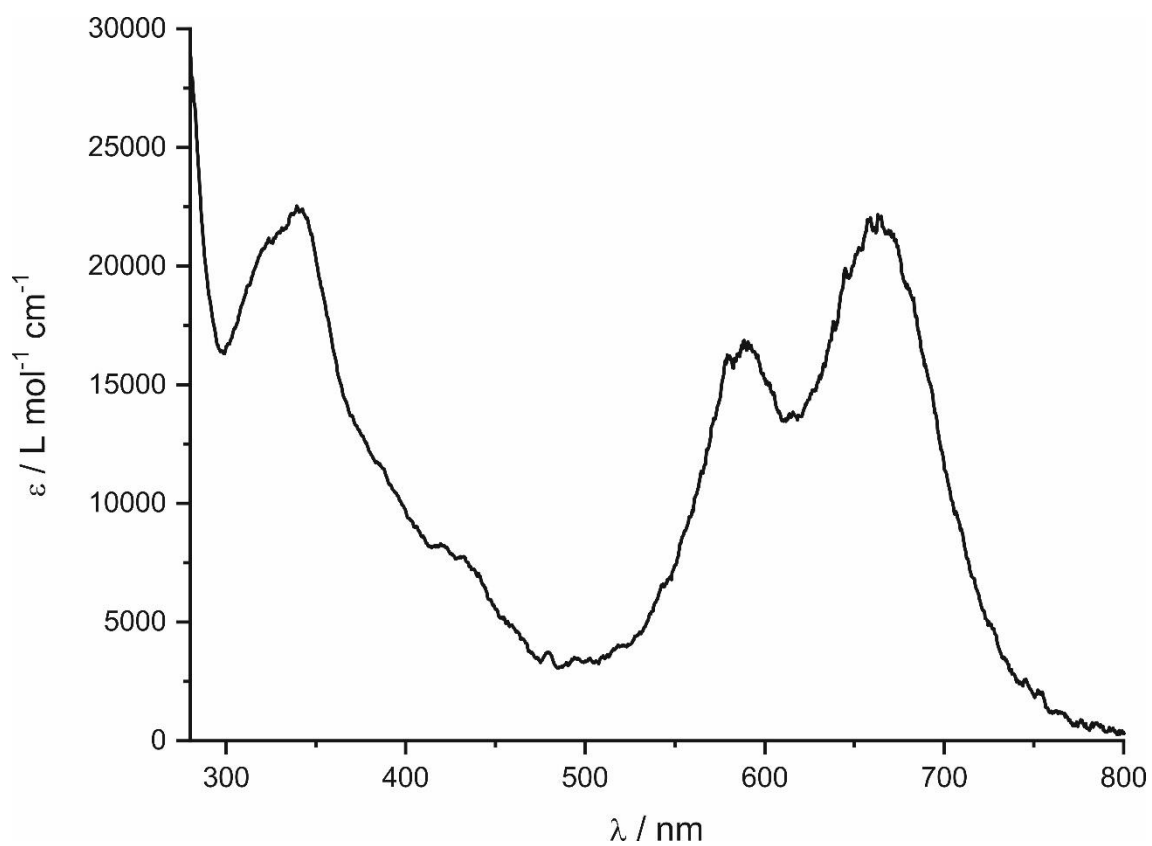
Figure S51. UV/vis spectrum of [(PHDI)Co(η^4-P$_5$(N(*i*Pr$_2$)$_2$)] (**4-N*i*Pr**) in THF.
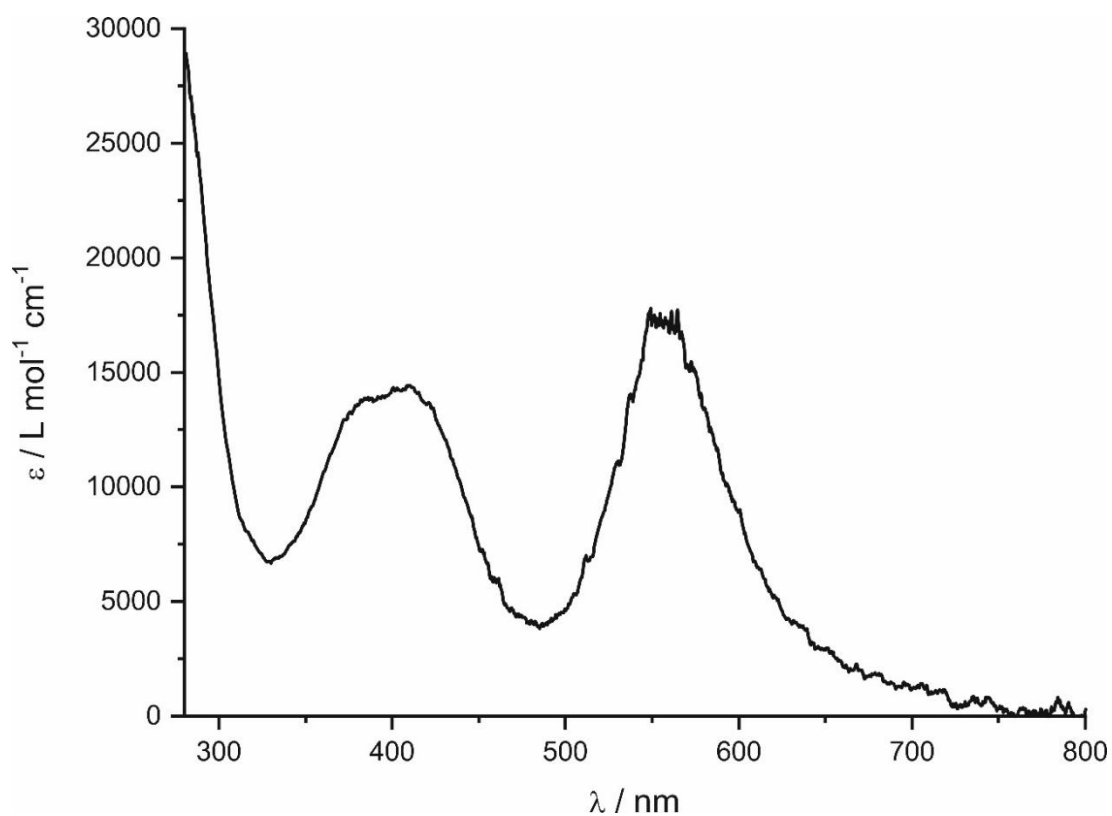
Figure S52. UV/vis spectrum of [*n*Bu₄N][(PHDI)Co(η³-P₃)(CN)] ([*n*Bu₄N]**5**) in THF.
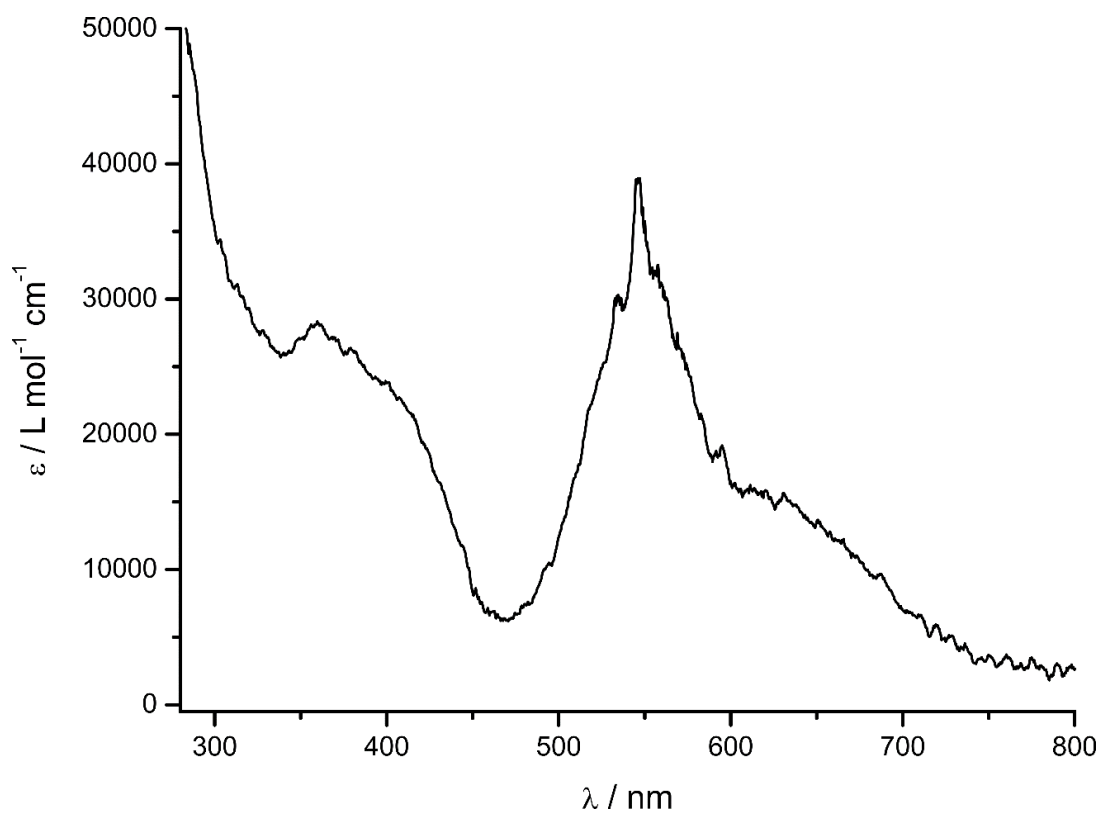
Figure S53. UV/vis spectrum of [Et₄N][(PHDI)Co(η³-P₅Mes₂)(CN)] ([Et₄N]**7**) in THF.

3.4.6   IR Spectra
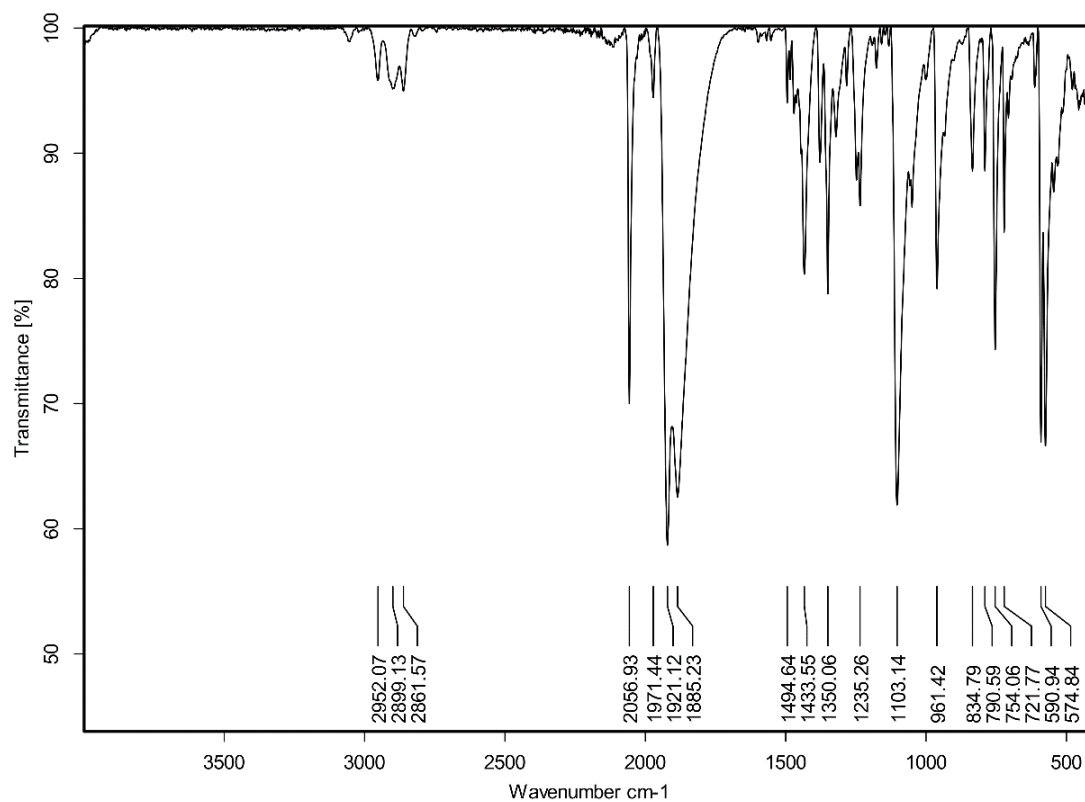
Figure S54. Solid state IR spectrum of [K(18c-6][(PHDI)Co(μ^2:η^1,η^4-P$_4$)W(CO)$_5$] ([K(18c-6]**3**).
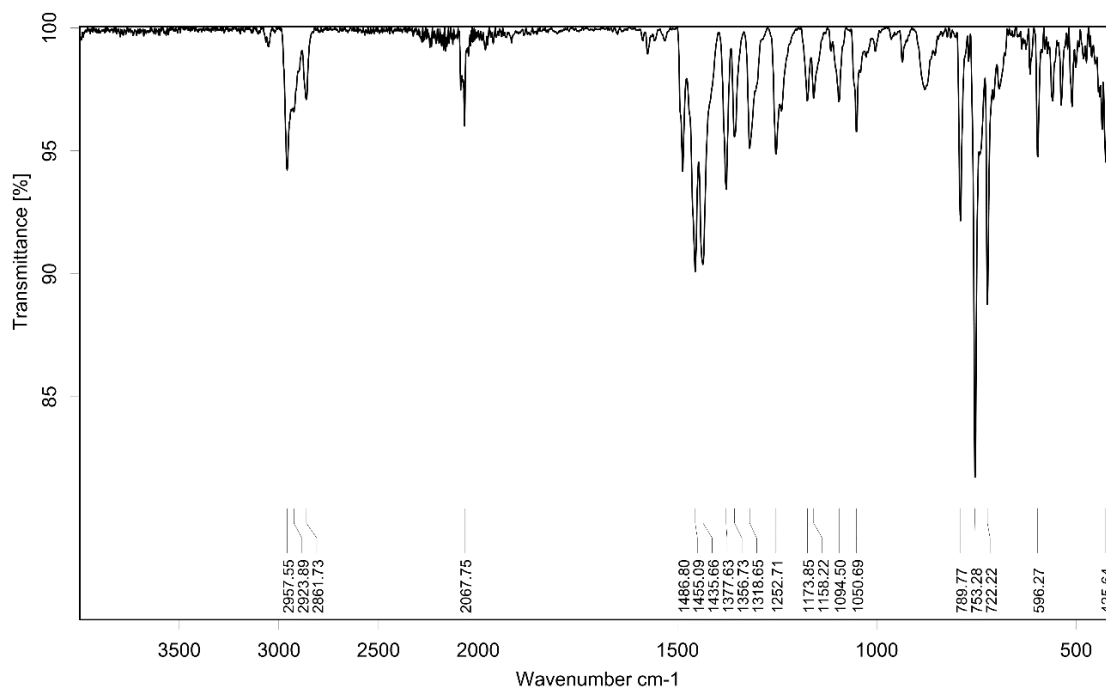
Figure S55. Solid state IR spectrum of [nBu$_4$N][(PHDI)Co(η^3-P$_3$)(CN)] ([nBu$_4$N]**5**).
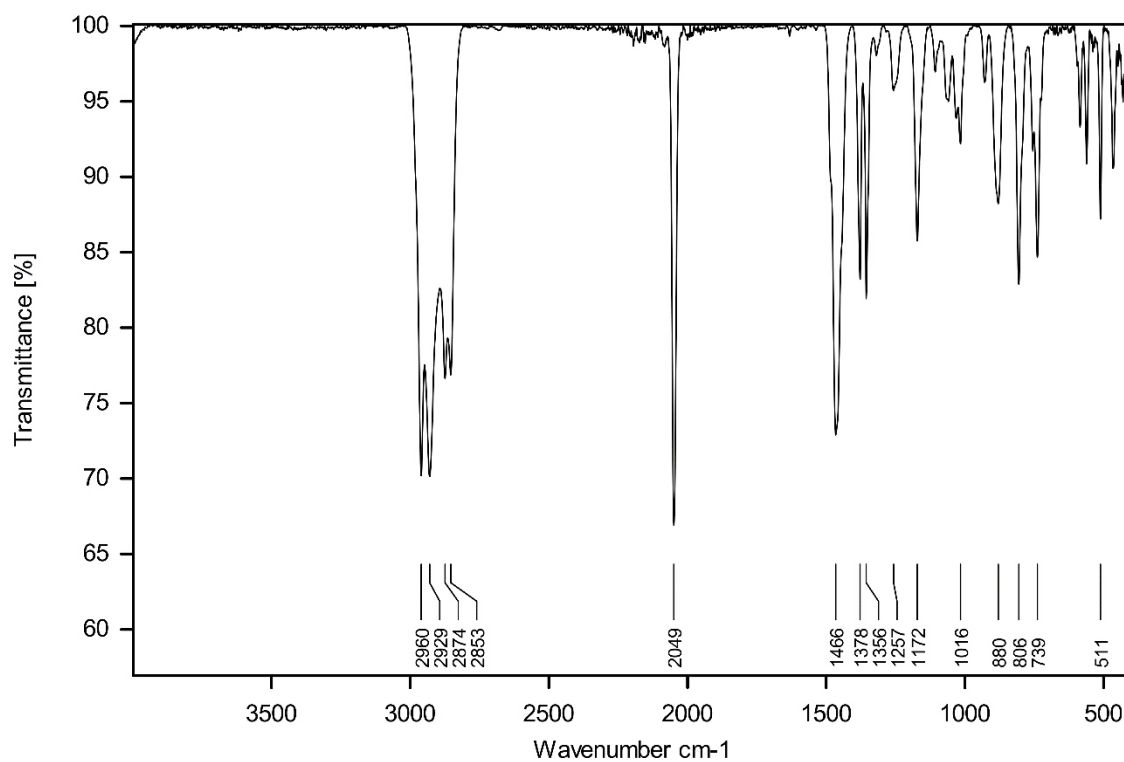
Figure S56. Solid state IR spectrum of [nBu4N][tBu2P(PCN)] ([nBu4N]6-*tBu*).
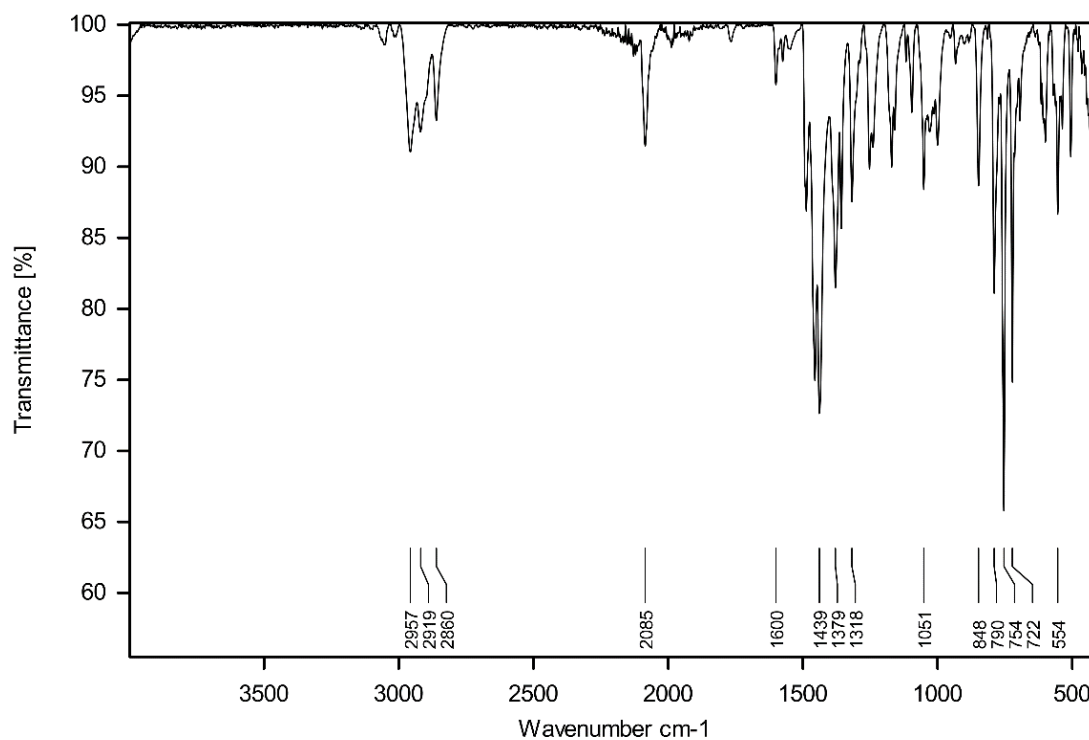
Figure S57. Solid state IR spectrum of [Et4N][(PHDI)Co(η³-P5Mes2)(CN)] ([Et4N]7).

3.4.7   X-Ray Crystallography

The single-crystal X-ray diffraction data were recorded on a Agilent Technologies SuperNova and a GV1000, TitanS2 diffractometer with Cu-K_α radiation ($\lambda = 1.54184$ Å). Either semi-empirical multi-scan absorption corrections[42] or analytical ones[43] were applied to the data. The structures were solved with SHELXT[44] and least-square refinements on F^2 were carried out with SHELXL.[45] The hydrogen atoms were located in idealized positions and refined isotropically with a riding model.

Twinning of the crystal of **4-Mes** was refined with a HKLF 5 BASF [0.215(2)] command. The crystal of [Et$_4$N]**7** contained six severely disordered molecules of Et$_2$O which were refined by using the solvent mask command (3 Et$_2$O: 126 e$^-$, found: 125.5 e$^-$ for each void).

CCDC 1940064-1940073 contain the supplementary crystallographic data for this paper. These data are provided free of charge by The Cambridge Crystallographic Data Centre (https://www.ccdc.cam.ac.uk/).
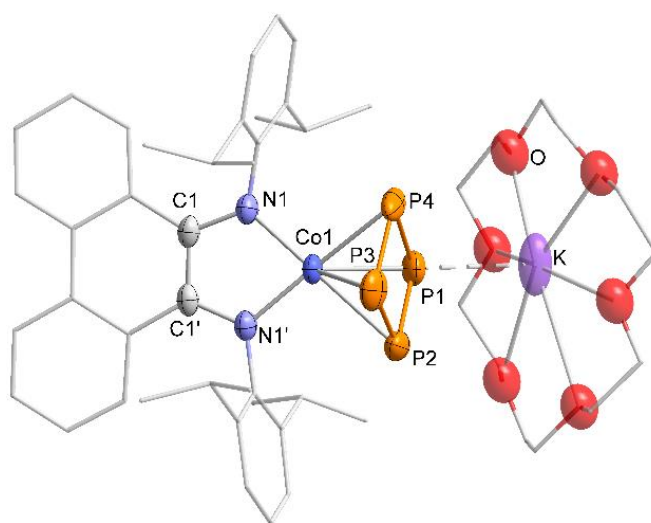
Figure S58. Solid-state molecular structure of [K(18c-6)][(PHDI)Co(η^4-P$_4$)] ([K(18c-6)]**2**). The asymmetric unit contains only half of the molecule, the full molecule is generated by the mirror plane perpendicular to the b axis. Hydrogen atoms are omitted for clarity and thermal ellipsoids are drawn at the 50% probability level. Selected bond lengths [Å] and angles [°]: P1–P2 2.037(9), P1–P4 2.234(8), P2–P3 2.130(6), P3–P4 2.158(7), Co1–P1 2.336(1), Co1–P2 2.403(8), Co1–P3 2.330(2), Co1–P4 2.297(8), Co1–N1 1.876(3), C1–N1 1.356(4), C1–C1' 1.431(7), P1–P2–P3 93.4(3), P2–P3–P4 89.4(1), P3–P4–P1 87.4(3), P2–P1–P4 89.7(2).

138
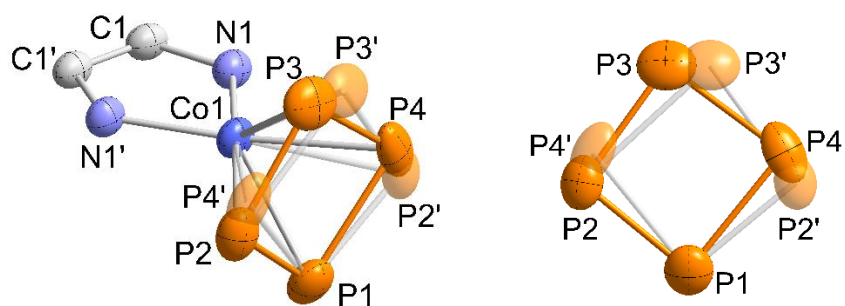
Figure S59. Side view (left) and front view (right) of the disordered P$_4$ ligand in the solid-state molecular structure of [K(18c-6)][(PHDI)Co(η^4-P$_4$)] ([K(18c-6)]**2**). The P$_4$ ring is disordered beyond the mirror plane perpendicular to the b axis. Part 1 and part 2 are 50% occupied each. Thermal ellipsoids are drawn at the 50% probability level.
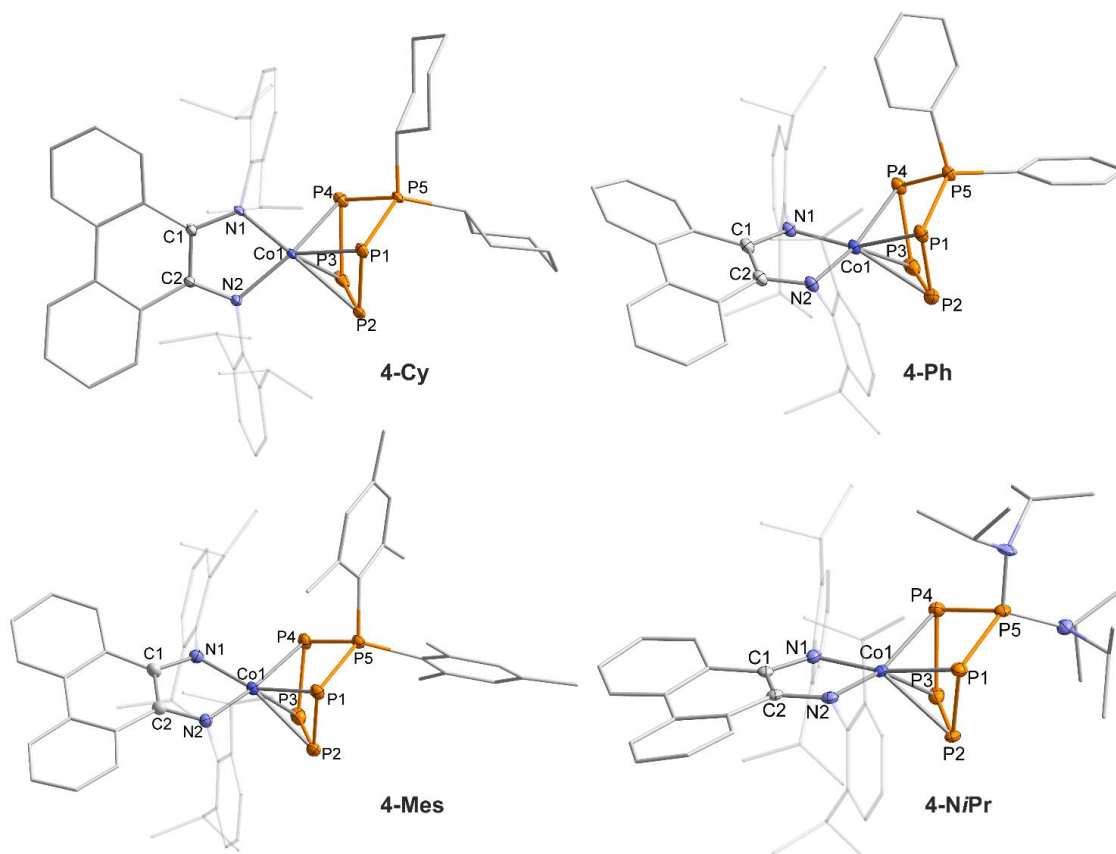
Figure S60. Solid-state molecular structures of complexes [(PHDI)Co(η^4-P$_5$R$_2$)] (**4-R**, R = Cy, Ph, Mes, NiPr$_2$). Ellipsoids are drawn at the 50% probability level; hydrogen atoms, solvent molecules and disorder in one of the N(iPr)$_2$ groups of **4-NiPr** are omitted for clarity. The crystal of **4-Mes** contained a second crystallographically independent molecule with very similar structural parameters; only one of these molecules is shown.

Table S9. Selected bond lengths (Å) and angles (°) of **4-R** (R = Cy, *t*Bu, Ph, Mes, N(*i*Pr)₂).

	4-Cy	**4-*t*Bu**	**4-Ph**	**4-Mes**[a]	**4-N*i*Pr**
P1−P2	2.1292(9)	2.1410(9)	2.1470(8)	2.139(1), 2.149(1)	2.140(1)
P1−P5	2.1504(8)	2.1596(8)	2.1346(7)	2.168(1), 2.170(1)	2.172(1)
P2−P3	2.147(1)	2.132(1)	2.1304(8)	2.126(2), 2.127(2)	2.136(1)
P3−P4	2.1197(9)	2.1394(9)	2.1395(7)	2.138(1), 2.144(1)	2.132(1)
P4−P5	2.1622(8)	2.1487(9)	2.1439(7)	2.182(1), 2.180 (1)	2.161(1)
Co1−P1	2.3682(7)	2.3687(7)	2.3583(5)	2.330(1), 2.316(1)	2.3749(9)
Co1−P2	2.3554(7)	2.3463(7)	2.3781(5)	2.395(1), 2.401(1)	2.3314(9)
Co1−P3	2.3243(6)	2.3236(7)	2.3313(6)	2.331(1), 2.332(1)	2.330(1)
Co1−P4	2.3811(7)	2.3928(7)	2.3836(6)	2.356(1), 2.358(1)	2.3813(9)
Co1−N1	1.876(2)	1.893(2)	1.888(2)	1.890(3), 1.886(3)	1.895(3)
Co1−N2	1.897(2)	1.896(2)	1.895(2)	1.907(3), 1.902(3)	1.900(3)
C1−N1	1.363(3)	1.360(3)	1.352(2)	1.356(5), 1.361(5)	1.357(4)
C2−N2	1.351(3)	1.360(3)	1.349(2)	1.351(5), 1.354(5)	1.362(4)
C1−C2	1.427(3)	1.427(3)	1.431(3)	1.428(6), 1.434(5)	1.422(4)
P1−P2−P3	105.58(4)	103.63(4)	105.84(3)	105.44(6), 104.96(6)	104.17(4)
P2−P3−P4	104.11(3)	105.11(4)	104.09(3)	102.05(5), 102.03(5)	103.40(5)
P3−P4−P5	98.60(4)	100.41(4)	100.49(3)	102.61(5),101.41(6)	98.97(4)
P4−P5−P1	97.34(3)	95.69(3)	98.60(3)	93.00(5), 92.57(5)	93.45(4)
P5−P1−P2	96.22(3)	100.63(3)	97.46(3)	97.87(5), 96.37(5)	97.74(4)

[a] Data for two crystallographically independent molecules.

Table S10. Crystallographic data and structure refinement of [K(18c-6)]**2** and [K(18c-6)]**3**.

	[K(18c-6)]**2**	[K(18c-6)]**3**
Empirical formula	$C_{50}H_{66}CoKN_2O_6P_4$	$C_{56}H_{68.5}CoKN_2O_{11.25}P_4W$
Formula weight / g·mol⁻¹	1012.95	1355.38
Temperature / K	122.9(2)	122.9(2)
Crystal system	monoclinic	monoclinic
Space group	$P2_1/m$	$C2/c$
a / Å	11.4558(5)	85.6114(9)
b / Å	19.7132(8)	13.0589(2)
c / Å	12.1033(5)	22.4458(3)
α /°	90	90
β /°	107.690(5)	90.025(1)
γ/°	90	90
V / Å³	2604.0(2)	25094.2(6)
Z	2	16
ρ_{calc} / g cm⁻¹	1.292	1.435
μ / mm⁻¹	4.841	7.426
F(000)	1086.0	11016.0
Crystal size / mm³	0.149 × 0.107 × 0.065	0.826 × 0.410 × 0.092
Radiation / Å	CuK$_\alpha$ (λ = 1.54184)	CuK$_\alpha$ (λ = 1.54184)

2Θ range for data collection /°	7.666 – 147.46	6.848 – 149.356
Diffractometer	GV1000, TitanS2	GV1000, TitanS2
Index ranges	$-14 \leq h \leq 13$	$-105 \leq h \leq 105$
	$-23 \leq k \leq 20$	$-16 \leq k \leq 16$
	$-13 \leq l \leq 14$	$-25 \leq l \leq 27$
Reflections collected	13745	179882
Independent reflections	5180 [R_{int} = 0.0364, R_{sigma} = 0.0397]	25277 [R_{int} = 0.0902, R_{sigma} = 0.0395]
Data/restraints/parameters	5180/132/300	25277/2339/1897
Goodness-of-fit on F^2	1.086	1.059
Final R indexes [I>=2σ (I)]	R_1 = 0.0654, wR_2 = 0.1785	R_1 = 0.0907, wR_2 = 0.2446
Final R indexes [all data]	R_1 = 0.0788, wR_2 = 0.1936	R_1 = 0.0996, wR_2 = 0.2532
Largest diff. peak/hole / e Å^{-3}	0.86/−0.56	1.71/−1.47
CCDC	**1940064**	**1940071**

Table S11. Crystallographic data and structure refinement of **4-Cy** and **4-tBu**.

	4-Cy	**4-tBu**
Empirical formula	$C_{53}H_{71}CoN_2P_5$	$C_{46}H_{60}CoN_2P_5$
Formula weight / g·mol^{-1}	949.89	854.74
Temperature / K	123.0(1)	123.0(1)
Crystal system	triclinic	monoclinic
Space group	$P\bar{1}$	$P2_1/n$
a / Å	11.1012(3)	17.1176(4)
b / Å	12.3491(5)	13.3206(3)
c / Å	20.9843(6)	20.6203(5)
α /°	89.104(3)	90
β /°	77.308(2)	110.948(3)
γ/°	63.865(3)	90
V / Å^3	2508.7(2)	4391.0(2)
Z	2	4
ρ_{calc} / g cm^{-1}	1.258	1.293
μ / mm^{-1}	4.461	5.039
F(000)	1010.0	1808.0
Crystal size / mm^3	$0.236 \times 0.089 \times 0.054$	$0.488 \times 0.353 \times 0.256$
Radiation / Å	CuK$_\alpha$ (λ = 1.54184)	CuK$_\alpha$ (λ = 1.54184)
2Θ range for data collection /°	8.01 – 147.532	8.07 – 148.386
Diffractometer	Agilent Technologies SuperNova	Agilent Technologies SuperNova
Index ranges	$-13 \leq h \leq 13$	$-20 \leq h \leq 21$
	$-13 \leq k \leq 15$	$-15 \leq k \leq 16$

	$-26 \leq 1 \leq 26$	$-25 \leq 1 \leq 18$
Reflections collected	39218	16674
Independent reflections	9887 [R_{int} = 0.0841, R_{sigma} = 0.0626]	8536 [R_{int} = 0.0425, R_{sigma} = 0.0540]
Data/restraints/parameters	9887/0/559	8536/0/501
Goodness-of-fit on F^2	1.030	1.046
Final R indexes [I>=2σ (I)]	R_1 = 0.0446, wR_2 = 0.1071	R_1 = 0.0531, wR_2 = 0.1350
Final R indexes [all data]	R_1 = 0.0533, wR_2 = 0.1142	R_1 = 0.0585, wR_2 = 0.1399
Largest diff. peak/hole / e Å^{-3}	0.66/−0.76	0.94/−0.89
CCDC	**1940072**	**1940073**

Table S12. Crystallographic data and structure refinement of **4-Ph** and **4-Mes**.

	4-Ph	**4-Mes**
Empirical formula	$C_{50}H_{52}CoN_2P_5$	$C_{59}H_{71}CoN_2P_5$
Formula weight / g·mol^{-1}	894.71	102.95
Temperature / K	123.0(1)	123.0(1)
Crystal system	monoclinic	triclinic
Space group	$P2_1/c$	$P\overline{1}$
a / Å	9.5803(2)	12.3113(3)
b / Å	22.1061(3)	12.9350(4)
c / Å	21.9485(3)	34.0646(9)
α /°	90	91.131(2
β /°	101.585(2)	93.275(2)
γ/°	90	97.108(2
V / Å^3	4553.6(1)	5372.2(3)
Z	4	4
ρ_{calc} / g cm^{-1}	1.305	1.264
μ / mm^{-1}	4.891	4.207
F(000)	1872.0	2164.0
Crystal size / mm^3	0.585 × 0.134 × 0.111	0.219 × 0.109 × 0.058
Radiation / Å	CuK$_α$ (λ = 1.54184)	CuK$_α$ (λ = 1.54184)
2Θ range for data collection /°	7.998 – 133.898	6.89 – 147.328
Diffractometer	Agilent Technologies SuperNova	Agilent Technologies SuperNova
Index ranges	$-11 \leq h \leq 11$ $-21 \leq k \leq 26$ $-25 \leq 1 \leq 26$	$-15 \leq h \leq 15$ $-16 \leq k \leq 16$ $-41 \leq 1 \leq 42$
Reflections collected	43994	21072
Independent reflections	8019 [R_{int} = 0.0649, R_{sigma} = 0.0377]	20172 [R_{int} = N/A, R_{sigma} = 0.0814]
Data/restraints/parameters	8019/0/531	21072/132/1265
Goodness-of-fit on F^2	1.017	1.093
Final R indexes [I>=2σ (I)]	R_1 = 0.0350, wR_2 = 0.0862	R_1 = 0.0609, wR_2 = 0.1495

Final R indexes [all data]	$R_1 = 0.0395$, $wR_2 = 0.0894$	$R_1 = 0.0753$, $wR_2 = 0.1574$
Largest diff. peak/hole / e Å⁻³	0.53/−0.43	0.60/−0.51
CCDC	**1940065**	**1940066**

Table S13. Crystallographic data and structure refinement of **4-N*i*Pr** and [K(18c-6)]**5**.

	4-N*i*Pr	[K(18c-6)]**5**
Empirical formula	$C_{50}H_{70}CoN_4P_5$	$C_{65}H_{82}CoKN_3O_6P_3$
Formula weight / g·mol⁻¹	940.88	1192.27
Temperature / K	123.0(1)	123.0(1)
Crystal system	monoclinic	Orthorhombic
Space group	*P2₁/c*	*Pbca*
a / Å	11.9652(2)	23.3457(3)
b / Å	20.9023(4)	22.1786(3)
c / Å	20.0633(4)	24.2379(3)
α /°	90	90
β /°	98.110(2)	90
γ /°	90	90
V / Å³	4967.7(2)	12549.8(3)
Z	4	8
ρ_{calc} / g cm⁻¹	1.258	1.262
µ / mm⁻¹	4.512	3.868
F(000)	2000.0	5056.0
Crystal size / mm³	0.246 × 0.163 × 0.044	0.523 × 0.272 × 0.158
Radiation / Å	CuK$_\alpha$ ($\lambda = 1.54184$)	CuK$_\alpha$ ($\lambda = 1.54184$)
2Θ range for data collection /°	7.464 – 147.92	6.596 – 147.908
Diffractometer	Agilent Technologies SuperNova	Agilent Technologies SuperNova
Index ranges	−14 ≤ h ≤ 13	−28 ≤ h ≤ 10
	−25 ≤ k ≤ 23	−26 ≤ k ≤ 19
	−23 ≤ l ≤ 24	−30 ≤ l ≤ 26
Reflections collected	31182	28077
Independent reflections	9854 [$R_{int} = 0.1025$, $R_{sigma} = 0.0968$]	12229 [$R_{int} = 0.0320$, $R_{sigma} = 0.0373$]
Data/restraints/parameters	9854/21/568	12229/6/750
Goodness-of-fit on F²	0.999	1.019
Final R indexes [I>=2σ (I)]	$R_1 = 0.0626$, $wR_2 = 0.1544$	$R_1 = 0.0364$, $wR_2 = 0.0842$
Final R indexes [all data]	$R_1 = 0.0818$, $wR_2 = 0.1751$	$R_1 = 0.0464$, $wR_2 = 0.0893$
Largest diff. peak/hole / e Å⁻³	0.77/−1.09	0.52/−0.45
CCDC	**1940069**	**1940070**

Table S14. Crystallographic data and structure refinement of [K(18c-6)]**6-*t*Bu** and [Et₄N]**7**.

	[K(18c-6)]**6-*t*Bu**	[Et₄N]**7**
Empirical formula	$C_{21}H_{42}KNO_6P_2$	$C_{62}H_{84}CoN_4P_5$
Formula weight / g·mol⁻¹	505.59	1135.14
Temperature / K	123.0(1)	123.0(1)
Crystal system	monoclinic	monoclinic
Space group	$P2_1/n$	$P2_1/n$
a / Å	16.6663(4)	18.6344(5)
b / Å	8.1532(2)	18.3344(3)
c / Å	21.7285(5)	21.3813(7)
α /°	90	90
β /°	112.545(3)	107.065(3)
γ/°	90	90
V / Å³	2726.9(1)	6983.3(3)
Z	4	4
ρ_{calc} / g cm⁻¹	1.232	1.080
μ / mm⁻¹	3.091	3.287
F(000)	1088.0	2416.0
Crystal size / mm³	$0.402 \times 0.319 \times 0.228$	$0.205 \times 0.162 \times 0.096$
Radiation / Å	CuK$_\alpha$ (λ = 1.54184)	CuK$_\alpha$ (λ = 1.54184)
2Θ range for data collection /°	8.474 – 147.294	6.918 – 148.858
Diffractometer	Agilent Technologies SuperNova	Agilent Technologies SuperNova
Index ranges	$-20 \leq h \leq 19$	$-21 \leq h \leq 23$
	$-9 \leq k \leq 9$	$-22 \leq k \leq 18$
	$-22 \leq l \leq 26$	$-25 \leq l \leq 26$
Reflections collected	9240	50550
Independent reflections	5256 [R_{int} = 0.0128, R_{sigma} = 0.0159]	13811 [R_{int} = 0.0684, R_{sigma} = 0.0621]
Data/restraints/parameters	5256/0/286	13811/0/694
Goodness-of-fit on F²	1.016	1.016
Final R indexes [I>=2σ (I)]	R_1 = 0.0237, wR_2 = 0.0616	R_1 = 0.0524, wR_2 = 0.1280
Final R indexes [all data]	R_1 = 0.0245, wR_2 = 0.0621	R_1 = 0.0771, wR_2 = 0.1420
Largest diff. peak/hole / e Å⁻³	0.24/−0.19	0.64/−0.35
CCDC	**1940068**	**1940067**

3.4.8   Quantum Chemical Calculations

3.4.8.1 Methods

Geometry optimization, frequency analysis, calculation of chemical shifts and NICS(0) values were carried out with the ORCA program package.[46] Geometry optimization for [(PHDI)Co(η^4-P$_4$)]$^-$ Anion (**2**) and [tBu$_2$P(PCN)]$^-$ anion (**6-tBu**) were performed at the OPBE-D3BJ/def2-TZVP[47–50], respectively BP86[51]-D3BJ/def2-TZVP with the auxiliary basis set def2/J[52] level of theory in gas phase. Frequency analysis were carried out to confirm the nature of stationary points found out by geometry optimizations. To save computational cost, all isopropyl groups were replaced by methyl groups. Calculation of chemical shifts and NICS(0)[53] values were performed at the OPBE-D3BJ/def2-TZVP level of theory in gas phase. NBO analysis and natural resonance analysis (NRT) was done with NBO6 program[54] implemented in Gaussian with BP86/def2-TZVP and B3LYP[55]/6-31G+∗.[56]

3.4.8.2 Results and Discussion

Density functional theory (DFT) studies at the OPBE/def2-TZVP[47–49] level of theory gave further insight into the nature of the *cyclo*-P$_4$ unit in anion **2**. The optimized model compound with *i*Pr substituted by Me features a square planar *cyclo*-P$_4$ ligand and P−P distances (2.148-2.152 Å) close to the crystallographically determined mean value of the *cyclo*-P$_4$ unit in anion **3** (2.147(7) Å). The aromaticity of the *cyclo*-P$_4$ ligand was investigated by nucleus independent chemical shift (NICS) DFT calculations.[53] In comparison to the NICS(0) values of aromatic species (benzene = 8.2, cyclobutadiene-diide = 10.7) and the anti-aromatic free P$_4^{2-}$ (−5.0),[12,57] the calculated NICS(0) value for complex **2** (9.4) indicates a substantial aromatic character. Similar observations were also reported by *Mézailles* for the P$_4^{2-}$ ligand in [(PhP(CH$_2$CH$_2$PCy$_2$)$_2$)Fe(η^4-P$_4$)].[12]

The molecular orbitals were visualized using GaussView 5.0[58] and shown with an isovalue = 0.05. The fully occupied orbitals with the highest energy are the orbitals **148**-**153**. Here, especially **148** (3d$_{z^2}$, and 3d$_{x^2-y^2}$), **150** (3d$_{xy}$), and **153 (HOMO)** (3d$_{z^2}$, and 3d$_{xy}$) exhibit a high d-orbital character. Therefore, a d^6-configuration can be concluded. Orbitals **149** and **151** show the lone pairs of the phosphorus unit. Orbital **152** represents the bonding interaction between the PHDI ligand and cobalt. By contrast, the unoccupied orbitals **154**, and **155** show antibonding character.

148 (occu.: 2.000, 51% $3d_{z^2}$, 16% $3d_{x^2-y^2}$, 18% $3d_{xz}$)

149 (occu.: 2.000)

150 (occu.: 2.000, 40% $3d_{xy}$)

151 (occu.: 2.000)

152 (occu.: 2.000)

153 (occu.: 2.000, 63% $3d_{x^2-y^2}$, 15% $3d_{xz}$, 4% $3d_{z^2}$)

154 (occu.: 0.000, 19% $3d_{xz}$, 7% $3d_{z^2}$))

155 (occu.: 0.000, 29% $3d_{yz}$)
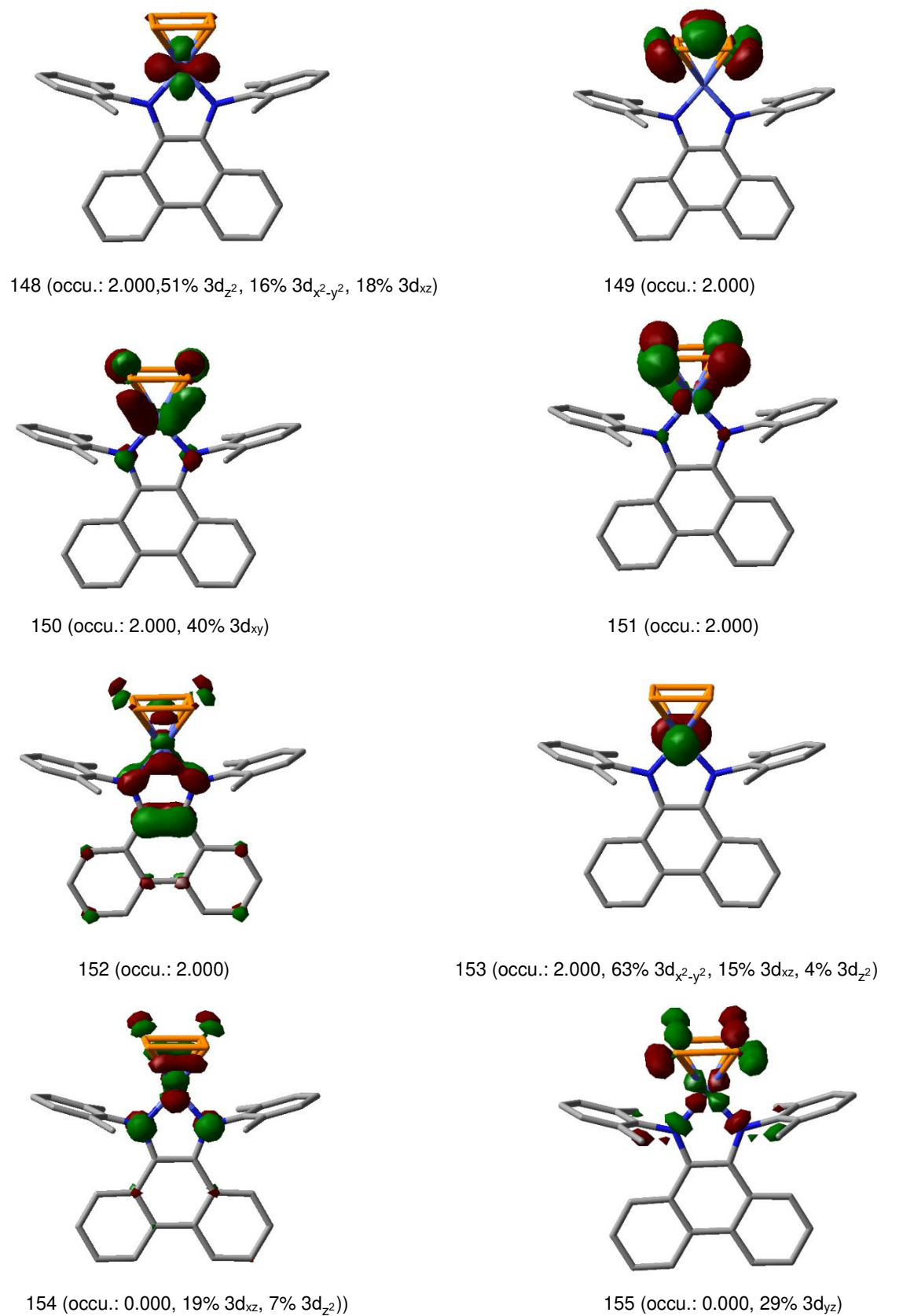
Figure S61. Molecular orbitals of the model compound [(Bis-(2,6-dimethylphenyl)-PHDI)Co(η^4-P$_4$)]$^-$ (c.f. **2**).

Table S15. Calculation of NICS(0) values.

Compound	NICS value	Character
Benzene C_6H_6	8.1	aromatic
Cyclobutadiene dianion $[C_4H_4]^{2-}$	10.4	aromatic
Tetraphosphacylobutadiene dianion $[P_4]^{2-}$	-4.7	anti-aromatic
DippPhDiCoP4	5.1	aromatic

Cartesian Coordinates for optimized structures

$[(Bis\text{-}(2,6\text{-}dimethylphenyl)\text{-}PHDI)Co(\eta^4\text{-}P_4)]^-$
(c.f. **2**)

Co	8.242792	4.917323	6.448956
P	7.710657	3.827674	4.524113
P	9.765875	3.836645	5.149448
N	7.829322	6.124645	7.755468
N	7.848255	3.713006	7.766403
P	9.759175	5.988608	5.136060
P	7.704552	5.978815	4.509396
C	7.464767	5.633789	8.959481
C	7.931926	7.484056	7.436808
C	7.475977	4.210742	8.966144
C	7.967163	2.351827	7.461862
C	7.098358	6.372989	10.136357
C	9.156445	8.140973	7.633359
C	6.819128	8.151034	6.901822
C	7.122239	3.477607	10.150874
C	9.200899	1.712656	7.659693
C	6.860525	1.665027	6.939374
C	7.072280	7.784156	10.183069
C	6.745250	5.653370	11.317618
C	9.257712	9.478023	7.258642
C	10.273266	7.404776	8.285378
C	6.960606	9.488136	6.539577
C	5.522026	7.428183	6.803822
C	7.119186	2.066767	10.212672
C	6.754937	4.203390	11.324170
C	9.317299	0.372853	7.299389
C	10.310929	2.468938	8.300275
C	7.017306	0.325912	6.591131
C	5.553442	2.369962	6.841084
H	7.337975	8.346012	9.299308

C	6.718410	8.469046	11.325670
C	6.391206	6.386447	12.463474
H	10.205862	9.994067	7.404161
C	8.171076	10.151381	6.710633
H	10.395983	6.432018	7.795664
H	6.102778	10.012358	6.120270
H	5.691272	6.446698	6.347155
H	7.395841	1.500088	9.335431
C	6.774176	1.387983	11.361604
C	6.408093	3.476531	12.476168
H	10.272527	-0.129676	7.445934
C	8.236819	-0.320072	6.763741
H	10.412229	3.442886	7.808392
H	6.164202	-0.213623	6.181735
H	5.707792	3.350029	6.376140
H	6.712317	9.557979	11.315456
C	6.373368	7.766599	12.483537
H	6.123296	5.858207	13.372594
H	8.267603	11.195485	6.416630
H	6.785989	0.299051	11.362673
C	6.411926	2.096532	12.510404
H	6.122372	4.009649	13.376967
H	8.345391	-1.365957	6.480469
H	6.092940	8.295187	13.393284
H	6.136533	1.572913	13.424556
H	4.835009	1.792561	6.252552
H	5.139427	2.543980	7.842293
H	11.255035	1.921337	8.231952
H	10.081832	2.658757	9.356475
H	4.798262	7.991520	6.208247
H	5.106100	7.256001	7.804593
H	10.037363	7.211026	9.339264
H	11.208548	7.968281	8.225713

Benzene C_6H_6

C	0.43000000	-1.32420000	0.00000000
C	1.36200000	-0.28970000	0.00000000
C	0.93200000	1.03450000	0.00000000
C	-0.43010000	1.32420000	0.00000000
C	-1.36200000	0.28970000	0.00000000
C	-0.93190000	-1.03460000	0.00000000
H	0.76490000	-2.35560000	0.00000000

H	2.42260000	-0.51570000	0.00000000
H	1.65770000	1.84030000	0.00000000
H	-0.76490000	2.35560000	0.00000000
H	-2.42260000	0.51560000	0.00000000
H	-1.65770000	-1.84020000	0.00000000

Tetraphosphacyclobutadiene dianion [P$_4$]$^{2-}$

P	-1.15940000	-0.99320000	0.00000000
P	0.99320000	-1.15940000	0.00000000
P	1.15940000	0.99320000	0.00000000
P	-0.99320000	1.15940000	0.00000000

Cyclobutadiene dianion [C$_4$H$_4$]$^{2-}$

C	0.73346300	0.73516400	-0.13584900
C	-0.73166700	0.73619000	0.13516100
C	-0.73331800	-0.73472600	0.13517600
C	0.73202100	-0.73672500	-0.13589100
H	-1.48320600	1.37215200	-0.39917800
H	-1.48677400	-1.36895900	-0.39932000
H	1.48225600	-1.37006000	0.40361900
H	1.48472400	1.36744400	0.40329600

[tBu$_2$P(PCN)]$^-$ (**6-tBu**)

P	-2.25025125563347	1.46192671541032	0.06975734399337
C	-1.48249263244720	2.17594792112246	-1.56153685577599
C	-1.48455801945431	2.42267082026686	1.55794906878339
P	-1.23987848344326	-0.46937869109669	0.34141605861631
C	-2.59131770451527	-1.45482890997712	-0.21938482498852
N	-3.42604970455938	-2.20287040093651	-0.58899826090662
C	-0.00890814923408	2.12996732136812	1.86030248655075
H	0.28850104598841	2.63184716430472	2.80029976826424
H	0.15366163529273	1.04908909600116	1.98500043077861
H	0.65625491822376	2.48697258893101	1.06415267995063
C	-2.32680274775500	1.94512485151463	2.75570272629607
H	-1.97601957428218	2.43592865827684	3.68194320869485
H	-3.39081336451527	2.18570375538604	2.61252911737995
H	-2.23750794117528	0.85520452483224	2.87278103511947
C	-1.68447024536416	3.93477806673562	1.39282391754249
H	-2.71809862051692	4.17335619021589	1.09902122557876
H	-1.47377363019754	4.44789060262598	2.34896223934258
H	-1.00636025142037	4.35701216985181	0.63809689467336
C	0.03978647055547	2.32052627655447	-1.56855263549650
H	0.40353547699629	2.54213205364143	-2.58959894627844
H	0.37794640056983	3.13780513320780	-0.91484395660917
H	0.50912971229198	1.38184548094550	-1.23447331094343
C	-2.16097534408618	3.50889528083265	-1.91222769787168
H	-1.85220039577094	4.32588780613163	-1.24719624440949
H	-1.90351356750635	3.80593909183214	-2.94559699835520
H	-3.25621946739542	3.41634314772173	-1.84843613425414
C	-1.88561511579211	1.14104853897979	-2.62499515855833
H	-2.97421889937842	0.97830770103936	-2.63220213298719
H	-1.57776192081769	1.49722751346534	-3.62481652358444
H	-1.40848810465767	0.17188779081476	-2.42172981054571

Natural theory analyses:

TOPO matrix for the leading resonance structure:

PCN unit: 4P 5C 6N

```
  Atom  1   2   3   4   5   6   7   8   9  10  11  12  13  14  15  16  17

       ---- --- --- --- --- --- --- --- --- --- --- --- --- --- --- --- ---
  1. P   1   1   1   1   0   0   0   0   0   0   0   0   0   0   0   0   0
  2. C   1   0   0   0   0   0   0   0   0   0   0   0   0   0   0   0   0
  3. C   1   0   0   0   0   0   1   0   0   0   1   0   0   0   1   0   0
  4. P   1   0   0   2   1   0   0   0   0   0   0   0   0   0   0   0   0
  5. C   0   0   0   1   0   3   0   0   0   0   0   0   0   0   0   0   0
  6. N   0   0   0   0   3   1   0   0   0   0   0   0   0   0   0   0   0
  7. C   0   0   1   0   0   0   0   1   1   1   0   0   0   0   0   0   0
  8. H   0   0   0   0   0   0   1   0   0   0   0   0   0   0   0   0   0
  9. H   0   0   0   0   0   0   1   0   0   0   0   0   0   0   0   0   0
 10. H   0   0   0   0   0   0   1   0   0   0   0   0   0   0   0   0   0
 11. C   0   0   1   0   0   0   0   0   0   0   0   1   1   1   0   0   0
 12. H   0   0   0   0   0   0   0   0   0   0   1   0   0   0   0   0   0
 13. H   0   0   0   0   0   0   0   0   0   0   1   0   0   0   0   0   0
 14. H   0   0   0   0   0   0   0   0   0   0   1   0   0   0   0   0   0
 15. C   0   0   1   0   0   0   0   0   0   0   0   0   0   0   0   1   1
 16. H   0   0   0   0   0   0   0   0   0   0   0   0   0   0   1   0   0
 17. H   0   0   0   0   0   0   0   0   0   0   0   0   0   0   1   0   0
 18. H   0   0   0   0   0   0   0   0   0   0   0   0   0   0   1   0   0
 19. C   0   1   0   0   0   0   0   0   0   0   0   0   0   0   0   0   0
 20. H   0   0   0   0   0   0   0   0   0   0   0   0   0   0   0   0   0
 21. H   0   0   0   0   0   0   0   0   0   0   0   0   0   0   0   0   0
 22. H   0   0   0   0   0   0   0   0   0   0   0   0   0   0   0   0   0
 23. C   0   1   0   0   0   0   0   0   0   0   0   0   0   0   0   0   0
 24. H   0   0   0   0   0   0   0   0   0   0   0   0   0   0   0   0   0
 25. H   0   0   0   0   0   0   0   0   0   0   0   0   0   0   0   0   0
 26. H   0   0   0   0   0   0   0   0   0   0   0   0   0   0   0   0   0
 27. C   0   1   0   0   0   0   0   0   0   0   0   0   0   0   0   0   0
 28. H   0   0   0   0   0   0   0   0   0   0   0   0   0   0   0   0   0
 29. H   0   0   0   0   0   0   0   0   0   0   0   0   0   0   0   0   0
 30. H   0   0   0   0   0   0   0   0   0   0   0   0   0   0   0   0   0


  Atom 18  19  20  21  22  23  24  25  26  27  28  29  30

       ---- --- --- --- --- --- --- --- --- --- --- --- ---
  1. P   0   0   0   0   0   0   0   0   0   0   0   0   0
  2. C   0   1   0   0   0   1   0   0   0   1   0   0   0
  3. C   0   0   0   0   0   0   0   0   0   0   0   0   0
  4. P   0   0   0   0   0   0   0   0   0   0   0   0   0
  5. C   0   0   0   0   0   0   0   0   0   0   0   0   0
  6. N   0   0   0   0   0   0   0   0   0   0   0   0   0
  7. C   0   0   0   0   0   0   0   0   0   0   0   0   0
  8. H   0   0   0   0   0   0   0   0   0   0   0   0   0
  9. H   0   0   0   0   0   0   0   0   0   0   0   0   0
 10. H   0   0   0   0   0   0   0   0   0   0   0   0   0
 11. C   0   0   0   0   0   0   0   0   0   0   0   0   0
 12. H   0   0   0   0   0   0   0   0   0   0   0   0   0
 13. H   0   0   0   0   0   0   0   0   0   0   0   0   0
 14. H   0   0   0   0   0   0   0   0   0   0   0   0   0
 15. C   1   0   0   0   0   0   0   0   0   0   0   0   0
```

```
16. H  0  0  0  0  0  0  0  0  0  0  0  0  0
17. H  0  0  0  0  0  0  0  0  0  0  0  0  0
18. H  0  0  0  0  0  0  0  0  0  0  0  0  0
19. C  0  0  1  1  1  0  0  0  0  0  0  0  0
20. H  0  1  0  0  0  0  0  0  0  0  0  0  0
21. H  0  1  0  0  0  0  0  0  0  0  0  0  0
22. H  0  1  0  0  0  0  0  0  0  0  0  0  0
23. C  0  0  0  0  0  0  1  1  1  0  0  0  0
24. H  0  0  0  0  0  1  0  0  0  0  0  0  0
25. H  0  0  0  0  0  1  0  0  0  0  0  0  0
26. H  0  0  0  0  0  1  0  0  0  0  0  0  0
27. C  0  0  0  0  0  0  0  0  0  0  1  1  1
28. H  0  0  0  0  0  0  0  0  0  1  0  0  0
29. H  0  0  0  0  0  0  0  0  0  1  0  0  0
30. H  0  0  0  0  0  0  0  0  0  1  0  0  0
```

```
        Resonance
   RS   Weight(%)          Added(Removed)
 -----------------------------------------------------------------------
   1*    68.81
   2*(2) 23.37   P  4- C  5, ( C  5- N  6), ( P  4),  N  6
   3     4.21   ( P  1- C  2),  P  1- P  4,  C  2, ( P  4)
   4     2.29   ( P  1- P  4),  P  4- C  5, ( C  5- N  6),  N  6
   5     1.31   ( P  4- C  5),  C  5- N  6,  P  4, ( N  6)
 -----------------------------------------------------------------------
       100.00   * Total *          [* = reference structure]
```

Summary of Natural Population Analysis:

		Natural Population			
	Natural	---			
Atom No	Charge	Core	Valence	Rydberg	Total
P 1	0.52853	9.99992	4.43056	0.04099	14.47147
C 2	-0.40171	1.99999	4.37938	0.02233	6.40171
C 3	-0.39640	1.99999	4.37514	0.02126	6.39640
P 4	-0.28387	9.99993	5.24593	0.03801	15.28387
C 5	-0.05061	2.00000	4.00045	0.05016	6.05061
N 6	-0.50036	2.00000	5.47046	0.02990	7.50036
C 7	-0.68031	2.00000	4.66779	0.01253	6.68031
H 8	0.21301	0.00000	0.78594	0.00105	0.78699
H 9	0.25577	0.00000	0.74314	0.00108	0.74423
H 10	0.22940	0.00000	0.76993	0.00066	0.77060
C 11	-0.68540	2.00000	4.67290	0.01251	6.68540
H 12	0.21311	0.00000	0.78596	0.00093	0.78689
H 13	0.23795	0.00000	0.76143	0.00062	0.76205
H 14	0.26053	0.00000	0.73778	0.00169	0.73947
C 15	-0.67318	2.00000	4.66141	0.01177	6.67318
H 16	0.23782	0.00000	0.76128	0.00090	0.76218
H 17	0.22022	0.00000	0.77869	0.00109	0.77978
H 18	0.22567	0.00000	0.77386	0.00047	0.77433
C 19	-0.67967	2.00000	4.66753	0.01215	6.67967
H 20	0.21577	0.00000	0.78310	0.00113	0.78423

H 21	0.21827	0.00000	0.78127	0.00046	0.78173
H 22	0.25453	0.00000	0.74384	0.00163	0.74547
C 23	-0.67488	2.00000	4.66285	0.01203	6.67488
H 24	0.22535	0.00000	0.77397	0.00068	0.77465
H 25	0.21758	0.00000	0.78131	0.00111	0.78242
H 26	0.24050	0.00000	0.75855	0.00095	0.75950
C 27	-0.68781	2.00000	4.67478	0.01303	6.68781
H 28	0.24469	0.00000	0.75459	0.00073	0.75531
H 29	0.21309	0.00000	0.78600	0.00091	0.78691
H 30	0.26240	0.00000	0.73614	0.00146	0.73760

===

* Total * -1.00000   39.99980   69.70597   0.29422   110.00000

3.5 References

[1] a) B. M. Cossairt, N. A. Piro, C. C. Cummins, *Chem. Rev.* **2010**, *110*, 4164–4177; b) M. Scheer, G. Balázs, A. Seitz, *Chem. Rev.* **2010**, *110*, 4236–4256; c) M. Caporali, L. Gonsalvi, A. Rossin, M. Peruzzini, *Chem. Rev.* **2010**, *110*, 4178–4235.

[2] a) A. Velian, C. C. Cummins, *Chem. Sci.* **2012**, *3*, 1003; b) P. Barbaro, A. Ienco, C. Mealli, M. Peruzzini, O. J. Scherer, G. Schmitt, F. Vizza, G. Wolmershäuser, *Chem. Eur. J.* **2003**, *9*, 5196–5210; c) S. Pelties, A. W. Ehlers, R. Wolf, *Chem. Comm.* **2016**, *52*, 6601–6604; d) E. Mädl, M. V. Butovskii, G. Balázs, E. V. Peresypkina, A. V. Virovets, M. Seidl, M. Scheer, *Angew. Chem. Int. Ed.* **2014**, *53*, 7643–7646, *Angew. Chem.* **2014**, *126*, 7774–7777; e) P. Barbaro, C. Bazzicalupi, M. Peruzzini, S. Seniori Costantini, P. Stoppioni, *Angew. Chem. Int. Ed.* **2012**, *51*, 8628–8631, *Angew. Chem.* **2012**, *124*, 8756–8759.

[3] G. Capozzi, L. Chiti, M. Di Vaira, M. Peruzzini, P. Stoppioni, *J. Chem. Soc., Chem. Commun.* **1986**, 1799–1800.

[4] B. M. Cossairt, M.-C. Diawara, C. C. Cummins, *Science* **2009**, *323*, 602.

[5] A. E. Seitz, M. Eckhardt, A. Erlebach, E. V. Peresypkina, M. Sierka, M. Scheer, *J. Am. Chem. Soc.* **2016**, *138*, 10433–10436.

[6] C. G. P. Ziegler, T. M. Maier, S. Pelties, C. Taube, F. Hennersdorf, A. W. Ehlers, J. J. Weigand, R. Wolf, *Chem. Sci.* **2019**, *10*, 1302–1308.

[7] Z. Li, J. E. Borger, F. Müller, J. R. Harmer, C.-Y. Su, H. Grützmacher, *Angew. Chem. Int. Ed.* **2019**, *58*, 11429–11433, *Angew. Chem.* **2019**, *131*, 11551–11555.

[8] S. Pelties, T. Maier, D. Herrmann, B. de Bruin, C. Rebreyend, S. Gärtner, I. G. Shenderovich, R. Wolf, *Chem. Eur. J.* **2017**, *23*, 6094–6102.

[9] F. Dielmann, A. Timoshkin, M. Piesch, G. Balázs, M. Scheer, *Angew. Chem. Int. Ed.* **2017**, *56*, 1671–1675, *Angew. Chem.* **2017**, *129*, 1693–1698.

[10] U. Chakraborty, J. Leitl, B. Mühldorf, M. Bodensteiner, S. Pelties, R. Wolf, *Dalton Trans.* **2018**, *47*, 3693–3697.

[11] P. Pyykkö, M. Atsumi, *Chem. Eur. J.* **2009**, *15*, 12770–12779.

[12] A. Cavaillé, N. Saffon-Merceron, N. Nebra, M. Fustier-Boutignon, N. Mézailles, *Angew. Chem. Int. Ed.* **2018**, *57*, 1874–1878, *Angew. Chem.* **2018**, *130*, 1892–1896.

[13] B. Gao, X. Luo, W. Gao, L. Huang, S.-m. Gao, X. Liu, Q. Wu, Y. Mu, *Dalton Trans.* **2012**, *41*, 2755–2763.

[14] a) N. A. Piro, C. C. Cummins, *J. Am. Chem. Soc.* **2008**, *130*, 9524–9535; b) C. Schwarzmaier, A. Noor, G. Glatz, M. Zabel, A. Y. Timoshkin, B. M. Cossairt, C. C. Cummins, R. Kempe, M. Scheer, *Angew. Chem. Int. Ed.* **2011**, *50*, 7283–7286, *Angew. Chem.* **2011**, *123*, 7421–7424.

[15] M. Di Vaira, M. P. Ehses, P. Stoppioni, M. Peruzzini, *Inorg. Chem.* **2000**, *39*, 2199–2205.

[16] a) A. E. Seitz, U. Vogel, M. Eberl, M. Eckhardt, G. Balázs, E. V. Peresypkina, M. Bodensteiner, M. Zabel, M. Scheer, *Chem. Eur. J.* **2017**, *23*, 10319–10327; b) M. Scheer, E. Leiner, P. Kramkowski, M. Schiffer, G. Baum, *Chem. Eur. J.* **1998**, *4*, 1917–1923; c) O. Kühl, *Phosphorus-31 NMR Spectroscopy*, *A Concise Introduction for the Synthetic Organic and Organometallic Chemist*, Springer-Verlag, Berlin Heidelberg, **2008**, pp. 21-22.

[17] a) K. A. Mandla, C. E. Moore, A. L. Rheingold, J. S. Figueroa, *Angew. Chem. Int. Ed.* **2019**, *58*, 1779–1783, *Angew. Chem.* **2019**, *131*, 1793–1797; b) O. J. Scherer, R. Winter, G. Wolmershuser, *Z. anorg. allg. Chem.* **1993**, *619*, 827–835; c) O. J. Scherer, J. Vondung, G. Wolmershäuser, *Angew. Chem. Int. Ed.* **1989**, *28*, 1355–1357, *Angew. Chem.* **1989**, *101*, 1395–1397; d) M. Herberhold, G. Frohmader, W. Milius, *J. Organomet. Chem.* **1996**, *522*, 185–196.

[18] M. H. Holthausen, S. K. Surmiak, P. Jerabek, G. Frenking, J. J. Weigand, *Angew. Chem. Int. Ed.* **2013**, *52*, 11078–11082, *Angew. Chem.* **2013**, *125*, 11284–11288.

[19] While this manuscript was under review, a related anionic complex (MeNHC)$_2$P][η^5-Cp^{tBu3}Co(η^3-P$_3$)] (MeNHC = 1,3,4,5-tetramethylimidazolin-2-ylidene) was published: M. Scheer, M. Piesch, S. Reichl, M. Seidl, G. Balázs **2019**, *Angew. Chem. Int. Ed.* DOI:10.1002/anie.201908397, *Angew. Chem.* DOI:10.1002/ange.201908397.

[20] C. Chan, A. E. Carpenter, M. Gembicky, C. E. Moore, A. L. Rheingold, J. S. Figueroa, *Organometallics* **2019**, *38*, 1436–1444.

[21] M. Di Vaira, L. Sacconi, P. Stoppioni, *J. Organomet. Chem.* **1983**, *250*, 183–195.

[22] W. W. Kramer, L. A. Cameron, R. A. Zarkesh, J. W. Ziller, A. F. Heyduk, *Inorg. Chem.* **2014**, *53*, 8825–8837.

[23] G. A. Abakumov, N. O. Druzhkov, T. N. Kocherova, K. A. Kozhanov, A. v. Murugova, E. N. Egorova, *Dokl. Chem.* **2016**, *467*, 109–112.

[24] R. van Belzen, R. A. Klein, H. Kooijman, N. Veldman, A. L. Spek, C. J. Elsevier, *Organometallics* **1998**, *17*, 1812–1825.

[25] R. van Belzen, R. A. Klein, W. J. J. Smeets, A. L. Spek, R. Benedix, C. J. Elsevier, *Recl. Trav. Chim. Pays-Bas* **1996**, *115*, 275–285.

[26] a) F. Cecconi, P. Dapporto, S. Midollini, L. Sacconi, *Inorg. Chem.* **1978**, *17*, 3292–3294; b) C. A. Ghilardi, S. Midollini, A. Orlandini, L. Sacconi, *Inorg. Chem.* **1980**, *19*, 301–306.

[27] a) P. Rigo, A. Turco, *Coord. Chem. Rev.* **1974**, *13*, 133–172; b) A survey in the Cambridge Cystal Structure Database (CCSD), version 5.39 update 4, 14/05/2019, revealed 96 cobalt complexes bearing only one terminal cyanide ligand with a mean Co–C distance of 1.900 Å (median 1.886 Å) and a mean C≡N distance of 1.134 Å (median 1.141 Å).

[28] W. S. Sheldrick, J. Kroner, F. Zwaschka, A. Schmidpeter, *Angew. Chem. Int. Ed.* **1979**, *18*, 934–935, *Angew. Chem.* **1979**, *91*, 998–1000.

[29] A. Schmidpeter, G. Burget, F. Zwaschka, W. S. Sheldrick, *Z. anorg. allg. Chem.* **1985**, *527*, 17–32.

[30] A. Schmidpeter, K.-H. Zirzow, G. Burget, G. Huttner, I. Jibril, *Chem. Ber.* **1984**, *117*, 1695–1706.

[31] a) S. Holand, F. Mathey, *Organometallics* **1988**, *7*, 1796–1801; b) A. Fischer, I. Neda, P. G. Jones, R. Schmutzler, *Phosphorus Sulfur Silicon Relat. Elem.* **1993**, *83*, 135–148; c) A. Vollbrecht, I. Neda, A. Fischer, P. G. Jones, R. Schmutzler, *Phosphorus Sulfur Silicon Relat. Elem.* **1995**, *107*, 69–78.

[32] S. Alidori, D. Heift, G. Santiso-Quinones, Z. Benkő, H. Grützmacher, M. Caporali, L. Gonsalvi, A. Rossin, M. Peruzzini, *Chem. Eur. J.* **2012**, *18*, 14805–14811.

[33] R. A. Bartlett, M. M. Olmstead, P. P. Power, G. A. Sigel, *Inorg. Chem.* **1987**, *26*, 1941–1946.

[34] a) M. Scheer, U. Becker, J. Magull, *Polyhedron* **1998**, *17*, 1983–1989; b) M. Scheer, M. Dargatz, P. G. Jones, *J. Organomet. Chem.* **1993**, *447*, 259–264.

[35] V. K. Cherkasov, N. O. Druzhkov, T. N. Kocherova, A. S. Shavyrin, G. K. Fukin, *Tetrahedron* **2012**, *68*, 1422–1426.

[36] P. Li, B. Lü, C. Fu, S. Ma, *Adv. Synth. Catal.* **2013**, *355*, 1255–1259.

[37] M. Fild, O. Stelzer, R. Schmutzler, G. O. Doak in *Inorganic Syntheses* (Eds.: A. Wold, J. K. Ruff), McGraw Hill, New York, **1973**, 4–9.

[38] K. Jonas, R. Mynott, C. Krüger, J. C. Sekutowski, Y.-H. Tsay, *Angew. Chem. Int. Ed. Engl.* **1976**, *15*, 767–768, *Angew. Chem.* **1976**, *88*, 808–809.

[39] H. H. Karsch, W. A. Herrmann, G. Brauer (Eds.) *Synthetic methods of organometallic and inorganic chemistry, / (Herrmann/Brauer). Ed. by Wolfgang A. Herrmann ; Vol. 3*, Thieme, Stuttgart, **1996**.

[40] *IvorySoft: gNMR for Windows*, *NMR Simulation Program,* P. H. M. Budzelaar, **2006**.

[41] a) S. Aime, R. K. Harris, E. M. McVicker, M. Fild, *J. Chem. Soc., Dalton Trans.* **1976**, 2144–2153; b) H. C. E. McFarlane, W. McFarlane, J. A. Nash, *J. Chem. Soc., Dalton Trans.* **1980**, 240–244; c) J. P. Albrand, H. Faucher, D. Gagnaire, J. B. Robert, *Chem. Phys. Lett.* **1976**, *38*, 521–523; d) J. E. Del Bene, J. Elguero, I. Alkorta, *J. Phys. Chem. A* **2004**, *108*, 3662–3667; e) E. G. Finer, R. K. Harris, *Mol. Phys.* **1967**, *13*, 65–75; f) M. A. M. Forgeron, M. Gee, R. E. Wasylishen, *J. Phys. Chem. A* **2004**, *108*, 4895–4908.

[42] a) SCALE3ABS, CrysAlisPro, Aglient Technologies Inc., Oxford, GB, 2012, b) G. M. Sheldrick, SADABS, Bruker AXS, Madison, USA, 2007.,

[43] R. C. Clark, J. S. Reid, *Acta Cryst. A* **1995**, *51*, 887–897.

[44] G. M. Sheldrick, *Acta Cryst. A* **2015**, *71*, 3–8.

[45] G. M. Sheldrick, *Acta Cryst. A* **2008**, *64*, 112–122.

[46] a) F. Neese, *WIREs Comput Mol Sci* **2012**, *2*, 73–78; b) F. Neese, *WIREs Comput Mol Sci* **2018**, *8*, e1327.

[47] M. Swart, A. W. Ehlers, K. Lammertsma, *Mol. Phys.* **2004**, *102*, 2467–2474.

[48] S. Grimme, S. Ehrlich, L. Goerigk, *J. Comp. Chem.* **2011**, *32*, 1456–1465.

[49] S. Grimme, J. Antony, S. Ehrlich, H. Krieg, *J. Chem. Phys.* **2010**, *132*, 154104.

[50] F. Weigend, R. Ahlrichs, *Phys. Chem. Chem. Phys.* **2005**, *7*, 3297–3305.

[51] A. D. Becke, *Phys. Rev. A* **1988**, *38*, 3098–3100.

[52] F. Weigend, *Phys. Chem. Chem. Phys.* **2006**, *8*, 1057–1065.

[53] Z. Chen, C. S. Wannere, C. Corminboeuf, R. Puchta, P. v. R. Schleyer, *Chem. Rev.* **2005**, *105*, 3842–3888.

[54] *NBO 6.0,* E. D. Glendening, J. K. Badenhoop, A. E. Reed, A. E. Carpenter, J. A. Bohmann, C. M. Morales, C. R. Landis, F. Weinhold, Theoretical Chemistry Institute, University of Wisconsin, Madison (WI), **2013**.

[55] A. D. Becke, *J. Chem. Phys* **1993**, *98*, 5648–5652.

[56] a) R. Ditchfield, W. J. Hehre, J. A. Pople, *J. Chem. Phys.* **1971**, *54*, 724–728; b) *Gaussian 09, Revision A.02,* M. J. Frisch, G. W. Trucks, H. B. Schlegel, G. E. Scuseria, M. A. Robb, J. R. Cheeseman, G. Scalmani, V. Barone, B. Mennucci, G. A. Petersson, Gaussian, Inc., Wallingford, CT, **2013**.

[57] J. O. C. Jiménez-Halla, E. Matito, J. Robles, M. Solà, *J. Organomet. Chem.* **2006**, *691*, 4359–4366.

[58] *GaussView,* R. Dennington, T. A. Keith, J. M. Millam, Semichem Inc., Shawnee Mission, KS, **2016**.

4   SYNTHESIS OF POLYPHOSPHIDO COBALT COMPLEXES USING A TETRAPHOSPHIDO COBALTATE PRECURSOR[a,b]

CHRISTIAN M. HOIDN, CLEMENS TAUBE, JAN J. WEIGAND, AND ROBERT WOLF
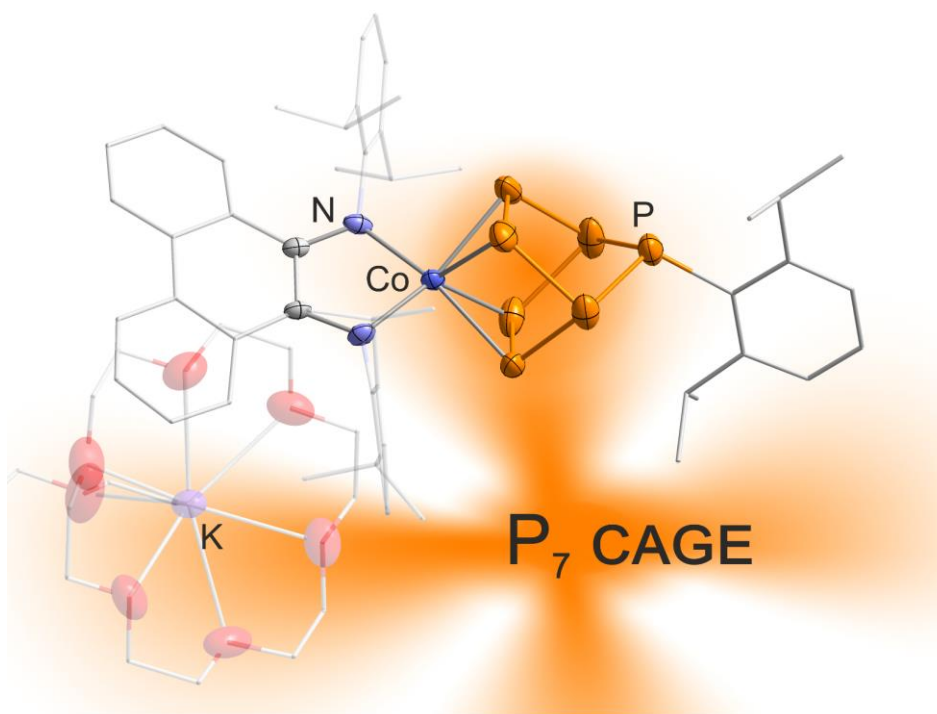
4.1   Introduction

Phosphorus possesses a pronounced tendency to form homoatomic frameworks, which is mostly explained by the diagonal relationship to carbon and the relative strength of the P−P single bond (200 kJ·mol^{-1}).[1] This feature is evident in the various different allotropes of elemental phosphorus and the existence of a variety of poly(cyclo)phosphanes. The pioneering work by *Baudler* and co-workers is particularly noteworthy, due to its pivotal contribution to the fundamental understanding of this compound class.[2–5] A selection of known polycyclophosphane frameworks is given in Figure 1. The most commonly observed cyclophosphane motifs consist of four, six, or seven phosphorus atoms (Figure 1a). By contrast, larger polyphosphane frameworks containing more than seven phosphorus atoms are rare (Figure 1b).
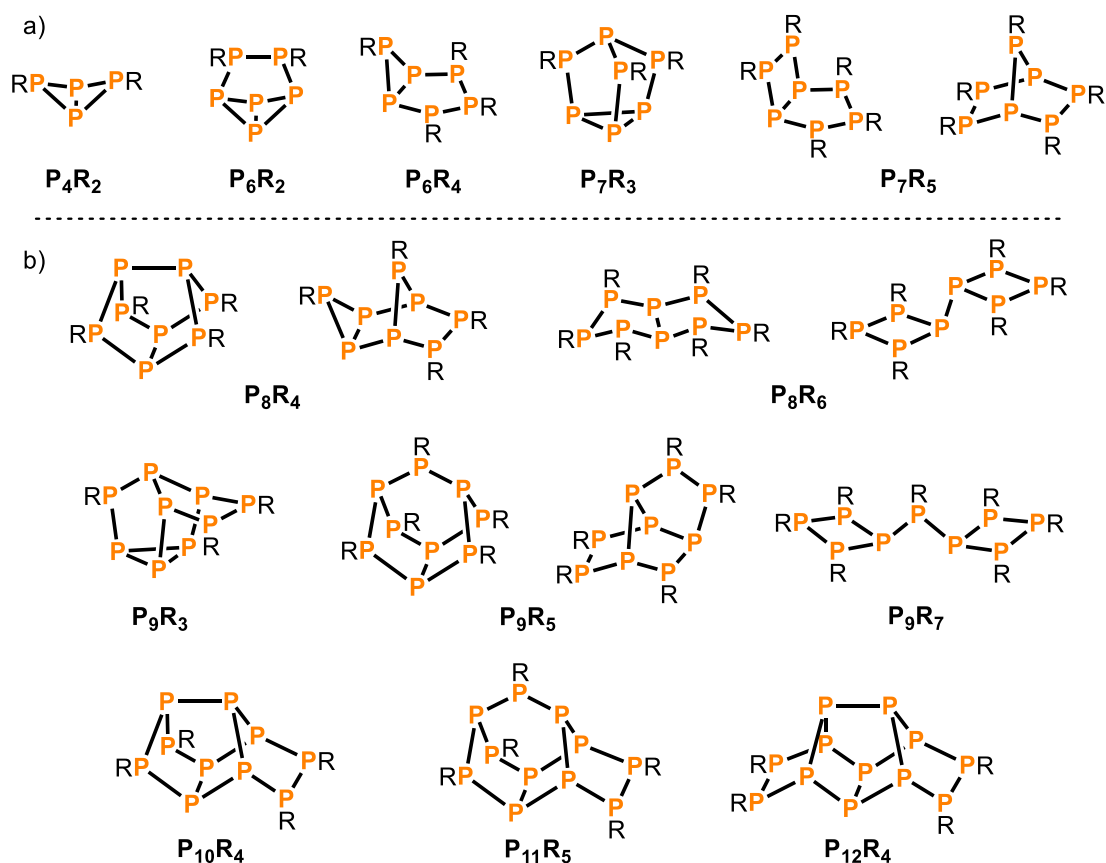
Figure 1. Selected examples of polycyclophosphane frameworks.

The traditional approach to the synthesis of polyphosphanes is the dehalogenation of chlorophosphanes in the presence of reducing agents such as magnesium or lithium aluminium hydride (Scheme 1a).[2,3] However, such methods often are very unselective, giving complicated and frequently inseparable product mixtures. The isolation of pure polyphosphanes from such reactions typically requires tedious work-up procedures

including column chromatography and fractional crystallization.[2–5] As a result, many of the polyphosphane motifs shown in Figure 1 have only been isolated in low yields. Fortunately, some alternative routes to polycyclophosphanes are also promising: for example, P−P bond formation by salt elimination reactions between alkali metal phosphanides and chlorophosphanes. Among other examples, this method has been used for the synthesis of LiP_9tBu_2 as shown in Scheme 1b.[6] P−N/P−H metathesis is another, fairly novel approach developed by *Weigand* and co-workers. This strategy is illustrated in Scheme 1c by the synthesis of a cationic heptaphosphane from a pyrazolyl-bridged diphosphorus trication and dicyclohexylphosphane.[7] Finally, *Bertrand* and co-workers have reported another, unusual method for the synthesis of polycyclophosphanes (Scheme 1d).[8] The reaction of *N*-heterocyclic carbenes (NHCs) with white phosphorus first leads to an opening of the P_4 tetrahedron. Subsequent aggregation processes can lead to polyphosphanes with a high nuclearity, such as $P_{12}R_2$ species.
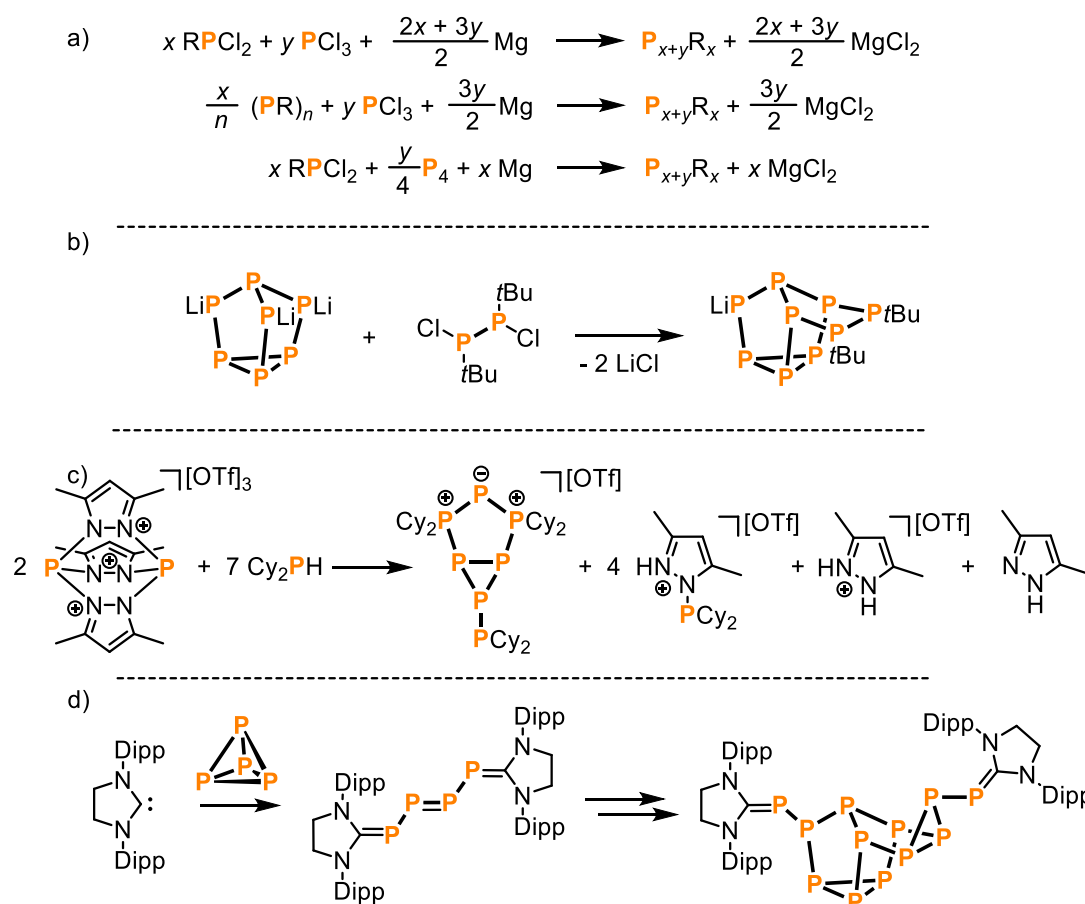
Scheme 1. Synthesis of polycyclophosphanes by: (a) dehalogenation of chlorophosphanes, (b) salt elimination, (c) P−N/P−H metathesis, and (d) P_4 aggregation with NHCs.

Related polycyclophosphide frameworks with up to 24 P atoms are accessible via the transition metal-mediated aggregation of white phosphorus (see the introduction of this

thesis, chapter 1, for an overview and Figure 2a for selected examples).[9] *Cummins* and co-workers obtained the diniobium complex **A**, which bears a remarkable P_8 cluster ligand, by reacting P_4 with a Nb(IV) precursor.[10] Another octaphosphido ligand was observed by *Roesky* and *Scheer* in the tetranuclear complexes **B**, synthesized by P_4 activation with either decamethylsamarocene or the Fe(I) β-diketiminato species [LFe(η^6-C_7H_8)] (L = CH[CMeN(2,6-Me$_2$C$_6$H$_3$)]$_2$).[11] The reaction of [(Cp'''Co)$_2$(η^4:η^4-C$_7$H$_8$)] (Cp''' = C$_5t$Bu$_3$H$_2$) with an excess of white phosphorus is unselective and gives several polycyclophosphido complexes including the impressive pentanuclear tetracosaphosphido complex **C**.[12] A different approach to polycyclophosphide species based on P-functionalization was demonstrated by *Scheer* and co-workers.[13] The reaction of the *cyclo*-P_5 compound [(C$_5$Me$_5$)Fe(P$_5$)] with the phosphorus nucleophile LiPH$_2$ afforded the dinuclear complex **D** bearing an extended HP$_{11}$ framework (Figure 2b).
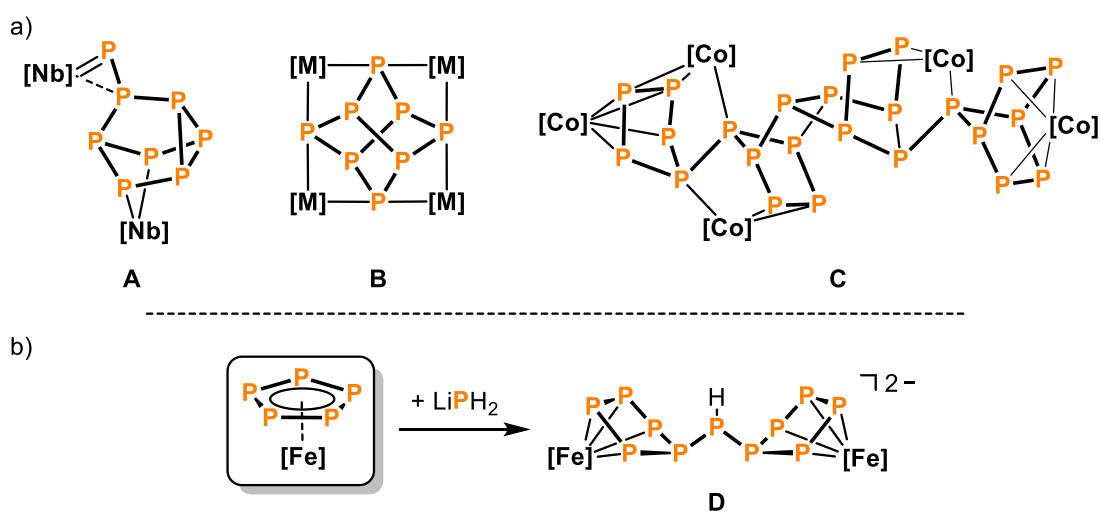
Figure 2. (a) Selected examples of polycyclophosphide ligands obtained by transition metal-mediated aggregation of P$_4$ and (b) functionalization of a *cyclo*-P$_5$ ligand with LiPH$_2$; [Nb] = [Nb(OR')$_3$] (OR' = (adamantane-2-ylidene)(mesityl)methanolate); [M] = [(C$_5$Me$_5$)$_2$Sm]; [Fe(L)] (L = CH[CMeN(2,6-Me$_2$C$_6$H$_3$)]$_2$); [Co] = [C$_5$H$_2t$Bu$_3$]; [Fe] = [(C$_5$Me$_5$)Fe].

We now present a new synthesis leading to polyphosphido complexes which is based on the reaction of nucleophilic *cyclo*-P_4 cobaltate **1** with the inversely polarized phosphaalkene **2**.[14] The reaction affords a mixture of unusual products including an anionic bicyclo[2.2.1]heptaphosphide compound **3** and a hexaphosphido complex **5**.

4.2   Results and Discussion

4.2.1   Reaction of [K(18c-6)][(PHDI)Co(η^4-*cyclo*-P$_4$)] with (^{Cl}Im^{Dipp})PP(Cl)Dipp

As shown in the preceding chapter of this thesis, the *cyclo*-P$_4$ cobalt compound [K(18c-6)][(PHDI)Co(η^4-*cyclo*-P$_4$)] (**1**, 18c-6 = 18-crown-6, PHDI = bis(2,6-diisopropylphenyl)-phenanthrene-9,10-diimine) is an excellent precursor for the construction of pentaphosphido complexes upon reaction with diorganochlorophosphanes. Intending to synthesize extended polyphosphorus frameworks, **1** was reacted with the P$_2$ species (^{Cl}Im^{Dipp})PP(Cl)Dipp (**2**, ^{Cl}Im^{Dipp} = *N,N'*-bis(2,6-diisopropylphenyl)-4,5-dichloroimidazolin-2-ylidene)[14] in toluene at room temperature (Scheme 2).
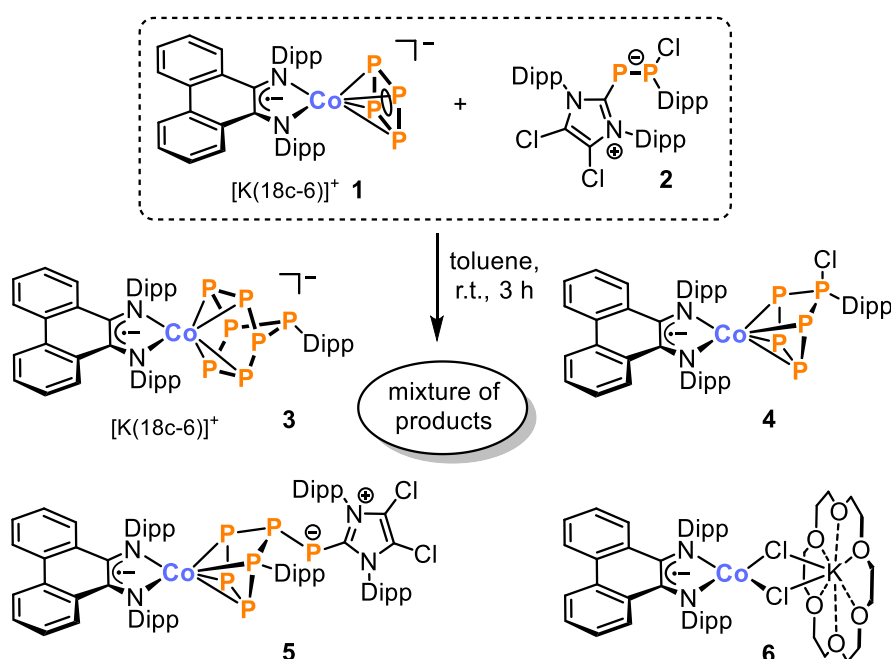
Scheme 2. Reaction of [K(18c-6)][(PHDI)Co(η^4-*cyclo*-P$_4$)] (**1**) with (^{Cl}Im^{Dipp})PP(Cl)Dipp (**2**)[14] resulting in a product mixture (18c-6 = 18-crown-6; PHDI = bis(2,6-diisopropylphenyl)phenanthrene-9,10-diimine; ^{Cl}Im^{Dipp} = *N,N'*-bis(2,6-diisopropylphenyl)-4,5-dichloroimidazolin-2-ylidene).

According to the ^{31}P{^{1}H} NMR spectrum of the reaction mixture (Figure 3), the reaction reaches completion within three hours and leads to the formation of several products. The major phosphorus containing species (marked with red circles in Figure 3) is the anionic heptaphosphido cobalt complex [K(18c-6)][(PHDI)Co(η^4-P$_7$Dipp] (**3**) featuring an AMM′XX′YY′ spin system with higher order multiplets at 101, −37, −64 and −131 ppm. The composition of **3** was confirmed by XRD analysis performed on crystals obtained by diffusion of Et$_2$O into a concentrated toluene extract (*vide supra*). Analogous NMR data

have been observed for related substituted heptaphosphido complexes such as [K(2,2,2-crypt)]$_2$[Fe(HP$_7$)$_2$][15] and [K(2,2,2-crypt)]$_2$[(RP$_7$)M(CO)$_3$] (M = Cr, R = H and M = W, R = H, Me, Et, nBu, CH$_2$Ph, SnCy$_3$).[16] It should be noted that the previously identified dinuclear $cyclo$-P$_4$ compound [{(PHDI)Co}$_2$(μ,η^4:η^4-P$_4$)] (262 ppm)[17] and the cation [(^{Cl}Im^{Dipp})P(Dipp)Cl]$^+$ (51 ppm) are minor by-products. [14] The latter species is a known decomposition product during the synthesis of **2**.
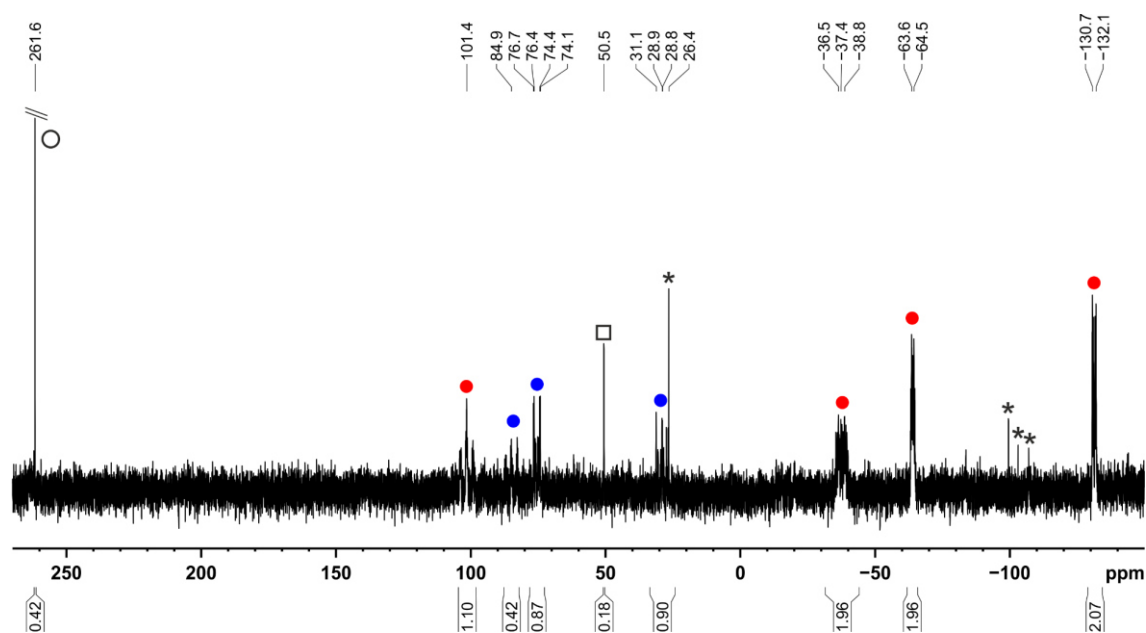
Figure 3. ^{31}P{^{1}H} NMR spectrum in toluene (C$_6$D$_6$-capillary) of the reaction mixture; ● AMM'XX'YY' spin system assigned to **3**; ● ABB'MM' spin system likely assignable to a $cyclo$-P$_5$ species; ○ [{(PHDI)Co}$_2$(μ,η^4:η^4-P$_4$)],[17] □ [(^{Cl}Im^{Dipp})P(Dipp)Cl]$^+$;[14] * minor unknown impurities and/or by-products.

The presence of an additional, new polyphosphorus species is evidenced by a second set of higher order multiplets at 85, 75 and 29 ppm in the ^{31}P{^{1}H} NMR spectrum (ABB'MM' spin system, marked with blue circles in Figure 3). These resonances, which have a lower intensity than those of the main product **3**, and are similar to those found for mononuclear $cyclo$-P$_5$R$_2$ complexes, e.g. [(^{Mes}BIAN)Co($cyclo$-P$_5$R$_2$)] (R = iPr, Cy, tBu, BIAN = 1,2-bis(arylimino)acenaphthene),[18] [(PHDI)Co($cyclo$-P$_5$R$_2$)] (R = Cy, tBu, Ph, Mes, N(iPr)$_2$; see Chapter 3) and [(C$_5$Me$_5$)Fe($cyclo$-P$_5$R)]$^-$ (R = CH$_2$SiMe$_3$, NMe$_2$).[19] The ^{31}P NMR data thus suggest the formation of a related complex [(PHDI)Co($cyclo$-P$_5$(Dipp)Cl)] (**4**), which is the expected product of the insertion of an intermediate [DippPCl]$^+$ fragment into the $cyclo$-P$_4$ ring of **1**. In addition, it should be mentioned that the resonance observed at +29 ppm and assigned to the MM' part of the ABB'MM' spin system is drastically downfield-shifted compared to the corresponding signal of analogous $cyclo$-P$_5$R$_2$

compounds (c.f. −158 ppm in [(PHDI)Co(*cyclo*-P₅Ph₂]; see Chapter 3). Further data supporting the formation of **4** could not be obtained so far.

In an attempt to separate **3** and **4**, the crude reaction mixture was evaporated to dryness and successively extracted with *n*-pentane, *n*-hexane, Et₂O and toluene. Dark blue single crystals were obtained from the *n*-pentane extract. XRD analysis of which revealed the additional formation of the neutral hexaphosphido complex [(PHDI)Co{η⁴-*cyclo*-P₅Dipp(P(ᶜˡImᴰⁱᵖᵖ))}] (**5**, *vide supra*), which is the expected product of a straightforward salt elimination reaction (Scheme 2). Unfortunately, no reliable NMR spectroscopic data of **5** could yet be recorded due to the low quantity of material obtained.

The ¹H NMR spectra of the fractions obtained by extraction with non-polar solvents (e.g. *n*-pentane, *n*-hexane, Et₂O) showed broad signals ranging from −25.3 to 83.6 ppm (Figure 4, top), which indicate the presence of a further, paramagnetic product. In fact, dark/green brown crystals were obtained from the *n*-hexane extracts. Weak diffraction prevented the measurement of a reliable XRD data set so far. Nevertheless, a preliminary data collection ("What is this experiment" supplied by CrysAlis Pro version 39.35c)
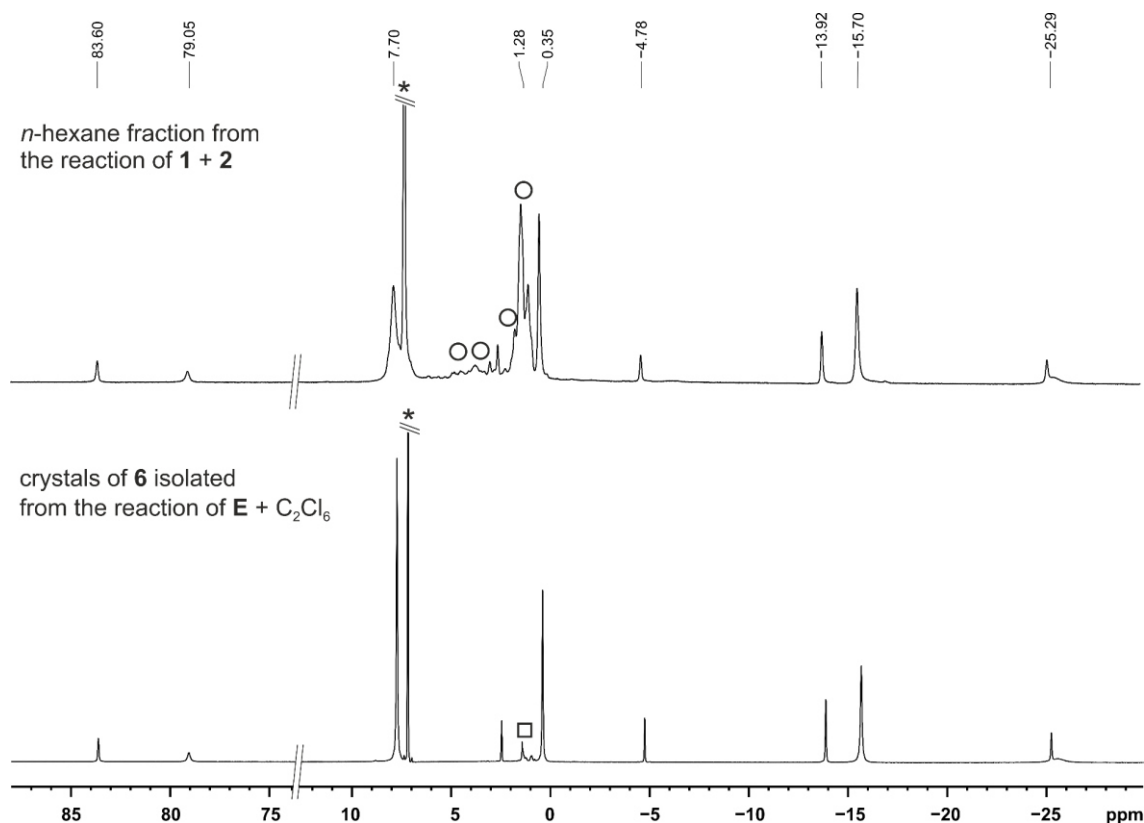
Figure 4. ¹H NMR spectra in C₆D₆ of the *n*-hexane extract from the reaction of [K(18c-6)][(PHDI)Co(P₄)] (**1**) with (ᶜˡImᴰⁱᵖᵖ)PP(Cl)Dipp (**2**, top) and of the isolated crystals obtained from the reaction of [K(18c-6)(thf)₂][(PHDI)Co(η⁴-1,5-cod)] (**E**) with C₂Cl₆ (bottom); □ cyclohexane, * C₆D₆, ○ unknown impurities and/or by-products.

revealed a dichlorido cobaltate species [{K(18c-6)}(μ-Cl)$_2${Co(PHDI)}] (**6**) as a paramagnetic by-product. A structurally very closely related β-diketiminato Fe(II) complex [{K(18c-6)}(μ-Cl)$_2${Fe(nacnac)}] (nacnac = CMe[CMeN(2,6-Me$_2$C$_6$H$_3$)]$_2$)[20] and similar paramagnetic lithium cobaltates(II) of the type [{Li(L$_2$)}(μ-Cl)$_2${Co(nacnac)}] (L = thf, Et$_2$O); nacnac = CH[CMeN(2,6-Me$_2$C$_6$H$_3$)]$_2$, CH[CMeN(Mes)]$_2$, CH[CMeN(Dipp)]$_2$, CH[C*t*BuN(Dipp)]$_2$) have been reported by *Holland*, *Power* and *Hannedouche*.[21]

Since attempts to separate **6** from the reaction mixture as a pure compound on a preparative scale were unsuccessful so far, **6** was synthesized independently as shown in Scheme 3. The reaction of [K(18c-6)(thf)$_2$][(PHDI)Co(η^4-1,5-cod)] (**E**) with one equivalent of C$_2$Cl$_6$ in THF-*d$_8$* immediately affords a dark brown reaction mixture. Brown crystals of **6** were obtained in 25% yield by diffusion of cyclohexane into a concentrated benzene solution. The ^{1}H NMR spectrum of the isolated crystals (Figure 4, bottom) shows an identical set of signals to those found in the reaction mixture of **1** and **2**. These data therefore confirm that the same paramagnetic molecule **6** is formed in both reactions.
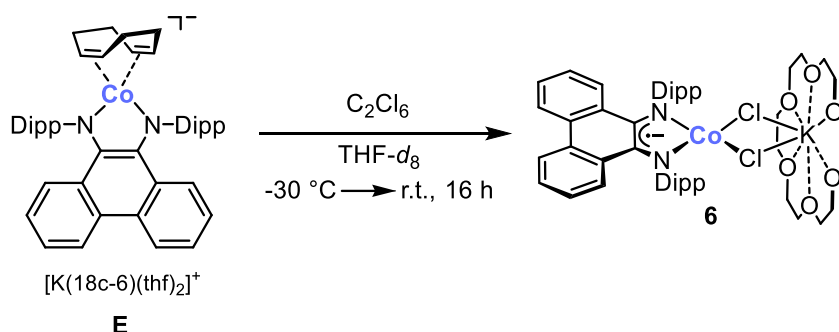
Scheme 3. Synthesis of [K(18c-6)][(PHDI)CoCl$_2$] (**6**) by oxidation of [K(18c-6)(thf)$_2$][(PHDI)Co(η^4-1,5-cod)] (**E**) with hexachloroethane.

In summary, the reaction of **1** with **2** is very unselective, probably due to different competing reaction pathways lead to a mixture of products (Scheme 4). The following pathway for the formation of the hexaphosphido complex **5** can be proposed: Initially, the reaction of **1** with **2** forms the imidazoliumyl-substituted diphosphene cation [(Dipp)P=P(^{Cl}Im^{Dipp})]$^+$ via elimination of [K(18c-6)Cl]. This cation is known to be formed upon reaction of **2** with chloride abstractors such as GaCl$_3$.[22] Next, the electrophilic, Dipp-substituted phosphorus atom inserts into the nucleophlic *cyclo*-P$_4$ unit of **1** to give compound **5′** (Scheme 4, path a). A subsequent 1,2 shift of the Dipp moiety then ultimately affords the hexaphosphido ligand observed in **5**. As the ^{31}P{^{1}H} NMR spectrum of the reaction mixture does not show the signals for an ABCDEF spin system

expected for **5** and only a few crystals of **5** were obtained, path (a) presumably plays only a minor role in the reaction.
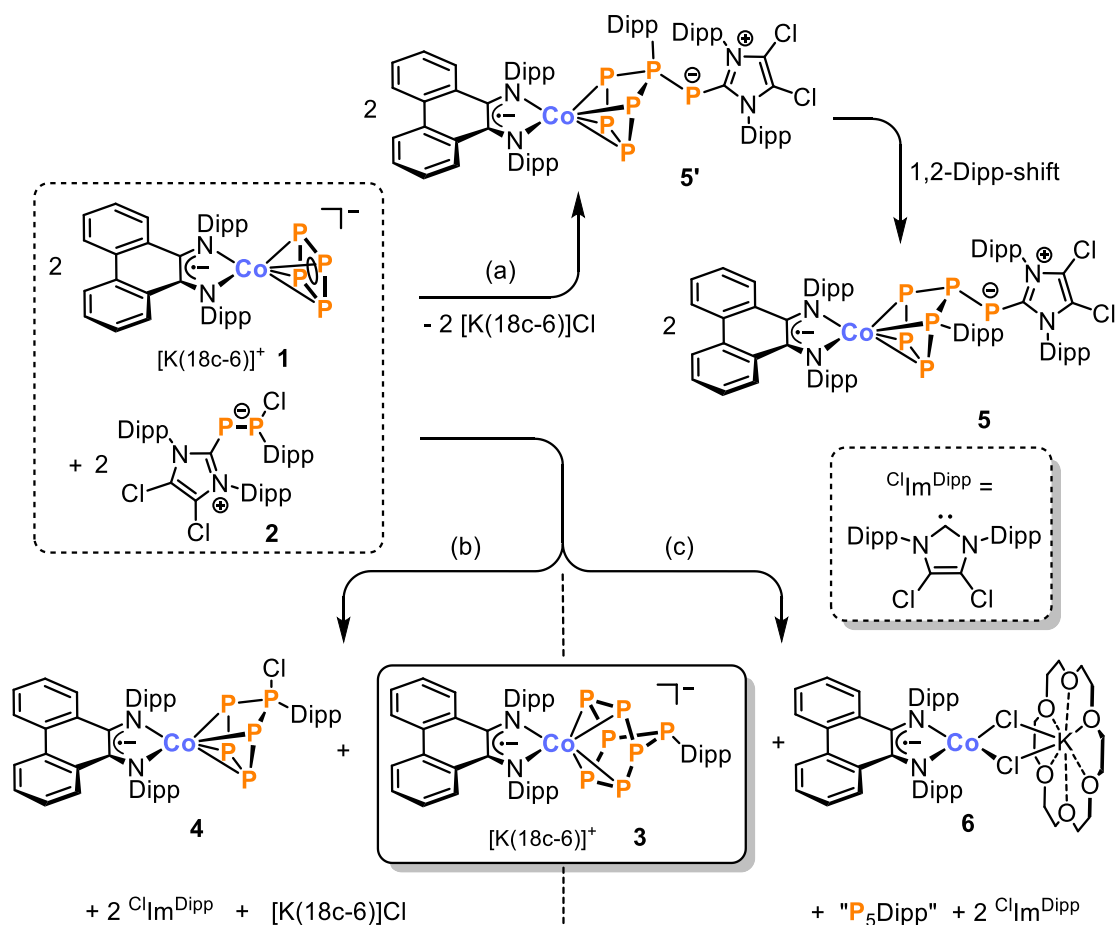
Scheme 4. Proposed synthetic pathways that lead to the formation of the detected products ($^{Cl}Im^{Dipp}$ = *N,N'*-bis(2,6-diisopropylphenyl)-4,5-dichloro-imidazolin-2-ylidene).

According to the $^{31}P\{^1H\}$ NMR spectrum of the reaction mixture, the main product is the heptaphosphido complex **3**. Based on the experimental data, two different pathways can be postulated that lead to the formation of **3** (Scheme 4). Following path (b), the reaction affords **3** and the pentaphosphido cobalt complex **4**, which could possibly give rise to the observed ABB′MM′ spin system in the $^{31}P\{^1H\}$ NMR spectrum (marked with blue circles in Figure 3). In this case, [K(18c-6)]Cl and two carbene molecules $^{Cl}Im^{Dipp}$ are the residual stoichiometric by-products. Path (c) involves the formation of **3** along with the paramagnetic dichlorido cobaltate **6**, which was identified by XRD analysis and its characteristic set of ^1H NMR signals. The fate of the missing "P$_5$Dipp" fragment remains presently unclear. It is tempting to speculate that "P$_5$Dipp" forms a carbene adduct with $^{Cl}Im^{Dipp}$. Indeed, the ABB′MM′ spin system found in the $^{31}P\{^1H\}$ NMR of the reaction mixture (Figure 3, marked blue and currently assigned to structure **4**) might alternatively

arise from such a molecule. The structural identity of the species corresponding to this spin system is therefore unclear.

4.2.2   Crystallographic Characterization of [K(18c-6)][(PHDI)Co(η^4-P$_7$Dipp] (3)

Green brown plates suitable for X-ray crystallography were obtained by diffusion of Et$_2$O into a saturated toluene solution of **3**. The solid-state molecular structure shows a [K(18c-6)(Et$_2$O)]$^+$ cation separated from a [(PHDI)Co(η^4-P$_7$Dipp)]$^-$ anion (Figure 5).
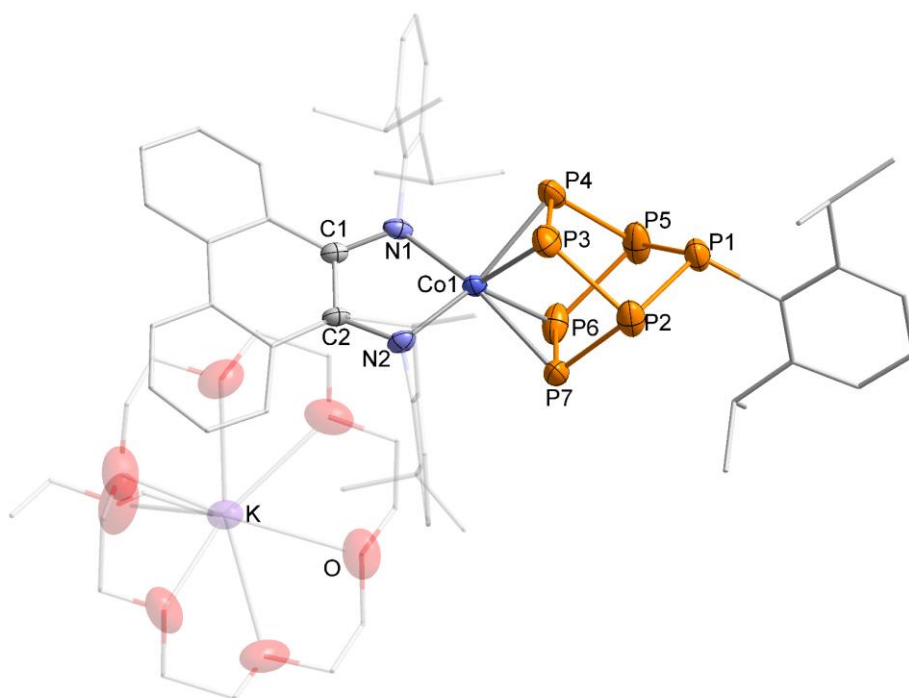
Figure 5. Displacement ellipsoid (40%) drawing of the heptaphosphido complex **3**. The hydrogen atoms are not shown for clarity. Selected bond lengths [Å]: Co1–N1 1.922(5), Co1–N2 1.910(5), Co1–P3 2.330(2), Co1–P4 2.337(2), Co1–P6 2.328(2), Co1–P7 2.335(2), P1–P2 2.159(3), P1–P5 2.154(3), P2–P3 2.211(3), P2–P7 2.209(3), P3–P4 2.140(3), P4–P5 2.193(4), P5–P6 2.224(3), P6–P7 2.115(3), C1–N1 1.358(8), C2–N2 1.362(8), C1–C2 1.433(8).

The cobalt atom is coordinated by the bidentate PHDI ligand, which is present in its radical anionic form according to the C−N (1.358(8), 1.368(8) Å) and C−C (1.433(8) Å) bond lengths in its backbone.[23] The second ligand is an η^4-coordinated 7-2,6-diisopropylphenyl-bicyclo[2.2.1]heptaphospha-2,5-diene cluster with P−P distances varying from 2.115(3) to 2.224(3) Å. Similar heptaphosphanorborna-2,5-diene ligands have been structurally elucidated in a few other complex anions, e.g. *Goicoechea*'s [Fe(HP$_7$)$_2$]$^{2-}$ and *Eichhorn*'s [(RP$_7$)W(CO)$_3$]$^{2-}$ (R = H, Et, SnCy$_3$). However, these compounds were obtained by attack of electrophiles at the heptaphosphido clusters

originally derived from Zintl P_7^{3-} anions. By contrast, **3** is synthesized by a completely different "bottom up" approach, and is, to the best of our knowledge, the first cobalt complex bearing a substituted RP_7^{2-} ligand. In good agreement with the reported bond parameters for other RP_7^{2-} ligands, the P−P distances between the metal coordinating phosphorus atoms (P3−P4 2.140(3) Å, P6−P7 2.115(3) Å) are somewhat shortened indicating a partial double bond character (c.f. calculated P−P single (2.22 Å) and P=P double bonds (2.04 Å)).[24]

4.2.3 Crystallographic Characterization of [(PHDI)Co{η^4-*cyclo*-P_5Dipp(P(^{Cl}Im^{Dipp}))}] (5)

Dark blue blocks of **5** suitable for XRD analysis were obtained from a concentrated *n*-pentane solution. The solid-state molecular structure shows a central cobalt atom coordinated by a hexaphosphido ligand in an η^4-fashion and a formally radical anionic PHDI$^{•-}$ ligand according to the C−N (1.338(2), 1.344(2) Å) and C−C (1.446(2) Å) distances in its backbone (Figure 6).[23] The hexaphosphido ligand features an aryl-substituted *cyclo*-P_5Dipp moiety bound to cobalt via its DippP1−P2−P3−P4 subunit. The P5 atom at the tip of the P_5 envelope points away from the metal center and is further connected to the two-coordinate phosphorus atom P6, which is stabilized by the NHC ^{Cl}Im^{Dipp}. The P6−C51 distance (1.777(2) Å) is in between the values calculated for P−C
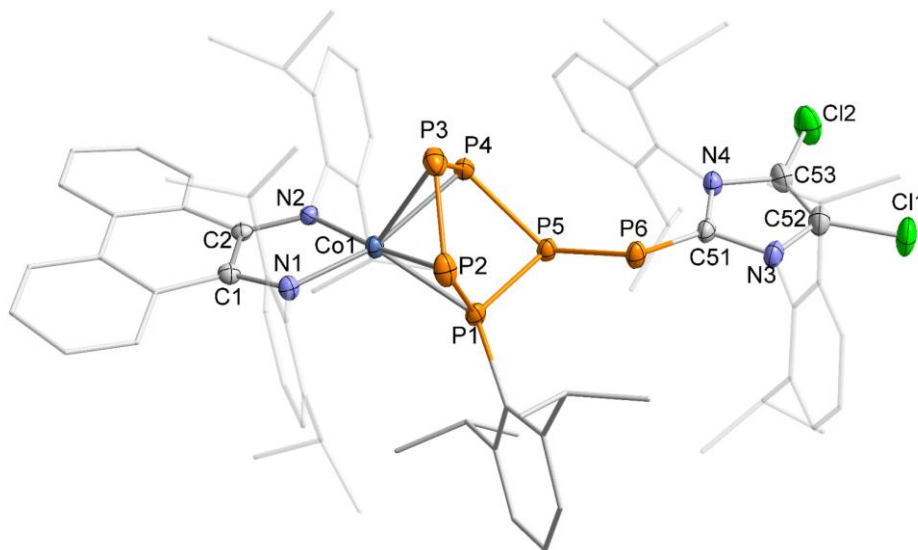
Figure 6. Displacement ellipsoid (40%) drawing of the hexaphosphido complex **6**. The hydrogen atoms and solvent molecules are not shown for clarity. Selected bond lengths [Å] and angles [°]: Co1−N1 1.931(2), Co1−N2 1.903(2), Co1−P1 2.3021(5), Co1−P2 2.3766(5), Co1−P3 2.3488(6), Co1−P4 2.3861(5), P1−P2 2.1510(7), P1−P5 2.1483(6), P2−P3 2.1160(8), P3−P4 2.1348(7), P4−P5 2.2410(6), P5−P6 2.1632(6), P6−C51 1.777(2) C1−N1 1.338(2), C2−N2 1.344(2), C1−C2 1.446(2), C51−N3 1.379(2), C51−N4 1.375(2), P1−P2−P3 98.14(3), P1−P5−P4 82.15(2), P1−P5−P6 97.68(2), P2−P3−P4 102.53(3), P3−P4−P5 110.50(3), P4−P5−P6 118.94(2), C51−P6−P5 102.92(6).

single (1.86 Å) and P=C double bonds (1.69 Å),[24] and is comparable to other NHC stabilized low coordinate phosphorus species such as *Arduengo*'s (IMes)PPh (1.763(6) Å, IMes = *N,N′*-bis(2,4,6-trimethylphenyl)-imidazolin-2-ylidene)[25] and *Robinson*'s (IMes)PP(IMes) (1.754(3) Å).[26] Analogously, the bonding at P6–^{Cl}Im^{Dipp} can be described by either a zwitterionic imidazolium phosphanide (**5a**) or a phosphaalkene resonance structure (**5b**, Figure 7a). The doubly-substituted *cyclo*-P$_5$ ligand in **5** is reminiscent of the related heterobimetallic species [(^{Mes}BIAN)Co(μ-η^4:η^1-P$_5t$Bu)GaCl(nacnac)] (**F**, Figure 7b, nacnac = CH(CMeNDipp)$_2$), which is obtained from the reaction of [K(dme)$_2${(^{Mes}BIAN)Co(μ-η^4:η^2-P$_4$)Ga(nacnac)}] with *t*BuCl$_2$.[18] Analogously to **F**, except for the P4−P5 bond (2.2410(6) Å), all other P−P distances (2.1160(8) to 2.1632(6) Å) are in a very close range. The shortening of these bonds with respect to a typical P–P single bond (2.22 Å)[24] may indicate some delocalized multiple bond character.
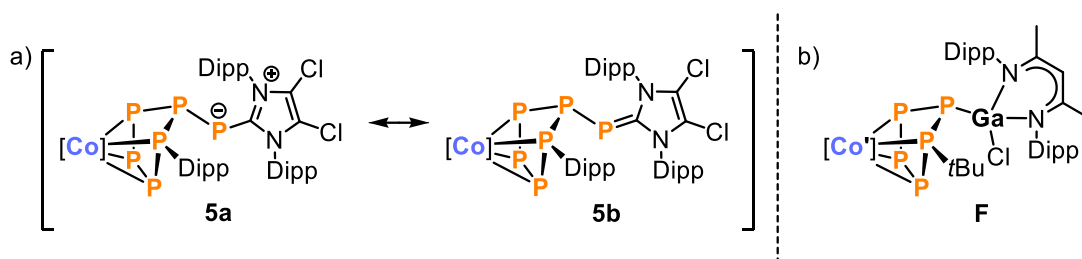
Figure 7. (a) Conceivable resonance structures describing the bonding within the hexaphosphido ligand in **5**; [Co] = [(PHDI)Co]; (b) related disubstituted *cyclo*-P$_5$ complex **F**;[18] [Co'] = [(^{Mes}BIAN)Co], (BIAN = 1,2-bis(arylimino)acenaphthene).

4.3   Conclusion

The reaction of $[K(18c\text{-}6)][(PHDI)Co(\eta^4\text{-}cyclo\text{-}P_4)]$ (**1**) with the inversely polarized phosphaalkene $(^{Cl}Im^{Dipp})PP(Cl)Dipp$ (**2**) leads to several products. The unprecedented hexaphosphido complex $[(PHDI)Co\{\eta^4\text{-}cyclo\text{-}P_5Dipp(P(^{Cl}Im^{Dipp}))\}]$ (**5**) was isolated from *n*-pentane extracts of the reaction, while an anionic heptaphosphido complex $[K(18c\text{-}6)][(PHDI)Co(\eta^4\text{-}P_7Dipp)]$ (**3**) was obtained from the toluene extracts. The latter compound appears to be the major product, and its formation is accompanied by the paramagnetic dichlorido cobaltate complex $[\{K(18c\text{-}6)\}(\mu\text{-}Cl)_2\{Co(PHDI)\}]$ (**6**), which was synthesized independently by oxidation of $[K(18c\text{-}6)(thf)_2][(PHDI)Co(\eta^4\text{-}1,5\text{-}cod)]$ (**E**) with C_2Cl_6. Compounds **3**, **5** and **6** have yet to be isolated as pure compounds, and have therefore not yet been fully characterized by elemental analysis, UV/Vis and NMR spectroscopy. Moreover, an EPR spectrum and the solution effective magnetic moment (Evans Method)[27] should be measured for paramagnetic **6**. Further experiments, including $^{31}P\{^1H\}$ NMR spectroscopic monitoring of the reaction, might give more insight into the mechanism of the formation of **3**. Nevertheless, the preliminary results reported in this chapter demonstrate that even larger polycyclopolyphosphane clusters can be synthesized by reaction of anionic polyphosphido complexes such as **2** with suitable polyphosphorus cations.

4.4   Supporting Information

4.4.1   General Procedures

All experiments were performed under an atmosphere of dry argon, by using standard Schlenk and glovebox techniques. Solvents were purified, dried, and degassed using an MBraun SPS800 solvent purification system. NMR spectra were recorded on Bruker Avance 400 spectrometer at 300 K and internally referenced to residual solvent resonances. $^{31}P\{^1H\}$ and ^{31}P NMR spectra were referenced externally to 85% $H_3PO_{4(aq.)}$. The starting materials $[K(18c-6)][(PHDI)Co(\eta^4\text{-}cyclo\text{-}P_4)]$ and $[K(18c-6)(thf)_2][(PHDI)Co(\eta^4\text{-}1,5\text{-}cod)]$ were prepared according to procedures presented earlier in this thesis. $(^{Cl}Im^{Dipp})PP(Cl)Dipp$ was prepared according to a literature procedure.[14] C_2Cl_6 was purchased from Sigma Aldrich.

4.4.2   Synthesis and Characterization

4.4.2.1 Synthesis of $[K(18c-6)][(PHDI)Co(\eta^4\text{-}P_7Dipp)]$ (3)

A deep yellow solution of **2** (34 mg, 0.047 mmol, 1.0 equiv.) in toluene (2 mL) was added dropwise to a dark turquoise suspension of **1** (49 mg, 0.047 mmol, 1.0 equiv.) in 2 mL toluene at room temperature. The resulting mixture was stirred for 16 h and a color change to dark green was observed. The solvent was removed *in vacuo*. The dark green residue was washed with Et$_2$O (25 x 1 mL) and extracted into toluene (10 x 1 mL). The dark green extracts were filtered, concentrated to ca. 5 mL, and layered with Et$_2$O (10 mL). Numerous small crystals formed over 10 days, which were isolated and washed quickly with Et$_2$O (1 mL). Yield: 2 mg (7%).

Melting point, elemental analysis, UV/vis and $^{13}C\{^1H\}$ NMR spectra were not obtained due to the low yield.

^{1}H NMR (400.30 MHz, 300 K, THF-d_8, in ppm): δ = 0.53 (d, $^3J_{HH}$ = 6.8 Hz, 12H, −CH(C*H*$_3$)$_2$ of Dipp), 0.94 (d, $^3J_{HH}$ = 6.8 Hz, 12H, −CH(C*H*$_3$)$_2$ of Dipp), 1.55 (d, $^3J_{HH}$ = 6.8 Hz, 12H, −CH(C*H*$_3$)$_2$ of Dipp), 2.51-2.57 (m, 2H, −C*H*(CH$_3$)$_2$ of P−Dipp), 3.61 (s, 24H, 18c-6), 3.73 (sept, $^3J_{HH}$ = 6.8 Hz, 4H, −C*H*(CH$_3$)$_2$ of N−Dipp), 6.58-6.63 (m, 2H, Ar−H), 6.80 (d, $^3J_{HH}$ = 7.7 Hz, 2H, Ar−H), 6.97 (t,

$^3J_{HH}$ = 7.6 Hz, 1H, C^4−H of P−Dipp), 7.03 (d, $^3J_{HH}$ = 8.9 Hz, 2H, Ar−H), 7.12-7.19 (m, 4H, Ar−H), 7.25-7.34 (m, 6H, Ar−H), 8.16 (d, $^3J_{HH}$ = 7.8 Hz, 2H, Ar−H). **^{31}P{^{1}H} NMR** (162.04 MHz, 300 K, THF-d_8, AMM′XX′YY′ spin system): δ / ppm = −129.5 - −128.2 (m, 2P, $P_{YY'}$), −65.1 - −63.5 (m, 2P, $P_{XX'}$), −42.4 - −37.6 (m, 2P, $P_{MM'}$), 97.6 (t, 1P, P_A).

4.4.2.2 Synthesis of [(PHDI)Co{η^4-*cyclo*-P$_5$Dipp(P(^{Cl}Im^{Dipp}))}] (5)

A deep yellow solution of **2** (28 mg, 0.039 mmol, 1.0 equiv.) in toluene (2 mL) was added dropwise to a dark turquoise suspension of **1** (40 mg, 0.039 mmol, 1.0 equiv.) in 2 mL toluene at room temperature. The mixture was stirred for 3 h and a color change to dark green was observed. The solvent was removed *in vacuo*. The dark green residue was extracted into *n*-pentane (10 x 1 mL). The resulting dark blue extracts were filtered, concentrated to ca. 4 mL, and stored at −30 °C. After one week a few small crystals were isolated and subjected to XRD analysis. The yield was not determined and further analysis was not performed due to the low quantity of product.

4.4.2.3 Synthesis of [{K(18c-6)}(μ-Cl)$_2${Co(PHDI)}] (6)
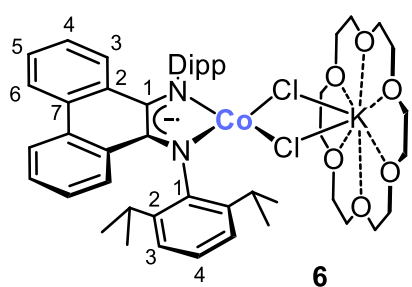
Solid C$_2$Cl$_6$ (2 mg, 0.008 mmol, 1.0 equiv.) was added to a dark green solution of [K(18c-6)(thf)$_2$][(PHDI)Co(η^4-1,5-cod)] (10 mg, 0.009 mmol, 1.0 equiv.) in THF-d_8 (1 mL) at −30 °C. An immediate color change to dark brown occurred, and the mixture was stirred for 18 h. The solvent was removed *in vacuo* and the dark brown residue was extracted into benzene (2 x 0.5 mL). The dark brown extracts were filtered and diffused with cyclohexane (ca. 2 mL). Small dark brown crystals formed over three weeks, which were isolated and washed with *n*-hexane (1 mL). Yield: 2 mg (25%).

Melting point, elemental analysis, UV/vis and ^{13}C{^{1}H} NMR spectra were not obtained due to the low quantity of isolated material.

^{1}H NMR (400.30 MHz, 300 K, C$_6$D$_6$, in ppm): δ = −25.59 (br s, 4 H) overlapping with −25.59 (s, 2H), −15.69 (br s, 12H, −CH(CH_3)$_2$ of Dipp), −13.90 (s, 4H), −4.78 (s, 2H), 0.37 (br s, 12H, −CH(CH_3)$_2$ of Dipp), 2.43 (s, 2H), 7.71 (br s, 24H, 18c-6), 79.05 (br s, 2H), 83.60 (s, 2H).
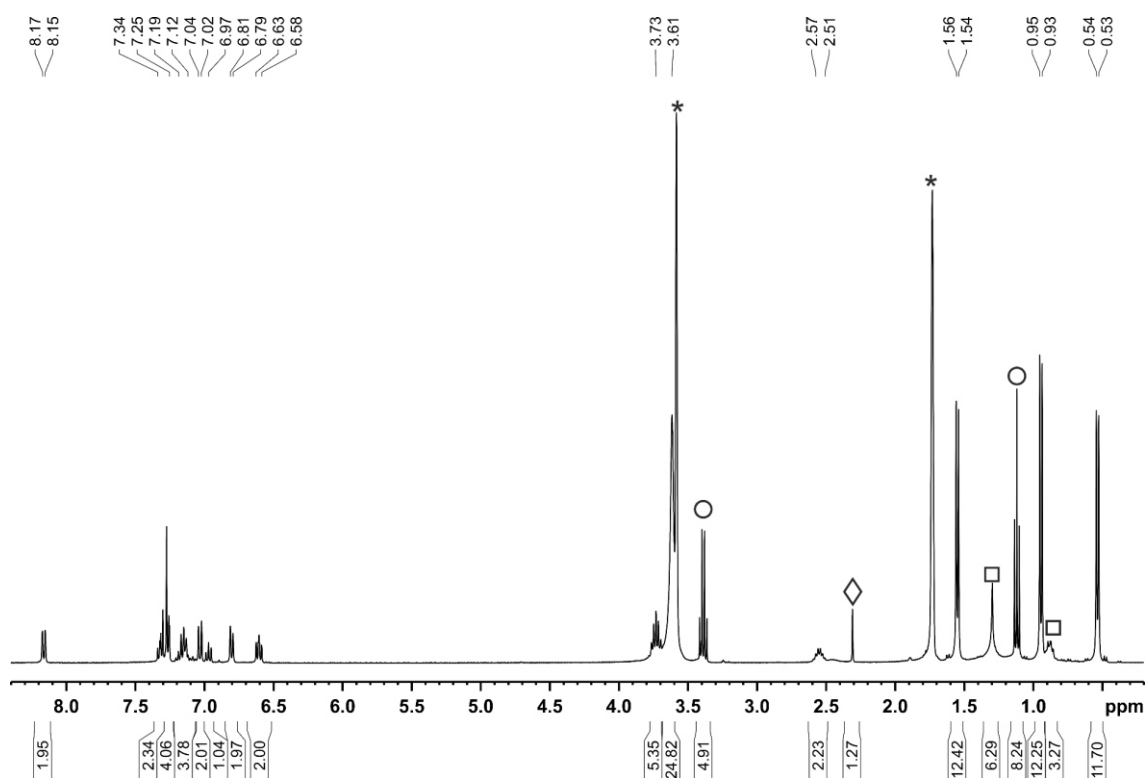
4.4.3   NMR Spectra

Figure S1. ^{1}H NMR spectrum (400.30 MHz, 300 K, THF-d_8) of [K(18c-6)][(PHDI)Co(η^4-P$_7$Dipp)] (**3**); * THF-d_8, □ n-hexane, ◊ toluene, ○ Et$_2$O.
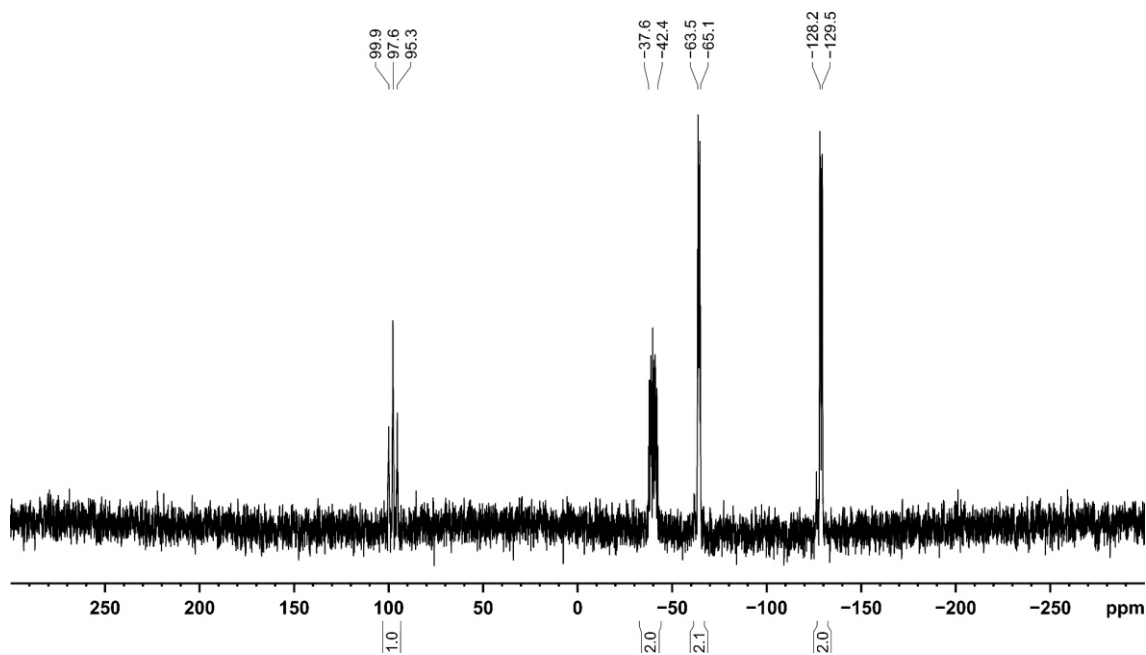
Figure S2. ^{31}P{^{1}H} NMR spectrum (162.04 MHz, 300 K, THF-d_8) of [K(18c-6)][(PHDI)Co(η^4-P$_7$Dipp)] (**3**).
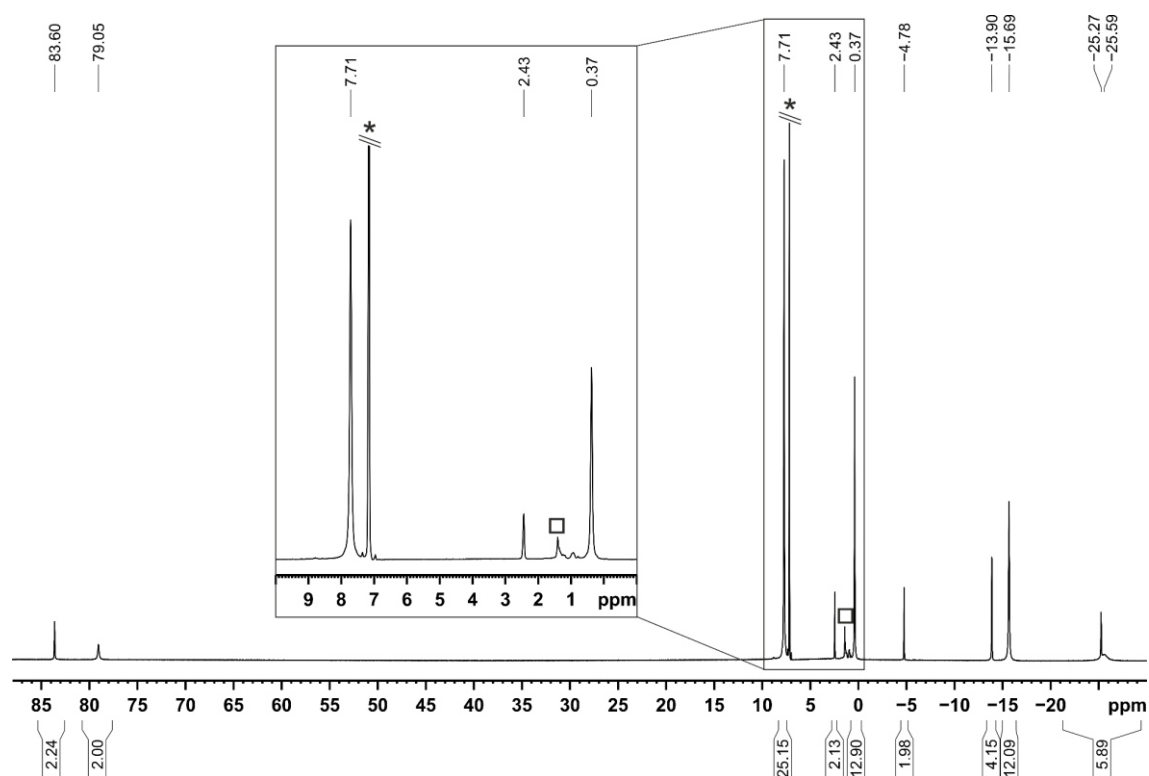
Figure S3. ^{1}H NMR spectrum (400.30 MHz, 300 K, C_6D_6) of [{K(18c-6)}(μ-Cl)$_2${Co(PHDI)}] (**6**); * C_6D_6, □ cyclohexane.

4.4.4   X-Ray Crystallography

The single-crystal X-ray diffraction data were recorded on an Agilent Technologies GV1000, TitanS2 diffractometer with Cu-K_α radiation (λ = 1.54184 Å). Either semi-empirical multi-scan absorption corrections[28] or analytical ones[29] were applied to the data. The structures were solved with SHELXT[30] and least-square refinements on F^2 were carried out with SHELXL.[31] The hydrogen atoms were located in idealized positions and refined isotropically with a riding model.

Table S1. Crystallographic data and structure refinement of **3** and **5**.

	3	**5**
Empirical formula	$C_{66}H_{93}CoKN_2O_7P_7$	$C_{82}H_{105}Cl_2CoN_4P_6$
Formula weight / g·mol^{-1}	1341.24	1462.34
Temperature / K	123.0(2)	123.0(1)
Crystal system	orthorhombic	monoclinic
Space group	$P2_12_12_1$	$C2/c$
a / Å	13.2421(3)	49.7345(5)
b / Å	17.9406(5)	10.5438(2)
c / Å	29.3437(6)	31.8043(4)
α /°	90	90
β /°	90	107.786(1)
γ /°	90	90
V / Å^3	6971.2(3)	15880.8(4)
Z	4	8
ρ_{calc} / g cm^{-1}	1.278	1.223
μ / mm^{-1}	4.385	3.793
F(000)	2840.0	6208.0
Crystal size / mm^3	0.202 × 0.108 × 0.026	0.618 × 0.300 × 0.183
Radiation / Å	CuK$_\alpha$ (λ = 1.54184)	CuK$_\alpha$ (λ = 1.54184)
2Θ range for data collection /°	7.324 – 148.27	7.466 – 147.714
Diffractometer	GV1000, TitanS2	GV1000, TitanS2
Index ranges	$-16 \leq h \leq 16$	$-61 \leq h \leq 60$
	$-21 \leq k \leq 21$	$-10 \leq k \leq 12$
	$-35 \leq l \leq 32$	$-39 \leq l \leq 39$
Reflections collected	25521	44464
Independent reflections	13471 [R_{int} = 0.0556, R_{sigma} = 0.0738]	15469 [R_{int} = 0.0360, R_{sigma} = 0.0327]
Data/restraints/parameters	13471/6/771	15469/0/878
Goodness-of-fit on F^2	1.039	1.021
Final R indexes [I>=2σ (I)]	R_1 = 0.0701, wR_2 = 0.1666	R_1 = 0.0407, wR_2 = 0.1085

Final R indexes [all data]	$R_1 = 0.0779$, $wR_2 = 0.1726$	$R_1 = 0.0442$, $wR_2 = 0.1123$
Largest diff. peak/hole / e Å⁻³	1.25/−0.65	0.61/−0.67
Flack parameter	−0.017(4)	

4.5 References

[1] a) J. J. Weigand, N. Burford in *Comprehensive inorganic chemistry II. From elements to applications* (Eds.: J. Reedijk, K. R. Poeppelmeier, A. M. Abakumov, A. V. Shevel′kov, Á. R. Álvarez, E. V. Antipov, J. W. Niemantsverdriet, L. Casella, N. Revaprasadu, P. O'Brien et al.), Elsevier, Amsterdam, **2013**, 119–149; b) A. F. Holleman, E. Wiberg, N. Wiberg, *Anorganische Chemie*, *Band 1 Grundlagen und Hauptgruppenelemente*, de Gruyter, Berlin, **2017**, pp. 846.

[2] M. Baudler, *Angew. Chem. Int. Ed. Engl.* **1982**, *21*, 492–512, *Angew. Chem.* **1982**, *94*, 520–539.

[3] M. Baudler, *Angew. Chem. Int. Ed. Engl* **1987**, *26*, 419–441, *Angew. Chem.* **1987**, *99*, 429–451.

[4] M. Baudler, K. Glinka, *Chem. Rev.* **1994**, *94*, 1273–1297.

[5] M. Baudler, K. Glinka, *Chem. Rev.* **1993**, *93*, 1623–1667.

[6] M. Baudler, W. Göldner, *Chem. Ber.* **1985**, *118*, 3268–3274.

[7] K.-O. Feldmann, J. J. Weigand, *Angew. Chem. Int. Ed.* **2012**, *51*, 7545–7549, *Angew. Chem.* **2012**, *124*, 7663–7667.

[8] a) J. D. Masuda, W. W. Schoeller, B. Donnadieu, G. Bertrand, *J. Am. Chem. Soc.* **2007**, *129*, 14180–14181; b) M. Scheer, G. Balázs, A. Seitz, *Chem. Rev.* **2010**, *110*, 4236–4256.

[9] a) B. M. Cossairt, N. A. Piro, C. C. Cummins, *Chem. Rev.* **2010**, *110*, 4164–4177; b) M. Caporali, L. Gonsalvi, A. Rossin, M. Peruzzini, *Chem. Rev.* **2010**, *110*, 4178–4235.

[10] B. M. Cossairt, C. C. Cummins, *Angew. Chem. Int. Ed.* **2008**, *47*, 169–172, *Angew. Chem.* **2008**, *120*, 175–178.

[11] a) F. Spitzer, C. Graßl, G. Balázs, E. M. Zolnhofer, K. Meyer, M. Scheer, *Angew. Chem. Int. Ed.* **2016**, *55*, 4340–4344, *Angew. Chem.* **2016**, *128*, 4412–4416; b) S. N. Konchenko, N. A. Pushkarevsky, M. T. Gamer, R. Köppe, H. Schnöckel, P. W. Roesky, *J. Am. Chem. Soc.* **2009**, *131*, 5740–5741.

[12] F. Dielmann, M. Sierka, A. V. Virovets, M. Scheer, *Angew. Chem. Int. Ed.* **2010**, *49*, 6860–6864, *Angew. Chem.* **2010**, *122*, 7012–7016.

[13] E. Mädl, M. V. Butovskii, G. Balázs, E. V. Peresypkina, A. V. Virovets, M. Seidl, M. Scheer, *Angew. Chem. Int. Ed.* **2014**, *53*, 7643–7646, *Angew. Chem.* **2014**, *126*, 7774–7777.

[14] M. H. Holthausen, S. K. Surmiak, P. Jerabek, G. Frenking, J. J. Weigand, *Angew. Chem. Int. Ed.* **2013**, *52*, 11078–11082, *Angew. Chem.* **2013**, *125*, 11284–11288.

[15] C. M. Knapp, J. S. Large, N. H. Rees, J. M. Goicoechea, *Chem. Commun.* **2011**, *47*, 4111–4113.

[16] a) S. Charles, J. C. Fettinger, B. W. Eichhron, *J. Am. Chem. Soc.* **1995**, *117*, 5303–5311; b) S. Charles, J. A. Danis, S. P. Mattamana, J. C. Fettinger, B. W. Eichhorn, *Z. anorg. allg. Chem.* **1998**, *624*, 823–829; c) S. Charles, J. A. Danis, J. C. Fettinger, B. W. Eichhorn, *Inorg. Chem.* **1997**, *36*, 3772–3778.

[17] S. Pelties, T. Maier, D. Herrmann, B. de Bruin, C. Rebreyend, S. Gärtner, I. G. Shenderovich, R. Wolf, *Chem. Eur. J.* **2017**, *23*, 6094–6102.

[18] C. G. P. Ziegler, T. M. Maier, S. Pelties, C. Taube, F. Hennersdorf, A. W. Ehlers, J. J. Weigand, R. Wolf, *Chem. Sci.* **2019**, *10*, 1302–1308.

[19] E. Mädl, M. V. Butovskii, G. Balázs, E. V. Peresypkina, A. V. Virovets, M. Seidl, M. Scheer, *Angew. Chem. Int. Ed.* **2014**, *53*, 7643–7646, *Angew. Chem.* **2014**, *126*, 7774–7777.

[20] M. M. Rodriguez, E. Bill, W. W. Brennessel, P. L. Holland, *Science* **2011**, *334*, 780–783.

[21] a) P. L. Holland, T. R. Cundari, L. L. Perez, N. A. Eckert, R. J. Lachicotte, *J. Am. Chem. Soc.* **2002**, *124*, 14416–14424; b) C. Chen, M. B. Hecht, A. Kavara, W. W. Brennessel, B. Q. Mercado, D. J. Weix, P. L. Holland, *J. Am. Chem. Soc.* **2015**, *137*, 13244–13247; c) A. Panda, M. Stender, R. J. Wright, M. M. Olmstead, P. Klavins, P. P. Power, *Inorg. Chem.* **2002**, *41*, 3909–3916; d) C. Lepori, P. Gómez-Orellana, A. Ouharzoune, R. Guillot, A. Lledós, G. Ujaque, J. Hannedouche, *ACS Catal.* **2018**, *8*, 4446–4451.

[22] K. Schwedtmann, M. H. Holthausen, C. H. Sala, F. Hennersdorf, R. Fröhlich, J. J. Weigand, *Chem. Commun.* **2016**, *52*, 1409–1412.

[23] B. Gao, X. Luo, W. Gao, L. Huang, S.-m. Gao, X. Liu, Q. Wu, Y. Mu, *Dalton Trans.* **2012**, *41*, 2755–2763.

[24] P. Pyykkö, M. Atsumi, *Chem. Eur. J.* **2009**, *15*, 12770–12779.

[25] A. J. Arduengo, J. C. Calabrese, A. H. Cowley, H. V. R. Dias, J. R. Goerlich, W. J. Marshall, B. Riegel, *Inorg. Chem.* **1997**, *36*, 2151–2158.

[26] Y. Wang, Y. Xie, P. Wei, R. B. King, H. F. Schaefer, P. v. R. Schleyer, G. H. Robinson, *J. Am. Chem. Soc.* **2008**, *130*, 14970–14971.

[27] D. F. Evans, *J. Chem. Soc.* **1959**, 2003.

[28] a) SCALE3ABS, CrysAlisPro, Aglient Technologies Inc., Oxford, GB, 2012, b) G. M. Sheldrick, SADABS, Bruker AXS, Madison, USA, 2007.

[29] R. C. Clark, J. S. Reid, *Acta Cryst. A* **1995**, *51*, 887–897.

[30] G. M. Sheldrick, *Acta Cryst. A* **2015**, *71*, 3–8.

[31] G. M. Sheldrick, *Acta Cryst. A* **2008**, *64*, 112–122.

5 SUMMARY

Chapter 1. Transition Metal-Mediated Transformations of White Phosphorus

This introductory chapter reviews the versatile chemistry of P_4 functionalization mediated by transition metal complexes. The chapter categorizes the current state of this research field into systematic subunits and delineates the synthetic methodologies used for exploring P_4 functionalization in detail. After a brief introduction concerning the relevance of P_4 transformations, this chapter first highlights the "one step activation and functionalization" of P_4 mediated by transition metals. "Functionalization of P_n ligands" is then discussed with this section further subdivided based on the number of phosphorus atoms within the ligand: P_{1-2}, P_3, P_4 and $P_{n \geq 5}$. Finally, transition metal-mediated methods for P_4 functionalization by radicals are described.

Chapter 2. Synthesis of Cyclic M_2E_2 Clusters (M = Fe, Co; E = Ge, Sn) Using M^- Synthons[1]

The major goal of this thesis was to synthesize and characterize novel low valent metal complexes and explore their potential in the activation and functionalization of white phosphorus. One of the low-valent metal clusters examined herein is the heterobimetallic Co_2Sn_2 cluster **2-1**. This tetranuclear species was synthesized by reaction of the anionic cobaltate salt $[K(thf)_{0.2}][Co(\eta^4\text{-}1,5\text{-cod})_2]$ with $[Ar'Sn(\mu\text{-Cl})]_2$ ($Ar' = C_6H_3\text{-}2,6(C_6H_3\text{-}2,6\text{-}i Pr_2)_2$) in toluene (Scheme 1). The data gathered from X-ray crystallography, Mössbauer spectroscopy and quantum chemical calculations indicate that compound **2-1** features strong intermetallic Co−Sn bonds, but a rather weak Sn−Sn interaction.
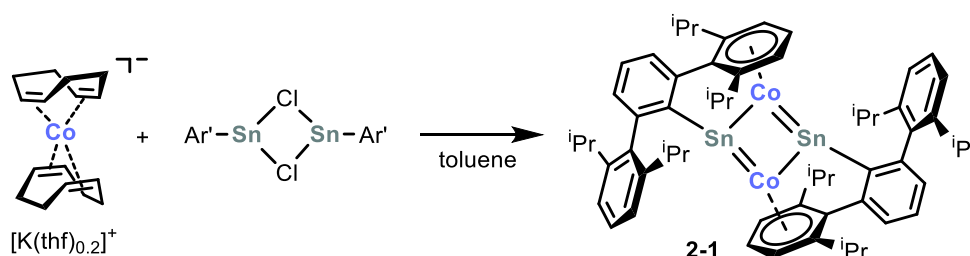
Scheme 1. Synthesis of Co_2Sn_2 compound **2-1**.

Compound **2-1** readily undergoes one electron oxidation when reacted with $[Cp_2Fe][BAr^F_4]$ ($Ar^F = 3,5\text{-}(CF_3)_2C_6H_3$) in THF. This reaction affords the paramagnetic compound $[Ar'_2Sn_2Co_2][BAr^F_4]$ (**2-2**), which contains a monocationic Co_2Sn_2 cluster

(Scheme 2a). The EPR spectrum of **2-2** is slightly rhombic and rather broad, but clearly indicates the presence of an S = ½ system. The crystallographically determined bond parameters of **2-2** closely resemble those found in the neutral precursor **2-1**. The reaction of **2-1** with white phosphorus cleanly affords the ternary cluster $[Ar'_2Sn_2Co_2P_4]$ (**2-3**, Scheme 2b). Notably, as one of the terphenyl moieties migrated from tin to phosphorus, this reaction represents a rare example of P_4 activation and functionalization in one step (see chapter 1.3.1 for further examples from the literature).
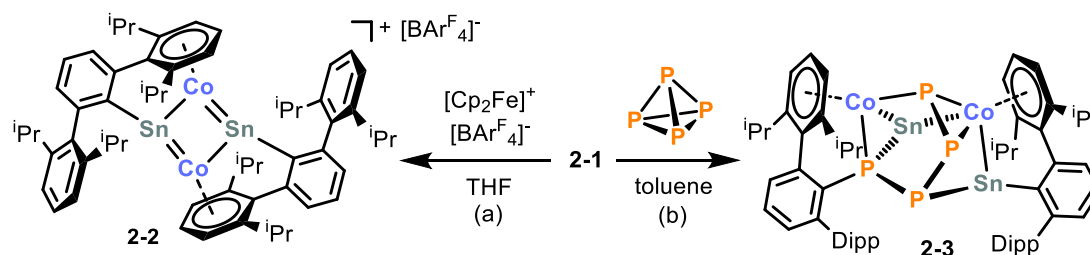
Scheme 2. Synthesis of the monocationic Co_2Sn_2 compound **2-2** and the ternary cluster **2-3**.

Furthermore, ^1H NMR spectroscopic evidence was gathered that the related Co_2Ge_2 cluster **2-4** was formed upon treatment of $[K(thf)_{0.2}][Co(\eta^4\text{-}1,5\text{-cod})_2]$ with $[Ar'GeCl]_2$, although attempts at the isolation of **2-4** as a pure species have been unsuccessful (Scheme 3a).
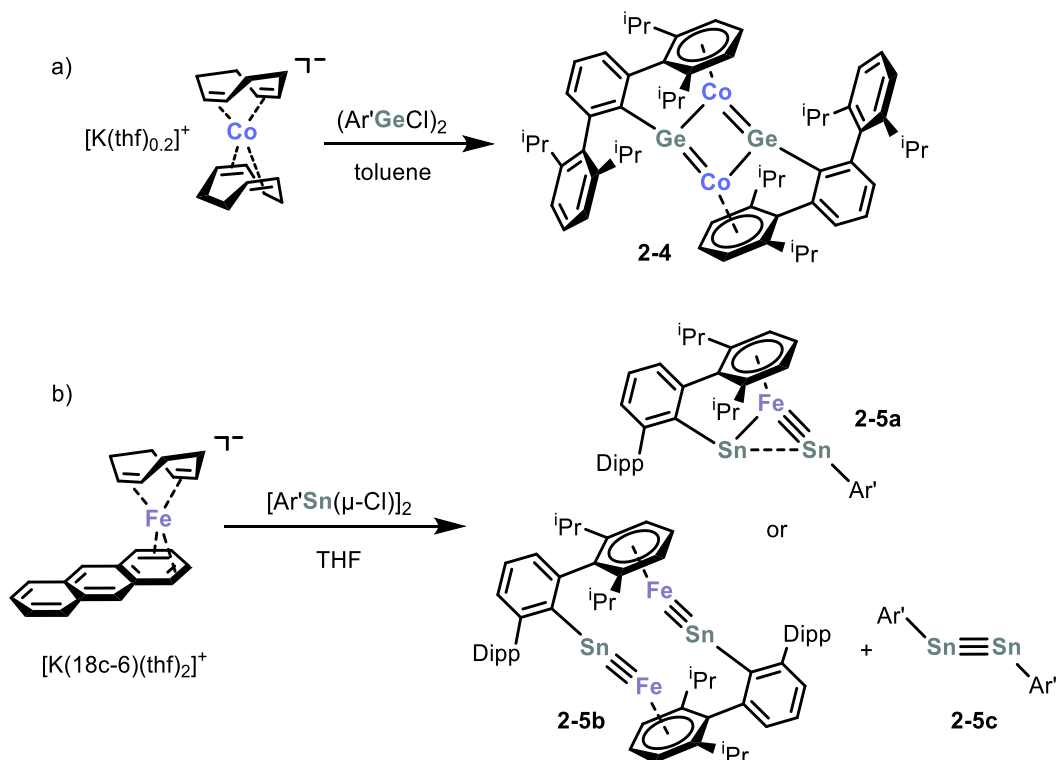
Scheme 3. Synthesis of cyclic heterobimetallic cluster compounds **2-4** and **2-5**

The reaction of the anionic ferrate salt $[K(18c\text{-}6)][Fe(\eta^4\text{-}1,5\text{-}cod)(\eta^4\text{-}C_{14}H_{10})]$ with $[Ar'Sn(\mu\text{-}Cl)]_2$ led to an iron/tin cluster compound **2-5**. However, the true composition of **2-5** remains ambiguous, since neither X-ray crystallography nor ^{1}H NMR spectroscopic analysis gave sufficient experimental evidence to distinguish between a disordered triangular Sn_2Fe compound **2-5a** or a co-crystallized mixture of the distannylidyne complex **2-5b** and the distannyne **2-5c**. Nonetheless, the latter option seems to be less likely, since both the bond parameters and the ^{1}H NMR spectroscopic data of **2-5c** differ from the values originally reported for the pure distannyne. Moreover, the results of quantum chemical calculations support the presence of the triangular compound **2-5a** over the dinuclear distannylidyne compound **2-5b**. Prospectively, several further experiments and analyses, such as mass spectrometry, ^{119}Sn NMR and Mössbauer spectroscopy need to be performed, in order to confirm the composition of **2-5** unambiguously.

The synthesis of compounds **2-1**, **2-4** and **2-5** demonstrates a promising avenue to new heterobimetallic species with strong intermetallic bonding. The application of this synthetic strategy to a range of other metalate anions and metal halides available across the periodic table may lead to a rich family of unprecedented clusters. The focus of future investigations will be the synthesis of further d-block/p-block species, and the exploration of their properties and reactivity.

Chapter 3. [3+2] Fragmentation of a Pentaphosphido Ligand by Cyanide[2]

This chapter addresses the use of low-valent α-diimine complexes for P_4 activation and subsequent functionalization.

The phenanthrene diimine complex $[K(18c\text{-}6)(thf)_{1.5}][(PHDI)Co(\eta^4\text{-}1,5\text{-}cod)]$ ($[K(18c\text{-}6)]$**3-1**, 18c-6 = 18-crown-6, PHDI = bis(2,6-diisopropylphenyl)phenanthrene-9,10-diimine, cod = cyclooctadiene) was synthesized by ligand exchange of 1,5-cod in $[K(18c\text{-}6)][Co(\eta^4\text{-}1,5\text{-}cod)_2]$ with PHDI. Reaction of $[K(18c\text{-}6)]$**3-1** with P_4 afforded an anionic *cyclo*-P_4 cobalt complex $[K(18c\text{-}6)]$**3-2** in a straightforward, high yielding synthesis (Scheme 4). The solid-state molecular structure of $[K(18c\text{-}6)]$**3-2** was heavily disordered, but the tungsten pentacarbonyl adduct $[K(18c\text{-}6)]$**3-3**, obtained quantitatively from the reaction with $[W(CO)_5(thf)]$, provided an ordered structure which allowed an analysis of the key structural parameters of the complex.

183
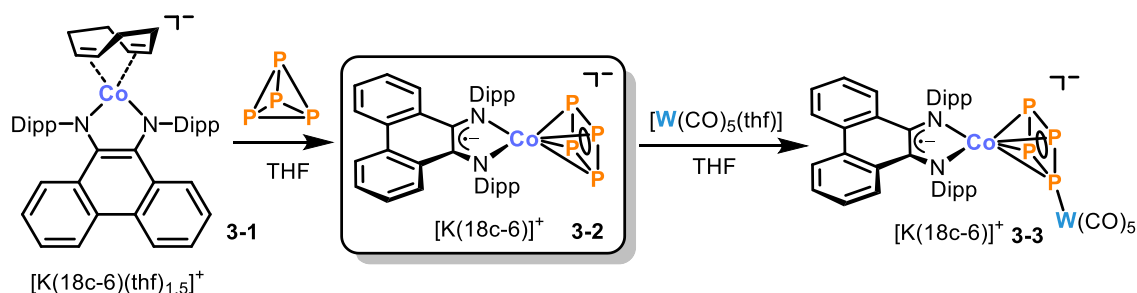
Scheme 4. Synthesis of compounds [K(18c-6)]**3-2** and [K(18c-6)]**3-3**.

Furthermore, a series of neutral pentaphosphido complexes (**3-4-R**) with an unprecedented range of alkyl, aryl and amino substituents was accessible by reacting [K(18c-6)]**3-2** with R_2PCl (Scheme 5a). Remarkably, the pentaphosphorus ligands of **3-4-R** undergo a [3+2] fragmentation upon reaction with two equivalents of cyanide, forming the anionic cyclotriphosphido cobalt complex **3-5** and rare cyanodiphosphan-1-ides **3-6-R** (Scheme 5b). Reaction of **3-4-Mes** with cyanide instead affords [Et_4N]**3-7**, which contains a rearranged P_5Mes_2 ligand (Scheme 5c). The structure of this complex suggests that tetraphosphido complexes are key intermediates *en route* to anions **3-5** and **3-6-R**.
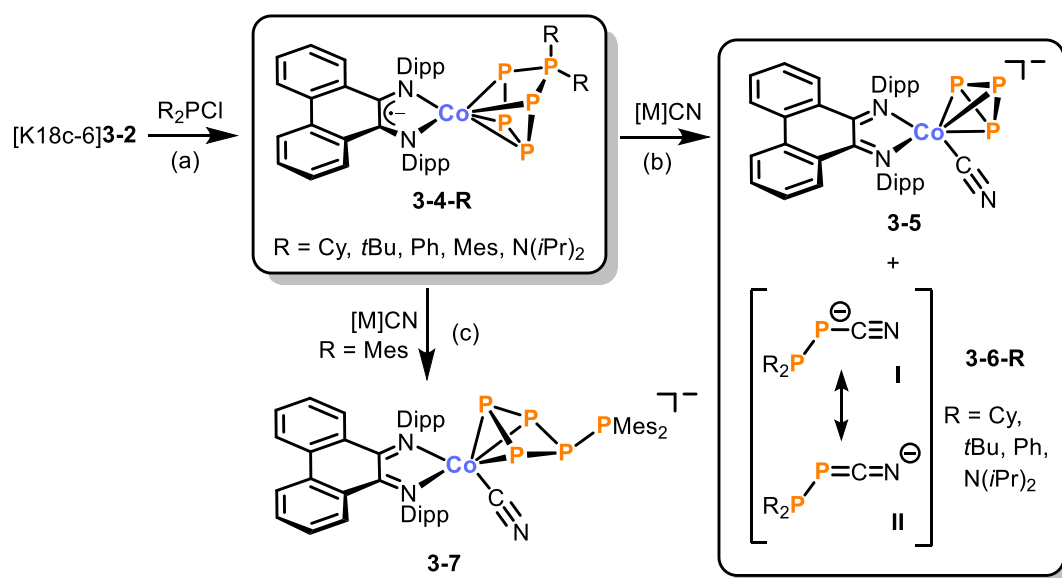
Scheme 5. Synthesis of the pentaphosphido complexes **3-4-R** (a) and their fragmentation (b) and rearrangement (c) depending on the substituent R.

The results of this work show that diimine cobalt complexes are an excellent platform for studying the degradation of polyphosphorus ligands with inorganic nucleophiles. An extension of this approach to a wider range of polyphosphides and other nucleophiles should give rise to further unusual phosphorus compounds. Furthermore, reactions of [K(18c-6)]**3-2** and [nBu_4N]**3-5** with electrophiles will likely give rise to novel

polyphosphanes and polyphosphido complexes (as already illustrated by preliminary work with [K(18c-6)]**2** reported in the next chapter).

Chapter 4. Synthesis of Polyphosphido Cobalt Complexes Using a Tetraphosphido Cobaltate Precursor

In extension to the previous chapter, which demonstrated that [K(18c-6)]**3-2** is an excellent precursor for the construction of pentaphosphido complexes, the potential of [K(18c-6)]**3-2** in the formation of more extended phosphorus frameworks was investigated.

The reaction of [K(18c-6)]**3-2** with the inversely polarized phosphaalkene ($^{Cl}Im^{Dipp}$)PP(Cl)Dipp (**4-1**, $^{Cl}Im^{Dipp}$ = *N,N'*-bis(2,6-diisopropylphenyl)-4,5-dichloro-imidazolin-2-ylidene) in toluene is unselective and affords several products (Scheme 6). The most easily accounted for product is the hexaphosphido complex [(PHDI)Co{η^4-*cyclo*-P$_5$Dipp(P($^{Cl}Im^{Dipp}$))}] (**4-2**), which was isolated as a few crystals from *n*-pentane extracts. Furthermore, the paramagnetic dichloride cobalt complex [{K(18c-6)}(μ-Cl)$_2${Co(PHDI)}] (**4-3**) was identified by its characteristic set of broad singlets in the ^{1}H NMR spectrum and by single-crystal XRD analysis. The heptaphosphido compound [K(18c-6)][(PHDI)Co(η^4-P$_7$Dipp] (**4-4**) crystallized in satisfactory purity from toluene extracts and was characterized by X-ray crystallography and multinuclear NMR spectroscopy.
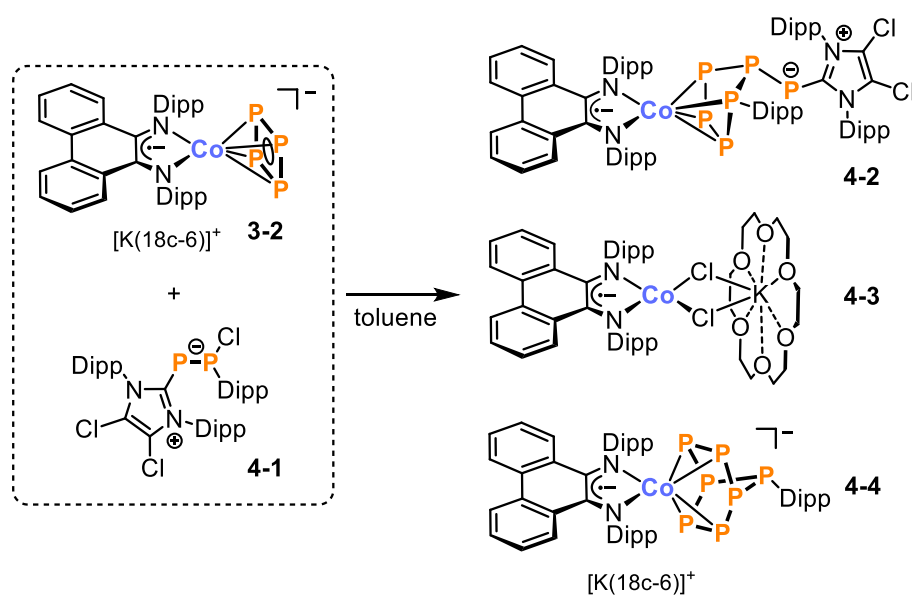
Scheme 6. Synthesis of the oligophosphido cobalt complexes **4-2** and **4-4**.

185

Prospective investigations will focus on the optimization of the reaction conditions and work-up procedures for this reaction. ^{1}H and ^{31}P{^{1}H} NMR monitoring experiments ought to give more insight into the mechanisms of the formation of the identified product species. Compounds **4-2** and **4-3** need to be isolated as pure compounds and fully characterized. Moreover, an EPR spectrum and the effective magnetic moment should be measured for paramagnetic **4-3**. Once **4-4** is accessible in sufficient quantities, further characterizations by elemental analysis and UV/Vis spectroscopy will be performed. Although the reaction is currently not fully understood, it offers valuable insight into the fundamental reactivity of polyphosphido complexes and demonstrates a novel method for the construction of extended polyphosphido frameworks in the coordination sphere of diimine cobaltate anions. The application of the same synthetic strategy to other low valent polyphosphido complexes may lead to a series of unprecedented polyphosphanido species. Finally, anionic P-containing products obtained from such reactions (e.g. **4-4**) are likely to serve as promising precursors for the construction of even larger extended polycyclophosphane scaffolds.

References

[1] C. M. Hoidn, C. Rödl, M. L. McCrea-Hendrick, T. Block, R. Pöttgen, A. W. Ehlers, P. P. Power, R. Wolf, *J. Am. Chem. Soc.* **2018**, *140*, 13195–13199.

[2] C. M. Hoidn, T. Maier, K. Trabitsch, J. J. Weigand, R. Wolf, *Angew. Chem. Int. Ed.* **2019**, *58*, 18931–18936, *Angew. Chem.* **2019**, *131*, 19107–19112.

6 ACKNOWLEDGEMENT

Zuletzt möchte ich mich bei folgenden Personen bedanken:

- Ganz besonders bei Prof. Dr. Robert Wolf für die hervorragende Betreuung, die interessante Aufgabenstellung, die anregenden Diskussionen, die exzellenten Arbeitsbedingungen und der großen Freiheit bei meiner Forschung.
- Prof. Dr. Manfred Scheer (Zweitgutachter), Prof. Dr. Frank-Michael Matysik (Drittprüfer) und Apl. Prof. Dr. Rainer Müller (Vorsitz) für die Bereitschaft, die Plätze der Prüfungskommission zu besetzen.
- Dr. Michael Bodensteiner, Dr. Stefanie Gärtner und Prof. Dr. Robert Wolf für die Hilfestellung bei der Röntgen-Einkristallstrukturanalyse.
- Den Mitarbeitern der zentralen Analytik und Werkstätten, insbesondere: Sabine Stempfhuber und Birgit Hischa (Röntgenstrukturanalyse), Annette Schramm, Georgine Stühler, Veronica Scheidler, Fritz Kastner und Ilya Shenderovich (NMR-Abteilung), Barbara Baumann und Helmut Schüller (Elementaranalyse), Josef Kiermaier und Wolfgang Söllner (Massenspektrometrie), Markus Lindner und Helena Ackermann (Glasbläserei).
- Meinen Kooperationspartnern Prof. Dr. Jan J. Weigand, Dr. Kai Schwedtmann, Clemens Taube, Julia Frötschel (TU Dresden), Prof. Dr. Philip P. Power, Madison L. McCrea-Hendrick (UC Davis), Prof. Dr. Rainer Pöttgen, Theresa Block, (WWU Münster), Dr. Andreas W. Ehlers (VU Amsterdam), Prof. Dr. Bas de Bruin (University of Amsterdam) für ihren wertvollen Beitrag, ihr hohes Engagement und die interessanten Diskussionen.
- Den aktuellen und früheren Arbeitskreismitgliedern: Anup Adhikari, Percia Beatrice Arockiam, Philipp Büschelberger, Jose Cammarata, Uttam Chakraborty, Peter Coburger, Sebastian Hauer, Dirk Herrmann, Gabriele Hierlmeier, John Kelly, Julia Leitl, Ulrich Lennert, Thomas Maier, Matt Margeson, Julia Märsch, Bernd Mühldorf, Stefan Pelties, Christian Rödl, Daniel Scott, Felix Seeberger, Marion Till, Franziska Urban, Thomas Wagner, Christoph Ziegler für die einmalige Stimmung im Arbeitskreis, die sehr kollegiale Atmosphäre, die lustigen Kaffeepausen, spontanen Feierabendbierchen, die Medien-Kompetenz-Seminare, die Lasertag-Besuche, die Weißwurst-Switch-Samstage, sowie die AK-Ausflüge.
- Insbesondere den Kollegen aus Labor 22 (it's-just-like-crazy-Anup, Utti, Dörk, Hauer-Bua, GaRbi, Hans, Lulu, Oberster-Bergführer-Uli) und meinem Office-Buddy, Fliegen-Peter.
- Thanks to John and Daniel for final proofreading.
- Der Stiftung der Deutschen Wirtschaft (sdw) für ein Promotionsstipendium, bei dem neben finanzieller, vielmehr noch eine ganz persönliche ideelle Förderung im Fokus steht, und der ganzen Regionalgruppe Regensburg für die großartige Zusammenarbeit.
- All meinen Freunden aus Regensburg und der Heimat, insbesondere den Quersties, der Zehnerleisbande und der Krimidinner-Truppe.

Unendlich dankbar bin ich meinen Eltern, Rudi und Beate, die mir mein ganzes Leben lang bedingungslosen Rückhalt gegeben haben und mich auf meinen Wegen immer uneingeschränkt unterstützt haben.

Tausend Dank an meine Brüder Matthias und Andreas, meine Schwägerin Christina, und meine kleine Nichte Hanna fürs Zuhören und das erfolgreiche Ablenken vom harten Unialltag.

Von ganzem Herzen möchte ich mich bei meiner Freundin Helena bedanken. Sie war während meiner gesamten Studien- und Promotionszeit immer für mich da, hat mich an schlechten Tagen aufgeheitert, viele wundervolle Momente mit mir geteilt und unvergessliche Abenteuer mit mir erlebt. Danke, Helena, dass du mich in diesem wichtigen Lebensabschnitt tagtäglich liebevoll begleitet hast.

7 CURRICULUM VITAE

Education

Since Nov. 2015	**Ph.D.** at the University of Regensburg, Germany (Institute of Inorganic Chemistry) in the group of Prof. Dr. R. Wolf: "Functionalization of White Phosphorus Mediated by Low Valent Cobalt Complexes"
Aug. – Oct 2016	**Research Visit** during the Ph.D. at the University of California, Davis, USA, Prof. Dr. Philip P. Power
Oct. 2013 – Sep. 2015	**Master of Science** in Chemistry at the University of Regensburg, Germany
	Master Thesis in the group of Prof. Dr. R. Wolf (Institute of Inorganic Chemistry): "Reactivity of an Anionic Iron Phosphinine Complex toward Main Group Electrophiles – a New Route to Phosphacyclohexadienyl Complexes"
May 2011 – Jul. 2013	**Bachelor of Science** in Chemistry at the University of Regensburg, Germany
	Bachelor Thesis in the group of Prof. Dr. R. Wolf (Institute of Inorganic Chemistry): "Synthese von niedervalenten Cobalt- und Nickelkomplexen durch Reduktion von NHC-Metallhalogeniden mit einer Magnesium(I)-Verbindung"
May 2011	**Abitur** (A-levels) at the Gymnasium Zwiesel

Awards & Scholarships

April 2019	Best Poster Award – 16th European Workshop on Phosphorus Chemistry in Bristol, UK
March 2018	Best Talk Award – 14th Koordinationschemie-Treffen in Heidelberg, Germany
June 2016	Graduation Award (Master's Degree) – Dr. Alfons Paulus Stiftung, University of Regensburg
June 2016 – May 2019	PhD Scholarship – Stiftung der Deutschen Wirtschaft (sdw)

Presentations

24. – 28.04.2019	Poster – 16th European Workshop on Phosphorus Chemistry in Bristol, UK
24. – 27.09.2018	Poster – 19th Vortragstagung für Anorganische Chemie der Fachgruppen Wöhler-Vereinigung und Festkörperchemie und Materialforschung in Regensburg, Germany
30.07. – 04.08.2018	Poster – 43th International Conference on Coordination Chemistry (ICCC) in Sendai, Japan
11. – 13.03.2018	Talk – 14th Koordinationschemie-Treffen in Heidelberg, Germany

20. – 25.08.2017	Talk – Wissenschaftliches Kolloquium von Arbeitsgruppen für Anorganische Chemie 2017 in Hirschegg, Austria
09. – 13.07.2017	Poster – 22nd European Conference on Organometallic Chemistry (EuCOMC) in Amsterdam, The Netherlands
20. – 22.03.2017	Poster – 14th European Workshop on Phosphorus Chemistry (EWPC) in Cluj-Napoca, Romania
07. – 09.03.2016	Talk – 13th European Workshop on Phosphorus Chemistry (EWPC) in Berlin, Germany
23. – 28.08.2015	Talk – Wissenschaftliches Kolloquium von Arbeitsgruppen für Anorganische Chemie 2015 in Hirschegg, Austria

8   LIST OF PUBLICATIONS

1) C. M. Hoidn, R. Wolf, *Dalton Trans.* **2016**, *45*, 8875−8884, *"Reaction of a 2,4,6-triphenylphosphinine ferrate anion with electrophiles: a new route to phosphacyclohexadienyl complexes"*

2) C. M. Hoidn, C. Rödl, M. L. McCrea-Hendrick, T. Block, R. Pöttgen, A. W. Ehlers, P. P. Power, R. Wolf, *J. Am. Chem. Soc.* **2018**, *140*, 13195−13199, *"Synthesis of a Cyclic Co₂Sn₂ Cluster Using a Co⁻ Synthon"*

3) C. M. Hoidn, J. Leitl, C. G. P. Ziegler, I. G. Shenderovich, R. Wolf, *Eur. J. Inorg. Chem.* **2019**, *2019*, 1567−1574, *"Halide-Substituted Phosphacyclohexadienyl Iron Complexes: Covalent Structures vs. Ion Pairs"*

4) C. M. Hoidn, T. M. Maier, K. Trabitsch, J. J. Weigand, R. Wolf, *Angew. Chem. Int. Ed.* **2018**, *58*, 18931−18936, *Angew. Chem.* **2019**, *131*, 19107−19112, *"[3+2] Fragmentation of a Pentaphosphido Ligand by Cyanide"*